Greenhouse gas observations across the Land-Ocean Aquatic Continuum: Multi-sensor applications for CO_2, CH_4 and O_2 measurements

Dissertation

zur Erlangung des Doktorgrades
der Mathematisch-Naturwissenschaftlichen Fakultät
der Christian-Albrechts-Universität zu Kiel

vorgelegt von

Anna Canning

Kiel

2020

Erste Gutachterin: Prof. Dr. Arne Körtzinger
Zweiter Gutachter: Prof. Dr. Bernhard Wehrli

Tag der mündlichen Prüfung: 24.04.2020
Zum Druck genehmigt: 24.04.2020

---

gez. Prof. Dr. Frank Kempken, Dekan

Erklärung

Hiermit erkläre ich an Eides Statt, dass ich die vorliegende Dissertation, abgesehen von der Beratung durch meinen Betreuer Prof. Dr. Arne Körtzinger, selbstständig und ohne fremde Hilfe angefertigt, keine anderen als die angegebenen Quellen und Hilfsmittel benutzt und die den benutzten Quellen wörtlich oder inhaltlich entnommenen Stellen als solche kenntlich gemacht habe. Diese Arbeit hat in gleicher oder ähnlicher Form noch keiner Prüfungsbehörde vorgelegen. Sie ist unter Einhaltung der Regeln guter wissenschaftlicher Praxis der Deutschen Forschungsgemeinschaft entstanden. Mir, Anna Rose Canning, wurde bis zum jetzigen Zeitpunkt noch kein akademischer Grad entzogen.

Kiel,03.03.2020

_____

(Anna Rose Canning)

Abstract

Carbon dioxide (CO_2) and methane (CH_4) are major greenhouse gases (GHG) and have been under constant monitoring for decades. Both gases have significantly increased in recent years due to anthropogenic activities, with fossil fuel CO_2 emissions peaking over 10 Gt C $yr^{-1}$for the first time in history in 2018. This has huge detrimental repercussions within natural systems including the warming of the planet. Although these GHG are extremely significant, there are also vast areas of study with little to no data in regards to emissions and budgets. These gaps are mainly within the aquatic regions (or the Land-Ocean Aquatic Continuum (LOAC)). As a consequence, there can be large discrepancies between budget numbers and in turn, scaling and future predictions.

One of the main reasons for discrepancies is due to differing regimes between the land and ocean where the two systems use different practices to optimise the instruments and measuring standards. Oceanographers, for example, focus more on accuracy and precision due to far smaller concentrations and variability. In order to combine oceanographic and limnological methods this thesis presents a novel sensor package and show its application in multiple campaigns across the entire LOAC.

The sensor set-up contained the sensors HydroC CO_2 FT (pCO_2), HydroC CH_4 FT (CH_4), HydroFlash O_2 (O_2) and a thermosalinograph for temperature and conductivity measuring all simultaneously. We extensively mapped inland regions and assessed the ways in which such high-resolution and accuracy measurements could potentially assist in filling some of these data gaps: First, the sensors' capabilities were tested in a range of salinities (saline to fresh) and across a range of seasons (spring, summer and autumn). We found the sensors performed well in all regions, however, to fully appreciate the data, extensive corrections had to be applied, vital within inland regions.

Following on from this we applied a simple model to calculate a continuous dataset for total alkalinity (TA) for the inland delta system. With this dataset, and our continuous pCO_2 data, we were able to calculate the full carbonate system. We found the whole delta system to be supersaturated in regards to CO_2, with each system (lakes, rivers or channels) showing very different dynamics. Both lakes and channels typically fluctuated between under and supersaturation (depending on season and region of the delta), while rivers were consistently supersaturated. Dissolved inorganic carbon (DIC) and O_2 ratios were extracted for each region (ΔDIC: ΔO_2), showing lakes tending to be heavily influenced by regions adjacent to them, such as wetlands that typically had the highest ranges of DIC. On top of this spatial-variability extraction, by extensive mapping techniques we were able to assess the presence of diel cycles. We found that lakes tended to have a strong diel cycle, with pCO_2 increasing during the night but typically returning to previous concentrations over the day. However, during these diel cycles, even though we observed a strong hysteresis, pCO_2 rarely rose above saturation ($\sim >$ 400 μatm).

This led us on to the final section where we extracted full diel cycles. Due to CH_4 being highly prominent in inland waters, the focus was mainly on the fluxes and concentrations. We found extreme diel cycles for CH_4, even more so than with pCO_2. In the lakes there was a clear hysteresis linking with sunrise and sunset. With the almost linear

CH_4 increase and O_2 decrease during the night (molar CH_4:O_2 ratio 1:50) this led to the explanation of strong stratification during the day, followed by nocturnal convection during the night. This would release the build-up of CH_4 in the bottom waters, mixing with the high O_2 surface waters. This was further confirmed by the concentrations reducing to initial conditions, such as with pCO_2, following sunrise as stratification occurred. In channels, however, this was slightly different yet still showed the potential of stratification within the water body, leading to CH_4 build-up in the bottom waters before release following the mixing during the night. Channel concentrations varied roughly a magnitude larger than lakes, however all regions of the delta were supersaturated with CH_4 in comparison with the atmosphere. We found channel CH_4 concentrations and fluxes potentially being underestimated by up to +25% and +20% respectively when not including a full diel cycle. In lakes however, we found the opposite, with an overestimation in concentration and fluxes (+3.3% and +4.2%) when not considering the diel cycle, although this greatly depends on time of the sampling.

Overall, this work presents a set-up that is capable to transverse across salinity boundaries, while gathering much needed, high-resolution, spatiotemporal data. We showed the possibilities that such a set-up can do, and the significance of sampling times in highly dynamic systems. These results confirm the existence of a diel cycle that, although have been noted before, are still not considered within the global budgets or within climate and environmental models.

Zusammenfassung

Kohlendioxid (CO_2) und Methan (CH_4) zählen zu den wichtigsten Treibhausgase (GHG). Deren Konzentration in derer Atmosphäre wird seit Jahrzehnten gemessen und hat durch anthropogene Aktivitäten deutlich zugenommen. CO_2-Emissionen aus fossilen Brennstoffen haben im Jahr 2018 erstmals 10 Gt C yr^{-1} überschritten. Diese Zunahme hat tiefreichende Auswirkungen auf chemischen (Ozeanversauerung) und physikalischen Prozesse (Erderwärmung) auf unserem Planeten und als Folge auf das gesamte Ökosystem der Erde. Obwohl diese Treibhausgase von großer Bedeutung sind, gibt es weite Bereiche, in denen nur wenige oder gar keine Daten zu Emissionen, Quellen und Senken vorliegen. Diese Lücken befinden sich hauptsächlich an der Schnittstelle vom limnologischen Ökosystem zum marinen Ökosystem (LOAC)). Als Folge davon gibt es große Diskrepanzen zwischen den Quellen und Senken in diesen Regionen und damit auch in den weltweiten Bilanzen und Modellen dieser Treibhausgase.

Die Hauptgründe für diese Diskrepanzen sind die unterschiedlichen Rahmenbedingungen dieser Regionen welche auch auf Messpraktiken, Messstandards und Instrumentierung Einfluss nehmen. Ozeanographen, zum Beispiel, fordern mehr Genauigkeit und Präzision, da in der marinen Region der LOAC die Konzentrationen der Gase und die Variabilität gering ist. Die limnologische Region bietet höhere Messsignale aber auch ein Vielfaches an Heterogenität.

Um ozeanographische und limnologische Methoden zu kombinieren, stelle ich ein neuartiges Sensorpaket vor und zeige seine Anwendung in mehreren Kampagnen über die gesamte LOAC.

Unser Sensoraufbau enthielt die Sensoren HydroC CO_2 FT (pCO_2), HydroC CH_4 FT (CH_4), HydroFlash O_2 (O_2) und einen Thermosalinographen zur gleichzeitigen Temperatur- und Leitfähigkeitsmessung. Ich habe räumlich-hochauflösende Messungen im limnologischen Bereiche durchgeführt um die Heterogenität dieser Region abzubilden und die Datenlücken zu schließen: Zunächst wurden die Fähigkeiten der Sensoren über eine Spannweite von Salinitäten (salzig bis frisch) und bei mehreren Jahreszeiten (Frühling, Sommer und Herbst) getestet. Die Sensoren funktionierten einwandfrei unter den schwierigen Bedingungen. Die Messignale mussten aber aufgrund der unterschiedlichen Umweltbedingungen umfangreichen Korrekturen unterworfen werden. Dies ist eben in den limnologischen Regionen von entscheidender Bedeutung. Darauf aufbauend habe ich mit einem einfachen Modell einen kontinuierlichen Datensatz für die Gesamtalkalinität (TA) des Binnendeltasystems berechnet. Mit diesem Datensatz und unseren kontinuierlichen pCO_2-Daten bin ich in der Lage, das vollständige Karbonatsystem zu berechnen.

Ich habe festgestellt, dass das gesamte Deltasystem in Bezug auf CO_2 übersättigt ist, wobei jedes System (Seen, Flüsse oder Kanäle) eine sehr unterschiedliche Dynamik aufweist. Sowohl die Seen als auch die Kanäle schwankten typischerweise zwischen Unter- und Übersättigung (je nach Jahreszeit und Region des Deltas), während die Flüsse durchweg übersättigt waren. Für jede Region wurde das Verhältnis zwischen gelösten anorganischen Kohlenstoff (DIC) und O_2 errechnet (ΔDIC: ΔO_2). Dabei zeigte sich, dass Seen tendenziell stark von den angrenzenden Regionen beeinflusst werden, wie z.B. Feuchtgebieten, die typischerweise die höchsten DIC-Werte aufweisen. Zusätzlich

zur räumlichen Variabilität konnte ich durch den umfangreichen Datensatz Tageszyklen analysieren. Seen weisen tendenziell einen starken Tageszyklus auf, bei dem der pCO_2 Wert in der Nacht ansteigt, aber im Laufe des Tages wieder abnimmt. Während dieser Tageszyklen stieg der pCO_2-Wert jedoch, wobei wir eine starke Hysterese beobachteten, selten über 400 μatm (vollständige Sättigung).

Zuletzt analysierte ich die Tageszyklen aller gemessenen Gase und deren Interaktion. Da CH_4 in Binnengewässern stark ausgeprägt ist, liegt der Schwerpunkt hauptsächlich auf den Flüssen und Konzentrationen dieses Treibhausgases. Die Tageszyklen sind bei CH_4 am stärksten und übertreffen sogar die von pCO_2. In den Seen gibt es eine deutliche Hysterese, die mit Sonnenauf- und Sonnenuntergang zusammenhängt. Der fast lineare CH_4-Anstieg und die O_2-Abnahme während der Nacht (molares CH_4:O_2-Verhältnis 1:50) führt zur Hypothese dass sich eine starke Schichtung während des Tages bildet, gefolgt von einer nächtlicher Konvektion während der Nacht. Dies Konvektion mischt das in der Nähe des Boden befindliche Wasser (hohe CH_4 Konz.) mit dem Oberflächenwasser (hohe O_2 Konz.). Darauf erfolgt eine CH_4 Anstieg im Oberflächenwasser und eine O_2 Abnahme ebendort. Dies wurde auch durch die pCO_2 Konzentrationen, bestätigt welche nach Einsetzen der Schichtung wieder auf die Anfangskonzentrationen zurückgehen. Kanäle zeigten ebenso Potenzial für einen Schichtungszyklus innerhalb des Wasserkörpers, was zu einer CH_4-Anreicherung im Bodenwasser vor der Freisetzung nach der Vermischung während der Nacht führte. Die Konzentrationen in den Kanälen schwankten ungefähr um eine Größenordnung größer als die der Seen, jedoch waren alle Regionen des Deltas im Vergleich zur Atmosphäre mit CH_4 übersättigt. Wir fanden heraus, dass die CH_4-Konzentrationen und -Flüsse im Kanal um bis zu 25% bzw. 20% höher sind, wenn man einen vollständigen Tageszyklus miteinbezieht. In Seen hingegen fanden wir das Gegenteil, nämlich eine Abnahme der Konzentration und der Flüsse um 3,3 % sowie 4,2 %, wenn man den Tageszyklus miteinbezieht. Dies ist allerdings stark von der Frequenz und dem Zeitpunkt der Probenahme abhängig.

In dieser Arbeit stelle ich ein Messsetup vor, welches in der Lage ist in einem großen Salzgehaltsbereich hochauflösende, räumlich und zeitlich, Messungen von CO_2, CH_4, O_2 zu machen. Ich habe gezeigt, welche Möglichkeiten ein solcher Aufbau bietet und welche Bedeutung die Abtastzeiten in hochdynamischen Systemen haben. Meine Ergebnisse bestätigen die Wichtigkeit des Tageszyklus in limnologischen Systemen. Dieser Zyklus wurde schon früher beobachtet, wird aber immer noch nicht in den globalen Klima- und Umweltmodellen berücksichtigt.

List of Figures

List of Tables

Manuscript Overview

1. **Anna Canning**, Arne Körtzinger, Peer Fietzek, Gregor Rehder: **Seamless gas measurements across Land-Ocean Aquatic continuum correction and evaluation of sensor data for CO_2, CH_4 and O_2 from contrasting field deployments, submitted to Marine Environmental Research**

   Author contribution: Anna Canning, Arne Körtzinger and Peer Fietzek discussed and designed the study together. Anna Canning collected and processed the sensor data and measured the discrete samples for alkalinity, dissolved inorganic carbon (excluding for M133) and methane, as well as processed the sensor data. Peer Fietzek assisted with processing of this sensor data. Gregor Rehder provided the reference system data for the Baltic Cruise. All authors reviewed the manuscript.

2. **Anna Canning** , Marie-Sophie Maier, Arne Körtzinger: **In-depth spatiotemporal analyses of carbon and oxygen dynamics using high-resolution data in Europe's second largest delta: the Danube River Delta**

   Author contribution: All authors contributions for the discussion and design of the fieldwork and analyses. Anna Canning collected and processed the sensor data and measured the discrete samples for alkalinity, dissolved inorganic carbon, Marie-Sophie Maier led and assisted work out in the field for data collection and mapping transects. Arne Körtzinger provided insightful ideas into the processing of the data. All authors reviewed the manuscript.

3. **Anna Canning**, Arne Körtzinger, Bernhard Werhli: **Methane in Europe's second largest delta (Danube River Delta): spatiotemporal patterns, lake day-night cycling and air-sea fluxes, In preparation for biogeosciences**

   Author contribution: Anna Canning and Arne Körtzinger discussed and designed the study from the results. Anna Canning collected and processed the sensor data. Benhard Werhli gave input and ideas. All authors reviewed the manuscript.

Contents

Introduction

1.1 Background

Since 1958, atmospheric carbon dioxide (CO_2) has been continuously measured by the Scripps Institute of Oceanography in Mauna Loa (Fig. 1.1), leading to one of the longest consistent measurement records in modern history. Within the first couple of years of the record, it became the first observation to show both a rise in atmospheric CO_2 and a seasonal cycle within concentrations (Keeling 1960). The continuing record, and the parallel atmospheric concentrations from NOAA (since 1974), has allowed for the expansion of our knowledge of atmospheric CO_2 and both the natural and anthropogenic impacts on these concentrations.

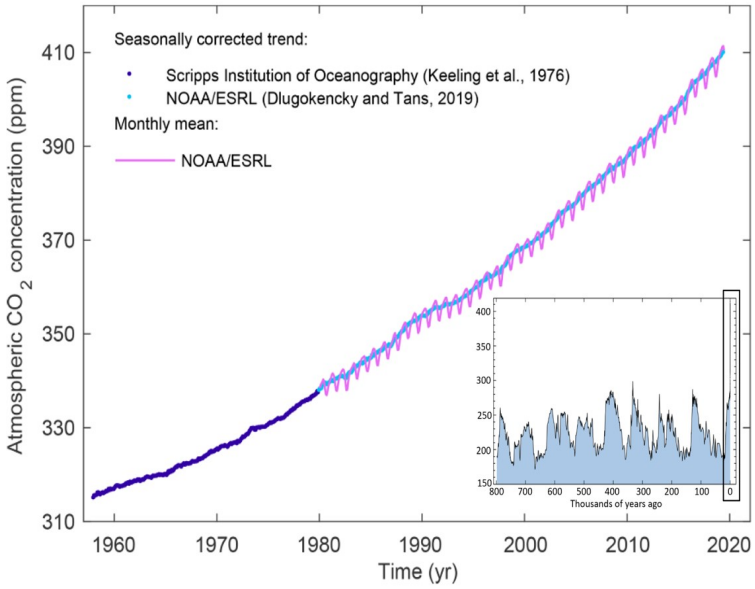

Figure 1.1: Atmospheric xCO_2 (ppm) measurements since 1958 (Friedlingstein et al. 2019) from NOAA and the Scripps Institute in Mauna Loa. Small insert showing the past 800,000 years (modified from Scripps Institution of Oceanography, Lüthi et al. (2008)) with the use of ice-core data before 1958, box indicating area of increased peak, note the difference in y-scale axis.

Since the beginning of the industrial revolution (1750), atmospheric CO_2 has increased from 279 ppm to over 409.09 ppm in 2019 (Dlugokencky and Tans, 2020), with a continuous overall increase as shown in figure 1.1. Initially, the increase following the industrial revolution due to land use change and deforestation (Ciais et al. 2013). Since around 1950 however, fossil fuel emissions have dominated our anthropogenic carbon source, further increasing to the present day (Friedlingstein et al. 2019). This ever-increasing excess in atmospheric CO_2 is either stored or used unevenly across three main simple reservoirs: terrestrial, oceanic and in the atmosphere (Cole et al. 2007). Within this thesis, focus is placed on two of the three reservoirs; inland waters therefore

terrestrial, and oceanic.

To first understand the purpose behind this research, we must consider a few preliminary questions; *what are the effects of CO_2 in the atmosphere? Has CO_2 changed from past records due to anthropogenic activities? What other gases are of interest?* Then bringing this background all together, *what are the implications of these increasing gases and are things being done to monitor or stop them?* With finally, *with this knowledge, which areas are in most need of data to help improve our understanding and how can we achieve this?*

Carbon Dioxide CO_2 is a greenhouse gas (GHG) that is sourced both naturally (i.e. respiration, fire) and also produced (i.e. combustion processes) and released to the atmosphere (Friedlingstein et al. 2019). Concentration of CO_2 in the atmosphere can influence the outbound solar radiation. Therefore, as CO_2 increases, there is a logarithmic increase in radiative forcing (RF) of the planet, causing it heat up (e.g. see the Keeling Curve or Myhre et al. (2013)). In the 15 years prior to the last International Panel on Climate Change (IPCC) report in 2013, CO_2 alone had accounted for approximately 80% of the increase of RF from GHG.

Once CO_2 is in the atmosphere there are four natural ways for removal (via in land or the ocean): Ocean invasion (seawater buffer), reaction with calcium carbonate, silicate weathering and land uptake through photosynthesis-respiration (Ciais et al. 2013). As CO_2 continues to increase that starts to put pressure on these particular areas. Between 1959-2018, fossil fuel emissions and land use change have accounted for 84% and 18% of all CO_2 emissions respectively. These emissions have been partitioned among land, ocean and atmosphere (29%, 24% and 45%), via such processes stated above, yet with 2% unaccounted for (Friedlingstein et al. 2019).

CO_2 emissions are constantly increasing and in 2018, fossil fuels reached over 10 ± 0.5 Gt C yr^{-1} (gigaton of carbon a year), which marks the first time in history for it to rise above 10 Gt C yr^{-1}, increasing 2.1%. When combined with land use change (1.5 ± 0.7 Gt C yr^{-1} (Friedlingstein et al. 2019)), the ocean sink accounted for 2.5 ± 0.6 GtC yr^{-1}. One implication of this oceanic CO_2 uptake pH reduction (see section 1.1.2), altering chemical balances leading to what is called ocean acidification (Doney et al. 2009). This lowers the calcium carbonate saturation states, ultimately impacting shell-forming organisms such as corals, molluscs and phytoplankton, which are the basis of life in the ocean. It also limits the oceans' ability to absorb CO_2 in the future.

CO_2 has been closely monitored for decades due to reasons above, however, it is not the only gas under constant watch.

Methane Since pre-industrial times, methane (CH_4) has been responsible for about 20% of the radiative climate forcing of all GHG (Weber et al. 2019). Although the concentrations of CH_4 are far lower than those of CO_2 within the atmosphere ($\sim$ 409.9 ppm CO_2 to 1876.2 ppb (NOAA 2020)), it's global warming potential (GWP) is 28 times that that of CO_2 (Myhre et al. 2013) over a 100-year time horizon, and ultimately contributes to CO_2 concentrations via hydroxyl radical (OH) oxidation. Due to the reaction with OH, the gas generates ozone up in the troposphere and reduces the oxidizing capacity of the atmosphere (Kirschke et al. 2013). In addition, other chemical compound changes also influene the forcing of CH_4 (such as nitrogen oxide and carbon monoxide) throughout its atmospheric lifetime (Saunois et al. 2019). As of late, CH_4 concentrations have seen an accelerated increase in the atmosphere from 1775 ppb to 1859 between 2006 to 2017 (Nisbet et al. 2019).

Currently, CH_4 global emissions are 568 Tg CH_4 y^{-1} (2003-2012: Saunois et al. (2016), 572 Tg CH_4 y^{-1} using top-down approach for 2008-2017: Saunois et al. 2019)

with $\sim$ 120 Tg CH_4 yr^{-1} (teragram CH_4 a year) from inland waters and 6–12 Tg CH_4 yr^{-1} from the ocean (Weber et al. 2019). Such as with CO_2, current levels have exceeded faster and/or higher than that seen in our geological records. A more recent study however, (Hmiel et al. 2020) suggested that the most recent anthropogenic CH_4 emissions are even between 25-40% underestimated than previously suggested.

When determining where the CH_4 comes from, it is broadly grouped into three sections, depending on how it is formed: thermogenic, pyrogenic and biogenic. These all have different isotopic signatures and can therefore be measured for contributions. Thermogenic CH_4 is formed geologically over millions of years and released either naturally (e.g. marine seeps) or via burning of fossil fuels. Pyrogenic CH_4 is formed with incomplete combustion of carbon soil and biomass, again through fossil fuels or more natural ways such as wildfires (Kirschke et al. 2013). The final one, bogenic, is the final product of decomposition of organic matter in anaerobic environments by Archaea. In this thesis this one will be focused on.

To understand the overall importance of these gas concentrations rising, one must understand the global and historical background.

Past variations and comparability During the past, atmospheric CO_2 has risen higher than it is today: mid-Pliocene (3.3-3 Myr) 350-450 ppm with temperatures 1.9-3.6 °C higher than pre-industrial, and Early Excene (52-48 Myr) above 1000 ppm and temps + 9-14 °C pre-industrial), however, the rate at which it is increasing is far greater than previously seen. During the last deglaciation (the period we are now in and following glacial maximums), the highest rates of increase which occurred, only managed to increase 1-1.5 °C over 1,000 years (Masson-Delmotte et al. 2013).

When looking at CH_4, compared to the geological record over the last 800,000 years, it has fluctuated between 300-800 ppb depending on Milankovitch cycles (10,000 years), orbital insolation cycles (23,000 years) and in more recent years, from the development of rice agriculture and early human activities (Fuller and Castillo 2014; Dean et al. 2018). Since the industrial revolution however, such as with CO_2, this change has shown a dramatic increase driven by anthropogenic activities to over 1800 ppb (Dean et al. 2018). These influences arise from multiple activities including burning of fossil fuels, industry work and land use change, ultimately leading to consequences within our earth's system. One of the commonly known consequence, in terms of public general knowledge, is the heating of the planet via the CH_4 increase as stated above.

Butterfly Effect This warming can have detrimental effects leading to increased melting of the polar ice caps, in turn, supplying the ocean with vast amounts of freshwater. This can increase sea level as well as reducing the albedo effect, ultimately increasing global temperatures (Ciais et al. 2013). The implications are already showing; with sea level rise showing higher rates of change between 19^{th}-20^{th} century than the last two millennia (Masson-Delmotte et al. 2013). These effects have impacts both on marine life and the chemistry within our water systems as stated before. Ultimately, this leads to a vicious cycle that is difficult to extract ourselves from and may eventually lead to a new norm. This is especially so, as the human population increases along with the need for more resources leading to increased land use change, excess pollution and therefore GHG increase.

Outcomes and issues so far The atmospheric carbon budget has received increased global attention in recent years and has led to multiple reports, of which the most influential being the IPCC special reports and assessments. Along with this, there are almost yearly global carbon and methane budgets released (see most recent: Friedlingstein et al.

2019 and Saunois et al. 2019, respectively), both these reports and budgets focusing more on the scientific and political community. These have ultimately led to increased global knowledge and international agreements (such as the Paris agreement in 2016 operating under the UN Framework Convention on Climate Change (UNFCCC)), acknowledging the impact of society on the heating of the planet and implementing change. Multiple countries have since acknowledged the need to reduce CO_2 emissions in an attempt to keep the temperature of the planet down, reduce pollution and the further destructive implications. This has been managed more recently on a global scale, with one example being the UN Sustainable Development Goals. Over 170 countries have signed up and are attempting to adopt new ways to combat climate change, through sustainable energy development; protecting marine ecosystems from pollution and addressing ocean acidification, while attempting to stick with the Paris agreement of limiting global mean temperatures of increasing by 2 °C, aiming at 1.5 °C. This increase of knowledge has not just impacted policy makers and the scientific communities, but now has become a global phenomenon with 2019 seeing the rise of 'Fridays for Future' and multiple movements around the globe.

These scientific reports and assessments have led communities around the world to start taking action, however they have also made it very clear that there remains huge gaps in our overall knowledge and budgets regarding the carbon-cycle.

Quantifying data As the majority of the planet is covered in water, this is closely coupled the carbon cycle, as it is the link between the terrestrial land (soil and plants) subsequently leading to the ocean via surface waters. Yet quantifying the entire aquatic zone has shown some difficulties, leading to two further questions:

Where are the areas of interest?
Why have they been left unquantified for so long?

These questions can be answered by immediately focusing on the Land-Ocean Aquatic Continuum (LOAC). It comprises largely of areas with little to no data in regard to understanding the global carbon system. This can be mainly attributed to a number of factors including; remote and inaccessible sample locations, often laborious methods that require collection of water samples and subsequent analysis in the laboratory. This is further combined with a complex interplay of biological, physical and chemical processes. The lack of data for CO_2 within rivers, lakes and ultimately the mixing zone between them and the ocean, can be seen in figure 1.2. In the global carbon budgets (Friedlingstein et al. 2019), inland waters are joined together under terrestrial land CO_2 sinks or ocean sinks, not included as their own regions or incorporating the LOAC, presented in figure 1.2.

Estimations of the global inland CO_2 budget are between 0.8 - 2.1 Pg C y^{-1} depending on literature (Cole et al. 2007 or Raymond et al. 2013). Large ranges and multiple methods for data collection has led to discrepancies in scaling up. The carbon budget has an estimated 0.4 Gt C y^{-1} unaccounted for, coming from either over estimations in data or unaccounted for sinks (Friedlingstein et al. 2019).

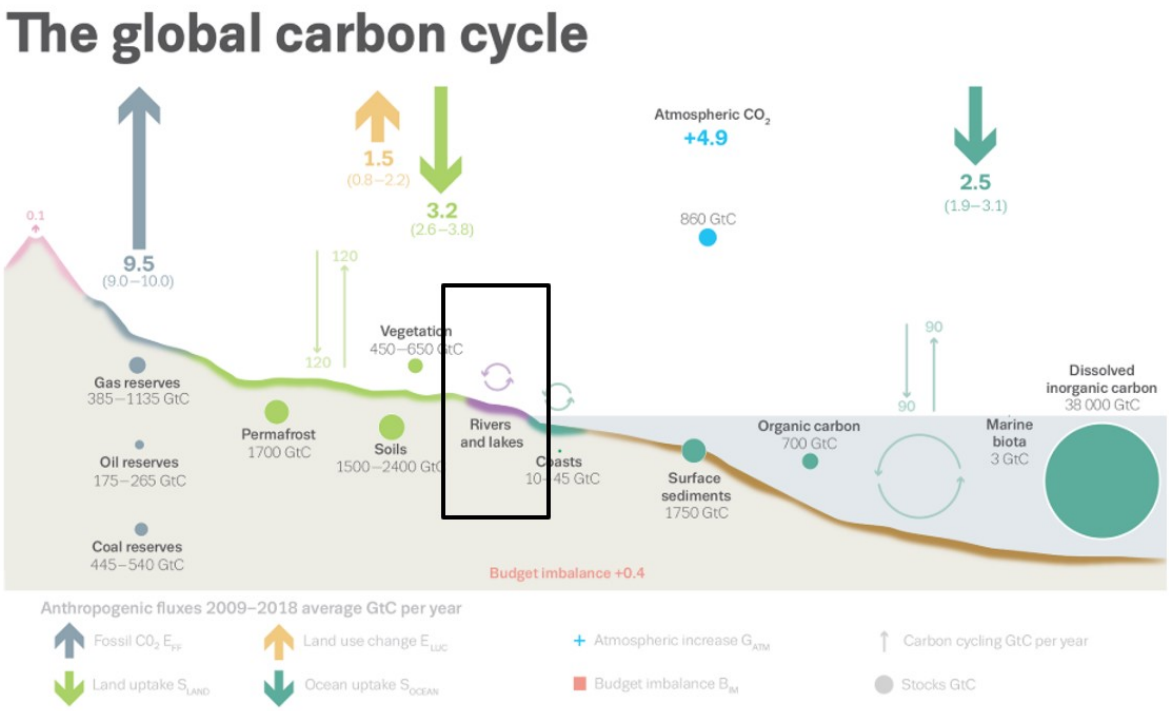

Figure 1.2: The most recent global carbon budget (Friedlingstein et al. 2019). All aspects described at the bottom, with all values in Gt C y^{-1}. Box indicating the area of interest and lack of quantified data.

In terms of human effects, anthropogenic perturbation has increased the amount of organic carbon exported from the terrestrial ecosystem to the aquatic system by 1.0 ± 0.5 Gt C y^{-1} (Regnier et al. 2013). This increase has multiple consequences throughout the LOAC, from increased storage to excess nutrients leading to eutrophication, potentially filling the gap to lost sinks. These regions are among the most sensitive to slight changes and therefore it is highly important to get a better combined picture from all important greenhouse gases to assess dynamics.

In terms of the global methane budget, Kirschke et al. (2013) and Saunois et al. (2016) suggested four main areas where there is significant lack of data or restraints that were needed. One of which was the high uncertainty in annual and decadal CH_4 emissions from natural sources (eg. wetlands and freshwater). Since then, work has been implemented by improving models and datasets, however there is still a need for more systematic measurements (Saunois et al. 2019). Although there has been progress to better quantify the CH_4 global budget, figure 1.3 shows clear discrepancies between methods of estimating the budgets which can be seen in 'other natural emissions' spanning from 222 to 37 Tg CH_4 y^{-1} (figure 1.3). This is due to the implementation of satellite data, and model variations from collect datasets.

These ranges seen in figure 1.3 are vast, especially in terms of all other categories within the budget. Due to multiple systems within the 'natural emissions', budgets get distorted whether it is bottom up or top down scaled. One of the reasons for this is that inland waters and the ocean, vary in biogeochemical processes, concentration ranges and the scale of complexity for each system.

For this reason, below is a description of the biogeochemical processes and concentrations ranges found for both oceanic and limnic systems, to fully grasp the differences between the regions.

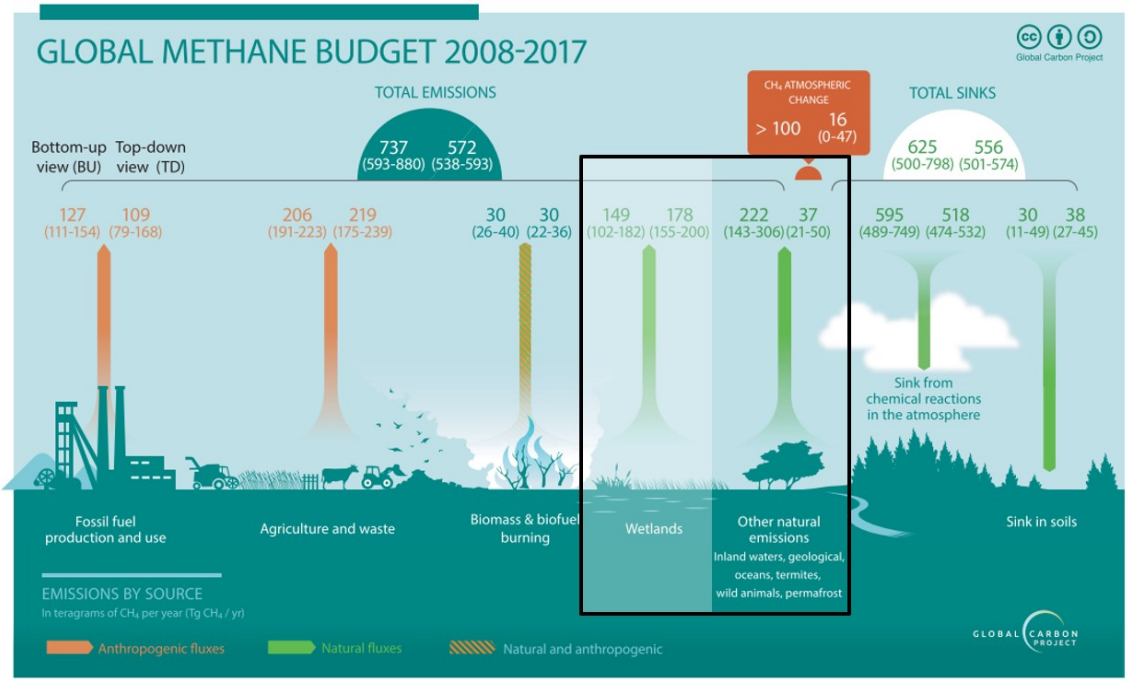

Figure 1.3: the global methane budget from the latest report (Saunois et al. 2019) showing bottom up and top down estimates. Box symbolizes are of which there is little to no data, such as with the global carbon budget (figure 1.2). The box is split into two: other natural emissions and wetlands. In this thesis we focus more on the natural wetlands (inland waters and ocean) however the region we work in is a wetland and so briefly touch on this.

Henry's Law

Henry's law states that 'at any given temperature, the amount of a given gas dissolved in a given type and volume of liquid is directly proportional to the partial pressure of that gas in equilibrium with that liquid'. It is the basis for and the reasoning behind taking measurements of surface concentrations in relation to our global understanding. Henry's law constant, i.e. the proportionality factor between gas partial pressure and dissolved gas concentration, is a gas-specific, temperature- and salinity-dependent property. For CO_2:

$$[CO_2] = K_H \cdot pCO_2 \tag{1.1}$$

Where K_H is Henry's law constant for CO_2 solubility in water (mol kg^{-1} atm^{-1}) with pCO_2 as the partial pressure of CO_2 (atm) in the gas phase in equilibrium with the liquid.

1.1.1 Aquatic CO_2 System

Aquatic CO_2 refers to CO_2 dissolved in water as well as carbonic acid and its dissociation products. It is governed by a suite of thermodynamic equations. In this thesis, I cover the full salinity gradient from freshwater to seawater, therefore the background within the carbon cycle is provided for both marine and limnic systems.

Dissolution of Carbon in Water

The aquatic CO_2 system is a major feature within all water bodies, regulating pH and controlling the concentration and hence air-water exchange of CO_2. It is governed by the following equilibria:

$$CO2(g) \rightleftharpoons CO2\,(aq) \tag{1.2}$$

$$CO2(aq) + H2O \rightleftharpoons H2CO3 \rightleftharpoons H^+ + HCO_3^- \tag{1.3}$$

$$HCO_3^- + H^+ \rightleftharpoons 2\,H^+ + CO_3^{2-} \tag{1.4}$$

Equation 1.2 represents the solubility of gaseous CO_2 in the water, which is described by Henry's law, where the Henry's law constant is typically referred to as KH (eq. 1.5). The dissolved $CO_2(aq)$ reacts with water forming carbonic acid (H_2CO_3), which is a moderately strong acid but only present in very small amounts relative to $CO_2(aq)$. Distinguishing between $CO_2(aq)$ and H_2CO_3 is analytically not possible. They are therefore lumped together to form the new species CO_2 (or H_2CO_3*) which is also referred to as carbonic acid, which is a weak acid.

$$KH=[CO2]/(pCO2) \tag{1.5}$$

$$K1=([HCO_3^-]\cdot[H^+])/([CO2]) \tag{1.6}$$

$$K2=[CO_3^{2-}][H^+]/([HCO_3^-]) \tag{1.7}$$

Equations 1.3 and 1.4 are the dissociation reactions of this carbonic acid which are characterized thermodynamically by the apparent dissociation constants for the first and second dissociation reaction of carbonic acid (K1 - eq. 1.6, K2, - eq. 1.7; in freshwater $10^{-6.35}$ and $10^{-10.3}$ at 25°C, Middelburg (2019)). Because of the highly non-ideal behavior of ionic species in the seawater matrix, thermodynamic constants in marine chemistry are typically expressed as stoichiometric constants, i.e. based on concentration rather than activities. This requires the activity constants to become part of the thermodynamic constant itself which renders this constant not only dependent on temperature but also on the composition of the salt matrix. The stoichiometric constants for seawater are therefore functions of temperature, salinity and pressure.

Parameters Determining Carbon System

Four main measurable quantities are available to analytically characterize the aquatic CO_2 system. One of these is dissolved CO_2, however, some authors refer to fugacity (fCO_2) instead of partial pressure (pCO_2). The difference between fugacity and partial pressure is similar to the difference between activity and concentration. Therefore, fugacity is the thermodynamically correct property to describe CO_2 solubility. However, as CO_2 in water behaves very nearly as an ideal gas, the difference between fCO_2 and pCO_2 is very small (on the order of 0.4%) and no distinction is made and pCO_2 is used instead of fCO_2. Therefore, pCO_2 is used throughout this work.

Following this, on top of pCO_2, the other three measurable quantities we focus on are, total alkalinity (TA), dissolved inorganic carbon (DIC) and pH. Each variable has a different use for extracting specific information about the aquatic CO_2 system. The main focus here is on pCO_2, which is the quantity that determines the equilibrium state for CO_2 between air and water and hence and any air-water CO_2 flux resulting from non-equilibrium conditions. TA is a measure of the water's acid binding capacity and is employed here for its strong conservative behavior in natural waters. Finally, we look at DIC, which is a book-keeping quantity for total dissolved inorganic carbon and as such can assist with identification of primary production and respiration dynamics both

in inland and ocean waters (Raymond et al. 2000; Fassbender et al. 2016; Bushinsky et al. 2019). pH is only touched on briefly and therefore shortly described below. With complete knowledge of all thermodynamic equations involved, only two of the four variables are needed to be measured to fully characterize the aquatic CO_2 system, such that the other two can be calculated using temperature and salinity (described further throughout the thesis). In the following, I provide a brief description of each of these four parameters.

CO_2 partial pressure (pCO_2) Partial pressure is a property only defined for a gas phase. When we refer to the pCO_2 of a water sample we in fact mean the pCO_2 of a gas phase that is in thermodynamic equilibrium according to Henry's law with this water sample. The definition of pCO_2 is thus the Henry's law expressed for CO_2 (eq. 1.5). According to Henry's law, if the water pCO_2 is below atmospheric pCO_2, the water will uptake CO_2, and vice versa. Therefore, knowing the dynamics of pCO_2 in the surface waters is vital to understand the exchange of CO_2 across the air-water-interface and the interactions between water and atmospheric pCO_2.

Total alkalinity (TA)

$$\begin{aligned} \mathrm{TA} = &[\mathrm{HCO_3^-}] + 2\,[\mathrm{CO_3^{2-}}] + \mathrm{B}[(\mathrm{OH})_4{}^-] + [\mathrm{OH^-}] + [\mathrm{HPO_4^{2-}}] \\ &+ 2\,[\mathrm{PO_4^{3-}}] + [\mathrm{H_3SiO_4^-}] + [\mathrm{NH_3}] + [\mathrm{HS^-}] - [\mathrm{H^+}]_\mathrm{F} \\ &- [\mathrm{HSO_4^-}] - [\mathrm{HF}] - [\mathrm{H_3PO_4}] \end{aligned} \tag{1.8}$$

Where $[H^+]_F$ refers the free concentration in the free pH-scale. In inland (natural) waters, TA includes contributions for inorganic bases and acids (at alkaline to neutral pH) (Williams et al. 2009; Hunt et al. 2011):

$$\begin{aligned} \mathrm{TA} = &[\mathrm{HCO_3^-}] + 2\,[\mathrm{CO_3^{2-}}] + \mathrm{B}[(\mathrm{OH})_4{}^-] + [\mathrm{OH^-}] + [\mathrm{HPO_4^{2-}}] \\ &+ 2\,[\mathrm{PO_4^{3-}}] + [\mathrm{H_3SiO_4^-}] + 2\,[\mathrm{H_2SiO_4^{2-}}] + [\mathrm{HS^-}] + 2\,[\mathrm{S^-}] \\ &+ [\mathrm{NH_3^+}] + [\mathrm{Org^-}] - [\mathrm{H^+}] - [\mathrm{H_3PO_4}] \end{aligned} \tag{1.9}$$

with the main difference from the ocean being Org^- which represents the organic acids. However, generally in inland waters, these are so small and combined with the absence of information about organic matter quality (e.g. for this thesis) it can be simplified:

$$\mathrm{TA} = [\mathrm{C_{TA}}] + [\mathrm{NC_{TA}}] + [\mathrm{OH^-}] - [\mathrm{H^+}] \tag{1.10}$$

Where $[C_{TA}]$ is the sum of carbonate and bicarbonate, and $[NC_{TA}]$ is the net contribution of non-carbonate species to TA (Hunt et al. 2011).

Total dissolved inorganic carbon (DIC) DIC is made up of several species: bicarbonate ion (HCO_3^-), carbonate ion (CO_3^{2-}) and dissolved CO_2 (sum of free CO_2(aq) and H_2CO_3). It is described as the mass balance of the carbon system:

$$\mathrm{DIC} = \mathrm{CO2} + \mathrm{HCO_3^-} + \mathrm{CO_3^{2-}} \tag{1.11}$$

The speciation of DIC as a function of pH can be seen in figure 1.4 which also shows the salinity effect on the carbonic acid dissociation constants as a slight shift to the left.

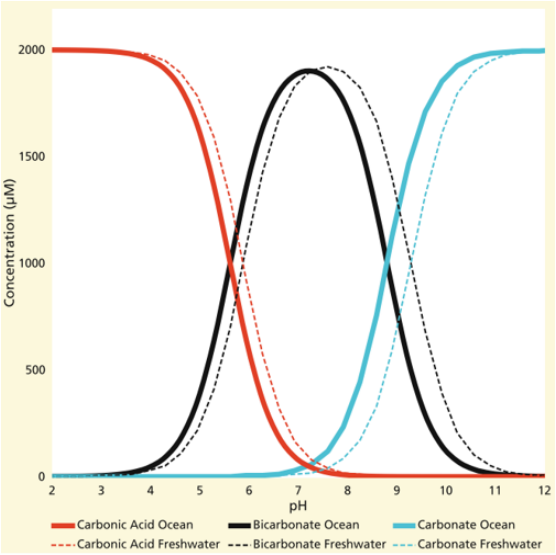

Figure 1.4: showing a Bjerrum plot of the DIC species within the ocean (solid lines) and inland waters (dashed lines), how they compare at DIC = 2000µM (Middelburg 2019).

pH value (pH) pH is the negative logarithm of the H^+ ion:

$$pH = -\log_{10}[H^+] \tag{1.12}$$

It is used to specify how basic or acidic the water is. Within most mineral-bearing waters the pH will be between 6-9 (Stumm and Morgan 1996). In recent years, the increased pCO_2 has led to an increased HCO_3^- , lowering pH and CO_3^{2-}, which ultimately has an effect on the ecosystem. The lower the pH, the more acidic the water becomes and over the past 15-30 years seawater pH has decreased by 0.0018 year, acidifying the ocean faster than before (Hönisch et al. 2012; Bates et al. 2014). To give an example, within the open ocean at roughly a pH of 8, around 86.5% will be HCO_3^-, 13% CO_3^{2-} and 0.5% dissolved CO_2 (figure 1.12 and Zeebe and Gladrow 2005). However, adding atmospheric CO_2 will increase HCO_3^- and H^+ concentrations, leading to lower CO_3^{2-} and pH (figure 1.12). Because of this process, over time there will be limitations on the oceans ability to absorb CO_2 form the atmosphere due the reduced CO_2 buffer capacity of the water, which is driven by the carbonate ion concentration.

Parameters closely linked

CH_4 CH_4, as described above is another significant GHG and of global significance. It is affected by the surrounding environments such as with CO_2. CH_4 is generally emitted via two paths within the ocean: via diffusive gas flux or ebullition, with inland waters also transported via macrophytes (Rejmánková. 2011). Most aquatic systems are over saturated in CH_4 from the ocean to inland waters, through microbial processes, such as archaeal methanogenesis. CH_4 is usually produced as the end product of organic matter degradation in anerobic conditions (Conrad 2009), however it is generally oxidized before reaching the surface of the water body (Boetius et al. 2000). The supersaturation of surface waters is found in all systems, and has been called the 'methane paradox' and has been under constant debate which is further described in section 6.

O_2 O_2 is produced via photosynthesis throughout the photic zone and consumed during respiration. This has a coupling effect with CO_2, and generally in a system governed by these two processes, the O_2 to CO_2 balance would roughly be 1:1 (explained further

in section 5). In both the oceans and inland waters you get a range of O_2, from anoxic (no O_2) to supersaturated in highly productive areas. In recent years however, the oceans have been of great interest due to ocean deoxygenation, where the combination of increased warming (therefore reduced solubility and enhanced stratification) and added anthropogenic nutrients fuelling primary production in the upper layers, are creating large oxygen minimum zones and hypoxic shelf systems (Stramma and Schmidtko. 2019).

1.1.2 Biogeochemical Processes

The Oceanic Carbon Cycle

Seawater CO_2 measurements have been long since conducted (beginning of the 19th century; Doney et al. (2009)). One reason for this continuing until present is due to our knowledge of the potential impact increased CO_2 can have on the oceans. Current estimates at 24% of anthropogenic CO_2 emissions being absorbed by the oceans (Friedlingstein et al. 2019). The majority of the ocean's sinks are within the deep ocean, with the surface being a relatively small carbon pool. However, this depends on region, upwelling potential, wind and other atmospheric conditions. One of the most dynamic, yet least measured parts of the ocean (when closely looking at the variability) is the Patagonian shelf in which two currents meet, bringing up nutrients and leading to high primary productivity. This reduces the amount of CO_2, making it highly variable within the ocean and focused on further in section 4.

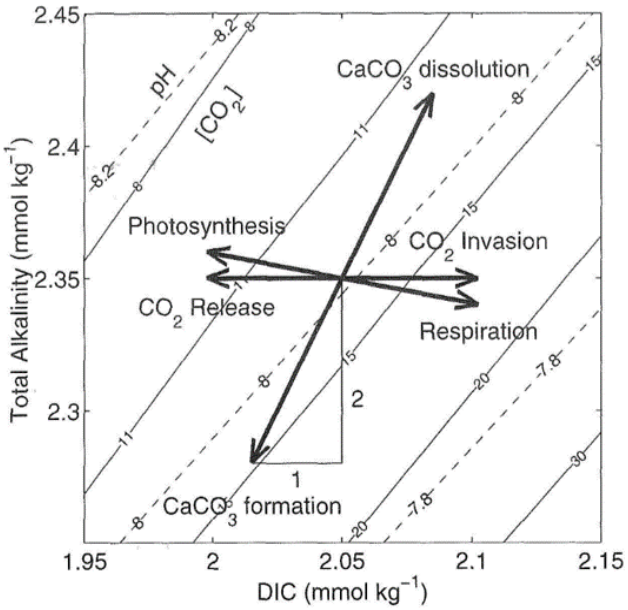

Figure 1.5: TA, DIC and CO_2 effects from different processes (arrows showing direction) within the ocean, the solid lines indicate CO_2 (µmol kg^{-1}) and pH as dashed lines, as a function of DIC and TA respectively (Zeebe and Wolf-Gladrow 2005).

Oceanic Carbonate System The main processes driving the carbonate system within the ocean include air-sea gas exchange and primary production and respiration as well as carbonate precipitation and dissolution. Figure 1.5 shows the relationship with TA, DIC, CO_2 concentration (solid lines) and pH (dashed lines). As CO_2 invades the ocean surface, DIC increases, pH will decrease (see section 1.1.1) but TA will stay the same because the charge balance doesn't change. TA is however affected by denitrification, sulfate reduction and $CaCO_3$ dissolution which all increase TA, whereas nitrification and sulfate reduction decrease it.

Photosynthesis and respiration influence the 4 parameters differently. During photosynthesis CO_2 is taken up and used, decreasing DIC and increasing pH, with slight increase in TA due to nutrient uptake (figure 1.5). The opposite is seen with respiration, as CO_2 is produced, it increases DIC and decreases pH and slightly decreases TA. Precipitation of $CaCO_3$ (figure 1.5 $CaCO_3$ formation) shows a ratio of 2:1 for TA and DIC due to as one mole of $CaCO_3$ is precipitated, one mole of double positively charged Ca^{2+} ions and one mole of carbonate are taken up. This process also slightly increases CO_2 and decreases pH. For dissolution however, it is the opposite with CO_2 decreasing and pH increasing, while both TA and DIC increase (as the same ratio).

CO_2 in seawater concentrations fluctuate depending on region, with each zone varying. However, TA is on average 2300 μmol kg^{-1} (Seelmann et al. 2019). DIC generally stays within a narrow range close to 2000 μM in surface waters within the ocean, although varies with salinity (Cole and Prairie 2014). pH is usually around 8.1, however, as stated before is consistently decreasing (Hönisch et al. 2012; Bates et al. 2014).

Oceanic CH_4 System Within the oceans, CH_4 is generally supersaturated, however the contribution to the overall global methane budget is extremely small at around 1-3 % and therefore, most efforts are focused more on continental CH_4 (Saunois et al. 2016). However, coastal and open ocean regions were observed to be sources with global fluxes estimated between 6-15 Tg CH_4 y^{-1} (Saunois et al. 2019), depending on the model used. The sources of marine CH_4 is under continuous debate but include production from marine sediments, emissions from destabilization of marine hydrates, geological marine seepage leaks and finally in situ production within the water column (Saunois et al. 2019). For brackish waters, CH_4 ranges vary from 3 to 7 Tg CH_4 $y^{-}1$ (Borges and Abril 2012; Laruelle et al. 2013) with a reported additional 4 Tg CH_4 y^{-1}, leading to numbers comparable to those of the ocean (Saunois et al. 2019).

The Limnic Carbon Cycle

Limnic Carbonate System Along with the same oceanic waters processes, inland water CO_2 and DIC concentrations also depend significantly on the freshwater system they are in and at which latitude. TA is affected far more greatly by processes compared to that of the ocean as it is closely linked with terrestrial and sedimentary influences, with little dilution (in comparison). In inland waters the photosynthetic assimilation of NH_4^+ and also NO_3^- causes an increase in TA, whereas the aerobic bacterial decomposition of biota to NO_3^- sees a decrease in TA (Stumm and Morgan 1996). The organic acids that may contribute to TA (eq. 1.8) are derived either via allochthonous or autochthonous processes, from photosynthesis in the water body or leached from plants and soils respectively (Hunt et al. 2011).

Ranges go from extremely low to extremely high ($<$ 45 ppm to 150,000 ppm CO_2 (ref)), in comparison to the ocean. Inland water TA is highly variably and tends to span large ranges of TA with low TA seen as $<$ 1000 μeq L^{-1} and high above 2000 μeq L^{-1}. DIC ranges from $<$20 μM to over 5000 μM when varying between acidic soft waters to harder alkaline waters, however most freshwaters stay within 100-1000 μM in surface waters (Cole and Prairie 2014). DIC is usually mainly consisting of HCO_3^-, however this can change in regions of low TA (soft waters), showing higher CO_2 and sometimes exceeding HCO_3^- (Cole and Prairie 2014). The speciation, however, is greatly influenced by the lithological nature of the surrounding regions as watersheds draining from rich carbonated rocky regions will have high pH, bicarbonate ions and therefore higher DIC and TA (Abril et al. 2015).

Limnic CH_4 System Like the ocean, inland waters are generally super saturated in terms of CH_4. Inland water CH_4 is generally produced within organic-matter rich, anoxic sediments within the floodplains or lakes. However, the majority of CH_4 (30-99%) produced within the aquatic system is oxidized to CO_2 through microbial CH_4 oxidation within the water column before reaching the atmosphere (Bastviken et al. 2008; Ward et al. 2017), such as with the ocean. However, given the shallower depths, ebullition and diffusive fluxes reach the surface faster and tend to have magnitudes higher concentrations (Saunois et al. 2019).

Most recent estimates and summaries show a range between 100-185 and 155-217 Tg CH_4 yr^{-1} (bottom up, top down respectively) for natural wetlands and for freshwaters between the years 2000-2009 at 117-212 Tg CH_4 yr^{-1} (Saunois et al. 2019).

Knowing some of the differences between the regions (oceanic and limnic), assists in to the understanding of how they may be combined (see following section).

Active and Passive Pipe

As mentioned before in 'Quantifying Data', the interface between the ocean and terrestrial regions within the carbon budget have been acknowledged as areas of little to no data (figures 1.2 and 1.3). These regions have had many attempts at classifying them in terms of the global budget. The transfer of carbon from land to the ocean, has been reported in the literature for decades (Meybeck 1982; Abril and Borges 2019), but had not been developed further partly due to no method being available to estimate fluxes across the land-ocean boundary directly. It was only first conceptualized by general assumptions in the literature during the 1970-1980's (Garrels and Mackenzie, 1971; Meybeck, 1982), creating the passive pipe theory (figure 1.6). This presented the carbon budget from inland to the ocean: from the flux calculated from inland outgassing (summed with burial in sediments) and the export of C to the coastal oceans. Since then, this interpretation has had many modifications, leading the 'active pipe' (Cole et al. 2007), where inland waters have been recognized to be far more complex than originally proposed. The most recent of which from Abril and Borges (2019) with the 'replumbed active pipe'. Within this 'replumed active pipe', there are still sections lacking of data both within inland waters and wetland regions (circles within figure 1.6), such as stated with both the global carbon and methane budgets (Friedlingstein et al. 2019; Saunois et al. 2019).

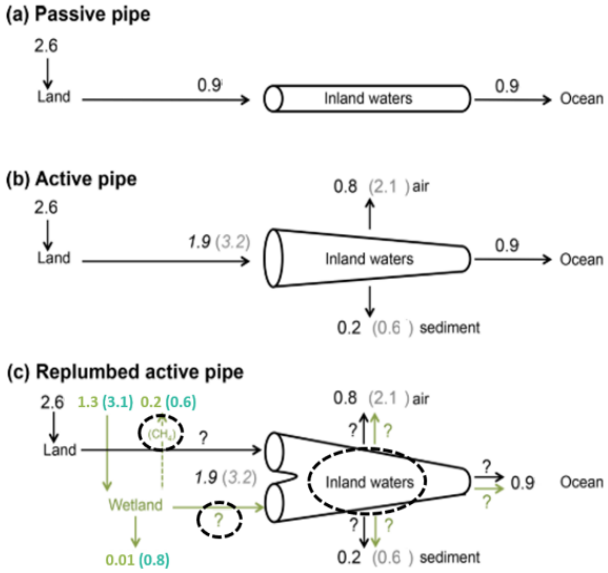

Figure 1.6: passive pipe evolution of inland water carbon to the ocean (PgC yr^{-1}) adapted from Abril and Borges (2019). It shows the evolution from the first 'pipe' to express the joining of the ocean and inland waters. Circles indicate areas in which we look at in this these

Major Differences

One of the main reasons behind this paucity of data stems from the differences between inland waters and the ocean. This can be classed into a few main sections: chemically (previously discussed and further throughout the thesis), environmentally such as surrounding regions leading to different biogeochemical processes (further discussed in sections 5 and 6), hydrologically and shorter time-scales on biochemical reactions (IPCC 2013) and finally methodologically. Although the final one does not originate from the natural environment, both limnologists and oceanographers have adapted their methodology to fit the surrounding environments. This difference inevitably leads to discrepancies and inconsistencies and is further discussed below.

1.1.3 Data Availability and the Problem of Under-sampling

Following on from 'Quantifying data', the replumed active pipe is a good example of where data is truly needed. This lack of data from inland waters, is shown from the database collection for surface water pCO_2 concentrations for the inland waters (Table 1.1). Although there are separate limnic databases for soils and specific regions (such as 'North Temperate Lakes'), up until 2014 (Hartmann et al. 2014) there was a lack of quality-controlled databases of measurements for inland rivers/water regimes. The 'Global database of methane concentrations and atmospheric fluxes for streams and rivers' is acquired data up until 2015 of concentrations, fluxes and other variables of all existing data found at the time.

GloRiCh (Hartmann et al. 2014) started in 2014, although it wasn't until 2019 when it was the first year it was published online. There are other databases focusing either on lakes or soils, but do not contain specific aquatic CO_2 measurements. The majority databases presented are for surface or oceanic waters. As the oceans have been under thorough observation for decades, this had led to multiple quality controlled checked databases. However, even with these databases, there is still a great paucity of CH_4 in both the ocean and inland waters.

Databases	**Region**	**CO_2/CH_4**
Surface ocean CO_2 atlas **(SOCAT)**	Ocean	CO_2
Integrated carbon observing system ocean thematic centre **(OTC)**	Surface	CO_2
Global surface pCO_2 **(LDEO)** database v2018	Surface	CO_2
Global ocean acidification observing network **(GOA-ON)** data portal	Ocean	CO_2
WMO-IOC joint technical commission for and marine meteorology **(JCOMM)**	Ocean	CO_2
GloRiCh global river chemistry database	Limnic - Rivers	CO_2
Global database of methane concentrations and atmospheric fluxes for streams and rivers *	Limnic (streams and rivers)	CH_4

* https://lter.limnology.wisc.edu/dataset/global-database-methane-concentrations-and-atmospheric-fluxes-streams-and-rivers

Table 1.1: The main global CO_2 databases for oceanic and limnic waters. Stating the region measured and if they record CO_2 or CH_4 or both.

1.1.4 Sensor Technologies

Sensor technologies also correlate with the lack of quality checked databases for limnic regions. Historically most sensor technologies are developed for ocean deployment, which is why there is a larger selection of oceanic databases with CO_2 information. Oceanic sensors have been developed over many years with an aim to have an accuracy of $\pm$ 2 μatm (Pierrot et al. 2009), to measure oceanic acidification over longer time scales. Whereas in inland waters, there was no specific quality assurance taken on a global level, until recently (see GloRiCh above). Table 1.2 shows some of the more recently available sensors for oceanic and inland water pCO_2 sensors, some of which have been utilized outside of their designed specification range.

Sensor Table

Main Operational Region	**CO_2 / CH_4**	**Author ***	**Company/ Name ****	**Accuracy(^{A}) or/ precision(^{p}) *****
Ocean	CO_2	Fietzek et al. (2014)	CONTROS HydroC CO_2 FT (see section 4)	$^{Offset \pm P}$ -0.6 ± 3.0 μatm
Ocean	CH_4	KMCON Manual	CONTROS HydroC CH_4 FT (see section 4)	^{A} ± 2 μatm or 3 % of reading
Ocean	CO_2	Pro-Oceanus data sheet	Pro-Oceanus, CO_2 -Pro (Pro-Oceanus Nova Scotia, Canada)	^{A} 0.50%
Ocean	CO_2 + CH_4	Picarro data sheet	Picarro G2401 CRDS	^{P} 10 – 50 ppb CO_2 0.3 – 1 ppb CH_4
Ocean	CO_2	Arruda et al. (2019)	OceanPack (SubCTech GmbH, Kiel, Germany)	^{A} <1.5%
Ocean	CO_2	Arruda et al. (2019)	GO-8050 (General Oceanics, Miami, U.S.)	^{A} ± 2 μatm
Ocean	CO_2	Clarke et al. (2017)	pCO_2 optode	^{P} 9.5 ± 9.5 μatm ^{A} ± 10μatm
Ocean	CO_2	Sutton et al. (2015)	Moored Autonomous pCO_2 ($MAPCO_2$)	^{uncertainty} < 2 μatm
Ocean	CO_2	Alliance for Coastal Technologies (ACT). (2010b)	Mini-Pro CO_2, Pro-Oceanus (See above)	^{A} + 9 ± 14 μatm
Ocean	CO_2	Alliance for Coastal Technologies (ACT). (2010a)	Sunburst, SAMI-CO_2	^{P} <1 μatm
Limnic	CO_2 + CH_4	Kotiaho (1996) Brennwald et al. (2016)	MIMS + ^{Mod} 'miniRuedi'	^{analyticaluncertainty} 1 – 3%
Limnic	CO_2	Hunt et al. (2017)	^{Mod}SIPCO_2	$^{A+P}$ 29 ± 6 μatm
Limnic	CO_2 + CH_4	www.lgrinc.com data sheet: LGR-ICO^{TM} MCEA1-911/915/927 + Cawford et al (2014)	Los Gatos (UGGA) (multiple types) ^{Mod}for CO_2: Fast Limnology Automated Measurement (FLAMe)	^{P} 0.02 – 0.4 ppm CO_2 0.03 – 3 ppb CH_4

Sensor Table Continued...

Main Operational Region	CO_2 / CH_4	Author *	Company/ Name **	Accuracy(^{A}) or/ precision(^{p}) ***
Limnic	CO_2	Vaisala Oyj. (2008); Johnson et al. (2010); Bastviken et al. (2015); Yoon et al. (2016)	^{Mod} Vaisala CARBOCAP® Carbon Dioxide Transmitter Series, GMT220	^{A} ± 1.5% of range + 2% of reading
Limnic	CO_2	Duvert et al. (2019) & https://eosense.com data sheet	eosGP, Eosense Inc., Canada	^{A} 1 % range + 1 % reading
Limnic	CO_2	Blackstock et al. (2019)	^{Mod} CO_2-LAMP (2 sensors)	^{A} sensor 1: ± 30 ppmv (± 3%) sensor 2: ± 300 ppmv (± 3 %)
Limnic	CO_2	Souza et al. (2019)	Csense, Turner Designs	^{A} 3 % of full scale
Limnic	CO_2	Alliance for Coastal Technologies (ACT). (2010a)	Sunburst SAMI- CO_2	$^P < 1$ μatm

***** where information was found or reference focusing on specific sensor.
****** ^{Mod} for modified set-up
******* some not specified which, ^{A} for accuracy, ^{P} for precision, some as uncertainty or offset, depending on how it is reported

Table 1.2: Some of the latest CO_2 and CH_4 sensor availability, either through companies or modified for specific needs and regions (oceanic or limnic).

High-accuracy, oceanic pCO_2 measuring systems have been established for decades (Körtzinger et al. 1996; Dickson et al. 2007; Pierrot et al. 2009) leading to well established global CO_2 databases (see table 1.1). Over the years these sea surface underway measurements of pCO_2 have dramatically increased, allowing for more in-depth analysis of the marine carbon cycle, especially within the coastal oceans (see examples Laruelle et al. 2010, Chen et al. 2013 and Bai et al. 2015). They have seen rapid development and extensive application on mobile and stationary platforms, research vessels, voluntary observing ships (VOS) and moorings (Byrne et al. 2010; Fietzek et al. 2011; Fiedler et al. 2013; Fietzek et al. 2014). Due to the size of the ocean, advancements on spatiotemporal data has been vastly improved by projects such as Argo or wave gliders (or equivalent) which have increased this resolution (Roemmich et al. 2009). This range of both platforms and sensors is mainly driven by the size and depth of the ocean, allowing for all types (large and small) of developments. From these developments, some have been adapted for limnic regions, however there tends to be little standardization in terms of accuracy, quality control and little work on inter-comparison between them. This lack of standardization is usually a result of vastly differing environments that inland water sensors would have to be exposed to, e.g. from high to low altitudes and swamps to lakes. On top of this, to collect spatiotemporal data from most inland locations, sensors would have to be portable and specific enough to adapt to a variety of vessels far smaller than compared to that of the ocean.

Showing the adaptation of sensors, table 1.2 presents a clear overlap with certain ocean specific sensors (e.g. Sunburst SAMI- CO_2) being used across the boundaries. However, even with the mixing of oceanic and limnic sensors, there is still very little focus on CH_4 sensor technologies, as with the databases, in both oceanic and limnic regions.

Sensors to measure pCO_2, generally use one of four main types of equilibrators: spray-type, marble-type, membrane-enclosed and manual head-spacing equilibrator. The most common are spray and marble-type equilibrators (Yoon et al. 2016), with spray-type equilibrators used across all water bodies and a standard for oceanic pCO_2 (Takahashi 1961; Dickson et al. 2007; Pierrot et al. 2009; Yoon et al. 2016). Marble-type equilibrators are more inland water based, for regions of high sediment loading, dynamic and high organic matter (Frankignoulle et al. 2001; Abril et al. 2006). Equilibration devices are a major difference between all regions, having a substantial effect on response time of the sensor, therefore failure to correct for this can have implications on the accuracy of the data (Webb et al. 2016).

However, in inland waters have extreme environmental differences to the ocean; highly particulate water columns, increased amounts of biological activity, inaccessibility and the extreme variability in concentrations, sensors are harder to develop for concise and accurate measurements. They must be easier to access and transport, and if left out autonomously allow for the risk of environmental impacts or being stolen. Therefore, a lot of studies have started using multiple sensors together, or air measuring sensors (see table 1.2) for inland waters (e.g. MIMS and FLAMe). They have to be relatively cheap (compared to oceanic equipment of up to \$100,000 + e.g. Los Gatos) for these reasons stated above. In situ stationary measurements within rivers and lakes, have also seen the increase use of EXO probes (YSI Inc. Yellow Springs, USA), which measure a range of parameters from dissolved O_2, pH and specific conductivity to nitrate, turbidity and chlorophyll. Generally, however, limnologists tend to adapt sensors to make them more efficient within the regions they need (see Crawford et al. 2014, Hunt et al. 2017 and Horgby et al. 2019 for CO_2 lake mapping, flux chambers and alpine stream adaptions).

Another collection methods is through remote sensing for pCO_2 and other gases in inland waters. Since the 1970/80s using LANDSAT data for primary production (Strong 1978; Platt and Sathyendranath 1988) and has since been used globally for CH_4 concentrations (Melack et al. 2004; Palmer et al. 2015). Both lead to increased errors, therefore having a system that does not need attending to (with calibration gases), easy to deploy, sturdy and stable but not too expensive is optimum for inland waters. A more desirable outcome is direct continuous measurements of pCO_2 and pCH_4 across the full LOAC. This would shed light on the two gases source and sink locations, the spatiotemporal concentration variability and provide an insight in understanding the biogeochemical processes and driving factors.

Motivation of intensified data collection across LOAC From the above, it is easy to understand the need for more regulated, accurate, and high-spatial data from inland and mixing regime waters for CO_2 and CH_4 concentrations. However, although the oceans are more regulated, the same data type is still needed. As stated before, in the ocean there is a goal of having an accuracy of $\pm$ 2 μatm for all ocean surface pCO_2 measurements so that the 'climate goal' can be achieved, giving a potential estimation of regional fluxes to an accuracy of 0.2 PgC yr^{-1} (Arruda et al. 2019; Wanninkhof et al. 2019). Yet, there is still a need for ocean waters to have optimized long-term continuous observations to monitor the carbon sink at adequate spatial and temporal resolution, as well as a need for targeted studies that address longer term and inter-annual variability (Peters et al. 2017). The same is needed for CH_4, with CH_4 sensors are still in their relatively early stages of development (compared to that of CO_2, see table 1.2).

Generally in inland waters, with many studies using adaptations of smaller sensors (Bastviken et al. 2015), there is need to fill regions with high-resolution data to look deeper into the dynamics within these systems and to look across the regions. Therefore, combining the two water bodies and looking spatiotemporally into biogeochemical cycles

is important for our understanding of how these systems work in relation to each other. A unified method of measuring underway has still not been perfected due to; large diel variations, steep horizontal and vertical concentration and temperature gradients, hard to reach areas and potential lack of adequate power and other resources within the inland waters. Therefore, the goal of this research is to, develop the ability to measure multiple gases continuously and accurately throughout the whole LOAC, in a universal way, ensuring as little human and technological error as possible.

However, for this to be fully implemented, important corrections of the sensor had to be clearly defined. Below are some of the corrections implemented or further discussed. Full in-depth corrections for all cruises can be found in section 4 and how some of the numbers were defined (for the response time correction) can be found in section 3.

Data processing and corrections Sensor processing and corrections are of absolute importance for both inland and oceanic waters. Extensive processing will be described in sections 3 and 4, here further corrections applicable to just the work done in this thesis are described. We have chosen to use the CONTROS HydroC® for multiple reasons, mainly due to their sensors needing no calibration gases, easy to transport, little power needed and on the lower range of oceanic sensor costs (yet with high accuracy). Therefore fitting the previous requirements already stated that is needed. The set-up consisted of the CONTROS HydroC® CO_2 FT (carbon dioxide partial pressure, pCO_2, HC-CO_2: Kongsberg Maritime Contros GmbH, Kiel, Germany (KMCON)), CONTROS HydroC® CH_4 FT (CH_4 partial pressure, pCH_4, HC-CH_4: KMCON), HydroFlash® O_2 (dissolved oxygen, O_2, KMCON) and a SBE 45 thermosalinograph (Sea-Bird Electronics, Bellevue, USA).

HC-CO_2 data processing As extended processing details can be found in section 4 and also in (Fietzek et al. 2014) here the main are just stated. One of the main corrections were for sensor drift from regular zeroing and flushing and on the bases of the pre- and post-deployment calibrations. Following this, temperature corrections (see below, also for HC-CH_4), extended calibrations for the limnic regions over 6,000 ppm (see below) and response time (RT: see below, also for HC-CH_4) were also corrected for.

Gas matrix effects A correction that is noted but not corrected for is the gas matrix effect. NDIR-based measurements of CO_2 in air have been shown to be affected by deviations of the gas matrix from the composition of standard air (e.g., Burch et al. 1962; Griffith 1982; Welles and McDermitt 2005) due to differences in pressure broadening. In surface water applications, such deviations are mostly due to deviations of the dissolved oxygen concentration from saturation with atmospheric oxygen levels. While this effect somewhat depends on the exact type of NDIR system, we used published information to estimate at $<+0.2$ % error in CO_2 per +1 % deviation of O_2 from saturation. For Romania, with median O_2 levels of 94 % ($\pm$ 10%, 25 and 75 percentiles), this translates to an underestimation of CO_2 by -0.7 % ($\pm$ 1.8%, 25 and 75 percentiles). Only in extreme situations (i.e., min./max O_2 saturation levels of up to 4%/125%) the effects become more significant (+4%/-17%). This only occurred for each limnic cruise over a maximum distance of $\sim$ 14.17 km, with the entire transect of $\sim$ 408 km. Note that due to a lack of a more quantitative characterization of the specific NDIR detectors used in HC-CO_2, no correction for the pressure broadening effect of the non-absorbing matrix gases was made to the data presented here as it far exceeds the aspect of this thesis.

Extended calibration In inland waters, an extended calibration was conducted proceeding the campaigns due to ranges found outside the manufacturer's calibration limits.

Due to the non-linearity of NDIR detectors, xCO_2 was calculated using the flow ratios of N_2 and CO_2 within laboratory conditions, over the upper range of the calibration limits ($>$ 6,000 ppm). These corrections are further explained in detail in section 4.

Response time correction For the HC-CO_2 and HC-CH_4, response time (RT) had to be corrected, which was one of the most important corrections for extracting high-spatial variability. Within the limnic regions, a time lag correction was applied following the derived e-folding time (dependent on flow and temperature, see section 3 and 4) which was then corrected following Fiedler et al. (2013). The same was done for the HC-CO_2 in the ocean and brackish, however the e-folding time was derived from the flush signal following the internal zeroing procedure.

Time lag correction Due to the sensors having a flow through set up, there was some time delay that had to be accounted for. From the speed of the water and the known length of the tubing, this was corrected for on most of the cruises (excluding the brackish cruise due to unknown length to water source). Further details are in section 3.

Temperature correction As the water travels from in situ to equilibrium where it is measured, through the passing of the tubes. Due to the dependence of temperature on both CO_2 and CH_4, yet different to one another, a correction for either the warming or cooling of the water had to be considered. It was chosen to follow Takahashi et al. (1993) temperature correction following experimental comparisons between discrete samples and sensor data and literature searches. This correction proved to be most applicable with the data. Further details are in section 4.

Specific O_2 optode sensor corrections Further post processing was conducted for the final limnic campaign (not described in section 4 due to being specific for just one campaign), for data quality insurance due to re-instalment of the optical unit following the initial set-up. This was done using the calibration coefficients and a modified Steinhart-Hart equation (Steinhart and Hart 1968) to correct the temperature:

$$\begin{aligned} T = \mathrm{A} + \mathrm{B} \cdot \ln(\mathrm{adcValue}/\mathrm{RN}) + \mathrm{C} \cdot \ln(\mathrm{adcValue}/\mathrm{RN})^2 \\ + \mathrm{D} \cdot \ln(\mathrm{adcValue}/\mathrm{RN})^3 \end{aligned} \tag{1.13}$$

T is the corrected temperature
adcValue = SampleR/1000
SampleR = Resistor Temperature (°C)
RN = 1000

The O_2 data was then corrected using the Uchida square mode, adapted from Uchida et al. (2008):

$$\mathrm{P}_0 = 1 - \mathrm{D}_0 \cdot \mathrm{T} \tag{1.14}$$

$$\mathrm{P}_c = \mathrm{D}_1 + \mathrm{D}_2 \cdot \mathrm{P}_r + \mathrm{D}_3 \cdot (\mathrm{P}_r)^2 \tag{1.15}$$

$$K_sv = C_0 + C_1 \cdot T + C_2 \cdot (t)^2 \tag{1.16}$$

$$[O2]=(((P0/Pc)-1))/\,K_sv \tag{1.17}$$

where P_r is the raw phase shift (Dphi), T is temperature in °C and D_X and C_X ($_X$=0,1...3) are the calibration coefficients.

1.2 References

Abril, G., and A. V. Borges. 2019. Carbon leaks from flooded land: do we need to replumb the inland water active pipe? Biogeosciences 769–784. doi:10.5194/bg-2018-239

Abril, G., S. Bouillon, F. Darchambeau, and others. 2015. Technical note: Large overestimation of pCO_2 calculated from pH and alkalinity in acidic, organic-rich freshwaters. Biogeosciences 12: 67–78. doi:10.5194/bg-12-67-2015

Abril, G., S. Richard, and F. Guérin. 2006. In situ measurements of dissolved gases (CO_2 and CH_4) in a wide range of concentrations in a tropical reservoir using an equilibrator. Sci. Total Environ. 354: 246–251. doi:10.1016/j.scitotenv.2004.12.051

Alliance for Coastal Technologies (ACT). 2010a. Performance Demonstration Statement for Sunburst Sensors SAMI-CO_2, ACT DS10-04 UMCES/CBL 10-094.

Alliance for Coastal Technologies (ACT). 2010b. Performance Demonstration Statement for Pro-Oceanus Systems Inc. PSI CO_2-ProTM, ACT DS10-03 UMCES/CBL 10-093.

Arruda, R., D. Atamanchuk, M. Cronin, T. Steinhoff, and D. W. R. Wallace. 2019. At-sea intercomparison of three underway pCO_2 systems. Limnol. Oceanogr. Methods 1. doi:10.1002/lom3.10346

Bai, Y., W.-J. Cai, X. He, W. Zhai, D. Pan, M. Dai, and P. Yu. 2015. A mechanistic semi-analytical method for remotely sensing sea surface pCO_2 in river-dominated coastal oceans: A case study from the East China Sea. J. Geophys. Res. Ocean. 120: 2331–2349. doi:10.1002/2014JC010632

Bastviken, D., J. J. Cole, M. L. Pace, and M. C. Van de-Bogert. 2008. Fates of methane from different lake habitats: Connecting whole-lake budgets and CH_4 emissions. J. Geophys. Res. Biogeosciences 113: 1–13. doi:10.1029/2007JG000608

Bastviken, D., I. Sundgren, S. Natchimuthu, H. Reyier, and M. Gälfalk. 2015. Technical Note: Cost-efficient approaches to measure carbon dioxide (CO_2) fluxes and concentrations in terrestrial and aquatic environments using mini loggers. Biogeosciences 12: 3849–3859. doi:10.5194/bg-12-3849-2015

Bates, N. R., Y. M. Astor, M. J. Church, and others. 2014. A time-series view of changing surface ocean chemistry due to ocean uptake of anthropogenic CO_2 and ocean acidification. Oceanography 27: 126–141. doi:10.5670/oceanog.2014.16

Blackstock, J. M., M. D. Covington, M. Perne, and J. M. Myre. 2019. Monitoring Atmospheric, Soil, and Dissolved CO_2 Using a Low-Cost, Arduino Monitoring Platform (CO_2-LAMP): Theory, Fabrication, and Operation. Front. Earth Sci. 7: 1–19. doi:10.3389/feart.2019.00313

Borges, A. V, and G. Abril. 2012. Carbon Dioxide and Methane Dynamics in Estuaries.

Brennwald, M. S., M. Schmidt, J. Oser, and R. Kipfer. 2016. A Portable and Autonomous Mass Spectrometric System for On-Site Environmental Gas Analysis. Environ. Sci. Technol. 50: 13455–13463. doi:10.1021/acs.est.6b03669

Burch, D. E., E. B. Singleton, and D. Williams. 1962. Absorption line broadening in infrared. Appl. Opt. 1: 359–363.

Bushinsky, S. M., Y. Takeshita, and N. L. Williams. 2019. Observing Changes in Ocean Carbonate Chemistry: Our Autonomous Future. Curr. Clim. Chang. Reports 5: 207–220. doi:10.1007/s40641-019-00129-8

Byrne, R. H., M. D. DeGrandpre, R. T. Short, and others. 2010. Sensors and Systems for in situ Observations of Marine Carbon Dioxide System Variables. Proc. Ocean. Sustain. Ocean Obs. Inf. Soc. 1. doi:10.5270/OceanObs09.cwp.13

Chen, C. T. A., T. H. Huang, Y. C. Chen, Y. Bai, X. He, and Y. Kang. 2013. Air-sea exchanges of coin the world's coastal seas. Biogeosciences 10: 6509–6544. doi:10.5194/bg-10-6509-2013

Ciais, P., C. Sabine, G. Bala, and others. 2013. The physical science basis. Contribution of working group I to the fifth assessment report of the intergovernmental panel on climate change. Chang. IPCC Clim. 465–570. doi:10.1017/CBO9781107415324.015

Clarke, J. S., E. P. Achterberg, D. P. Connelly, U. Schuster, and M. Mowlem. 2017. Developments in marine pCO_2 measurement technology; towards sustained in situ observations. TrAC - Trends Anal. Chem. 88: 53–61. doi:10.1016/j.trac.2016.12.008

Cole, J. J., and Y. T. Prairie. 2014. Dissolved CO_2 in Freshwater Systems. Ref. Modul. Earth Syst. Environ. Sci. doi:10.1016/b978-0-12-409548-9.09399-4

Cole, J. J., Y. T. Prairie, N. F. Caraco, and others. 2007. Plumbing the Global Carbon Cycle: Integrating Inland Waters into the Terrestrial Carbon Budget. Ecosystems 10: 172–185. doi:10.1007/s10021-006-9013-8

Crawford, J. T., L. C. Loken, N. J. Casson, C. Smith, A. G. Stone, and L. A. Winslow. 2014. High-speed limnology: Using advanced sensors to investigate spatial variability in biogeochemistry and hydrology. Environ. Sci. Technol. 49: 442–450. doi:10.1021/es504773x

Dean, J. F., J. J. Middelburg, T. Röckmann, and others. 2018. Methane Feedbacks to the Global Climate System in a Warmer World. Rev. Geophys. 56: 207–250. doi:10.1002/2017RG000559

Dickson, A. G. 1981. An exact definition of total alkalinity and a procedure for the estimation of alkalinity and total inorganic carbon from titration data. Deep Sea Res. Part A, Oceanogr. Res. Pap. 28: 609–623. doi:10.1016/0198-0149(81)90121-7

Dickson, A. G., C. L. Sabine, and J. R. Christian. 2007. Guide to Best Practices for Ocean CO_2 Measurements, PICES Special Publication.

Doney, S. C., V. J. Fabry, R. A. Feely, and J. A. Kleypas. 2009. Ocean Acidification: The Other CO_2 Problem. Ann. Rev. Mar. Sci. 1: 169–192. doi:10.1146/annurev.marine.010908.163834

Duvert, C., M. Bossa, K. J. Tyler, J. G. Wynn, N. C. Munksgaard, M. I. Bird, S. A. Setterfield, and L. B. Hutley. 2019. Groundwater-Derived DIC and Carbonate Buffering Enhance Fluvial CO_2 Evasion in Two Australian Tropical Rivers. J. Geophys. Res. Biogeosciences 124: 312–327. doi:10.1029/ 2018JG004912

Fassbender, A. J., C. L. Sabine, and M. F. Cronin. 2016. Global Biogeochemical Cycles Mooring measurements. 250–267. doi:10.1002/2015GB005205.Received

Fiedler, B., P. Fietzek, N. Vieira, P. Silva, H. C. Bittig, and A. Körtzinger. 2013. In situ CO_2 and O_2 measurements on a profiling float. J. Atmos. Ocean. Technol. 30: 112–126. doi:10.1175/JTECH-D-12-00043.1

Fietzek, P., B. Fiedler, T. Steinhoff, and A. Körtzinger. 2014. In situ quality assessment of a novel underwater pCO_2 sensor based on membrane equilibration and NDIR spectrometry. J. Atmos. Ocean. Technol. 31: 181–196. doi:10.1175/JTECH-D-13-00083.1

Fietzek, P., S. Kramer, and D. Esser. 2011. Deployments of the HydroCTM

(CO_2/CH_4) on stationary and mobile platforms - Merging trends in the field of platform and sensor development. Ocean. Mts/Ieee Kona 1–9. doi:10.23919/OCEANS.2011.6107129

Frankignoulle, M., A. Borges, and R. Biondo. 2001. A new design of equilibrator to monitor carbon dioxide in highly dynamic and turbid environments. Water Res. 35: 1344–1347. doi:10.1016/S0043-1354(00)00369-9

Friedlingstein, P., M. W. Jones, M. O'Sullivan, and others. 2019. Global Carbon Budget 2019. Earth Syst. Sci. Data 1783–1838. doi:10.5194/essd-11-1783-2019

Fuller, D. Q., and C. Castillo. 2014. Rice: Origins and Development. Encycl. Glob. Archaeol. 6339–6343. doi:10.1007/978-1-4419-0465-22185

Griffith, D. W. T. 1982. Calculations of carrier gas effects in non-dispersive infrared analyzers. I. Theory. Tellus 34: 376–384.

Hartmann, J., R. Lauerwald, and N. Moosdorf. 2014. A Brief Overview of the GLObal RIver Chemistry Database, GLORICH. Procedia Earth Planet. Sci. 10: 23–27. doi:10.1016/j. proeps.2014.08.005

Hmiel, B., V. V Petrenko, M. N. Dyonisius, and others. 2020. anthropogenic fossil CH_4 emissions. Nature 578: 10–14. doi:10.1038/s41586-020-1991-8

Hönisch, B., A. Ridgwell, D. N. Schmidt, and others. 2012. The geological record of ocean acidification. Science (6072). 335: 1058–1063. doi:10.1126/science.1208277

Horgby, Å., P. L. Segatto, E. Bertuzzo, R. Lauerwald, B. Lehner, A. J. Ulseth, T. W. Vennemann, and T. J. Battin. 2019. Unexpected large evasion fluxes of carbon dioxide from turbulent streams draining the world's mountains. Nat. Commun. 10. doi:10.1038/s41467-019-12905-z

Hunt, C. W., J. E. Salisbury, and D. Vandemark. 2011. Contribution of non-carbonate anions to total alkalinity and overestimation of pCO_2 in New England and New Brunswick rivers. Biogeosciences 8: 3069–3076. doi:10.5194/bg-8-3069-2011

Hunt, C. W., L. Snyder, J. E. Salisbury, D. Vandemark, and W. H. McDowell. 2017. SIPCO_2: A simple, inexpensive surface water pCO_2 sensor. Limnol. Oceanogr. Methods 15: 291–301. doi:10.1002/lom3.10157

Johnson, M. S., M. F. Billett, K. J. Dinsmore, M. Wallin, K. E. Dyson, and R. S. Jassal. 2010. Direct and continuous measurement of dissolved carbon dioxide in freshwater aquatic systems—method and. Ecohydrology 3: 68–78. doi:10.1002/eco.95

Keeling, C. D. 1960. The Concentration and Isotopic Abundances of Carbon Dioxide in the Atmosphere. Tellus 12: 200–203. doi:10.3402/tellusa.v12i2.9366

Kirschke, S., P. Bousquet, P. Ciais, and others. 2013. Three decades of global methane sources and sinks. Nat. Geosci. 6: 813–823. doi:10.1038/ngeo1955

Körtzinger, A., H. Thomas, B. Schneider, N. Gronau, L. Mintrop, and J. C. Duinker. 1996. At-sea intercomparison of two newly designed underway pCO_2 systems - Encouraging results. Mar. Chem. 52: 133–145. doi:10.1016/0304-4203(95)00083-6

Kotiaho, T. 1996. On-site environmental and in situ process analysis by mass spectrometry. J. Mass Spectrom. 31: 1–15. doi:10.1002/(SICI)1096-9888(199601)31:1<1::AID-JMS295>3.0.CO;2-J

Laruelle, G. G., H. H. Dürr, R. Lauerwald, J. Hartmann, C. P. Slomp, N. Goossens, and P. A. G. Regnier. 2013. Global multi-scale segmentation of continental and coastal waters from the watersheds to the continental margins. Hydrol. Earth Syst. Sci. 17: 2029–2051. doi:10.5194/hess-17-2029-2013

Laruelle, G. G., H. H. Dürr, C. P. Slomp, and A. V. Borges. 2010. Evaluation of sinks and sources of CO_2 in the global coastal ocean using a spatially-explicit typology of estuaries and continental shelves. Geophys. Res. Lett. 37: 1–6. doi:10.1029/2010GL043691

Lüthi, D., M. Le Floch, B. Bereiter, T. Blunier, J.-M. Barnola, U. Siegenthaler, D. Raynaud, J. Jouzel, H. Fischer, K. Kawamura, and T.F. Stocker. 2008. High-resolution carbon dioxide concentration record 650,000-800,000 years before present. Nature, Vol.

453, pp. 379-382, 15 May 2008.

Masson-Delmotte, V., M. Schulz, A. Abe-Ouchi, J. Beer, A. Ganopolski, J.F. González Rouco, E. Jansen, K. Lambeck, J. Luterbacher, T. Naish, T. Osborn, B. Otto-Bliesner, T. Quinn, R. Ramesh, M. Rojas, X. Shao and A. Timmermann, 2013: Information from Paleoclimate Archives. In: Climate Change 2013: The Physical Science Basis. Contribution of Working Group I to the Fifth Assessment Report of the Intergovernmental Panel on Climate Change [Stocker, T.F., D. Qin, G.-K. Plattner, M. Tignor, S.K. Allen, J. Boschung, A. Nauels, Y. Xia, V. Bex and P.M. Midgley (eds.)]. Cambridge University Press, Cambridge, United Kingdom and New York, NY, USA.

Melack, J. M., L. L. Hess, M. Gastil, B. R. Forsberg, S. K. Hamilton, I. B. Lima, and E. M. Novo. 2004. Regionalization of methane emissions in the Amazon Basin with microwave remote sensing JOHN. Glob. Chang. Biol. 530–544. doi:10.1111/j.1529-8817.2003.00763.x

Meybeck, M. 1982. Carbon, nitrogen, and phosphorus transport by world rivers. Am. J. Sci. 282: 401–450. doi:10.2475/ajs.282.4.401

Middelburg, J. J. 2019. Marine Carbon Biogeochemistry: A Primer for Earth System Scientists,.

Myhre, G., D. Shindell, F.-M. Bréon, and others. 2013. Anthropogenic and Natural Radiative Forcing. In: Climate Change 2013: The Physical Science Basis. Contribution of Working Group I to the Fifth Assessment Report of the Intergovernmental Panel on Climate Change [Stocker, T.F., D. Qin, G.-K. Plattner, M. Ti. Cambridge Univ. Press. Cambridge, United Kingdom New York, NY, USA, Chapter 8: 659–740. doi:10.1017/CBO9781107415324.018

Nisbet, E. G., M. R. Manning, E. J. Dlugokencky, and others. 2019. Very Strong Atmospheric Methane Growth in the 4 Years 2014–2017: Implications for the Paris Agreement. Global Biogeochem. Cycles 33: 318–342. doi:10.1029/2018GB006009

NOAA. (2020) Global Monitoring Division program and the data is available at https:// www.esrl.noaa.gov/gmd/ccgg/trendsch4/ (last access: 07 January 2020)

Palmer, S. C. J., T. Kutser, and P. D. Hunter. 2015. Remote sensing of inland waters: Challenges, progress and future directions. Remote Sens. Environ. 157: 1–8. doi:10.1016/j.rse.2014.09.021

Peters, G. P., C. Le Quéré, R. M. Andrew, and others. 2017. Towards real-time verification of CO_2 emissions. Nat. Clim. Chang. 7: 848–850. doi:10.1038/s41558-017-0013-9

Pierrot, D., C. Neill, K. Sullivan, and others. 2009. Recommendations for autonomous underway pCO_2measuring systems and data-reduction routines. Deep. Res. Part II Top. Stud. Oceanogr. 56: 512–522. doi:10.1016/j.dsr2.2008.12.005

Platt, T., and S. Sathyendranath. 1988. Oceanic primary production: estimation by remote sensing at local and regional scales. Science (80-.). 241: 1613–1620.

Raymond, P. A., J. E. Bauer, and J. J. Cole. 2000. Atmospheric CO_2 evasion, dissolved inorganic carbon production, and net heterotrophy in the York River estuary. Limnol. Oceanogr. 45: 1707–1717. doi:10.4319/lo.2000.45.8.1707

Raymond, P. A., J. Hartmann, R. Lauerwald, and others. 2013. Global carbon dioxide emissions from inland waters. Nature 503: 355–359. doi:10.1038/nature12760

Regnier, P., P. Friedlingstein, P. Ciais, and others. 2013. Anthropogenic perturbation of the carbon fluxes from land to ocean. Nat. Geosci. 6: 597–607. doi:10.1038/ngeo1830

Roemmich, D., G. Johnson, S. Riser, and others. 2009. The Argo Program: Observing the Global Oceans with Profiling Floats. Oceanography 22: 34–43. doi:10.5670/oceanog.2009.36

Saunois, M., P. Bousquet, B. Poulter, and others. 2016. The global methane budget 2000-2012. Earth Syst. Sci. Data 8: 697–751. doi:10.5194/essd-8-697-2016

Saunois, M., A. R. Stavert, B. Poulter, and others. 2019. The Global Methane Budget 2000-2017. Earth Syst. Sci. Data. doi:10.1017/CBO9781107415324.004

Seelmann, K., S. Aßmann, and A. Körtzinger. 2019. Characterization of a novel autonomous analyzer for seawater total alkalinity: Results from laboratory and field tests. Limnol. Oceanogr. Methods 17: 515–532. doi:10.1002/lom3.10329

Souza, R., R. Aquino, S. De Santana, J. Tota, R. Silva, M. Roberval, A. Marcos, and D. De Andrade. 2019. Comparison of headspace and compact sensor measurements of tropical lakepCO 2. IOSR J. Environ. Sci. Toxicol. Food Technol. 13: 08–14. doi:10.9790/2402-1303030814

Steinhart, J. S., and S. R. Hart. 1968. Calibration curves for thermistors. Deep Sea Res. Oceanogr. Abstr. 15: 497–503. doi:10.1016/0011-7471(68)90057-0

Stramma, L. and Schmidtko, S., 2019. Global evidence of ocean deoxygenation. IUCN.

Strong, A. E. 1978. Chemical whitings and chlorophyll distributions in the Great Lakes as viewed by Landsat. Remote Sens. Environ. 7: 61–72. doi:10.1016/0034-4257(78)90007-X

Stumm, W. and Morgan, J.J., 1996. Chemical equilibria and rates in natural waters. Aquatic chemistry, 1022.

Sutton, A. J., C. L. Sabine, S. Maenner-Jones, and others. 2015. A high-frequency atmospheric and seawater pCO_2 data set from 14 open-ocean sites using a moored autonomous system. Earth Syst. Sci. Data 6: 353–366. doi:10.3334/CDIAC/OTG.TSM

Takahashi, T. 1961. Carbon dioxide in the atmosphere and in Atlantic Ocean water. J. Geophys. Res. 66: 477. doi:10.1029/JZ066i002p00477

Takahashi, T., J. Olafsson, J. G. Goddard, D. W. Chipman, and S. C. Sutherland. 1993. Seasonal variation of CO_2 and nutrients in the high-latitude surface oceans: A comparative study. Global Biogeochem. Cycles 7: 843–878. doi:10.1029/93GB02263

Uchida, H., T. Kawano, I. Kaneko, and M. Fukasawa. 2008. In situ calibration of optode-based oxygen sensors. J. Atmos. Ocean. Technol. 25: 2271–2281. doi:10.1175/2008JTECHO549.1

Vaisala Oyj. 2008. Vaisala CARBOCAP Carbon Dioxide Transmitter Series User's Guide, Helsinki, Finland.

Wanninkhof, R., P. A. Pickers, A. M. Omar, and others. 2019. A surface ocean CO_2 reference network, SOCONET and associated marine boundary layer CO_2 measurements. Front. Mar. Sci. 6. doi:10.3389/fmars.2019.00400

Ward, N. D., T. S. Bianchi, P. M. Medeiros, M. Seidel, J. E. Richey, R. G. Keil, and H. O. Sawakuchi. 2017. Where Carbon Goes When Water Flows: Carbon Cycling across the Aquatic Continuum. Front. Mar. Sci. 4: 1–27. doi:10.3389/fmars.2017.00007

Webb, J. R., D. T. Maher, and I. R. Santos. 2016. Automated, in situ measurements of dissolved CO_2, CH_4, and $\delta^{13}C$ values using cavity enhanced laser absorption spectrometry: Comparing response times of air-water equilibrators. Limnol. Oceanogr. Methods 14: 323–337. doi:10.1002/lom3.10092

Weber, T., N. A. Wiseman, and A. Kock. 2019. Global ocean methane emissions dominated by shallow coastal waters. Nat. Commun. 10: 1–10. doi:10.1038/s41467-019-12541-7

Welles, J. M., and D. K. McDermitt. 2005. Measuring carbon dioxide in the atmosphere. Micrometeorol Agr. Syst. Agron. Monogr 47: 287–320.

Williams, A. J., C. Brannon Andersen, and G. P. Lewis. 2009. Evaluating the effects of sample processing treatments on alkalinity measurements. J. Hydrol. 377: 455–464. doi:10.1016/j.jhydrol.2009.09.007

Yoon, T. K., H. Jin, N.-H. Oh, and J.-H. Park. 2016b. Technical note: Applying equilibration systems to continuous measurements of pCO_2; in inland waters. Biogeo-

sciences Discuss. 2: 1–34. doi:10.5194/bg-2016-54

Thesis Outline

From all the details above, this has led to the motivation of implementing and assessing oceanic sensors into limnic systems research, in the attempt to bridge the gap between the marine and limnic world. The high accuracy, resolution, consistency, and versatility found within ocean observation technology is needed for inland waters. All of these characteristics will hopefully improve our understanding of the dynamics and overall carbon budgets, especially in areas where there is a deficiency of data. This could potentially assist with validation of models, scaling up budgets and improve our overall standing on future predictions. Here we look into the efforts of developing and using such a system from pre-existing oceanic sensors for application across the LOAC, testing the sensors across contrasting environments. The focus is on the two main gases described previously: pCO_2 and CH_4, alone with O_2 and temperature and salinity. This thesis primarily focuses on the suitability and performance and then further explores into what can be extracted from this. With the fate of the carbon cycle ultimately determined by present and future anthropogenic activities, in depth knowledge of how these systems function is very much needed. Therefore, the thesis investigates the following questions:

1. **Can a set of oceanographic sensors provide high-quality data across the entire Land-Ocean Aquatic Continuum and under a wide range of operation conditions?**

   Although sensors have been used in both oceanic and limnic waters, the two systems vary drastically in concentration and spatial-variability ranges. This variability leads to differences in sampling techniques, leading to methodological inconsistencies and different standardization of sensors. Most inland water sampling is collected via discrete sampling methods, ultimately leading to both human error and discrepancies. In this chapter, using industry manufactured oceanic sensors for pCO_2, pCH_4, O_2 and temperature and conductivity, we measured across the entire salinity range (oceanic, brackish and fresh waters). For each campaign, the set-up was combined with either reference systems or discrete sampling for validation. Through this we assess the abilities of the sensors in both calm and highly dynamic regions. Further discussions on the sensor's performance as well as its utility for assessing both temporal and spatial variability, including small-spatial scale, are included. (Chapter 4: SENSOR SET-UP DEVELOPMENT AND ASSESSMENT)

2. **Can high-resolution mapping data be applied to a simple model to predict TA and further carbonate species measurements, while enabling diel extractions?**

   Collecting continuous TA and DIC measurements with sensors is currently not feasible, especially within inland waters. Therefore, there is an almost complete paucity of high-resolution datasets in terms of diel cycles and continuous measurements for these two parameters. These variables are important in terms of

understanding the carbon cycle dynamics and biogeochemical cycles in inland waters. Therefore, in this chapter, using a basic model of the relationship between TA and both temperature and specific conductivity along with a few discrete samples, we were able to produce a continuous dataset for the TA and hence the full carbonate system from our continuous dataset of pCO_2, temperature and specific conductivity. Furthermore, extraction of diel cycles was found to be possible with the use of extensive mapping. These extractions were further confirmed with the analyses of extraction full diel variabilities. The dynamics within the inland waters in the Danube Delta for the carbonate system and processes, are discussed in detail. (Chapter 5: INLAND MODELLING OF CARBONATE SYSTEM VARIABLES)

3. **Can high-spatio-temporal methane data and diel-cycle extraction advance the improvement of methane budget estimates?**

   Diel cycles within inland waters are known to potentially have significant implications for understanding CH_4 processes and dynamics within inland waters. Due to the inaccessibility and difficulties with sampling however, they are rarely measured leading to potential biases in budget and flux assessments. Using the high-resolution data from the completion of multiple diel-cycle measurements from one location (two different regions: lakes and channels), we were able to extract the diel cycle dynamics of CH_4. The processes behind the diel variability and then re-calculated fluxes, using both the day data only and the combined, are further discussed. (Chapter 6: INLAND METHANE DYNAMICS AND DIEL CYCLES)

Technologies and Methods

3.1 Sensors

The set up consisted of the HydroC® CO_2 FT (HC-CO_2: Kongsberg Maritime Contros GmbH, Kiel, Germany: KMCON) for pCO_2, HydroC® CH_4 FT (HC-CH_4: KMCON) for pCH_4, SeaBird Thermosalinograph 45 (Sea-Bird Electronics, Bellevue, USA) for temperature, conductivity and salinity, and the HydroFlash® O_2 optode (KMCON). This combination allowed for the interactions between the parameters and possible biogeochemical processes to be assessed. CO_2, CH_4 and O_2 could be used to focus on biological processes while the SBE would pick up the more physical processes. The sensors were from the same water source, described further below.

All sensors are commercially manufactured, with the HC-CO_2, HC-CH_4 and optode used commercially and thoroughly tested (Fietzek et al. 2011, 2014; Fiedler et al. 2013; McGinnis et al. 2016; Bittig et al. 2018).

3.2 Discrete Sample Analyses

All discrete samples used throughout this thesis, were collected from the same water source during all campaigns (slightly differing in brackish waters). The samples were measured using different methods depending on sample type and location. Described below are the laboratory details following collection. Further details on specific collection techniques see section 4.

3.2.1 Discrete Sample Measurements

TA and DIC The samples for TA and DIC were collected following the DOE guidelines (Dickson et al 2007). Samples of either 500 mL Duran or 100 mL borosilicate glass bottles poisoned with either 100 μL or 20 µL saturated $HgCl_2$ solution (for the ocean and limnic campaigns respectively). Samples for the ocean and brackish waters were then analyzed using the SOMMA for DIC (Johnson et al. 1987) or the VINDTA for TA (Mintrop et al. 2000). For inland waters the Apollo DIC Analyzer and the Apollo TA Titrator were used. Details on accuracy or duplicates are in section 4.

Methane Samples were collected for each cruise and measured all almost the same way (excluding limnic regions, see below). A static equilibration method was used to analyse the samples. This is where a head space of 10ml Helium (Air Liquid GmbH, Dusseldorf) was injected into the glass vial and left to equilibrate with the head space for at least 2 hours. Sub-samples were then sampled from this head space of approximately 9ml of head space volume. This was then injected into the gas chromatographic system. For limnic cruises, due to the high rates of CH_4 found within the samples, and reference gases far under that of what was needed (up to 11,000 μatm), the extracted head space sample was diluted and scaled. The scales were based on a ratio for each sample to helium

from a pressurized chamber and depended on sample concentration (higher, larger the ratio for helium). Using two standard gas mixtures for calibration, the dry mole fraction of CH_4 was then determined from the FID signal peak. Three lots of four calibration mixtures were injected everyday with highest standard of 25,000 ppb for daily calibration. The methane content (nmol) was then calculated following the Ideal Gas Law, with the solubility described by Henry's Law. The effects of temperature and salinity on the solubility of the gases was considered by using values determined by Wiesenburg and Guinasso (1979) (eq. 3.1) (Weiss 1970) which is included in the calculation of the dissolved gas concentration from its dry mole fraction within the gas phase. The equation used (nmol L^{-1}):

$$C = \exp\left\{A_1 + \frac{A_2}{T} \cdot 100 + A_3 \ln\left(\frac{T_{\text{eq}}}{100}\right) + A_4\left(\frac{T_{\text{eq}}}{100}\right) + S\left[B_1 + B_2\left(\frac{T_{\text{eq}}}{100}\right) + B_3\left(\frac{T_{\text{eq}}}{100}\right)^2\right]\right\} \cdot x_{\text{HS}} P \tag{3.1}$$

Where the exponential term is called the Bunsen coefficient and this is used as equivalent to Henry's law. Ax and Bx are constants from Wiesenburg and Guinasso (1979) for nmol L^{-1} and Teq is temperature (°C + 273.15). Using this, the total concentration of the sample was then calculated from the water phase volume and methane content. Saturation was calculated using the equilibrium concentration as described in section 6.

Oxygen O_2 samples were collected in 100 mL borosilicate glass bottles for the oceanic cruise. Any sample with bubbles was discarded immediately. Following sampling they were immediately spiked with fixation solution (NaOH/NaI and $MnCl_2$) before being shaken for 30 seconds. They were titrated using the Winkler Method (Winkler 1888) within 40 min to 16 h between sampling and measuring. Standard protocols followed Grasshoff et al. (1999), chap. 4: Determination of oxygen.

3.3 Preliminary Experiments with Novel Sensor Package

Preliminary excursions and laboratory experiments were conducted to ensure the set-up work sufficiently in the decided flow regime with collection of discrete samples as well as conducting experiments to test the response times of the sensor (HC-CO_2).

3.3.1 Preliminary Laboratory Experiments

Laboratory experiments were conducted during 2016 in preparation for sea-going research cruises. They were conducted at GEOMAR Helmholtz Centre for Ocean Research, Germany within the temperature-controlled laboratory. The set up involved a 100 L tank with a small submersible pump used to pump the water in a closed circuit to the HydroC CO_2 FT. Each room was set to a specific temperature (either 5°C, 10°C, 16°C and 20°C), attempting to span the range in which we may experience in the field. The tank was left for a minimum of 12 hours before experiments were conducted to ensure all the water was of the correct temperature.

Temperature dependence Solubility, molecular diffusion coefficient and permeability of as given gas in the membrane are all temperature-dependent which makes the sensor's response time temperature-dependent to. Temperature experiments were therefore conducted following the work of Fietzek et al. (2014). The response time (RT)

was measured via the flushing and zeroing sequence (schematic figure 3.1) within the HC-CO_2 (described further in chapter 4).

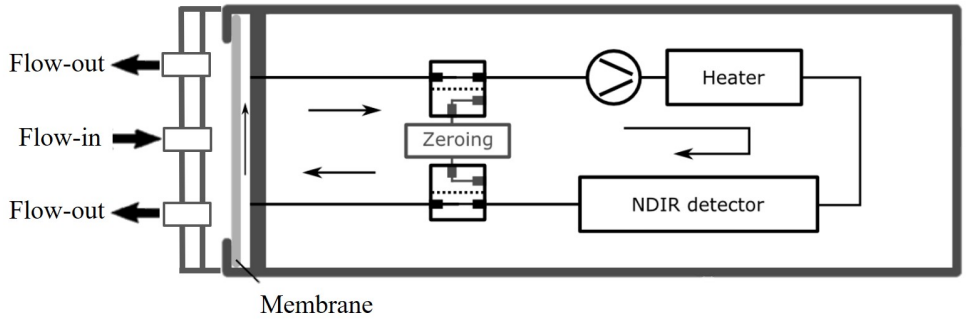

Figure 3.1: Modified schematic from Fietzek et al.(2014) showing the flow through type head and the zeroing loop.

The RT was estimated from the signal recovery after each of the zeroing interval (figure 3.1), by fitting an exponential function to the signal (Fiedler et al. 2013). In the laboratory, a series of zeroing and flushing sequences were continuously run (2 min zero, 15 min flush) under controlled temperature conditions. The acquired RT of the sensor is denoted at t63, representing the e-folding time scale of the sensor (Miloshevich et al. 2004).

The results showed the least amount of error between each repeated zeroing and flush sequence with 5 L min^{-1} (Table 3.1). Using this, and along manufacturer recommendation is 5 L min^{-1} (between 2-16 L min^{-1}), it was decided to flag any flow below 5 and try to stay around 6. Figure 3.2 shows an example of the different fits for 2 L min^{-1}, 5 L min^{-1} and 8 L min^{-1} within 5°C room with RT (seconds) shortening with increased flow.

Flow Speed		**5°C**	**10°C**	**16°C**	**20°C**
2 L min^{-1}	RT	2:27[2:35]	2:25[2:30]	2:21[2:30]	2:12[2:17]
	RT-err	0.3[0.4]	0.4[0.5]	0.3[0.68]	0.3[0.4]
5 L min^{-1}	RT	1:42[1:47]	1:34[1:38]	1:30[1:35]	1:29[1:33]
	RT-err	0.3	0.3[0.4]	0.3	0.2[0.5]
8 L min^{-1}	RT	1:18[1:20]	1:15[1:23]	1:13[1:16]	1:09[1:14]
	RT-err	0.2[0.4]	0.3[0.6]	0.2[0.4]	0.2[0.5]

Table 3.1: Results from the temperature-controlled response time (RT) experiments for the HydroC CO_2 FT measuring pCO_2. The sensor measured in 4 temperatures (5°C, 10°C, 16°C and 20°C) with continuous zeroing and flushing intervals. For each of these intervals the response time (RT) and error (RT-err) is estimated from fitting and exponential function and acquiring t_{63} which is when the sensor signal has accommodated 63 % of the step's amplitude.

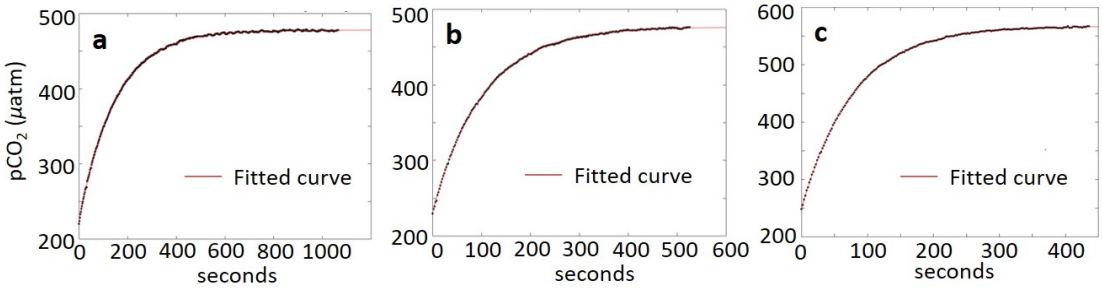

Figure 3.2: HydroC CO_2 FT flushing sequence in which the exponential functions to the signal increase. This is denoted as t_{63}, which represents the sensor time response where 63% of the sensor signal has accommodated the steps amplitude. (a) is the fit at 5°C at 2L min^{-1}, (b) is the fit at 5°C at 5 L min^{-1} and (c) is the fit at 5°C at 8 L min^{-1}. Notice the seconds along the bottom decreasing with increasing flow speed.

3.3.2 Preliminary Field Experiments

Between May and June 2016, three 1-day cruises to Boknis Eck Time-Series Station (Figure 3.3) in Eckernförde Bay, western Baltic Sea were conducted onboard the RV Littorina. This experiment proved that all sensors worked well in the water set-up and it was possible to easily collect discrete samples in parallel (Figure 3.3). From the laboratory experiments and previous knowledge, the flow for the HydroC sensors was only monitored, via a visual platform for these cruises but later logged for response time corrections (see section 4), and the HC-CO_2 was placed prior to the HC-CH_4 due to its greater dependence on temperature with the potential of warming through the system. During this time discrete samples for total alkalinity (TA) and dissolved inorganic carbon (DIC) were collected (as described in section 3.2.1 and 4) from the same water source for use of practice and reference to ensure systems were working correctly. The data was logged and for the HydroC sensors was immediately visible using the KMCON software.

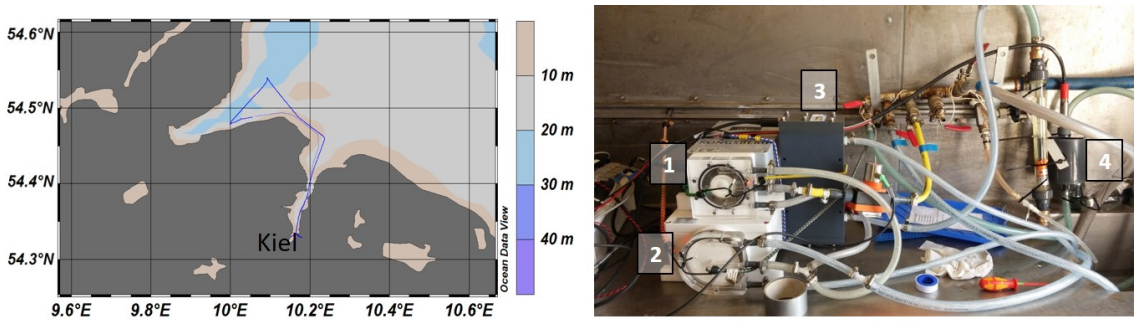

Figure 3.3: Showing the cruise track from Kiel to Boknis Eck and the original set-up on the RV Littorina 2016. In the set-up: (1) HC-CO_2 for pCO_2, (2) HC-CH_4 for pCH_4, (3) SeaBird Thermosalinograph 45 for temperature and salinity, and (4) HydroFlash® O_2 for O_2, with a flow gauge and flow meter to measure the water for the SeaBird and HydroC sensors respectively.

Discrete samples were then measured at GEOMAR Helmholtz Centre for Ocean Research Kiel described in the following sections.

TA / DIC and pCO_2 Samples were measured in the laboratory using the VINDTA and SOMMA respectively, details of which are described in sections 3 and 4. From this pCO_2 was calculated through the open access software CO_2SYS (Lewis et al. 1998) with the constants for brackish water (Millero et al. 2006), previously used by others in the same region: Baltic Sea (Schneider et al. 2014). These results were then compared to the processed sensor data. A time lag was noticed between discrete samples and sensors, due

to the tubing length. However due to this, the tubing size not measured and without a fully logged flow data, a time lag correction could not be accurately accounted. With this noted as highly important and therefore measured and accounted for, for each preceding cruise.

CH_4 Discrete samples were measured as described in section 3.4. Triplicates were taken for each sample. This data was converted into partial pressure using Henry's constant following (Wiesenburg and Guinasso 1979) to be comparable to that of the sensor. Due to only monitoring of the flow speed during these excursions, a standard 5 L min^{-1} was used for the response time correction for the pCH_4 data. Given this, the RT increased the R^2 of the discrete samples to the sensor data (R^2 = 0.27 raw data, to R^2 = 0.85 RT-Corr data). The mean and standard deviation from each triplicate improved from 5.3 ± 17.2 μatm to 2.6 ± 7.7 μatm. During the transect, the dataset stayed roughly around the lower values, with the higher ranges only within the fjord close to the Schwentine channel, known to have higher concentrations of CH_4 (McGinnis et al. 2016).

These cruises assessed the possibility of the system of continuously running over a period of time, while discrete reference data was able to be collected simultaneously.

3.4 General sampling procedure

Most methods of data collection within inland waters still rely on the collection of discrete samples, in which combined errors coming from sampling, sample storage and processing as well as from the measurement itself can be substantial. Over the years, attempts have been made to be reduce them by establishing verified standard operation procedures particularly in oceanography (e.g. CO_2: Dickson et al. (2007), O_2: Winkler (1888) and CH_4: McAuliffe (1971)). With each of these techniques having their own limitations and advantages, the main discrepancy issues usually come from those not characterized and standardised. Yet even when verified, basic sampling procedures still tend to differ (see Balmer and Downing 2011 and Selvam et al. 2014 for inland CO_2 and CH_4 sampling showing small variations; and see Bange et al. 2010, Repeta et al. 2016, and Wilson et al. 2018 for oceanic CH_4 extraction).

3.4.1 Method comparison

As established before, the techniques between limnology and oceanography often differ and even between independent limnology methods. Given this, a comparison exercise on sample preservation was completed during the Romanian cruises where discrete samples for TA and DIC were both poisoned (following oceanic techniques, see section 3 and 4) and non-poisoned (widespread limnic practice) were taken in parallel and stored in dark and cool place. Sample measurement occurred at the same time. Although TA and pH are more worldly used in terms of pCO_2 calculation in inland waters, here we still assess the effects on TA and DIC. For TA, the mean difference between non-poisoned and poisoned samples (± SD) was 31.7 ± 31.6, 19.5 ± 74.5 and 24.8 ± 13.9 μmol kg^{-1} for May, Aug and Oct respectively (figure 3.4). DIC at 28.3 ± 139.6, 174.1 ± 88.9 and -12.4 ± 218.1 µmol kg^{-1} had a much higher variability The combined effect of TA and DIC increases during storage of non-poisoned samples on calculated pCO_2 led to values of 368.9 ± 2079.5, 3630.8 ± 2053.9 and 435.4 ± 949.2 μatm for May, Aug and Oct respectively.

Aug showed the largest overall variation with un-poisoned samples, which was to be expected given the sample's high biological activity, not just with mass macrophytes

which dominated in May. Large offsets could also occur due to moving which sampling or in regions of highly dynamics concentrations where there was likely to have highly patchy areas of particle rich conditions. As most are positive this shows a growth in TA and DIC over time however, there was no significant correlation between duration of storage and TA/DIC offset between poisoned and non-poisoned samples ($p > 0.05$). Changes with both TA and DIC from poisoned and non-poisoned, highly distorting the calculated pCO_2 calculations.

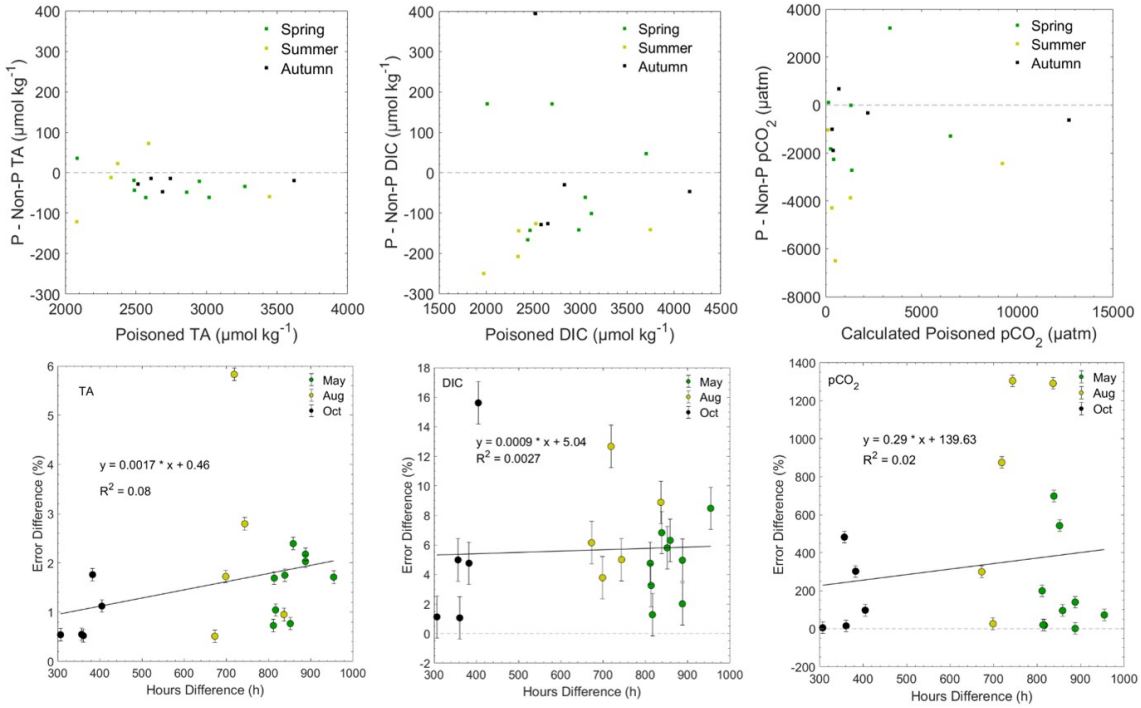

Figure 3.4: Discrete samples for total alkalinity (TA), dissolved inorganic carbon (DIC) and calculated pCO_2 (from TA and DIC using CO_2SYS (Lewis et al. 1998)) during the 3 seasons in the Danube delta, Romania (May, August (Aug) and October (Oct) 2017). Replicates were taken either poisoned (P) or left non-poisoned (NP) for comparison but stored in a dark refrigerator until measured. The top graphs show the difference (P – NP) in TA, DIC (μmol kg^{-1}) or pCO_2 (μatm) over the poisoned samples concentration. The bottom graphs show this difference in error percentage (%) over hours from time sampled to measured.

TA and DIC are not often used for pCO_2 calculations via CO_2SYS, normally TA and pH are used, however this varies between techniques and research institutes. Although TA only moderately changes (maximum of 6%), with DIC showing higher variability due to the use of CO_2 via biological processes and therefore significantly distorts the final pCO_2 calculations, it still changes enough to have implications on the calculations.

3.4.2 Time Lag

Given the tubing length from the pump to where the discrete sample collection point and sensors were placed, a time lag correction was needed to reference discrete samples to in situ observations. This was calculated separate for each cruise, depending on length of tubing and flow speed. To correct for this, we divided the water volume in the tubing (i.e. area of cross section of tubing times length of tubing, all converted to L) by the flow rate (L min^{-1}) which yields the passage time in minutes. For each cruise this changed and varied. During the oceanic cruise there was roughly 1-minute time lag and during Romania $\sim$ 23 seconds from the discrete sampling point to the sensor ($\sim$ 45 seconds from the water to the sensor).

3.4.3 Limitations

The biggest limitations were apparent in Romania where vast amounts of macrophytes within the shallow waters influenced the data. With high water flow speeds, although biofouling did not occur upon the membranes and had no noticeable impact, which was previously found with Yoon et al. (2016), other organisms such as macrophytes became an issue during certain seasons and locations (mainly lakes in May and Aug). Due to reducing the effects of the vessel itself on the data, the pump was placed at the front on the boat so bubbling or vessel disturbance was at a minimum when sailing. However, this resulted in large amounts of macrophytes would get stuck around the pump depending on regions and season. This was logged for later flagging as often as possible as it was immediately seen within the data due to a micro climate being created (spikes in figure 3.5). Even though these events were rare overall and primarily occurred within lakes of the Danube Delta system, difficulty to distinguishing between 'unnatural' or 'natural' surface waters was extremely difficult, therefore all data was just flagged for later further analyses. Challenges in logging boat passing movement also had an impact on the overall data as owing to the shallowness of some of the water bodies data peaks were immediately visible from waters coming from either the sediment (boats causing change in pressure) or below the stratified layer depending on season, vessel size and proximity to the houseboat.

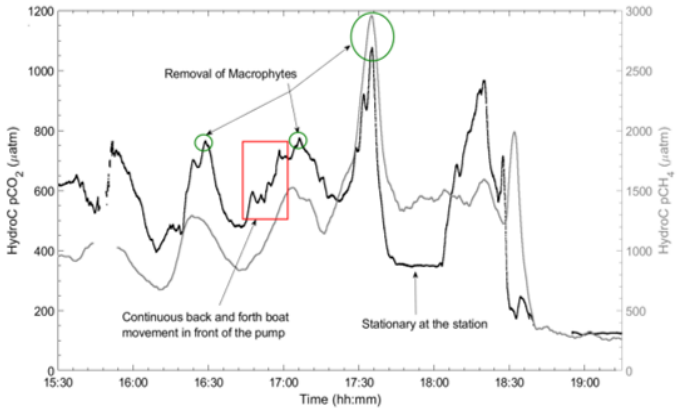

Figure 3.5: Example of impacts on pCO_2 μatm (black line) and pCH_4 μatm (grey line) from macrophytes getting stuck around the pumping system and speedboat passing impacts during Rom2 (summer campaign). Removal of macrophytes (green circles) and continuous back and forth movement of a speed boat in front of the pump (red square) are shown within the data, with clearer representation shown for the pCO_2. (Right) An example of macrophytes within a lake system.

Given the boat was continuously moving, there was no opportunity to keep the head of pump completely clear of macrophytes the entire time. A small cage was built which enabled the easier removal of these during the transects.

3.5 References

Balmer, M., and J. Downing. 2011. Carbon dioxide concentrations in eutrophic lakes: undersaturation implies atmospheric uptake. Inl. Waters 1: 125–132. doi:10.5268/IW-1.2.366

Bange, H. W., K. Bergmann, H. P. Hansen, A. Kock, R. Koppe, F. Malien, and C. Ostrau. 2010. Dissolved methane during hypoxic events at the Boknis Eck time series station (Eckernförde Bay, SW Baltic Sea). Biogeosciences 7: 1279–1284. doi:10.5194/bg-7-1279-2010

Bittig, H. C., A. Körtzinger, C. Neill, and others. 2018. Oxygen Optode Sensors: Principle, Characterization, Calibration, and Application in the Ocean. Front. Mar. Sci. 4: 1–25. doi:10.3389/fmars.2017.00429

Casper, P., S. C. Maberly, G. H. Hall, and B. J. Finlay. 2000. Fluxes of methane and carbon dioxide from a small productive lake to the atmosphere. Biogeochemistry 49: 1–19. doi:10.1023/A:1006269900174

Dickson, A. G., C. L. Sabine, and J. R. Christian. 2007. Guide to Best Practices for Ocean CO_2 Measurements, North Pacific Marine Science Organization.

Dlugokencky, E. and Tans, P.: Trends in atmospheric carbon dioxide, National Oceanic and Atmospheric Administration, Earth System Research Laboratory (NOAA/ ESRL), available at: http:// www.esrl.noaa.gov/gmd/ccgg/trends/global.html, last access: 29 January 2020

Fiedler, B., P. Fietzek, N. Vieira, P. Silva, H. C. Bittig, and A. Körtzinger. 2013. In situ CO_2 and O_2 measurements on a profiling float. J. Atmos. Ocean. Technol. 30: 112–126. doi:10.1175/JTECH-D-12-00043.1

Fietzek, P., B. Fiedler, T. Steinhoff, and A. Körtzinger. 2014. In situ quality assessment of a novel underwater pCO_2 sensor based on membrane equilibration and NDIR spectrometry. J. Atmos. Ocean. Technol. 31: 181–196. doi:10.1175/JTECH-D-13-00083.1

Fietzek, P., S. Kramer, and D. Esser. 2011. Deployments of the HydroC® (CO_2/CH_4) on stationary and mobile platforms - Merging trends in the field of platform and sensor development. Ocean. Mts/Ieee Kona 1–9. doi:10.23919/OCEANS.2011.6107129 Grasshoff, K., Kremling, K., and Ehrhardt, M. (1999). Methods of Seawater Analysis. Weinheim, Germany: Wiley-VCH Verlag GmbH.

Johnson, K. ., J. M. Sieburth, P. J. le. Williams, and L. Brändström. 1987. Coulometric total carbon dioxide analysis for marine studies: Automation and calibration. Mar. Chem. 21: 117–133. doi:10.1016/0304-4203(87)90033-8

Lewis, E., D. Wallace, and L. J. Allison. 1998. Program developed for CO_2 system calculations, carbon dioxide information analysis center.

McAuliffe, C. 1971. Gas Chromatographic Determination of Solutes by Multiple Phase Equilibrium. Chem. Technol. 1: 46–51.

McGinnis, D. F., N. Bilsley, M. Schmidt, P. Fietzek, P. Bodmer, K. Premke, A. Lorke, and S. Flury. 2016. Deconstructing Methane Emissions from a Small Northern European River: Hydrodynamics and Temperature as Key Drivers. Environ. Sci. Technol. 50: 11680–11687. doi:10.1021/acs.est.6b03268

Millero, F. J., T. B. Graham, F. Huang, H. Bustos-Serrano, and D. Pierrot. 2006. Dissociation constants of carbonic acid in seawater as a function of salinity and temperature. Mar. Chem. 100: 80–94. doi:10.1016/j.marchem.2005.12.001

Miloshevich, L. M., A. Paukkunen, H. Vömel, and S. J. Oltmans. 2004. Development and validation of a time-lag correction for Vaisala radiosonde humidity measurements. J. Atmos. Ocean. Technol. 21: 1305–1327.

Mintrop, L., F. F. Pérez, M. González-Dávila, M. Santana-Casiano, and A. Körtzinger. 2000. Alkalinity determination by potentiometry: intercalibration using three different methods. 26: 23–37.

Repeta, D. J., S. Ferrón, O. A. Sosa, C. G. Johnson, L. D. Repeta, M. Acker, E. F. DeLong, and D. M. Karl. 2016. Marine methane paradox explained by bacterial degradation of dissolved organic matter. Nat. Geosci. 9: 884–887. doi:10.1038/ng$eO_2$837

Schneider, B., W. Gülzow, B. Sadkowiak, and G. Rehder. 2014. Detecting sinks and sources of CO_2 and CH_4 by ferrybox-based measurements in the Baltic Sea: Three case studies. J. Mar. Syst. 140: 13–25. doi:10.1016/j.jmarsys.2014.03.014

Selvam, B. P., S. Natchimuthu, and L. Arunachalam. 2014. Methane and carbon

dioxide emissions from inland waters in India - implications for large scale greenhouse gas balances. 3397–3407.

Wiesenburg, D. A., and N. L. Guinasso Jr. 1979. Equilibrium solubilities of methane, carbon monoxide, and hydrogen in water and sea water. J. Chem. Eng. Data 24: 356–360. doi:10.1021/je60083a006

Winkler, L. W. 1888. Die bestimmung des im wasser gelösten sauerstoffes. Berichte der Dtsch. Chem. Gesellschaft 21: 2843–2854.

Sensor Set-up Development and Assessment

submitted as: Anna Canning, Arne Körtzinger, Peer Fietzek and Gregor Rehder: Technical Note: Seamless gas measurements across Land-Ocean Aquatic Continuum - corrections and evaluation of sensor data for CO_2, CH_4 and O_2 from field deployments in contrasting environments. [submitted to Biogeosciences, doi: 10.5194/bg-2020-128]

4.1 Abstract

Comparatively the ocean and inland waters are two separate worlds, with concentrations in greenhouse gases having orders of magnitude in difference between the two. Together they create the Land-Ocean Aquatic Continuum (LOAC), which comprises itself largely of areas with little to no data in regards to understanding the global carbon system. Reasons for this include remote and inaccessible sample locations, often tedious methods that require collection of water samples and subsequent analysis in the lab, as well as the complex interplay of biological, physical and chemical processes. This has led to large inconsistencies, increasing errors and inevitably leading to potentially false upscaling. Here we demonstrate successful measurements even in remote inland areas over extreme concentration ranges in high detail and accuracy with a set-up using a combination of pre-existing oceanographic sensors. The set-up consists of 4 sensors measuring pCO_2, pCH_4 (both flow-through, membrane-based NDIR and TDLAS sensors) O_2, and a thermosalinograph at high-resolution from the same water source simultaneously. The flexibility of the system allowed deployment from freshwater to open ocean conditions on varying vessel sizes, where we managed to capture day-night cycles, repeat transects and also delineate small scale variability. Our work demonstrates the need for increased spatiotemporal monitoring, and shows a way to homogenize methods and data streams in the ocean and limnic realms.

4.2 Introduction

Both carbon dioxide (CO_2) and methane (CH_4) are significant players in the Earth's climate system, with 2016 being the first full year atmospheric CO_2 rose above 400 parts per million (ppm), with an average of 402.8 ± 0.1 ppm (Le Quéré et al. 2017). Since 1750 it has risen from 277 ppm. A similar trend has been seen with CH_4, increasing by 150% in the atmosphere to 1803 ppb between 1750 - 2011 (Ciais et al. 2013), with an acceleration in recent years to 1850 ppb in 2017 (Nisbet et al. 2019). With the oceans being a sink for an estimated 24% of anthropogenic CO_2 emissions (Friedlingstein et al. 2019), they have been under continuous observation and study, resulting in the collection of large global databases (e.g., Takahashi et al. 2009; Bakker et al. 2016). Such observations have shown both regional and/or temporal variabilities between a source and sink for CO_2, yet typically a low to moderate CH_4 source (roughly 0.4-1.8 Tg CH_4 yr^{-1}; Bates et al. 1996; Borges et al. 2018; Rhee et al. 2009), increasing in coastal regions (Bange 2006). Inland waters however, are a different story and although it has

been known for 50 years that they are mostly supersaturated with CO_2 (Park 1969), up until recently their budgets have been of little focus. Regions such as lakes, rivers and reservoirs, are only more recently becoming recognized as significant elements of the global carbon budget (e.g. Regnier et al. 2013; Borges et al. 2015); with global CO_2 and CH_4 emissions from inland waters estimated at 2.1 Pg C yr^{-1}(Raymond et al. 2013) and 0.7 Pg C yr^{-1} (Bastviken et al. 2011) respectively. Mixing regimes (e.g. deltas and estuaries) as well as streams and smaller bodies of water are known to be overly important within these inland systems (Holgerson and Raymond 2016; Natchimuthu et al. 2017; Grinham et al. 2018), yet there is very little data coverage with respect to both these parameters (Borges et al. 2018), even more so when evaluated together.

One issue leading to little data coverage is that the combination of both inland waters and the ocean, the land-ocean aquatic continuum (LOAC), usually not studied continuously but rather split between oceanographers and limnologists. Although significant progress has been made recognizing the importance of the LOAC as a whole system (e.g. Raymond et al. 2013; Regnier et al. 2013; Downing 2014; Palmer et al. 2015; Xenopoulos et al. 2017), huge knowledge gaps are still present, particularly related to limited field data availability (Meinson et al. 2016). Often this is due to using different measuring techniques and protocols, both with respect to in-situ/autonomous observations and the collection of discrete data. Furthermore, this is empathized by pCO_2, pCH_4 and dissolved O_2 being controlled by several factors including biological effects, vertical and lateral mixing and temperature-dependent thermodynamic effects (Bai et al. 2015). These effects are exacerbated within inland waters where variability is far higher due to variations in environmental conditions and the magnitude of biological processes and anthropogenic influences (Cole et al. 2007). The high spatial and temporal variability within the inland/mixing waters (Wehrli 2013) only increases these difficulties, ultimately leading to the interface between the ocean and inland to be considered one of the hardest systems to observe accurately and adequately. This has led to limitations and lack of verifications, leading to errors, discrepancies and unreliability of scaling up the data. Inland waters tend to exhibit extreme ranges of CO_2 partial pressure (pCO_2, < 100 to $>10{,}000$ μatm; Abril et al. 2015) in comparison to oceanic waters (100 – 700 μatm; Valsala and Maksyutov 2010), while also showing extreme variabilities for both O_2 and CH_4. Given the much smaller concentration changes and gradients, oceanic sensors and methods have been specifically tailored to assure high accuracy over oceanic concentration ranges, in comparison to inland waters.

One way of tackling these limitations and measurement technique differences is through sensors, ensuring a unified way of measuring with well-constrained accuracy and precision. In specific regions, this has become more widespread and reviewed numerous times within the coastal and open ocean (see Atamanchuk et al. 2015 and Clarke et al. 2017 for examples). Multiple seagoing methods have been applied since the 1960's (see examples Takahashi 1961 and DeGrandpre et al. 1995 to more recent; Waugh et al. 2006; Pierrot et al. 2009; Schuster et al. 2009; Becker et al. 2012) to measure and estimate greenhouse gases, such as CO_2 across a variety of aquatic regions. Inland water investigations have also seen clear progress with the development of continuous, autonomous measurement techniques (e.g. Degrandpre et al. 1999; Baehr and Degrandpre 2004; Crawford et al. 2014; Meinson et al. 2016; Brandt et al. 2017). Yet, only few studies have employed membrane-based equilibration sensors with NDIR detection (non-dispersive infrared spectrometry) (e.g. Johnson et al. 2009; Bodmer et al. 2016; Yoon et al. 2016; Hunt et al. 2017, adapting atmospheric sensors (see Bastviken et al. 2015). These methods often focus on only one gas (usually CO_2) and none of these methods covers both waters types. Given the biological and physical parameters of inland waters, multi-gas analyses is the way forward, which was previously noted by in

the work of Brennwald et al. (2016), where they worked on the development of the membrane inlet mass-spectrometric (MIMS) 'miniRuedi'. This system measured as a nearly fully autonomous multi-gas mass spectrometer, however despite advances in both inert and reactive gas measurements the need for a filter and gas standards for extreme gradients gives this set-up a disadvantage in highly diverse inland waters. This highlights one issue with extremely variable environments, and showing that there is need for developing a robust, fully autonomous sensor system that is portable enough for small and simple platforms. The development needs to be able to measure a full range of concentrations accurately and precisely which is usually out of the specifications of sensors designed for one region. It needs to have the potential to measure multiple gases and ancillary parameters in unison across salinity and regional boundaries (including extreme concentrations), enabling us to measure throughout the LOAC, bridging the ocean-limnic gap both technically and by reducing discrepancies and errors. This is essential for improved monitoring, provides in-need high spatial variability data, tracking the global carbon budget (Le Quéré et al. 2017) and potential application in areas of highest uncertainties, with potentially high anthropogenic input (Schimel et al. 2016).

Here we used state-of-the-art membrane-based equilibrator NDIR and TDLAS (tunable diode laser absorption spectroscopy) sensors for pCO_2 and pCH_4 respectively, an oxygen optode and a thermosalinograph to create a set-up allowing measurements in a continuous flow-through system. To assess the versatility, performance, portability and measurement quality of the set-up, it was deployed across the three main aquatic environments: oceanic, brackish and limnic. We present the technical findings from the campaigns, showing the need for such high-resolution data, however biogeochemical implications will not be further investigated. The main objective of the work presented here was to realize a fully versatile, portable, and robust flow-through system to accurately and autonomously measure multiple dissolved gases (CO_2, CH_4, O_2) and ancillary parameters (T, S, water flow) simultaneously. The set-up was subsequently deployed in each region of selected salinities (ocean, brackish and inland waters) to allow for both spatial and temporal measurements. Extensive post field campaign corrections were assessed to see the need for their adaptation over all the regions, and for the more precise corrections, small-scale variability was used for this purpose. Discrete samples were collected, and reference systems were deployed alongside to provide quality assessment of the performance of the flow-through set-up.

4.3 Material and Methods

4.3.1 Sensors and ranges

The set-up featured four separate sensors measuring 3 dissolved gases as well as standard hydrographic parameters (Table 4.1).

The CONTROS HydroC® CO_2 FT (HC-CO_2) and CONTROS HydroC® CH_4 FT (HC-CH_4) (Kongsberg Maritime Contros GmbH, Kiel, Germany; KMCON) are both commercially manufactured sensors which use membrane-based equilibrators combined with NDIR and TDLAS gas detectors, respectively. Both sensors are of flow-through type, in which water is pumped through a plenum with a planar semi-permeable membrane across which dissolved gas partial pressure equilibrium is established with the head space behind, as described by Fietzek et al. (2014). The CONTROS HydroFlash® O_2 (KMCON, Kiel, Germany) is an optical sensor (optode) based on the principle of fluorescence quenching (see Bittig et al. (2018) for an optode technology review). As the sensor is only available as submersible type, a flow-through cell was built around the sensor head for integration in the flow-through system. The SBE 45 Micro Thermos-

alinograph (Sea-Bird Electronics, Bellevue, USA) was used to measure temperature and conductivity to calculate salinity, at a frequency of up to 1 Hz.

Model	Deployment Type	Detector Type	Resolution	Accuracy	Response Time (t_{63})	Specified Flow Rate (L/min)	Power Consumption	Dimensions (mm)	Weight (kg)	Range of Factory Calibration
CONTROS HydroC® CO2 FT** (KMCON*)	FT** membrane equilibration	NDIR	< 1 µatm	± 1 % of reading	t_{63} ~ 1:32 min @ 16°C, 5 L/min	2-15	350 mA @ 12 V	325 x 240 x 126	5.3	0 - 6,000 µatm
CONTROS HydroC® CH4 FT** (KMCON*)	FT** membrane equilibration	TDLAS	< 0.01 µatm	± 2 µatm or 3 % of reading	t_{63} ~ 22:46 min @ 17°C, 7 L/min	6-15	600 mA @ 12 V	452 x 283 x 142.5	8.5	< 2 - 40,000 µatm
CONTROS HydroFlash® O2 (KMCON*)	Submersible	Fluorescence quenching	< 0.1 %	± 1 %	t_{63}< 3 s	N/A	0.1 J per sample	23 x 197 with connector	0.17 air, 0.11 water	0 - 400 mbar pO_2
SBE 45 Salinity***	FT**	Conductivity Cell	0.00001 S/m	± 0.0003 S/m	N/A	0.6-1.8	30 mA @ 12-30 V	338 x 134.4 x 76.2	4.6	0 to 7 S/m
SBE 45 Temperature ***	FT**	Thermistor	0.0001 °C	± 0.002 °C	N/A	0.6-1.8	30 mA @ 12-30 V	338 x 134.4 x 76.2	4.6	-5 to +35 °C

* Kongsberg Maritime Contros GmbH, ** Flow-Through, ***Thermosalinograph, Sea-Bird Scientific

Table 4.1: Sensors and their manufacturer specifications, along with calibration range (for the CONTROS HydroC® CO_2 FT and CH_4 FT factory calibration ranges were specific for the campaigns).

4.3.2 Initial procedures and background

Initial experiments were conducted within the laboratory at GEOMAR, Kiel, Germany and during short sea trials on-board RV Littorina during 2016 to ensure the optimal performance of all sensors (data not shown here). HC-CO_2 was placed within the set-up upstream of HC-CH_4 due to higher sensitivity and dependence of the parameter pCO_2 to temperature changes. The water flow was split between sensors due to differing flow range requirements. A flow meter and pressure valves were installed to provide optimal flow speeds, as shown in the schematic of the overall set-up (Fig. 4.1).

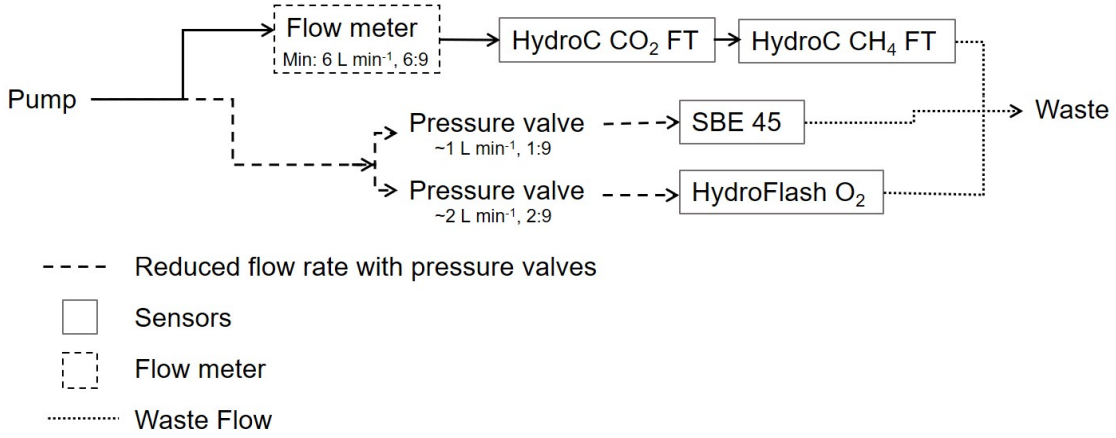

Figure 4.1: Flow schematic of the set-up, including minimal flow ratios. The flow rate was measured only for the main flow. For the side flows the rate was adjusted by pressure valves to be a fraction (i.e. 1:9 and 2:9) of the total flow.

Depending on the vessel type and location of the measurement system therein, the pump was placed either in the 'moon pool' of the ship or at the front of the boat (limnic cruises, see Table 2). The total flow was regulated by multiple pressure valves to a pump rate of approximately 9-10 L min^{-1}. The HC-CO_2 and HC-CH_4 show a distinct dependence of their response time (RT), on the water flow rate, with the demand for the HC-CO_2 flow rates ranging from 2-16 L min^{-1} (manufacturer recommendation is 5 L min^{-1}) and for the HC-CH_4 flow rates from 6-16 L min^{-1}. Based on this information combined with preliminary testing and power accessibility considerations across all regions, 6 L min^{-1} was used as the target flow rate for the HC-CO_2 and HC-CH_4. Data acquired with any flow rate below 5 L min^{-1} were flagged questionable.

The data was logged on an internal logger for the HC-CO_2 and HC-CH_4 in unison, and displayed live using the CONTROS Detect software from KMCON. The SBE Thermosalinograph and HydroFlash O_2 were logged on SeatermV2 software and a terminal programme (Tera Term) respectively. The sensors have the capability to set the timestamps for logged data, allowing alignment among all sensor systems and/or local time for discrete sample collection. Water flow was measured using LabJack Software and any power cuts (or other circumstances such as and boats passing near to the house boat during the limnic cruises) were logged manually to ensure the best quality processing which is described in the next sections.

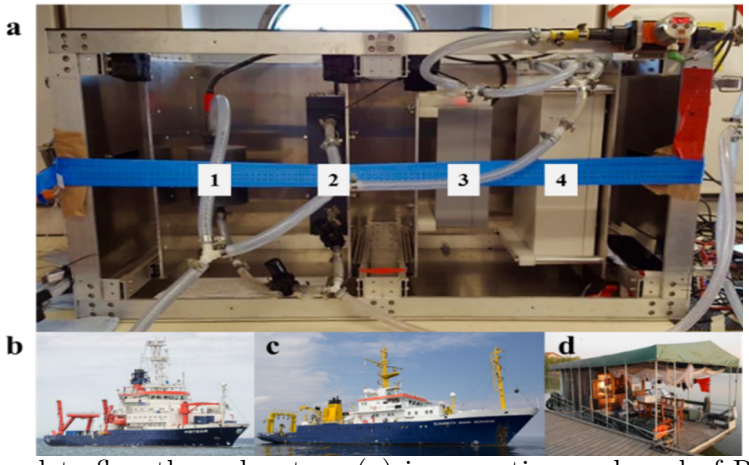

Figure 4.2: Complete flow-through set-up (a) in operation on board of RV Meteor indicating the easily accessible sensors for O_2 (1), T and S (2), pCO_2 (3) and CH_4 (4). Besides the operation on RV Meteor (b) across the Atlantic, M133, the set-up was also deployed on RV Elisabeth Mann Borgese (c) within the Baltic Sea, EMB 142, and on a houseboat in the Danube Delta (d), Romania, Rom1-3 for spring (Rom1), summer (Rom2) and autumn (Rom3).

The set-up was tested in three different locations: South Atlantic Ocean (oceanic), western Baltic Sea (brackish) and the Danube river delta (limnic), Romania between 2016 and 2017 (Fig. 4.2 and 4.3). This ensured the sensors were tested in the field across the full salinity range, from freshwater to seawater, from moderate to tropical temperatures and from low concentrations near atmospheric equilibrium to extreme cases of super- (CH_4, CO_2) or undersaturation (CO_2, O_2). The choice of cruises also allowed testing the versatility of the set-up with deploying it on a range of vessel types (Fig. 2 and Table 4.2, in section: Set-up evaluation).

4.3.3 Expeditions

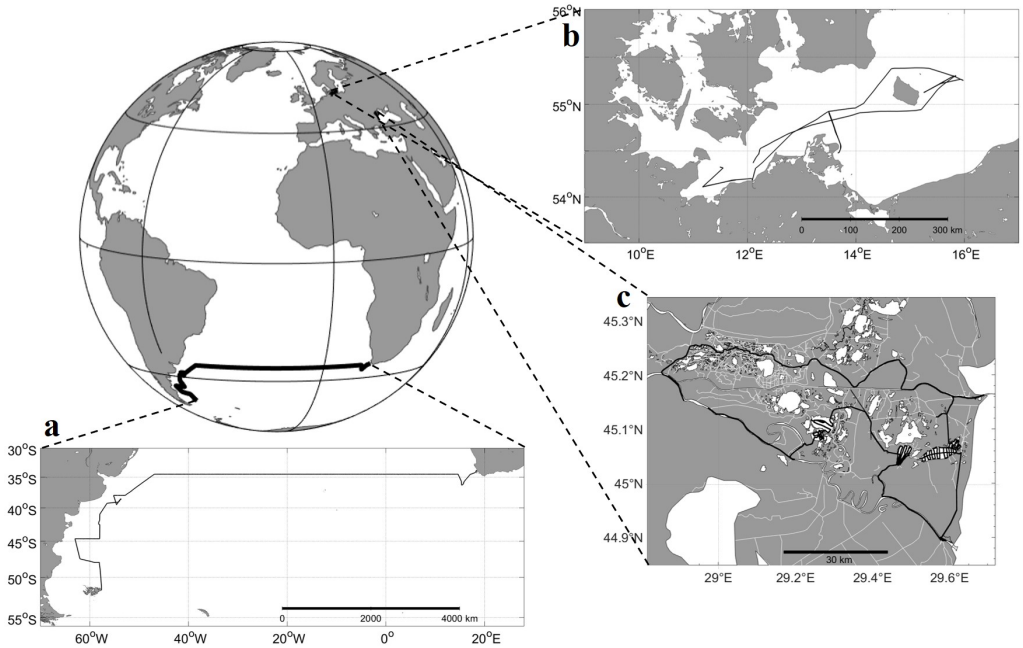

Figure 4.3: Transects for all test sites: (a) Oceanic: South Atlantic, RV Meteor cruise M133 Ocean (Cape Town, South Africa – Stanley, Falklands), (b) Brackish: RV Elisabeth Mann Borgese cruise EMB 142, Western Baltic Sea, (c) Limnic: Danube Delta, Romania. For further information see Table 2.

Meteor Cruise M133 to South Atlantic (oceanic)

The system was set up on the RV Meteor (cruise M133) during the SACROSS campaign, from Cape Town, South Africa to the Falkland Islands, UK between 15.12.2016 - 13.01.2017 (open to shelf oceanic waters). Discrete samples were collected throughout the cruise for total alkalinity (TA), dissolved inorganic carbon (DIC), CH_4 and O_2. The water was pumped up by means of a submersible pump installed in the ship's moon pool at about 5.7 m depth. The system logged once every minute which was deemed sufficient until the Patagonian Shelf was reached, where the measurement frequency was increased to 1 Hz. Sea surface temperature data was measured with a temperature sensor (SBE 38, Sea-Bird Electronics, Bellevue/WA, USA) installed at the seawater intake in the moon pool, which was used for temperature correction of the flow-through system data. Sea surface salinity was taken from the ship's thermosalinograph (SBE 21, SeaCAT TSG, Sea-Bird Scientific) and was used for the carbonate system calculations related to the discrete reference. CH_4 data collected during this cruise and half of the brackish cruise stated below was not used due to an internal issue of the detector related to absorption peak identification. This data was automatically flagged within the sensor diagnostic values and subsequently excluded. This issue was fixed for the limnic campaigns by installation of a reference gas cell in the absorption path of the detector.

Elisabeth Mann Borgese EMB 142 to Western Baltic Sea (brackish)

The sensor package was run on board of RV Elisabeth Mann Borgese (EMB 142) to the western Baltic Sea between 15.-22.10.2016 (brackish waters). The cruise was one of the main field activities of the Scientific Committee on Oceanic Research (SCOR) working group 142 (Dissolved N_2O and CH_4 measurements: Working towards a global network of ocean time series measurements of N_2O and CH_4) and entirely dedicated to the inter-comparison of continuous and discrete N_2O and CH_4 measurement techniques (see Wilson et al. 2018), but some of the systems also measured pCO_2 continuously. Discrete samples were collected for validation of the CO_2 and CH_4 sensors. All analyzers and the discrete sampling line were connected to the same water supply from a submersible pump system installed in the ship's 'moon pool' (depth 3 m), ensuring that the same water was used by all groups. A back-pressure regulation system assured independent flow assurance of the individual set ups. The sensors logged continuously at a rate of between once per second and once per minute, depending on local variability. During this cruise, only half the CH_4 data was used due the same technical reason as stated for the oceanic cruise.

Romania 1-3 Cruises to the Danube River Delta, Romania (limnic)

Excursions over three consecutive seasons were conducted during three field campaigns throughout the Danube Delta in Romania (limnic) in 2017: during spring (Rom1: 17-26.06.2017), summer (Rom2: 03-12.08.2017) and fall (Rom3: 13.-23.10.2017). The Danube Delta is situated at the border of Romania and Ukraine on the edge of the Black Sea. It is the second largest river delta in Europe with a diverse wetland area of about 300,000 ha with a variety of lakes, rivers and channels. The equipment was set-up on board a small houseboat, giving access to smaller channels and 'hard to reach' areas. A small power generator or car batteries were used to power the system. With an 11-24 V power source the set-up can take a reading at up to 1 Hz. In combination with the flow-through set-up, discrete samples were collected using the same water inlet as the sensors. Data acquisition was only interrupted when there were unexpected rainstorms or problems with the power supply, i.e. power cuts due to lack of fuel. Bilge pumps were

deployed from the bow of the house boat to reduce water body perturbations caused by the boat that would affect the flow-through measurements. The excess water was discarded over the side, away from the pump location. Due to measuring in parallel, during times where there was no SBE data, temperature was used from the optode (mean offset from the SBE for all cruises 0.16 ± 0.1 °C), although this was rare.

4.3.4 Method Validation

To validate the sensor measurements, discrete samples were collected simultaneously from the same water source (vessel-dependent) using tubing connected to the manifold to which the sensors were connected to.

TA and DIC samples were collected in 500 mL Duran glass bottles (100 ml borosilicate glass bottles for inland waters) following the standard operating procedure for water sampling for the parameters of the oceanic carbon dioxide system (SOP 1, Dickson et al. 2007) with 87, 8 and 68 discrete samples from the oceanic, brackish and inland water cruises, respectively. The samples were poisoned with 100 μL (20 μL inland) of saturated $HgCl_2$ solution to stop biological activity from altering the carbon distributions in the sample container before analysis, a procedure not typically performed in limnic research. During the limnic excursions both poisoned and un-poisoned samples were taken to do further analysis between techniques, only poisoned are shown here for reference. A headspace of approximately 1% of the bottle volume was left to allow for water expansion and the greased stopper was put in place and secured in an airtight manner using an elastic strap. The samples were then stored in a dark, cool place until measured. The VINDTA (Versatile Instrument for the Determination of Titration Alkalinity, Marianda Analytics and Data, Kiel, Germany) and SOMMA (Single Operator Multiparameter Metabolic Analyzer, University of Rhode Island, Narragansett Bay/MA, USA) were used to measure TA (Mintrop et al. 2000) and DIC (Johnson et al. 1987) in the brackish and seawater samples. Freshwater samples were measured using the Apollo Total Alkalinity Titrator (Model AS-ALK2, Apollo SciTech, Newark, USA) and DIC Analyzer (Model AS-C3, Apollo SciTech, Newark, USA). Measurements were calibrated with certified reference material (CRM) provided by A. Dickson (University of California, San Diego/CA, USA) with a determined precision of ±1.64 μmol kg^{-1} and ±1.15 μmol kg^{-1}, respectively for DIC and TA. TA and DIC were then used to compute pCO_2, using the open-access software CO_2SYS software (Lewis et al. 1998) employing the Millero et al. (2010, 2006) and Millero et al. (1979) carbonic acid dissociation constants (K1 and K2) for seawater, brackish and freshwater samples, respectively.

CH_4 samples were collected in 20 mL bottles, poisoned with 50 μL of saturated solution $HgCl_2$ and crimp-sealed. The samples were then stored until measurement. CH_4 in these water samples was measured with a gas chromatographic method following a procedure described by Weiss and Price (1980) and A. Kock (unpubl.) with an average standard deviation of the mean CH_4 concentration of 2.7% calculated following A. Kock (unpubl.) and David (1951). During transportation and storage, some CH_4 samples developed air bubbles due to warming causing some of the gases (e.g., nitrogen, oxygen) to become supersaturated and eventually outgas; these samples were discarded.

During the brackish water cruise, the MESS (mobile equilibrator sensor system, Leibniz Institute for Baltic Sea Research) was used as a reference system. The system consists of an open mixed showerhead-bubble type equilibrator, with an auxiliary equilibrator attached to the main exchange vessel. Water flow was adjusted to approximately 6 L min^{-1} during the cruise. Three Cavity Enhanced Absorption Spectrometers (CEAS) were attached in parallel from which only the results of the Los Gatos Research (LGR) GHG analyzer (Los Gatos Research, San Jose, California, USA) determining xCO_2 and xCH_4 are used for the comparison purposes in this study. Total air flow through the

pumps of the sensors and an additional air pump was set to approximately 1 L min^{-1}. A set of calibration gas runs covered a range from 1806 to 24944 ppb for methane and 201.3 to 1001.5 ppm for CO_2. Source of the calibration gases was the off-axis integrated cavity output spectroscopy (OA-ICOS) central calibration facility of the European Integrated Carbon Observation Research Infrastructure (ICOS CAL). The high standard was produced by NOAA as initiative of the SCOR working group 143. The response time for methane and CO_2 for the chosen flow rates were determined prior to the cruise to be approximately $\sim$ 330 s and $\sim$ 35 s respectively, at roughly 6 L min^{-1} with a gas flow of 4.7 L min^{-1}. Similar system operations and details of the post processing of data are given in Gülzow et al. (2011), which is installed on a VOS line and regularly reporting the data to the SOCAT data base (Bakker et al. 2016). However, the equilibrator system used in this study had been optimized for a shorter RT.

Oxygen was sampled in 100 mL borosilicate glass bottles with precisely known volume and titrated using the Winkler Method (Winkler 1888) on the oceanic cruise. The precision of the Winkler-titrated oxygen measurements was 0.29 μmol L^{-1} and based on 120 duplicates, from the mathematical average of standard deviations per replicate. Samples containing any air bubbles were discarded immediately.

4.3.5 Sensor data processing

The main corrections on the raw pCO_2 output from the HC-CO_2 sensor were for sensor drift (both zero and span), any observed warming of the sampled water at the sensor with respect to the seawater intake temperature, extended calibrations (over 6000 ppm, i.e. upper limit of manufacturer calibration range) and the effect of the sensor response time (RT), all described below. Sensor drift for the HC-CO_2 was corrected on the basis of pre- and post-deployment calibrations and the regular in situ zeroings using the sensor's auto-zero function, in which CO_2 is scrubbed from the measured gas stream using a soda lime cartridge. This zero measurement is then used in post-processing to correct for the drift over the deployment, details of which are described by Fietzek et al. (2014). The zeroings were carried out at regular intervals of 4 to 12 h in the various field campaigns and the shape of the zero drift was employed in the correction of the span drift between pre- and post-cruise factory calibration

The temperature correction was applied for all pCO_2 data to correct for any temperature difference between measurement in the flow-through setup and in situ temperature. After a time-lag correction due to in situ temperature and equilibrium temperature mismatch, resulting from the travelling time of the water from intake to sensor spot, the Takahashi et al. (1993) temperature correction was used for pCO_2:

$$\mathrm{pCO_2}(T_{in-situ}) = \mathrm{pCO_{2(}}_{T_{equ})} \cdot \exp\left[0.0423 \cdot (\mathrm{T}_{in-situ} - \mathrm{T}_{equ})\right] \tag{4.1}$$

where $T_{in-situ}$ is the in-situ temperature (i.e. SST), and T_{equ} is the equilibration temperature. For CH_4, the correction following Gülzow et al. (2011) was applied:

$$\mathrm{pCH4} = \mathrm{pCH_{4,}}_{equ} \cdot (\mathrm{CH_{4,}}_{sol,equ} \,/\, \mathrm{CH_{4,}}_{sol,insitu}) \tag{4.2}$$

where pCH_4 is the final pCH_4 (atm), $pCH_{4,equ}$ is the pCH_4 (atm) at equilibrium, $CH_{4,sol,equ}$ is the solubility (mol/(L $\cdot$ atm) of CH_4 at equilibrium and $CH_{4,sol,in}$ situ is the solubility (mol/(L $\cdot$ atm) at the in situ conditions.

During the Danube river field campaigns, pCO_2 data sometimes exceeded 6,000 ppm, i.e. the upper limit of the factory calibration range. NDIR detectors such as the one

used in the HC-CO_2 sensor, show a non-linear signal response, therefore extrapolation over the factory-calibrated range could not be done safely and an extended calibration was conducted. Prior to the extended calibrations, a further 'post' processing calibration was conducted at the KMCON manufacturer. The polynomial was compared to that of the initial post calibration from Rom2, revealing an average offset between the two of - 0.766 ± 0.94 (±SD) ppm. This proved that the HC-CO_2 had shown little change over the period, ensuring the extended calibration was applicable and could be applied to this expedition. The extended lab calibration was performed on manually produced gas mixtures. The xCO_2 of these mixtures was calculated considering the precisely measured flow ratios of the mixed gases N_2 and CO_2. The prepared calibration gas was wetted and routed to the HC-CO_2 membrane equilibrator. An extended calibration curve was then estimated to reduce the measurement uncertainty over an extended range 5,000-30,000 ppmv, while still increasing the measurement error at this range by an estimated 3 % compared to the ± 1% accuracy for measurements within the regular factory calibration range. This was due to larger uncertainties of the calibration reference (N_2 and CO_2: AIR LIQUIDE Deutschland GmbH, Düsseldorf, Germany, 99.999 % and 99.995 % accuracy respectively), the flow error of the mass flow controllers and the smaller sensor sensitivities at higher partial pressures.

The HC-CO_2 sensor response time (RT) for the corresponding flow rate and temperature was estimated from the signal recovery after each zeroing interval, by fitting an exponential function to the signal increase following the zeroing. Sensor time response is typically denoted as t63, which represents the e-folding time scale of the sensor, i.e. the time over which, following a stepwise change in the measured property, the sensor signal has accommodated 63% of the step's amplitude (Miloshevich et al. 2004). This correction was carried out by following a RT correction (RT-Corr) routine by Fiedler et al. (2013). However, the conditions within the limnic regions were simply too variable compared to the available in situ RT determinations and the in situ RT-dependencies that could be derived from the in situ measurements. Therefore, prior to the first expeditions, experiments were conducted within temperature-controlled culture rooms to see how the e-folding time of the HC-CO_2 flow-through sensor was affected by flow and temperature. These characterizations were used as the basis for the HC-CO_2 RT-Corr for the limnic cruises, as described below for HC-CH_4. Procedures for RT-Corr are further described by Fiedler et al. (2013) and Miloshevich et al. (2004).

Due to the HC-CH_4 using a TDLAS detector, drift correction was not needed as it produces a derivative signal that is directly proportional to CH_4 eliminating offsets in a 'zero baseline technique', along with a narrow band detection, therefore reducing signal noise (Werle 2004). However, compared to the HC-CO_2, the HC-CH_4 sensor has an approx. 15 times longer RT due multiple combined reasons: lower solubility, lower CH_4 permeability of the membrane material, and the comparatively larger internal gas volume. To enable a meaningful analysis of all the dissolved gas sensor signals, the CH_4 data therefore needed a RT-Corr. This was derived in a different way to the HC-CO_2 as no zeroing process within the HC-CH_4 allowed regular phenomenological estimation of the in-situ RT during measuring. To quantify the CH_4 sensor's t_{63}, laboratory experiments with a modified sensor unit were conducted at different flow rates (5.7, 6.5 and 7 L min^{-1}) and temperatures (11.06, 15.05, 18.04°C) to determine the RT as a function of these parameters. The HC-CH_4 used for the RT determination experiments was modified by the installation of two additional valves in the internal gas circuit (c.f. the sensor schematic in the Fietzek et al 2014). Switching these valves enables bypassing the membrane equilibrator and causes e.g. equilibrated, low pCH_4 gas to be continuously circulated through the detector. Now the pCH_4 in the calibration tank can be increased. As soon as a stable pCH_4 level is reached in the tank, the valves within the HydroC are

switched back and the gas passes the membrane equilibrator again. From the resulting signal increase the time constant for the equilibration process i.e. the sensor RT can be determined.

These modifications have only affected the internal gas volume and flow properties to a small extend. An effect on the determined RT compared to the RT of a standard HC-CH_4 is therefore considered negligible.

This information was then applied to the raw HC-CH_4 field data considering the measured flow rate and temperature and the method of Fiedler et al. (2013).

Post processing of the HydroFlash O_2 followed the SOP provided by KMCON using Garcia and Gordon (1992) combined fit constants. Further processing to convert the output into gravimetric (μmol kg^{-1}) and volumetric units (μmol L^{-1}) for comparison with other sensors and the discrete samples is described in the SCOR WG142 recommendations on O_2 quantity conversions (Bittig 2016).

The output from the factory-calibrated SBE 45 thermosalinograph had no need for post processing. All accuracies of the sensors are shown in Table 4.1.

4.4 Results

The set-up was easily adapted to each power source, managing to measure across the range of salinities and concentrations (Table 4.2). Due to the design, physical placement and high flow speed, no clogging or biofouling of the membranes of the HC-CO_2 and HC-CH_4 occurred even within particle-rich environments, with very little settlement.

Cruise Information				Observed Parameter Ranges									
Cruise ID	**Location**	**Vessel Size (m)**	**Excursion Date**	**pCO_2 (µatm) min:max**		**pCH_4 (µatm) min:max**		**O_2 (µmol/kg) min:max**		**Temperature (°C) min:max**		**Salinity (PSU) min:max**	
RV Elisabeth Mann Borgese (**EMB 142**)	Baltic Sea	56.5	15.10.2016 - 22.10.2016	378.0	623.8	**1.5**	6.6	98.2	313.9	11.0	13.4	7.40	15.87
RV Meteor (**M133**)	South Atlantic Ocean	98	15.12.2016- 13.01.2017	214.9	428.6	N/A	N/A	217.7	306.4	**8.5**	23.3	33.25	**36.25**
Romania (**Rom1**): Spring Cruise	Danube Delta, Romania	~10	17.05.2017 - 26.05.2017	**14.1**	**>6,000**	76.2	8,656.6	173.4	**431.2**	14.2	23.2	0.11	0.25
Romania (**Rom2**): Summer Cruise	Danube Delta, Romania	~10	03.08.2017 - 12.08.2017	24.8	**>6,000**	118.4	**11,633.1**	26.7	377.3	25.4	**34.6**	**0.02**	0.37
Romania (**Rom3**): Fall Cruise	Danube Delta, Romania	~10	13.10.2017 - 21.10.2017	177.9	**>6,000**	103.9	9,425.6	**6.9**	376.7	14.2	17.8	0.11	0.26

Table 4.2: Cruise table for all field campaigns in 2016 and 2017, with cruise/ship names (cruise ID in bold), areas, as well as observed maximum to minimum values for all measured parameters (in bold). For pCO_2, the sensor is only factory-calibrated up to 6,000 ppm; therefore this was deemed as the maximum in these circumstances.

4.4.1 Extended calibration

Compared with the prior calibration curve from the conducted calibration at KMCON factory, the final extended 5-degree polynomial had to be shifted slightly (690 ppm), which was expected due to slightly different calibration methods, so that both polynomials matched at the top of the calibration range from KMCON ($\sim 6,000$ ppm). The sensor was able to reach values of nearly 30,000 ppm before starting to reach saturation (Fig. 4.4). Given this range was of similar magnitude as discrete samples and previous pCO_2 data from the Danube Delta (M. S. Maier unpubl.: reaching values of up to and over 20,000 ppm), the correction was applied to all data above 6,000 ppm. However, note the general uncertainty of the sensor at this range is larger than that at company 'operational values' and due to the longer time period between deployments, spring and summer excursions have an unquantified increased error. We assume 3% as a conservative estimate of the overall accuracy of the xCO_2 measurements in the extended range ($>$ 6,000 ppm). From the noise of the signal during the calibrations, the estimated precision is $\pm$ 1% of the CO_2 reading and we believe even at this reduced accuracy the observations in the high pCO_2 range are of significant scientific value.

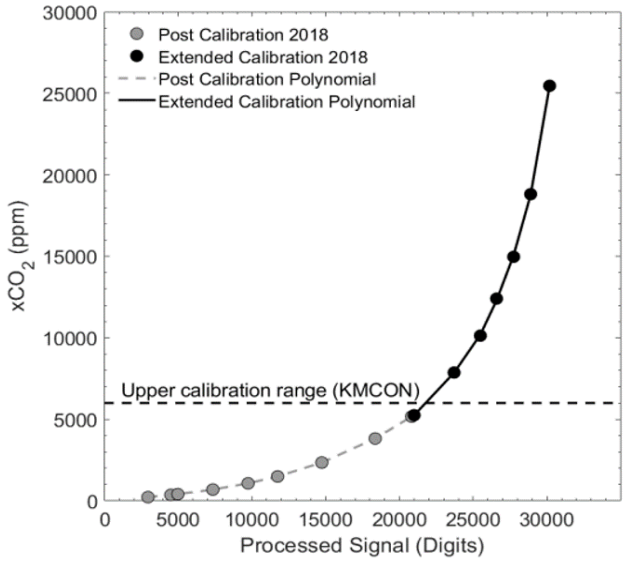

Figure 4.4: Calibration polynomial from the post-cruise manufacturer calibration (grey dots) (KMCON) and the manual extended calibration curve (black dots), with the top range of the KMCON calibration range indicated (dashed line) above which the non-linear behavior of the NDIR (non-dispersive infrared spectrometry) sensor becomes stronger. Processed signal was calculated from the raw and reference signal data during processing.

4.4.2 RT-Correction analysis

Although RT-Corr is not a new method within the ocean/brackish waters (see e.g. Fiedler et al. 2013; Gülzow et al. 2011; Miloshevich et al. 2004), the results of both the HC-CO_2 and HC-CH_4 corrections show high promises and absolute need in freshwaters for such sensors measuring in highly diverse regions. The HC-CO_2 RT-Corr laboratory experiments quantitatively show the effect of temperature and flow and point to the importance of recording the flow data (Fig. 4.5). An example of the estimation of t_{63} is given in Fig. 4.5(b), which shows the signal recovery following a 'zeroing' procedure, with $t_{63} = 93$ s. Both, increased flow rate and temperature reduce the RT of the sensor significantly. As stated before, due to varying flow and temperature, the HC-CO_2 RT was determined by the laboratory experiments shown in Fig. 4.5(a) for limnic regions.

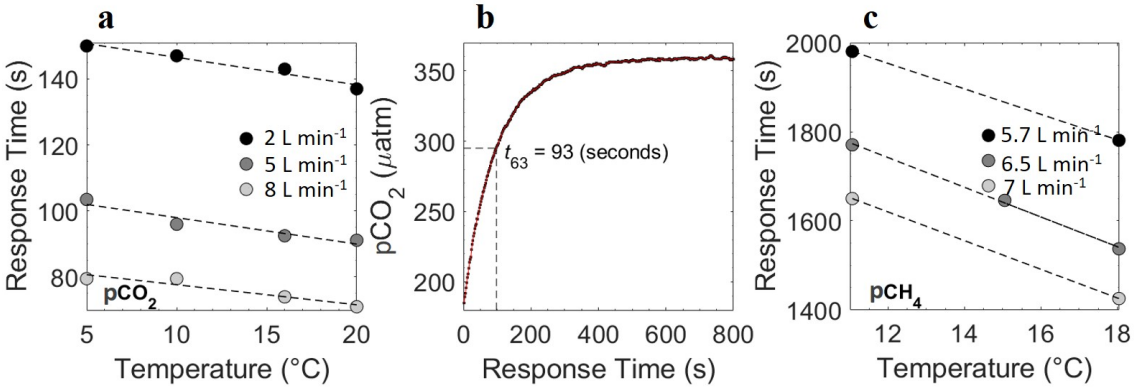

Figure 4.5: Response Time (RT) (s) of the HC-CO_2 determined at 4 temperatures within controlled laboratory conditions for different water flow rates (2, 5 and 8 L min^{-1}) with errors too small to see (a). An example of the output (b) shows how t63 is retrieved after a zeroing interval with t_{63} determined by the models fit (fit line in red). RT for pCH_4 also shown (c) for flow rates of 5.7, 6.5, and 7 L min^{-1} conducted in controlled conditions within KMCON.

The RT of the HC-CH_4 was far higher than for CO_2 and varied between 1,425 – 1,980 s (Fig. 4.5c) depending on temperature and flow, with both higher temperature and flow rate yielding shorter RT. This was then applied to the raw HC-CH_4 data and compared with the pO_2, which has an RT of < 3 s (KMCON HydroFlash user manual) and therefore does not require an RT correction, to qualitatively assess the suitability of the correction (Fig. 4.6). Note the inverted pO_2 due to typically having an inverse relationship with pCH_4.

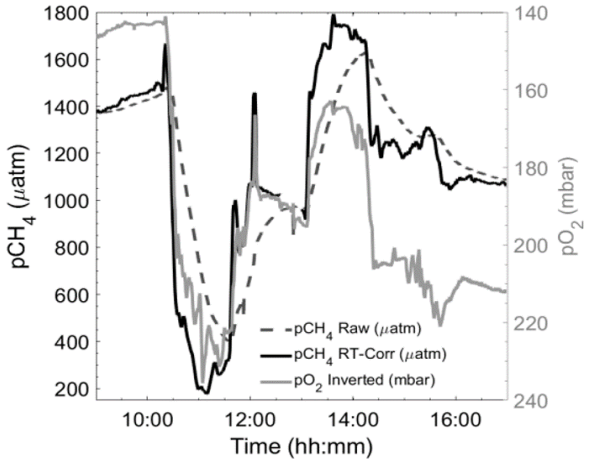

Figure 4.6: Section of a 24hr-cycle of data from the autumn limnic cruise (Rom3), showing raw (black dashed) and RT-Corr (black solid line) pCH_4 μatm measured by the HC-CH_4 with inverted pO_2 mbar (grey) as a reference for true spatiotemporal variability.

4.4.3 Verification by discrete sample comparison

CO_2

Discrete pCO_2 was calculated from TA and DIC measurements, with an average precision from replicates of 1.48 μmol kg^{-1} (TA) and 1.04 μmol kg^{-1} (DIC) after removal of one outlier sample. During the oceanic cruise, this provided a mean difference within the open ocean of -0.28 $\pm$ 5.48 μatm ($\pm$SD) to the data measured by the HC-CO_2 flow through system (HC-CO_2 pCO_2 – calculated pCO_2 [DIC and TA]), with the mean increasing with more variability and productivity within the water along the Patagonia Shelf waters up to 5.26 $\pm$ 4.22 μatm ($\pm$SD) (possibly pointing at the onset of a biofouling issue within the tubing). Oceanic pCO_2 sensors are needed to operate with an overall

accuracy of ± 2 μatm (Pierrot et al. 2009), therefore this sensor performance throughout the open ocean was considered very good. A comparison between the performances of the HC-CO_2 is shown in Fig. 4.7, where each region has been separated. The comparison for the brackish water is against the calibrated data from the state-of-the-art equilibrator set up using an LGR oa-ICOS (Gülzow et al. 2011) showing an offset of -2.87 ± 7.71 (±SD) μatm (HC-CO_2 – Reference pCO_2). Note the change in pCO_2 for each region, varying from under saturated (mainly oceanic waters) to supersaturated (brackish waters) and almost 20,000 μatm within the limnic waters during Rom1 (Fig. 4.7).

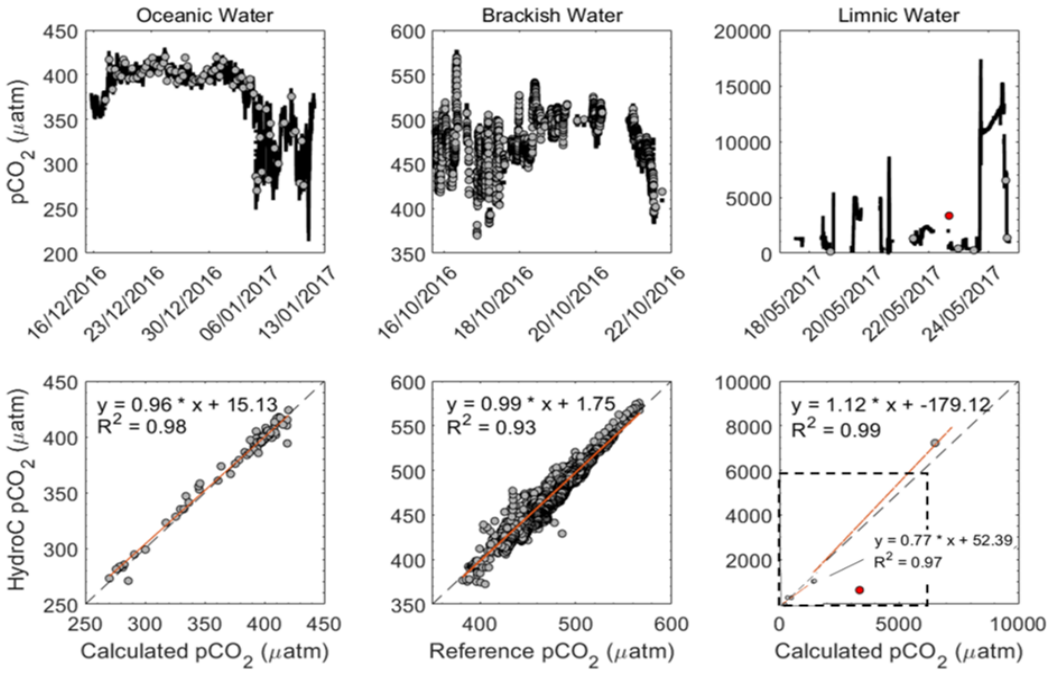

Figure 4.7: pCO_2 (μatm) from the HC-CO_2 within the 3 regions: oceanic (including the open ocean and the Patagonian shelf), brackish and limnic waters with the reference data used. The top graphs show the overall transects with HC-CO_2 data as black line and the reference data as grey dots (date as d/month/yr). The lower are property-property plots showing the 1:1 line (dashed) and line of best linear fit (orange). For validation of our system we used calculated pCO_2 from TA and DIC using CO_2SYS for both oceanic and limnic waters, whereas a reference system for the brackish waters as described above. During the Rom1 (limnic cruise), only poisoned samples were used as a reference (n = 7), with the outlier in red (sample with unclear match to flow-through data excluded from fit), with the box (dashed) indicating the 6,000 ppm KMCON calibration limit.

Between calculated pCO_2 (from TA and DIC) and measured pCO_2 (HC-CO_2) in the limnic cruise, the deviation was not unexpected due to the likely presence of organic alkalinity that causes an unknown TA bias that leads to an offset in the calculated pCO_2 (Abril et al. 2015). These input measurements of TA and DIC themselves had an average precision based on replicates of 1.03 μmol kg^{-1} and 0.27 μmol kg^{-1} for TA and DIC respectively.

CH_4

The average offset of the reference system to the HC-CH_4 during the first half of the brackish cruise was -0.95 ± 0.19 (±SD) μatm for the RT-Corr pCH_4 data (Fig. 4.8). This gave an average offset within the manufacturer accuracy specification range of ±2 μatm, with a mean offset of 0.79 ± 0.64 (±SD) μatm. Both sensors showed the same variability and magnitude to one another even with the offset (Fig. 4.8). With little

noise from both systems, natural variability was witnessed by both to further assure the system was running efficiently.

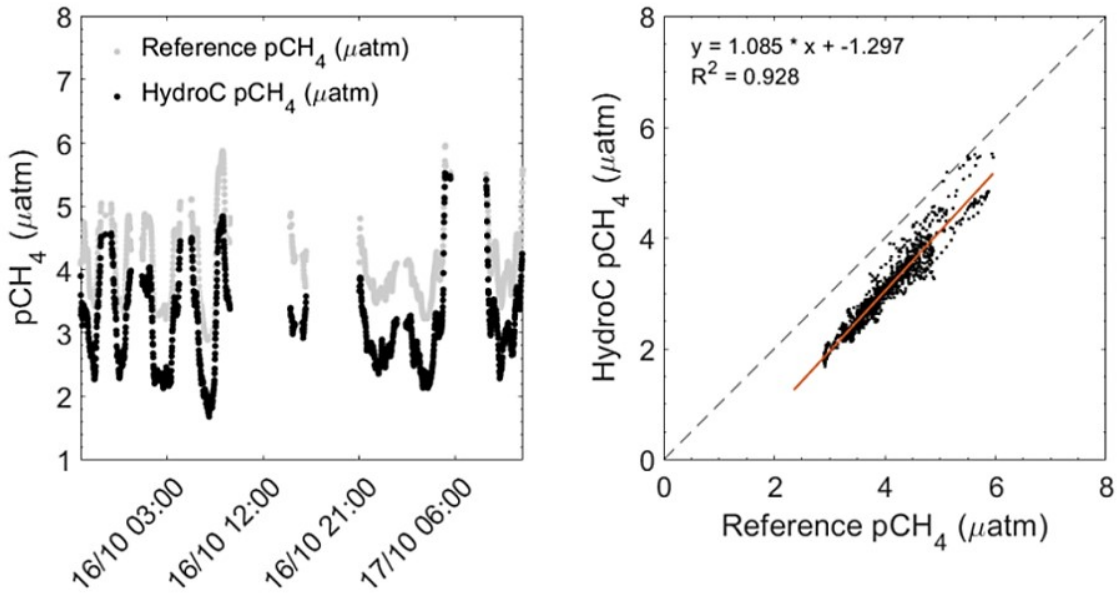

Figure 4.8: pCH_4 μatm data from the HC-CH_4 during the brackish cruise (EMB 142: R/V Elisabeth Mann Borgese) expedition in the Western Baltic Sea with the reference system over the first half of the cruise. Left shows the HC-CH_4 data with a negative offset resulting in lower concentrations compared to that of the reference data. Right gives a 1:1 plot with regression line (R^2 = 0.928), illustrating the constant offset, but similar slope of data. Within the brackish waters, the offset was within the specifications from KMCON, yet both values (reference and HC-CH_4) were in the range of that previously found within the region (Gülzow et al. 2013).

During the limnic campaigns, CH_4 showed extreme spatial and temporal differences, which highlights the need of high spatiotemporal coverage. Given the previous evaluation of the RT-Corr, this heavily improved the accuracy of the HC-CH_4 within the limnic system of Romania (HC-CH_4 – measured pCH_4: Rom1: from -164.3 ± 1,117.3 (±SD) μatm to 182.6 ± 591.3 (±SD) μatm; Rom2: from 609.3 ± 1,065 (±SD) μatm to 537.9 ± 1,145 (±SD) μatm and Rom3: from 466.5 ± 383 (±SD) μatm to 457.1 ± 376 (±SD) μatm (Rom1 shown in Fig. 4.9). Matching discrete sample data with continuous sensor data that has a long RT, becomes very complicated in highly variable situations. The effect of variable situations was also noticeable within the triplicates of the discrete samples, some varying by over 400 μatm (with an average variability between repeated samples at 122.6 ± 100.9 (±SD) μatm), leading to the offset with the HC-CH_4 seeming reasonable. The agreement between sensor data and discrete samples increased significantly with the RT-Corr, shown in Fig. 9 with the R^2 improving from 0.33 to 0.93 and the slope from 0.36 to 1.25. Peaks within the data are also observed within the discrete measurements (Fig. 4.9 bottom) in combination with the sensor data e.g. in the lower graph of Fig. 4.9 between 20/05 and 21/05. It has to be noted that the determination of dissolved CH_4 concentrations from discrete samples is also not fully mature and shows significant inter-laboratory offsets (Wilson et al. 2018) and thus, the observed discrepancy is likely not to be entirely caused by our sensor-based measurements.

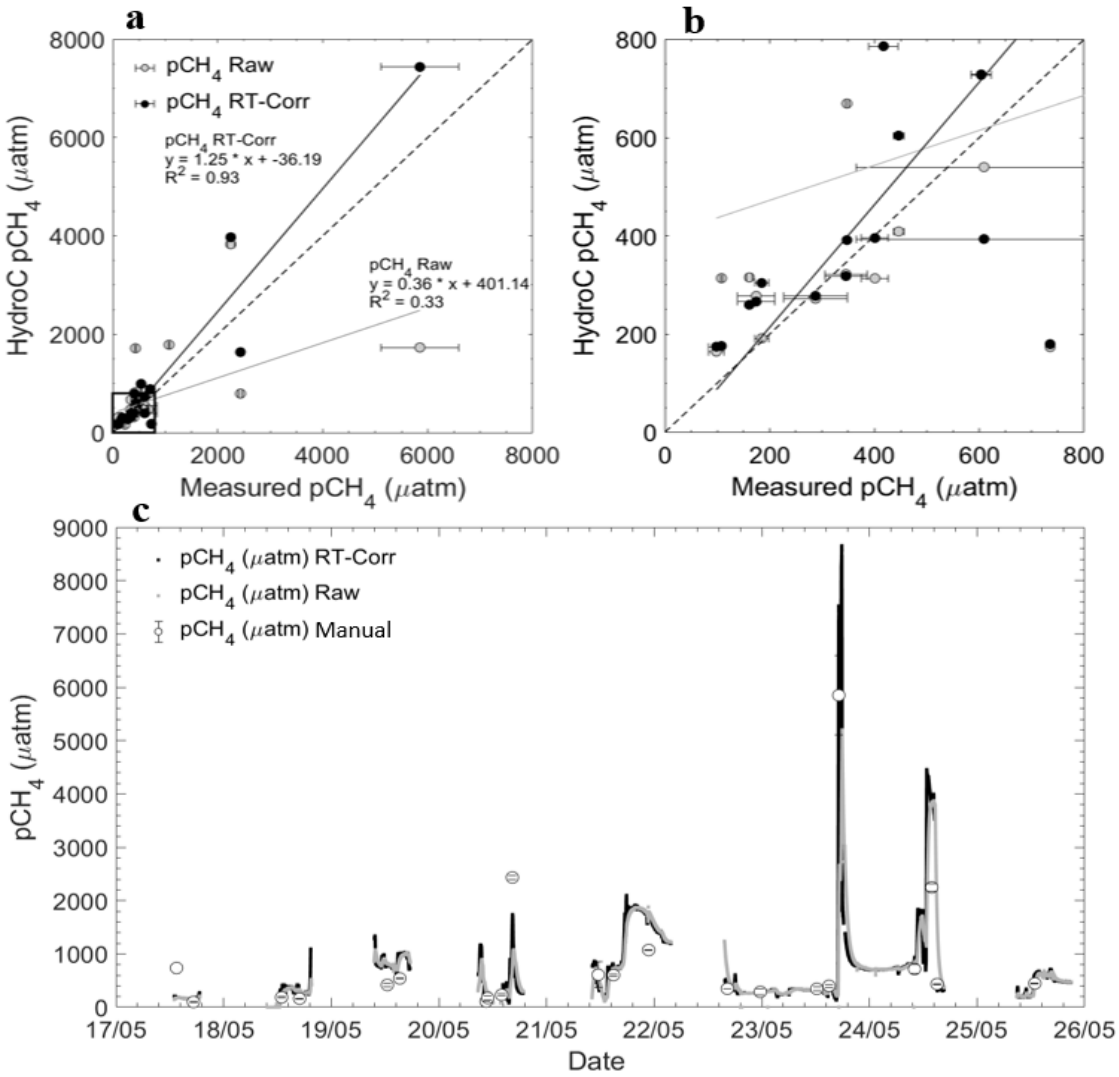

Figure 4.9: (a) Rom1 pCH_4 μatm data versus measured discrete samples of pCH_4 μatm with both raw HC-CH_4 data and response time corrected (RT-Corr) data over the full range of concentrations. (b) A close up view of the lower 800 μatm with errors for the measured samples against the HC-CH_4 data. The grey line signaling the line of best fit for the raw pCH_4 and black line signaling the RT-Corr pCH_4 μatm. (c) Full transect with discrete pCH_4 μatm samples for the spring cruise over time (date in dd/mm), error bars too small to see.

O_2

During the oceanic cruise, after the post offset-correction (stated above), O_2 μmol L^{-1} had an average offset of -0.1 $\pm$ 3.4 ($\pm$SD) μmol L^{-1} (HydroFlash O_2 – discrete samples O_2) over the whole transect (Fig. 4.10). The offset increased during the Patagonian Shelf waters due to the higher concentration ranges and gradients found along the shelf, possibly indicating an emerging biofouling issue of the sensor or within the casing surrounding the sensor. This demonstrated the overall long-term stability and reliability of the O_2 optode even in an area with such extreme hydrographic variability. This was expected due to optodes being used widely in multiple environments (see Bittig et al. 2018, Kokic et al. 2016 and Wikner et al. 2013 for oceanic, coastal and fresh water examples).

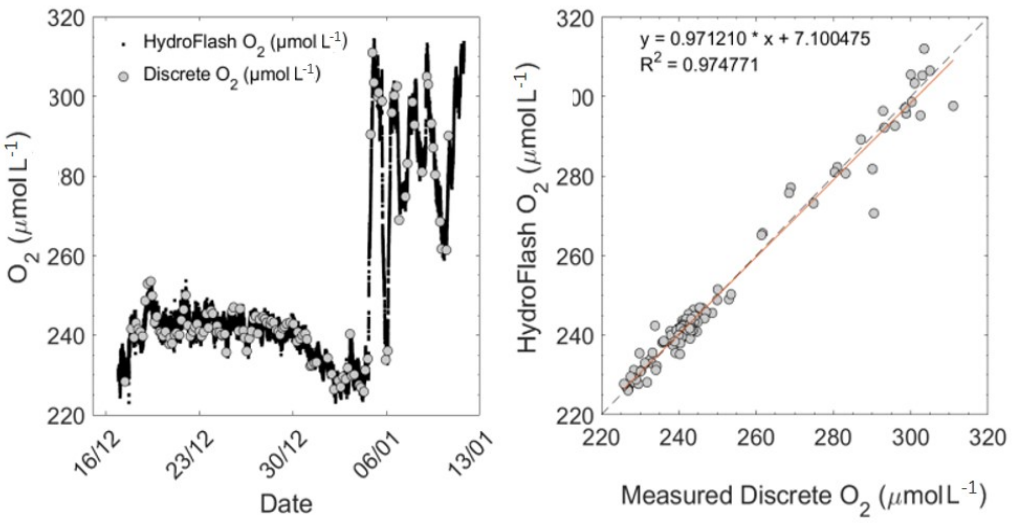

Figure 4.10: Oxygen concentration during M133 from re-calibrated continuous optode and discrete Winkler titration measurements (left panel), and property-property plot (right panel). For the open ocean and shelf waters the mean offset is -0.08 ± 1.89 (±SD) μmol L^{-1} and -0.15 ± 6.49 (±SD) μmol L^{-1}, respectively. Higher variability towards the end of the transect is due to entering the productive Patagonian Shelf (dd/mm: 06/01 - 13/01, 2017), also seen in higher concentrations of O_2.

4.5 Discussion

We have presented a portable, easily accessible, quick to set up multi-gas measurement system that can autonomously measure across the entire LOAC. The operational boundaries of these sensors were tested over long deployment durations (1 month), small spatial scales and under a wide range of operational environmental conditions. The limnic cruises were ideally suited to test the flexibility of these sensors, with concentration ranges reaching almost 30,000 μatm for pCO_2, over 10,000 μatm for pCH_4, and O_2 ranging from supersaturated to suboxic. Direct comparisons with the CH_4 and CO_2 concentrations show relatively similar variations as previous measurements within the Danube Delta lakes (Durisch-Kaiser et al. 2008; Pavel et al. 2009). Overall the set-up showed a good performance with continuous data collection providing values within the expected ranges for pCO_2 across different salinity areas and when split into lakes rivers and channels (Hope et al. 1996; Bouillon and Dehairs 2007; Lynch et al. 2010). However, in comparison to rivers and streams of similar size, pCH_4 determined in this study, had generally higher overall concentrations (Wang et al. 2009; Crawford et al. 2017) and higher overall medians (Stanley et al. 2015). Yet, they are within the range found for other freshwater systems, and on a similar scale with other regions showing abnormal peaks (Bange et al. 2019). Below we present data examples from our various field campaigns illustrating the utility and observational power of our approach to resolve both spatial and temporal variability in parallel for all measured quantities and at very high resolution

4.5.1 Temporal variability

In the Danube delta, portability of the set-up allowed to focus on temporal variability for specific regions. Fig. 4.11 displays data from a two-week field campaign (Rom3), with areas of stationary measurements over extended time periods (grey shading in Fig. 11). Data were continuously logged for all parameters throughout the campaigns, with interruptions only when the houseboat docked. During each campaign, temporal

variability showed differences between the regions (lakes, rivers and channels). When looking at Fig. 4.11. this can be seen between each stationary zone (grey shading). The first of which was in a channel next to lake Isac (Fig. 4.11, grey box on 16/10, duration 15h:26 min). An instant peak in CO_2 and CH_4 can be seen when entering the channel from the lake, coinciding with a drop in O_2. Over this diel cycle, CO_2 and O_2 are apparently governed by production and respiration, as to be expected (Nimick et al. 2011), yet with relatively constant and high CH_4 concentrations. However, during the second stationary zone (Fig. 4.11, 19/10) conducted within a lake, pCO_2 is shown to be far lower than the channel and has a steady increase from the point of stationary. The same diel pattern is shown in the final station zone (Fig. 4.11, 23/10), which is located in one of the northern channels, far from any lake. These comparisons (from channel to lake variabilities) throughout the transects show the temporal variabilities within a short distance over various regions (rivers, channels and lakes) and how they can vastly differ in both magnitude and diel pattern, even when comparing the same region (channel next, 16/10, to lake Isac to a northern channel, 23/10 Fig. 4.11).

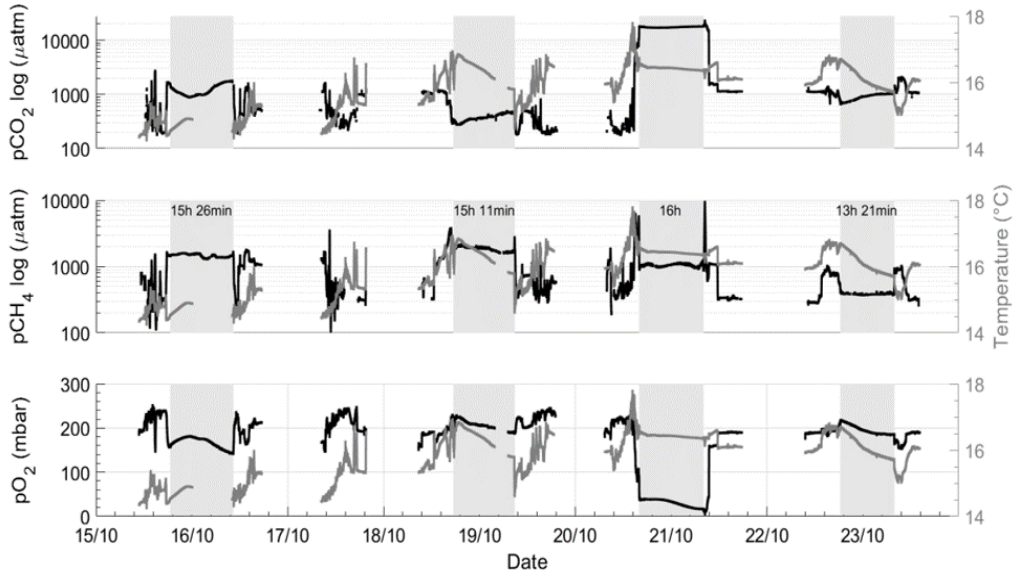

Figure 4.11: Sections acquired during the autumn limnic cruise: Rom3, showing pCO_2 (μatm, logarithmic scale), pCH_4 (μatm, logarithmic scale) and pO_2 (in mbar) and temperature (°C) (grey) across the entire deployment. Shaded areas indicate periods of stationary observations when anchored in one location, with station-keeping durations in hours and minutes given in the middle row. Gaps in data collection refer to the systems being switched off.

Looking closer into specific temporal variabilities, Fig. 4.12 shows an exemplary 24h-cycle within a small channel. This location was marked as a 'hot spot' within our transect, showing drastic concentration changes with clear coupling between O_2, pCO_2 and temperature. The pCO_2 increases from 5,000 μatm to nearly 17,000 μatm over the night, then decreases back to initial levels during the day, coinciding with sunrise and sunset, while the opposite trend for both temperature and pO_2 was observed. Timing and amplitude of these diel trends could have been lost with discrete sampling alone. Due to the same diel variation observed from this location over two of the three months (Rom1 and Rom2), uncertainties behind this variation, such as passing of water parcels anomalies or wind driven variation as suggested before (Serra et al. 2007; Bogert et al. 2012), can be ruled out as possible explanation. Although diel cycles in inland waters have been further investigated (see Nimick et al. 2011; Maher et al. 2015; Andersen et al. 2017; van Bergen et al. 2019 for channels, estuarine, lakes and pond investigations

respectively) they are generally left out when it comes to average concentrations and corresponding fluxes. Evaluating our data gives evidence that such practices have to be critically evaluated, especially given the abundance and magnitude of diel cycles observed in these regions. Any study aiming to measure representative concentrations and fluxes for limnic systems with significant diel variability will have to address this. Adequate sampling/observation schemes should be implemented to avoid strong biases (e.g. by both day-night sampling or by convoluting spatial and temporal variability in 24 h non-stationary mapping exercises).

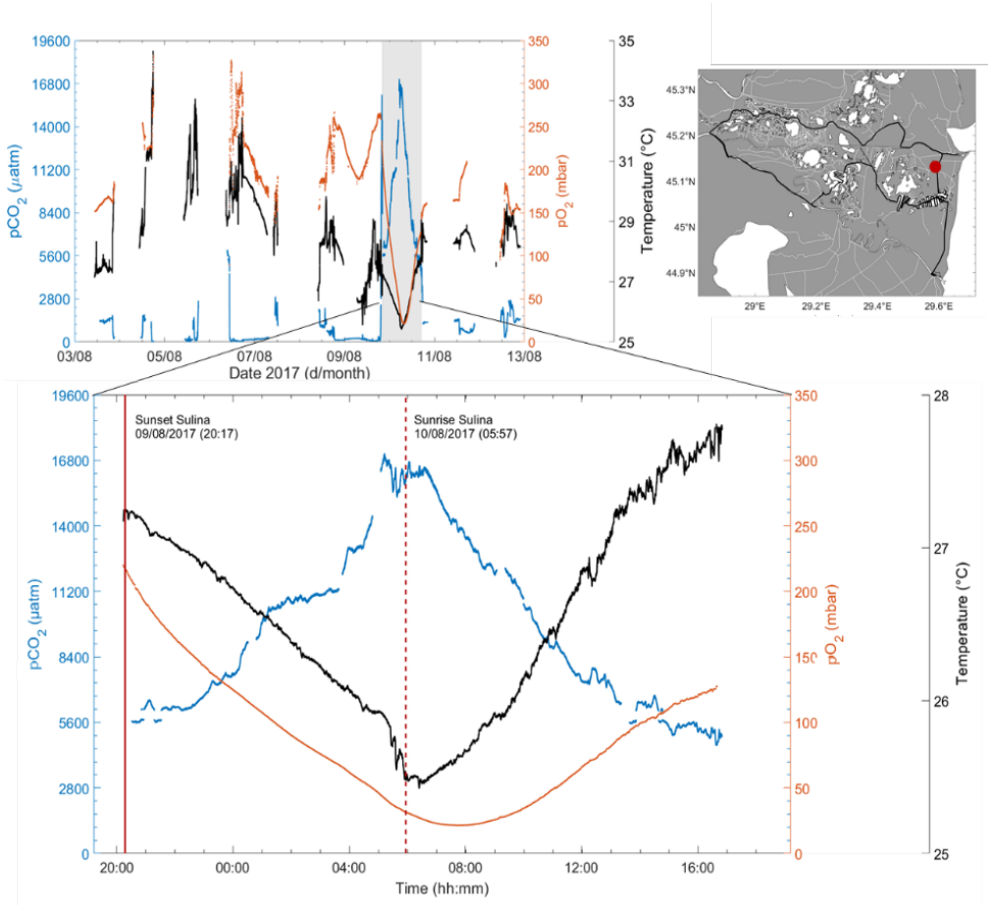

Figure 4.12: Measurements of pCO_2 (in μatm, blue), pO_2 (in mbar, orange) and temperature (in °C, black), during the Danube river campaign Rom2 in summer 2017 (top). The grey rectangle highlights a 24 h cycle acquired at a fixed location in a channel (see red dot on map). Close up of this 24 h cycle (bottom) with sunset (solid red), sunrise (dashed line red) indicated, showing extreme variability on the diel cycle time scale.

4.5.2 Spatial variability

Both system stability and sensitivity could be demonstrated nicely during the oceanic cruise (15.12.2016 – 13.01.2017: Fig. 4.13). The little spatial variability was expected over the large distance when crossing the open ocean waters of the South Atlantic Gyre. The fact that even these small variations in pCO_2, O_2, and temperature still show clear correlations, points at the very low noise level of the measurements. When entering the Patagonian shelf, two currents, the Brazil Current and Malvinas Current, meet, creating upwelling with fresh nutrients and therefore strongly increased primary production (Matano et al. 2010). These waters are characterized by high productivity with higher pO_2 and lower pCO_2 (Fig. 4.13) and increased overall variability compared to the open ocean. Some of these variabilities show the dynamic mixing between the contrasting waters masses of the confluent surface currents. This region is one of the most pro-

ductive and energetic regions throughout the ocean and is generally poorly described within models due to such dynamics (Arruda et al. 2015). The area is therefore an ideal location to demonstrate the high spatiotemporal resolution of our continuous, automatic multi-parameter approach.

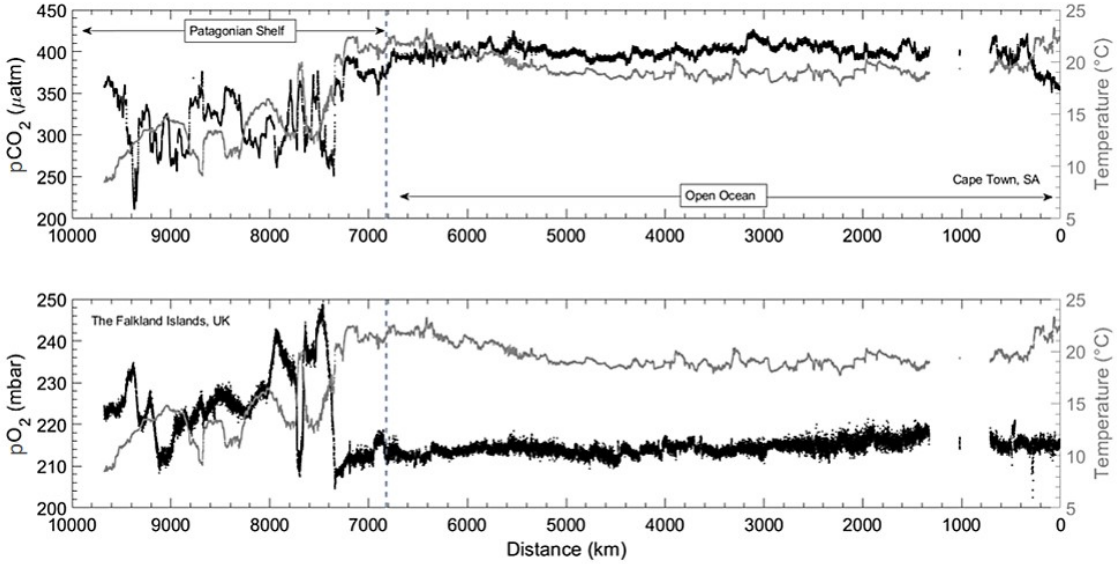

Figure 4.13: Data from the RV Meteor cruise M133 across the Atlantic Ocean (Cape Town/South Africa to the Falkland Islands/UK). Note the inverted x-axis to coincide with the direction on the map: pCO_2 (in μatm, top, black points) and pO_2 (in mbar, bottom, black points) with water temperature (in °C, grey), with an indication of the Patagonian Shelf area (left of the dashed line) and open ocean (right of the dashed line).

In contrast to the utility for reliably mapping vast ocean regions, Rom1-3 enabled to observe very small-scale spatial variability. Channels were noticeably playing a part in the spatial distribution of high pCO_2 and pCH_4 throughout the Danube Delta, as for most freshwater areas (Crawford et al. 2017). This is clearly observed during mapping of the St George river branch (Fig. 4.14). Although the variability of pCO_2 is relatively small ($\sim \pm 60$ μatm), the higher concentrations are still picked up and observed to originate from a side channel, dispersing down the river branch. Although expected, due to the real-time measurement visualization provided by the KMCON software, spatial impacts from the channels within more sensitive regions were immediately noticed, allowing for data-guided mapping. The versatility enabled us to complete small spatial scale transects, with repetitions over time to ensure the concentration changes were primarily due to spatial and not temporal variability (see multiple transects in Fig. 4.14). This enables spatial dispersion distances to be measured on such small scales.

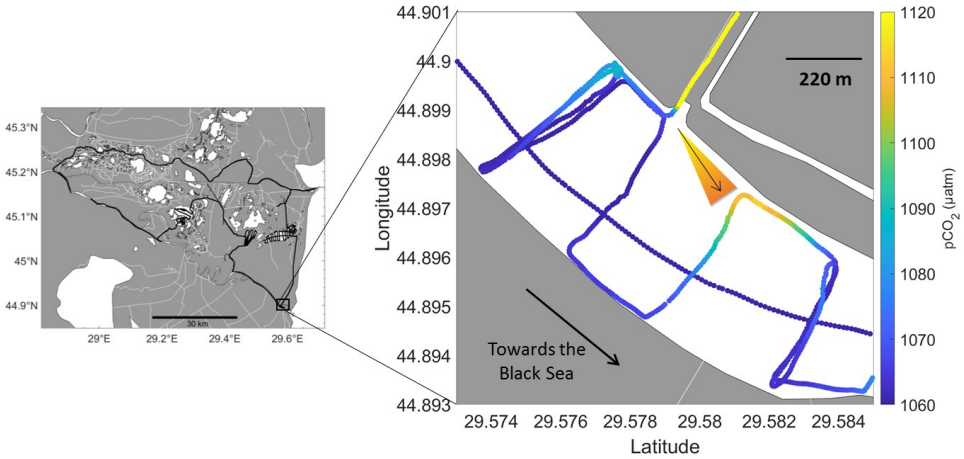

Figure 4.14: Small-scale spatial variability in pCO_2 (μatm) recorded in the Danube Delta from our river transects next to the entrance of a channel near St. George. Direction of the water flow was visible even with small changes in concentrations (arrow and interpretation of concentration gradient and flow direction is indicated to support interpretation).

In more extreme cases, small-scale spatial changes were observed in areas of joining channels during Rom3, where the pCO_2 values decreased from 14,722 μatm to 1,623 μatm in just over 4 min (Fig. 4.15). With the house boat travelling between 2-3 knots this corresponds to a distance of about 400 m (Fig. 4.15). This change was detected within a manmade channel joining Lake Roşulette towards the Sulina River Branch, arriving from the highest pCO_2 and pCH_4, along with the lowest O_2 throughout the delta transect (pCO_2 indicated on the map in Fig. 4.15). Also shown in Fig. 4.15 are the processed as well as the raw output from the HC-CO_2 (orange dashed), exemplifying the need for all corrections and post-processing steps described above to fully reveal the true spatial distribution. 'Hot spots' and areas of spatially extreme dynamics could be easily passed over with discrete or intermediate sampling. Therefore, this ability to gather such data allows for better classification of individual systems.

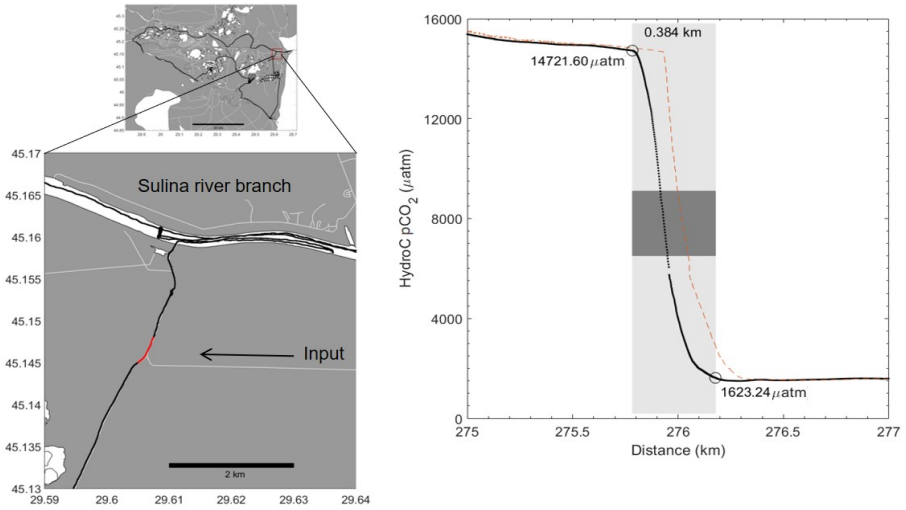

Figure 4.15: Extreme pCO_2 concentration gradient over a short time period ($\sim$ 4 min indicated by the red line on the map (left), and light grey box on graph (right)) during Rom3. Raw pCO_2 (orange dashed), compared with post-processed, response time corrected (RT-Corr) pCO_2 data (black), narrowing and improving the spatial extend of the gradient region by $\sim$ 100 m. The gradient occurred over a distance of about 400 meters due to another channel providing a different water source (left, white line indicating channel). The dark grey box symbolizes the area over the concentration change in which the houseboat passed the entrance of the entering channel.

Although not shown here, even concentration fluctuations due to vessels passing were picked up immediately within the data, usually leading to increasing CO_2 and CH_4 concentrations. With recreational activities and boat usage within some regimes increasing, this should be considered when measuring both fluxes and overall concentrations.

4.6 Conclusion

As the importance of seamless observation across the entire LOAC is becoming more apparent, enabling and openly assessing a variety of techniques across all water types is essential to improve our understanding of carbon budgets and processes especially within the inland regions. We have therefore tried to introduce oceanic precision and attention to detail into the field observations in inland water regions. The results clearly demonstrate the observational power this technology can provide, but at the same time illustrates the need for dedicated data processing addressing major sensor issues (drift, calibration range, time constants etc.) for achievement of high data quality. Although improvements can be made in terms of size and accessibility, this setup and data readings show the vitality of having high resolution multi-gas data for mapping and diel cycle extraction, which can further assist with modelling efforts and assessing concentrations and fluxes. Given there is much need for both high spatial data coverage and accurate concentrations for inland CO_2 and CH_4 measurements (Crawford et al. 2014; Meinson et al. 2016; Natchimuthu et al. 2017; Grinham et al. 2018), this type of dataset can help fill the gap in this specific region, and can further show areas of much needed improvement as previously suggested. This can enable better classification of regions, thus furthering monitoring activities and overall carbon budget investigations which benefit from enhanced data acquisitions on higher spatial and temporal resolutions. The main use of this continuous, high resolution data can be split into four main sections: (a) large scale monitoring and mapping efforts, (b) temporal variability observations (i.e., with observations in a fixed location or in Lagrangian perspective), (c) spatial variability observation (with a moving platform, often resulting in a convolution of spatial

and temporal variability) and (d) the assessment of the coupling between the different continuously observed parameters. The use of separate techniques from oceanography to limnology are slowly becoming unnecessary but there is a definite need for standardized corrections in limnology, such as in the ocean.

4.7 Acknowledgements

The research leading to these results has received funding from the European Union's Horizon 2020 research and innovation program under the Marie Sklodowska-Curie grant agreement No 643052 (C-CASCADES project) as well as Digital Earth which is coordinated by GEOMAR Helmholtz Centre for Ocean Research Kiel. We thank the captain and crews of the R/V Elizabeth Mann Borgese, R/V Meteor, R/V Littorina and from the Romanian cruises. We would also like to thank Marie-Sophie Maier, Bernhard Wahrli and Christian Teodoru, ETH Zürich, for the project collaboration and Romanian cruise assistance. Also to thank all of the KMCON team with their support and help throughout and Matthias Zimmerman, Eawag Kastanienbaum, for the development of the boat logger. Finally, we also thank those who helped with either laboratory or processing assistance; Björn Fiedler, Tobias Steinhoff, Tobias Hahn, Katharina Seelmann, Alexander Zavarsky, Dennis Booge and Jennifer Clarke, all originally from GEOMAR, Kiel.

4.8 References

Abril, G., S. Bouillon, F. Darchambeau, and others. 2015. Technical note: Large overestimation of pCO_2 calculated from pH and alkalinity in acidic, organic-rich freshwaters. Biogeosciences 12: 67–78. doi:10.5194/bg-12-67-2015

Andersen, M. R., T. Kragh, and K. Sand-Jensen. 2017. Extreme diel dissolved oxygen and carbon cycles in shallow vegetated lakes. Proc. R. Soc. B Biol. Sci. 284. doi:10.1098/rspb.2017.1427

Arruda, R., P. H. R. Calil, A. A. Bianchi, S. C. Doney, N. Gruber, I. Lima, and G. Turi. 2015. Air-sea CO_2 fluxes and the controls on ocean surface pCO_2 seasonal variability in the coastal and open-ocean southwestern Atlantic Ocean: A modeling study. Biogeosciences 12: 5793–5809. doi:10.5194/bg-12-5793-2015

Atamanchuk, D., A. Tengberg, D. Aleynik, P. Fietzek, K. Shitashima, A. Lichtschlag, P. O. J. Hall, and H. Stahl. 2015. Detection of CO_2 leakage from a simulated sub-seabed storage site using three different types of pCO_2 sensors. Int. J. Greenh. Gas Control. doi:10.1016/j.ijggc.2014.10.021

Baehr, M. M., and M. D. Degrandpre. 2004. In situ pCO_2 and O_2 measurements in a lake during turnover and stratification: Observations and modeling. 49: 330–340.

Bai, Y., W.-J. Cai, X. He, W. Zhai, D. Pan, M. Dai, and P. Yu. 2015. A mechanistic semi-analytical method for remotely sensing sea surface pCO_2 in river-dominated coastal oceans: A case study from the East China Sea. J. Geophys. Res. Ocean. 120: 2331–2349. doi:10.1002/2014JC010632

Bakker, D. C. E., B. Pfeil, C. S. Landa, and others. 2016. Surface Ocean CO_2 Atlas (SOCAT) V4. PANGAEA 8: 383–413. doi:10.1594/PANGAEA.866856

Bange, H. W. 2006. Nitrous oxide and methane in European coastal waters. Estuar. Coast. Shelf Sci. 70: 361–374. doi:10.1016/j.ecss.2006.05.042

Bange, H. W., C. H. Sim, D. Bastian, J. Kallert, A. Kock, A. Mujahid, and M. Müller. 2019. Nitrous oxide (N_2O) and methane (CH_4) in rivers and estuaries of northwestern Borneo. Biogeosciences Discuss. 1–25. doi:10.5194/bg-2019-222

Bastviken, D., I. Sundgren, S. Natchimuthu, H. Reyier, and M. Gälfalk. 2015. Technical Note: Cost-efficient approaches to measure carbon dioxide (CO_2) fluxes and con-

centrations in terrestrial and aquatic environments using mini loggers. Biogeosciences 12: 3849–3859. doi:10.5194/bg-12-3849-2015

Bastviken, D., L. J. Tranvik, J. A. Downing, P. M. Crill, and A. Enrich-Prast. 2011. Freshwater methane emissions offset the continental carbon sink. Science 331: 50. doi:10.1126/ science.1196808

Bates, T. S., K. C. Kelly, J. E. Johnson, and R. H. Gammon. 1996. A reevaluation of the open ocean source of methane to the atmosphere. J. Geophys. Res. Atmos. 101: 6953–6961. doi:10.1029/95JD03348

Becker, M., N. Andersen, B. Fiedler, P. Fietzek, A. Körtzinger, T. Steinhoff, and G. Friedrichs. 2012. Using cavity ringdown spectroscopy for continuous monitoring of $\delta 13C(CO_2)$ and $\check{N}CO_2$ in the surface ocean. Limnol. Oceanogr. Methods 10: 752–766. doi:10.4319/lom.2012.10.752

van Bergen, T. J. H. M., N. Barros, R. Mendonça, and others. 2019. Seasonal and diel variation in greenhouse gas emissions from an urban pond and its major drivers. Limnol. Oceanogr. 64: 2129–2139. doi:10.1002/lno.11173

Bittig, H. 2016. Recommendations on the conversion between oxygen quantities for Bio-Argo floats and other autonomous sensor platforms Recommended implementation.

Bittig, H. C., and A. Körtzinger. 2015. Tackling oxygen optode drift: Near-surface and in-air oxygen optode measurements on a float provide an accurate in situ reference. J. Atmos. Ocean. Technol. 32: 1536–1543. doi:10.1175/JTECH-D-14-00162.1

Bittig, H. C., A. Körtzinger, C. Neill, and others. 2018. Oxygen Optode Sensors: Principle, Characterization, Calibration, and Application in the Ocean. Front. Mar. Sci. 4: 1–25. doi:10.3389/fmars.2017.00429

Bodmer, P., M. Heinz, M. Pusch, G. Singer, and K. Premke. 2016. Carbon dynamics and their link to dissolved organic matter quality across contrasting stream ecosystems. Sci. Total Environ. 553: 574–586. doi:10.1016/J.SCITOTENV.2016.02.095

Bogert, M. C. Van De, D. L. Bade, S. R. Carpenter, J. J. Cole, M. L. Pace, P. C. Hanson, and O. C. Langman. 2012. Spatial heterogeneity strongly affects estimates of ecosystem metabolism in two north temperate lakes. 57: 1689–1700. doi:10.4319/lo.2012.57.6.1689

Borges, A. V., G. Abril, and S. Bouillon. 2018. Carbon dynamics and CO_2 and CH_4 outgassing in the Mekong delta. Biogeosciences 15: 1093–1114. doi:10.5194/bg-15-1093-2018

Borges, A. V., F. Darchambeau, C. R. Teodoru, and others. 2015. Globally significant greenhouse-gas emissions from African inland waters. Nat. Geosci. 8: 637–642. doi:10.1038/ngeO$_2$486

Bouillon, S., and F. Dehairs. 2007. Biogeochemistry of the Tana estuary and delta (northern Kenya). Limnol. Oceanogr. 52: 46–59.

Brandt, T., M. Vieweg, G. Laube, R. Schima, T. Goblirsch, J. H. Fleckenstein, and C. Schmidt. 2017. Automated in Situ Oxygen Profiling at Aquatic-Terrestrial Interfaces. Environ. Sci. Technol. 51: 9970–9978. doi:10.1021/acs.est.7b01482

Brennwald, M. S., M. Schmidt, J. Oser, and R. Kipfer. 2016. A Portable and Autonomous Mass Spectrometric System for On-Site Environmental Gas Analysis. Environ. Sci. Technol. 50: 13455–13463. doi:10.1021/acs.est.6b03669

Ciais, P., C. Sabine, and G. Bala. 2013. Carbon and Other Biogeochemical Cycles. In: Climate Change 2013: The Physical Science Basis. Contribution of Working Group I to the Fifth Assessment Report of the Intergovernmental Panel on Climate Change [Stocker, T.F., D. Qin, G.-K. Plattner, M. Tignor,.

Clarke, J. S., E. P. Achterberg, D. P. Connelly, U. Schuster, and M. Mowlem. 2017. Developments in marine pCO_2 measurement technology; towards sustained in situ observations. TrAC - Trends Anal. Chem. 88: 53–61. doi:10.1016/j.trac.2016.12.008

Cole, J. J., Y. T. Prairie, N. F. Caraco, and others. 2007. Plumbing the Global Carbon Cycle: Integrating Inland Waters into the Terrestrial Carbon Budget. Ecosystems 10: 172–185. doi:10.1007/s10021-006-9013-8

Crawford, J. T., L. C. Loken, N. J. Casson, C. Smith, A. G. Stone, and L. A. Winslow. 2014. High-Speed Limnology: Using Advanced Sensors to Investigate Spatial Variability in Biogeochemistry and Hydrology. Environ. Sci. Technol. 49: 442–450. doi:10.1021/es504773x

Crawford, J. T., L. C. Loken, W. E. West, and others. 2017. Spatial heterogeneity of within-stream methane concentrations. J. Geophys. Res. Biogeosciences 122: 1036–1048. doi:10.1002/2016JG003698

David, A. H. A. 1951. Further Applications of Range to the Analysis of Variance. Biometrika 38: 393–409.

Degrandpre, M. D., M. M. Baehr, and T. R. Hammar. 1999. Calibration-Free Optical Chemical Sensors. 71: 1152–1159.

DeGrandpre, M. D., F. L. Sayles, T. R. Hammar, and S. P. Smith. 1995. In situ measurements of seawater. Limnol. Oceanogr. 40: 969–975.

Dickson, A. G., C. L. Sabine, and J. R. Christian. 2007. Guide to Best Practices for Ocean CO_2 Measurements, North Pacific Marine Science Organization.

Dlugokencky, E., and P. Tans. 2016. Trends in atmospheric carbon dioxide. Natl. Ocean. Atmos. 98 Adm. Earth Syst. Res. Lab. NOAA/ESRL. www.esrl.noaa.gov/gmd/ccgg/trends/global.html.

Downing, J. A. 2014. Limnology and oceanography: Two estranged twins reuniting by global change. Inl. Waters 4: 215–232. doi:10.5268/IW-4.2.753

Durisch-Kaiser, E., A. Pavel, A. Doberer, J. Reutimann, S. Balan, S. Sobek, S. RĂDAN, and B. Wehrli. 2008. Nutrient retention, total N and P export, and greenhouse gas emission from the Danube Delta lakes. Geo-Eco-Marina 81–90. doi:10.5281/zenodo.57332

Fiedler, B., P. Fietzek, N. Vieira, P. Silva, H. C. Bittig, and A. Körtzinger. 2013. In situ CO_2 and O_2 measurements on a profiling float. J. Atmos. Ocean. Technol. 30: 112–126. doi:10.1175/JTECH-D-12-00043.1

Fietzek, P., B. Fiedler, T. Steinhoff, and A. Körtzinger. 2014. In situ quality assessment of a novel underwater pCO_2 sensor based on membrane equilibration and NDIR spectrometry. J. Atmos. Ocean. Technol. 31: 181–196. doi:10.1175/JTECH-D-13-00083.1

Friedlingstein, P., M. W. Jones, M. O'Sullivan, and others. 2019. Global Carbon Budget 2019. Earth Syst. Sci. Data 1783–1838. doi:10.5194/essd-11-1783-2019

Garcia, H. E., and L. I. Gordon. 1992. Oxygen solubility in seawater: Better fitting equations. Limnol. Oceanogr. 37: 1307–1312. doi:10.4319/lo.1992.37.6.1307

Grinham, A., S. Albert, N. Deering, M. Dunbabin, D. Bastviken, B. Sherman, C. E. Lovelock, and C. D. Evans. 2018. The importance of small artificial water bodies as sources of methane emissions in Queensland, Australia. Hydrol. Earth Syst. Sci. 22: 5281–5298. doi:10.5194/hess-22-5281-2018

Gülzow, W., G. Rehder, J. S. V. Deimling, T. Seifert, and Z. Tóth. 2013. One year of continuous measurements constraining methane emissions from the Baltic Sea to the atmosphere using a ship of opportunity. Biogeosciences 10: 81–99. doi:10.5194/bg-10-81-2013

Gülzow, W., G. Rehder, B. Schneider, J. Schneider, and B. Sadkowiak. 2011. A new method for continuous measurement of methane and carbon dioxide in surface waters using off-axis integrated cavity output spectroscopy (ICOS): An example from the Baltic Sea. Limnol. Oceanogr. Methods 9: 176–184. doi:10.4319/lom.2011.9.176

Holgerson, M. A., and P. A. Raymond. 2016. Large contribution to inland water CO_2 and CH_4emissions from very small ponds. Nat. Geosci. 9: 222–226. doi:10.1038/nge$O_2$654

Hope, D., T. K. Kratz, and J. L. Riera. 1996. Relationship between pCO_2 and Dissolved Organic Carbon in Northern Wisconsin Lakes. Journal of environmental quality, 25(6):1442-1445

Hunt, C. W., L. Snyder, J. E. Salisbury, D. Vandemark, and W. H. McDowell. 2017. $SIPCO_2$: A simple, inexpensive surface water pCO_2 sensor. Limnol. Oceanogr. Methods 15: 291–301. doi:10.1002/lom3.10157

Johnson, K. ., J. M. Sieburth, P. J. le. Williams, and L. Brändström. 1987. Coulometric total carbon dioxide analysis for marine studies: Automation and calibration. Mar. Chem. 21: 117–133. doi:10.1016/0304-4203(87)90033-8

Johnson, M. S., M. F. Billett, K. J. Dinsmore, M. Wallin, K. E. Dyson, and R. S. Jassal. 2009. Direct and continuous measurement of dissolved carbon dioxide in freshwater aquatic systems-method and applications. Ecohydrology 3:1. doi:10.1002/eco.95

Kokic, J., E. Sahlée, A. Brand, and S. Sobek. 2016. Low sediment-water gas exchange in a small boreal lake. J. Geophys. Res. Biogeosciences 121: 2493–2505. doi:10.1002/2016JG003372

Lewis, E., D. Wallace, and L. J. Allison. 1998. 1998. CO_2SYS-Program developed for the CO_2 system calculations. Carbon Dioxide Inf Anal Center Report ORNL/CDIAC-105

Lynch, J. K., C. M. Beatty, M. P. Seidel, L. J. Jungst, and M. D. Degrandpre. 2010. Controls of riverine CO_2 over an annual cycle determined using direct , high temporal resolution pCO_2 measurements. 115: 1–10. doi:10.1029/2009JG001132

Maher, D. T., K. Cowley, I. R. Santos, P. Macklin, and B. D. Eyre. 2015. Methane and carbon dioxide dynamics in a subtropical estuary over a diel cycle: Insights from automated in situ radioactive and stable isotope measurements. Mar. Chem. 168: 69–79. doi:10.1016/j.marchem.2014.10.017

Matano, R. P., E. D. Palma, and A. R. Piola. 2010. The influence of the Brazil and Malvinas Currents on the Southwestern Atlantic Shelf circulation. Ocean Sci. 6: 983–995. doi:10.5194/os-6-983-2010

Meinson, P., A. Idrizaj, P. Nõges, T. Nõges, and A. Laas. 2016. Contunious and high-frequency measurements in limnology: History, applications and future challenges. Environ. Rev. 24: 52–62. doi:10.1139/er-2015-0030

Millero, F. J. 1979. The Thermodynamics of the Carbonate System in seawater. Geochim. Cosmochim. Acta 43: 1651–1661.

Millero, F. J. 2010. Carbonate constants for estuarine waters. Mar. Freshw. Res. 61: 139–142. doi:10.1071/MF09254

Millero, F. J., T. B. Graham, F. Huang, H. Bustos-Serrano, and D. Pierrot. 2006. Dissociation constants of carbonic acid in seawater as a function of salinity and temperature. Mar. Chem. 100: 80–94. doi:10.1016/j.marchem.2005.12.001

Miloshevich, L. M., A. Paukkunen, H. Vömel, and S. J. Oltmans. 2004. Development and validation of a time-lag correction for Vaisala radiosonde humidity measurements. J. Atmos. Ocean. Technol. 21: 1305–1327.

Mintrop, L., F. F. Pérez, M. González-Dávila, M. Santana-Casiano, and A. Körtzinger. 2000. Alkalinity determination by potentiometry: intercalibration using three different methods. 26: 23–37.

Natchimuthu, S., M. B. Wallin, L. Klemedtsson, and D. Bastviken. 2017. Spatio-temporal patterns of stream methane and carbon dioxide emissions in a hemiboreal catchment in Southwest Sweden. Sci. Rep. 7: 1–12. doi:10.1038/srep39729

Nimick, D. A., C. H. Gammons, and S. R. Parker. 2011. Diel biogeochemical processes and their effect on the aqueous chemistry of streams: A review. Chem. Geol. 283: 3–17. doi:10.1016/j.chemgeo.2010.08.017

Nisbet, E. G., M. R. Manning, E. J. Dlugokencky, and others. 2019. Very Strong

Atmospheric Methane Growth in the 4 Years 2014–2017: Implications for the Paris Agreement. Global Biogeochem. Cycles 33: 318–342. doi:10.1029/2018GB006009

Palmer, S. C. J., T. Kutser, and P. D. Hunter. 2015. Remote sensing of inland waters: Challenges, progress and future directions. Remote Sens. Environ. 157: 1–8. doi:10.1016/j.rse.2014.09.021

Park, P. K. 1969. Oceanic CO_2 system: an evaluation of ten methods of investigation. Limnol. Oceanogr. 14: 179–186. doi:10.4319/lo.1969.14.2.0179

Pavel, A., E. Durisch-kaiser, S. Balan, S. Radan, S. Sobek, and B. Wehrli. 2009. Sources and emission of greenhouse gases in Danube Delta lakes. Environ. Sci. Pollut. Res. 16: 86–91. doi:10.1007/s11356-009-0182-9

Pierrot, D., C. Neill, K. Sullivan, and others. 2009a. Recommendations for autonomous underway pCO_2 measuring systems and data-reduction routines. Deep. Res. Part II Top. Stud. Oceanogr. 56: 512–522. doi:10.1016/j.dsr2.2008.12.005

Pierrot, D., C. Neill, K. Sullivan, and others. 2009b. Recommendations for autonomous underway pCO_2 measuring systems and data-reduction routines. Deep. Res. Part II Top. Stud. Oceanogr. 56: 512–522. doi:10.1016/j.dsr2.2008.12.005

Le Quéré, C., R. M. Andrew, P. Friedlingstein, and others. 2017. Global Carbon Budget 2017. Earth Syst. Sci. Data 1–79. doi:10.5194/essd-2017-123

Raymond, P. a, J. Hartmann, R. Lauerwald, and others. 2013. Global carbon dioxide emissions from inland waters. Nature 503: 355–359. doi:10.1038/nature12760

Regnier, P., P. Friedlingstein, P. Ciais, and others. 2013. Anthropogenic perturbation of the carbon fluxes from land to ocean. Nat. Geosci. 6: 597–607. doi:10.1038/ngeo 1830

Rhee, T. S., A. J. Kettle, and M. O. Andreae. 2009. Methane and nitrous oxide emissions from the ocean: A reassessment using basin-wide observations in the Atlantic. J. Geophys. Res. 114: D12304. doi:10.1029/2008JD011662

Schimel, D., P. Sellers, B. Moore III, and others. 2016. Observing the carbon-climate system. arXiv Prepr. arXiv1604.02106.

Schneider, B., W. Gülzow, B. Sadkowiak, and G. Rehder. 2014. Detecting sinks and sources of CO_2 and CH_4 by ferrybox-based measurements in the Baltic Sea: Three case studies. J. Mar. Syst. 140: 13–25. doi:10.1016/j.jmarsys.2014.03.014

Schuster, U., A. Hannides, L. Mintrop, and A. Körtzinger. 2009. Sensors and instruments for oceanic dissolved carbon measurements. Ocean Sci. 5: 547–558. doi:10.5194/os-5-547-2009

Serra, T., J. Vidal, X. Casamitjana, M. Soler, and J. Colomer. 2007. The role of surface vertical mixing in phytoplankton distribution in a stratified reservoir. 52: 620–634.

Stanley, E. H., L. C. Loken, J. T. Crawford, S. K. Oliver, N. J. Casson, and S. T. Christel. 2015. The ecology of methane in streams and rivers: patterns, controls, and global significance. Ecol. Monogr. 86: 146–171. doi:10.1890/15-1027.1

Takahashi, T. 1961. Carbon dioxide in the atmosphere and in Atlantic Ocean water. J. Geophys. Res. 66: 477. doi:10.1029/JZ066i002p00477

Takahashi, T., J. Olafsson, J. G. Goddard, D. W. Chipman, and S. C. Sutherland. 1993. Seasonal variation of CO_2 and nutrients in the high-latitude surface oceans: A comparative study. Global Biogeochem. Cycles 7: 843–878. doi:10.1029/93GB02263

Takahashi, T., S. C. Sutherland, R. Wanninkhof, and others. 2009. Climatological mean and decadal change in surface ocean pCO_2, and net sea-air CO_2 flux over the global oceans. Deep. Res. Part II Top. Stud. Oceanogr. 56: 554–577. doi:10.1016/j.dsr2.2008.12.009

Valsala, V., and S. Maksyutov. 2010. Simulation and assimilation of global ocean pCO_2 and air–sea CO_2 fluxes using ship observations of surface ocean pCO_2 in a sim-

plified biogeochemical offline model. Tellus B Chem. Phys. Meteorol. 62: 821–840. doi:10.1111/j.1600-0889.2010.00495.x

Wang, D., Z. Chen, W. Sun, B. Hu, and S. Xu. 2009. Methane and nitrous oxide concentration and emission flux of Yangtze Delta plain river net. Sci. China, Ser. B Chem. 52: 652–661. doi:10.1007/s11426-009-0024-0

Waugh, D. W., T. M. Hall, B. I. Mcneil, R. Key, and R. J. Matear. 2006. Anthropogenic CO_2 in the oceans estimated using transit time distributions. Tellus B Chem. Phys. Meteorol. 58: 376–389. doi:10.1111/j.1600-0889.2006.00222.x

Wehrli, B. 2013. Conduits of the carbon cycle. Nature 503: 9–10. doi:10.1038/503346a

Weiss, R. F., and B. A. Price. 1980. Nitrous Oxide Solubility in Water and Seawater. Mar. Chem. 8: 347–359.

Werle, P. W. 2004. Diode-Laser Sensors for In-Situ Gas Analysis. Laser Environ. Life Sci. 223–244. doi:10.1007/978-3-662-08255-311

Wikner, J., S. Panigrahi, A. Nydahl, E. Lundberg, U. Båmstedt, and A. Tengberg. 2013. Precise continuous measurements of pelagic respiration in coastal waters with Oxygen Optodes. Limnol. Oceanogr. Methods 11: 1–15. doi:10.4319/lom.2013.11.1

Wilson, S. T., H. W. Bange, D. L. Arévalo-Martínez, and others. 2018. An intercomparison of oceanic methane and nitrous oxide measurements. Biogeosciences 15: 5891–5907. doi:10.5194/bg-15-5891-2018

Xenopoulos, M. A., J. A. Downing, M. D. Kumar, S. Menden-Deuer, and M. Voss. 2017. Headwaters to oceans: Ecological and biogeochemical contrasts across the aquatic continuum. Limnol. Oceanogr. 62: S3–S14. doi:10.1002/lno.10721

Yoon, T. K., H. Jin, N.-H. Oh, and J.-H. Park. 2016. Technical note: Assessing gas equilibration systems for continuous pCO_2 measurements in inland waters. Biogeosciences 13: 3915–3930. doi:10.5194/bg-13-3915-2016

Inland modelling of carbonate systems variables

In preparation as: Anna Canning, Marie-Sophie Maier, Arne Körtzinger 'In-depth spatiotemporal analyses of carbon and oxygen dynamics using high-resolution data in Europe's second largest delta: the Danube River Delta.' [In prep.]

5.1 Abstract

With the complexity of inland waters, especially with the river-ocean interface being known to be one of the most dynamic systems, acquiring data at high spatiotemporal resolution to fully assess the dynamics of the aquatic systems is becoming increasingly important. However, inland regions are generally studied either using discrete sample data, or sensor data specifically from one location which typically miss the full spatiotemporal variability. Here, with the use of a novel sensor package to acquire continuous data for pCO_2, pCH_4, O_2 and temperature/conductivity at a frequency of up to 1 Hz, we were able to create an in-depth assessment of the Danube River Delta, across lakes, rivers and channels and over three seasons with special focus on CO_2/O_2 dynamics. Focus was also put on specific aspects such as 'hot spots' as well diel cycles. Using this data, as well as data from collected discrete samples, we were also able to create a continuous dissolved inorganic carbon (DIC) and alkalinity (TA) dataset enabling us to analyze and make informed assumptions of the potential influence of reed beds, groundwater impacts and the possibility of carbonate buffering within the system. We found that the regions (lakes, rivers and channels) varied differently with their ΔDIC / ΔO_2 relationship, with rivers and channels being mainly supersaturated in pCO_2 while undersaturated in oxygen. Further analyses also divulged that regions showed clear lateral connectivity throughout the delta depending on months and flow regimes, e.g. channel dynamics influencing lakes. The data also shed light on the magnitude of diel cycles which can have significant impacts on sampling strategies for inland waters.

5.2 Introduction

River delta systems host some of the most diverse ecosystems, with the rivers depositing sediment over centuries creating diverse wetlands (Overeem and Syvitski, 2009). They are highly dynamic and vulnerable, yet extremely important, ecosystems (Kalcheva et al., 2014), not just by supporting vast biodiversity, but also within the carbon cycle and have seen growing amounts of research (e.g., Borges et al., 2018, Cunada et al., 2018, Overeem and Syvitski, 2009 and Rößger et al., 2019).

Dissolved inorganic carbon (DIC) is made up of CO_2, HCO_3^- and CO_3^{2-}, and represents the sum of the concentrations of all these inorganic carbon species. In aquatic systems, DIC is the primary source of carbon dioxide (CO_2) for photosynthesis (Duarte et al., 2008), and a good indicator of net biological productivity (Song et al., 2013). The dynamics of the DIC pool depend on multiple processes including respiration or photo-oxidation (Song et al., 2013; Tranvik et al., 2009; Wilson and Xenopoulos, 2009),

photosynthesis, CO_2 invasion/evasion and $CaCO_3$ dissolution (Crawford et al., 2014a; Karim et al., 2011; Kempe, 1979; Koehler et al., 2012), or via external abiotic processes such as drainage/groundwater water sources (Deirmendjian and Abril, 2018; Duvert et al., 2019; Tweed et al., 2016) and weathering or precipitation of carbonate/silicate minerals (Tamooh et al., 2013).

Dissolved oxygen (O_2) also shows sensitivity to a variety of processes with the concentrations mainly driven by photosynthesis, where it is produced by autotrophs during the daylight, respiration, where is it consumed, and exchange with the atmosphere (Muraoka et al., 2018; Staehr et al., 2010). Also, like with DIC, it is affected by additional processes via mixing and inflow waters. O_2 is one of the fundamental parameters within these systems and a critical factor within the structuring of biological communities (Couture et al., 2015). It can be used to measure net metabolism, and in turn better our understanding of habitat conditions (Obertegger et al., 2017). For example, excess carbon (i.e., DIC in excess of the equilibrium concentration) and dissolved oxygen deficits (i.e., amount of oxygen missing for air-sea equilibrium) indicate dominance of net heterotrophy, while the opposite is indicative of net autotrophy. Both DIC and O_2 are two of the most useful quantities to establish and understand the internal dynamics and balances within the limnic carbon cycle.

These dynamics can be studied by looking at the speciation of the aquatic CO_2 system, which is possible if at least two of the four measurement parameters of the aquatic CO_2 system (i.e., pH, pCO_2, DIC, TA) are available. When combined with oxygen, the waters' sink/source function for atmospheric CO_2 and O_2 via their respective air-sea equilibrium status can be used as an insight into the drivers of observed variability using the ratio between the spatiotemporal variations in DIC and O_2 disequilibria.

O_2 concentration, having been easier to measure than inorganic carbon, due to the availability of both a reliable wet-chemical methods as well as robust sensors, has had a long track record of being recorded in limnic systems such as lakes (Istvánovics and Honti, 2018). Many of these studies have used sensors within lakes to measure metabolism (Antenucci et al., 2013) leading to the use of respiration and production models (Hanson et al., 2008; Istvánovics and Honti, 2018; Staehr et al., 2010). However, as stated by Istvánovics and Honti (2018), this is not always straightforward and therefore combining together both O_2 and DIC concentrations may help to shed light on biologically driven DIC changes and hence distinguish between physical and biogeochemical processes within the waters. For a reliable interpretation of such spatial data, it is important to assess the temporal variability in the mapped region. Sensors are often used stationary, resulting in time series with high temporal resolution at a defined location. This way, daily or longer-term fluctuations can be assessed. Mapping regional concentration gradients with sensors results in a convolution of both spatial and temporal variability patterns, thus, spatial differences may become severely masked with the temporal (i.e. typically diel) fluctuations of a parameter approaching or even surpassing spatial variability. For a reliable interpretation of spatial data, it is therefore vital to assess the diel fluctuation expected within the mapped regions. If there is adequate information on the diel fluctuations, the spatial data can ideally be corrected to a common time, which would allow to look at a spatial patterns with no or minimal influence of temporal differences.

Although lakes have been the main focus for many spatiotemporal studies, all three main regions – streams/channels, lakes and rivers – are typically sources of atmospheric CO_2. Most riverine carbon inputs are terrestrial from both CO_2-rich ground waters and dominant heterotrophic processes (Cole et al., 2007; Duarte and Prairie, 2005; Tamooh et al., 2013), with both rivers and streams together constituting to about 45% of all terrestrial ecosystem carbon transfer (Kuhn et al., 2017; Raymond et al., 2012, 2013). And yet, there still remain large gaps in terms of data coverage (Drake et al.,

2017), mainly due to the size, limited accessibility and largely unknown spatiotemporal variability (Marx et al., 2017). This is especially so in terms of the carbon system variability covering specific regions and joining zones, although it is becoming more recognised as the most important way to collect such data and to assess the interactions between regions (Crawford et al., 2014a, 2014b; Hanson et al., 2007; Hotchkiss et al., 2018; Palmer et al., 2015). With the interlinking between systems having potential influences on other areas, either through the reed beds or via channels, most limnic locations cannot be treated individually in a 1D sense.

Therefore, to add to this well needed dataset, we focused on the Danube River Delta, Romania, which is a temperate riverine dominated delta. With the ability of continuous underway measurement systems (e.g., Canning et al. subm.) it was feasible to measure across boundaries and assess each region's individual characteristics and how they interact with each other. Therefore, based on three seasonal campaigns during 2017 (spring, summer and autumn), spatiotemporal dynamics of CO_2, DIC, TA and O_2 were measured and will be discussed here.

The objectives of this study were: (1) observe and understand the aquatic CO_2 and dissolved oxygen systems in terms of spatiotemporal dynamics, through determination of TA and DIC on discrete water samples in combination with continuous sensor data of pCO_2 and O_2, (2) explore the connected carbon and oxygen dynamics between lakes, rivers and channels within the delta, and (3) see how these patterns change seasonally and over diel cycles, assessing this variability splitting between biological influence and physical processes.

5.3 Study Region, Cruises, Materials and Methods

5.3.1 The Danube Delta

The Danube River Delta is the second largest river delta in Europe after the Volga Delta (Pavel et al., 2009), situated on the boarder of Ukraine and Romania (44°25' - 45°30'N and 28°45' - 29°46'E) where it flows into the Black Sea. It is classified as a temperate riverine delta, yet experiences extreme water temperatures, varying seasonally from below freezing to 29.5°C (2017: ICPDR URL 1: from Sulina or St. George). The average annual discharge of the Danube River at Reni, an observation station ∼50 km upstream of the delta's apex, was 6760 m^3 s^{-1} in the period 2000-2014. Discharge peaks are from April to June due to meltwater from both the Alps and the Carpathians, with the lowest discharge being observed in autumn. The delta itself, besides the main river stems, consists of a variety of lakes, rivers and channels spanning over 300,000 ha and has the vastest compact zone of reed beds in the world (Oosterberg and Bogdan 2000; Pavel et al., 2009). The wetlands and delta systems receive approximately 10% of the Danube River's total discharge (Oosterberg et al., 2000), through which the delta dampens water level fluctuations at the downstream sections of the main river. Originating within Germany, the Danube travels across 2,857 km to reach the sea, with a drainage basin of 817,000 km^2 (Panin, 2003). As a consequence of this, the delta receives water from across Europe, with multiple studies looking into the effects of pollutants both within the delta and the effect on the Black Sea (e.g: Matache et al., 2013; Woitke et al., 2003; Yiğiterhan and Murray, 2008), especially now recovering from eutrophication up until the late 1980's (Coops et al., 1999; Enache et al., 2019; Geta et al., 2004). However, considering its complexity, anthropogenic influence, its potential within the carbon cycle and its diverse biological dynamics, few studies have focus on these (Durisch-Kaiser et al., 2008; Pavel et al., 2009), even less so as a whole.

Using the basic river continuum concept (RCC: Vannote et al., 1980), the headwater-

to-mouth gradient of physical conditions in rivers elicits responses in the biological systems that strongly influence producer and consumer communities and hence the trophic balance of the water. With this, measuring throughout the Danube River Delta, which consists of a diverse range of lakes, channels and wetlands on top of its main rivers, could enable picking up such activities throughout this system.

5.3.2 Sampling and Analytical Techniques

Sampling took place over three seasons during 2017: spring (May 17-26), summer (August 3-12) and autumn (October 13-23). An underway flow-through sensor set-up was installed on a small houseboat to collect continuous CO_2, CH_4, dissolved O_2 and physical parameters at a sampling frequency of up to 1 Hz (Canning et al. subm., specific details described in section 4). All parameters were measured across the entire delta in parallel on the same pumped water flow. The CONTROS HydroC® CO_2 FT, CONTROS HydroC® CH_4 FT, and HydroFlash® O_2 sensors (Kongsberg Maritime Contros GmbH, Kiel, Germany) were used to measure CO_2 partial pressure (pCO_2), methane partial pressure (pCH_4) and dissolved O_2, respectively. The sensors for pCO_2 and pCH_4 employ membrane-based equilibration of a headspace gas volume with continuous gas analysis using non-dispersive infrared (NDIR and tuneable diode laser (TDLAS) technologies. The HydroFlash® O_2 optode uses the principle of fluorescence quenching (see Bittig et al., 2018) and was placed in a small custom-made flow-through cell due to it being of submersible type. Discrete samples for measurements of TA and DIC (from same sample) were routinely collected from the same water source. Samples were collected following the standard operating procedure SOP1 (Dickson et al., 2007), according to which they were poisoned with saturated $HgCI_2$ solution immediately after collection. For comparison with the typically unpoisoned sampling procedures in limnic methods we also took unpoisoned duplicate samples (see section 3.4.1). Once sealed, the samples were stored in a cool, dark place until measured. TA was measured using the Apollo Total Alkalinity Titrator (Model AS-ALK2, Apollo SciTech, Newark, USA) and DIC was measured using the DIC Analyzer (Model AS-C3, Apollo SciTech, Newark, USA) which were calibrated with certified reference material (CRM) provided by A. Dickson (University of California, San Diego/CA, USA) with a determined accuracy of $\pm$ 1.15 μmol kg^{-1} and $\pm$1.64 μmol kg^{-1}, and an average uncertainty of the samples based on replicates of 1.028 μmol kg^{-1} and 0.272 μmol kg^{-1} for TA and DIC respectively.

A small house boat was used to travel throughout the entire delta, allowing for shallow water deployment (Fig. 5.1). This enabled extensive mapping of the lake regions and the observation of diel cycles and throughout each cruise. The cruise track followed almost the same route for all 3 seasonsal campaigns, with changes only occurring due to environmental external reasons.

The delta was initially studied as a whole, yet given the diversity of each region and for the purpose of this paper, the dataset was then split by season (May, Aug and Oct) and water type (R - river, L - lake, Ch - channel, Fig. 5.1) to closer explore it in terms of seasonality and water type. This was to reflect the diversity of the systems, to reduce the error and skewness of the distributions coming from 'hot spots' (indicated in Fig. 5.1b), so that a more accurate representation of the overall system could be achieved. Given the complexity of the system and its forever changing characteristics, classification of specific regimes was completed both visually (and by clear concentration change boundaries from one region to the other (Fig. 5.1). Each season was almost comparable in terms of spatial coverage throughout the transects, therefore allowing for the exact sectioning throughout the 3 seasons. Lake Roşu (Fig. 5.1c) is used as an example as it was the largest and most well mapped of the 5 lakes we sampled (Lake Isac, Lake Roşu, Lake Roşulette, Lake Puiu and Lake Uzlina, Fig. 5.1 and appendix

5.15).

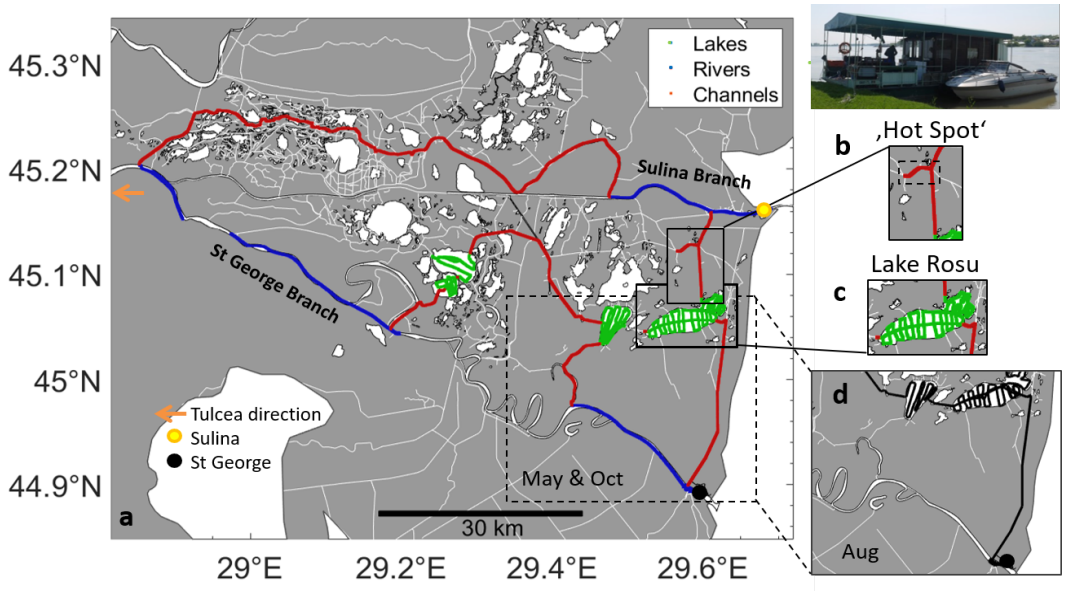

Figure 5.1: The Danube River Delta with the cruise tracks of the three seasonal campaigns carried out with a houseboat (top right). The cruises followed the same track, with only slight variations in the south-eastern part due to blockages in channels or slightly different mapping (see insert d). The main river branches are indicated: St. George Branch and Sulina Branch (both blue). The route went down to St. George from the direction of Tulcea (just off the map), then up to Sulina and back to near Tulcea. Colour sectioning of the Danube Delta from the Oct cruise shows the separation between lakes (green), main rivers (blue) and channels (red). Places of interest for this paper are highlighted, with (b) indicating the 'hot spot' channel and surrounding channels and, (c) indicating Lake Roșu.

Carbonate system calculations

A continuous TA dataset was calculated from the observed strong relationship found between specific conductivity (SC, μS cm^{-1}), temperature (T, °C) and the TA measured from discrete samples (μmol kg^{-1}). Using these, we chose a linear plus quadratic term model fit on the basis of the statistical significance and performance compared to simpler versions. From this predicted TA and measured pCO_2, DIC was calculated using the software package CO_2SYS (Lewis et al., 1998) with the freshwater dissociation constants for carbonic acid from Millero (1979). Predicted values for TA and DIC were then compared with the discrete samples collected to assess the performance of our predictive equation for TA and the accuracy of the consecutive calculation of DIC. In this paper, we present super- or undersaturation of the species as positive or negative ΔO_2, ΔCO_2 and ΔDIC. These quantities were calculated from the observations (X_{obs}) and the expected concentration at equilibrium with atmospheric CO_2 and O_2 ($X_{equilibrium}$), respectively as:

$$\Delta\mathrm{DIC} = \mathrm{DIC}_{obs} - \mathrm{DIC}_{equilibrium} \tag{5.1}$$

$$\Delta\mathrm{CO_2} = \mathrm{CO_{2,obs}} - \mathrm{CO_{2,equilibrium}} \tag{5.2}$$

$$\Delta\mathrm{O_2} = \mathrm{O_{2,obs}} - \mathrm{O_{2,equilibrium}} \tag{5.3}$$

$DIC_{equilibrium}$ was calculated with CO_2SYS using the mean global atmospheric CO_2 mole fraction (ppmv) of the respective month (i.e. 409.65, 405.07 and 403.64 ppm for May, Aug and Oct respectively) converted to partial pressure in μatm using observed instantaneous barometric pressure and in situ temperature, estimated TA, and in situ temperature. $O_{2,equilibrium}$ was calculated the same using the atmospheric O_2 mole fraction (Glueckauf, 1951) and the oxygen solubility constants from Garcia and Gordon (1992).

The observed slope between ΔDIC / ΔO_2 , i.e. the correlation between variations in the disequilibria of inorganic carbon and oxygen, can be interpreted (if other influences are negligible) in terms of the phenomenological respiratory quotient (RQ), which is the dimensionless ratio of CO_2 released to O_2 consumed (Münzner and Berggren, 2019; Tsutsui et al., 2015).

Methane sensor data analyses were used in assessment of the data within a 'hot spot'. Oxygen data from a membrane-inlet mass spectrometer (MIMS, Brennwald et al., 2016; Maier et al., in prep.) were used for the 'hot spot' in May, as the data from the HydroFlash® O_2 could not be used during this time due to a sensor malfunction.

5.3.3 Statistical analyses

For statistical analyses between the parameters, a non-parametric Spearman's rank correlation was used due to the non-normal distribution of the data. The respiratory quotient was estimated from the slope of the relationship between the DIC and O_2 disequilibria (i.e., ΔDIC /ΔO_2) for each system and region. We realize that the phenomenological relationship is affected by a variety of processes including for example air-sea gas exchange. We hypothesize, however, that biological autotrophic and heterotrophic respiration are the major drivers of the relationship such that the slope can be interpreted mostly in a biogeochemical sense.

Extracting temporal variability of certain selected regions was possible via crossing these regions at different times throughout one day. The resulting dataset therefore contained information on both spatial variability as well as temporal variability on diel (or shorter) time scales. For pCO_2 in lakes, an anomaly with respect to the average lake pCO_2 ($pCO_{2,mean}$) was calculated for each data point as follows:

$$pCO_{2,anom} = pCO_{2,obs} - pCO_{2,mean} \tag{5.4}$$

in which $pCO_{2,obs}$, is the observed value at each point of the lake survey, and the $pCO_{2,mean}$ is the mean pCO_2 for the entire lake survey (here Lake Roşu, appendix 5.15). Given the data set not covering a full 24-h cycle, this anomaly was then plotted against local time and fitted with a simple harmonic function:

$$pf(t) = a \cdot \sin(b \cdot t + c) \tag{5.5}$$

where t is time, a is the amplitude, b is the period and c the phase shift. This approach assumes that studied region (here: lake) has enough internal consistency to follow a common diel cycle which is of at least similar magnitude as any spatial gradient. The fact that we were able to fit a harmonic function to the temporal distribution of the anomalies speaks for the general validity of this assumption. When this common diel cycle is removed from the lake data via the harmonic function, the resulting pattern should, within in the validity of the above assumption, be largely free of variability on the diel scale and thus mostly reveal small-scale spatial variability.

In order to confirm the existence of a strong diel cycle as evidenced by magnitude and phase of the harmonic function, we analysed the DIC of all crossovers, i.e. the locations of the lake survey that were covered twice. We then plotted the ΔDIC between the 1^{st} and 2^{nd} observation at each crossover against the Δtime interval between the 1^{st} and 2^{nd} observation. The resulting linear trend was then compared to the phase of the harmonic function. The observed slope of the ΔDIC : Δtime relationship was applied to correct the DIC over the transects.

5.4 Results and discussion

5.4.1 Prediction of TA and DIC

A careful overall analysis revealed a small but statistically significant relationship of TA with water T (ρ = -0.39, p = 0.01). We therefore added T and a quadratic term for specific conductivity (SC^2) and temperature (T^2) (table 5.1) thereby taking into account the slightly non-linear relationship and reducing the average error by -1.19 % and R^2 by -0.12 for TA. Each cruise was treated separately due to varying T for each season and T/SC relationship with TA from the discrete samples (Fig. 5.2).

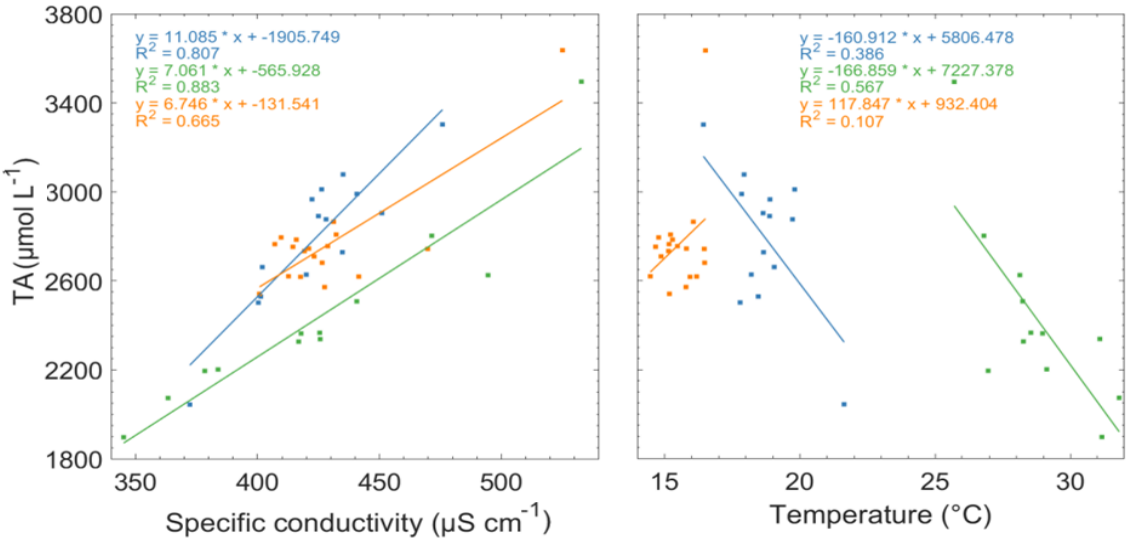

Figure 5.2: Specific conductivity (SC, μS cm^{-1}), temperature (T, °C) with total alkalinity (TA, μmol L^{-1}) across all three transects, showing high correlation between the two properties for spring (May, blue) and summer (Aug, green), although slightly misfit with autumn (Oct, orange) with a more clustered distribution, for TA/SC (R^2 at 0.81, 0.88, 0.67 respectively). TA/T had a lower correlation (R^2 at 0.39, 0.57, 0.11 respectively) but, when used together with SC, was found to increase the fit (table 1)

Using this, a mixed linear regression with quadratic term model was applied to all seasons to yield predictive equations for TA (eq.5.6 coefficients and statistics in table 5.1).

$$\mathrm{TA} = a\,(\mathrm{SC}) + b\,(\mathrm{T}) + c\,(\mathrm{SC})^2 + d\,(\mathrm{T})^2 + e \tag{5.6}$$

coefficients are shown in table 5.1 with e as the intercept, where SC is specific conductivity (μS cm^{-1}) and T is temperature (°C).

Aug and May show a stronger dependence with SC and T compared to that of Oct (Fig. 5.2), this could be due to a previous flood event (that occurred just before the expedition) that created a different TA-SC relationship, with comparatively little TA

change throughout (seen in Fig. 5.2). The predicted TA show good overall agreement with TA measured for May and Aug from discrete samples over all cruises (R^2 = 0.85 to 0.97, slope = 0.88 to 0.97, Fig. 5.3). DIC calculated from predicted TA, measured pCO_2, T and salinity showed similarly good agreement with DIC measured from discrete samples (R^2 = 0.69 to 0.96, slope = 0.83 to 1.07, Fig. 5.3). Overall this proves the validity of our approach to construct a continuous TA and DIC dataset complementing the continuous pCO_2 measurements from combining the continuous T, SC, and pCO_2 data with discrete TA and DIC data. The small variations in the slope between the three seasons, however, are largely due to different TA and DIC ranges observed and the fact that only a relatively small number of samples were available for this validity test.

The resulting residuals for TA ($TA_{predicted}$ – $TA_{measured}$, Fig. 5.3) were 2.3 ± 114.6 μmol kg^{-1} (±SD), -0.8 ± 74.2 μmol kg^{-1} (±SD) and 0.1 ± 92.0 μmol kg^{-1} (±SD) for May, Aug and Oct respectively. For DIC, the residuals ($DIC_{predicted}$ – $DIC_{measured}$) were a bit higher at -52.0 ± 18.4 μmol kg1^{-1} (±SD), -100.4 ± 114.5 μmol kg^{-1} (±SD) and -77.1 ± 233.7 μmol kg^{-1} (±SD) pointing at a slight underestimation of DIC by about 2-3 %. Given the large ranges in both TA and DIC and the relatively small number of discrete samples to establish the predictive equations, these fits were deemed successful and applied throughout the three cruises.

Cruise Month	**a**	**b**	**c**	**d**	**R^2**	**Adjusted R^2**	p	**Error (%)**
May	157.20	-1658.78	-0.17	43.54	0.86	0.77	7.22E-04	5.00
Aug	5.35	-1826.84	1.84E-04	30.63	0.97	0.94	2.76E-05	3.82
Oct	-62.55	2473.25	0.077	-81.78	0.85	0.78	3.32E-05	3.81

Table 5.1: Coefficients used in the total alkalinity (TA) calculation using the specific conductivity (SC), temperature (T) (eq. 5.6). The intercept, R^2, p-value and error (%) are all expressed with Aug showing the largest adjusted R^2 of 0.94 and Oct having the smallest relative TA error (3.81%).

With this method, the full range of TA and DIC was covered, especially during the May and Aug campaigns (Fig. 5.3). However, Oct showed little correlation with both SC and T (ρ =0.24 (p =0.34) and ρ =0.05 (p =0.85) respectively). There was a definite temperature dependence with TA as seen before (Lee et al., 2006), which ensured this fit. Overall, we can conclude that the chosen procedure predicts TA and DIC across the entire ranges spanned by the discrete samples without any systematic biases. The linear model regressions do not always show this as clearly as they suffer from the clustering of the data points in a small part of the parameter range giving little weight to the few but important data points at the extremes.

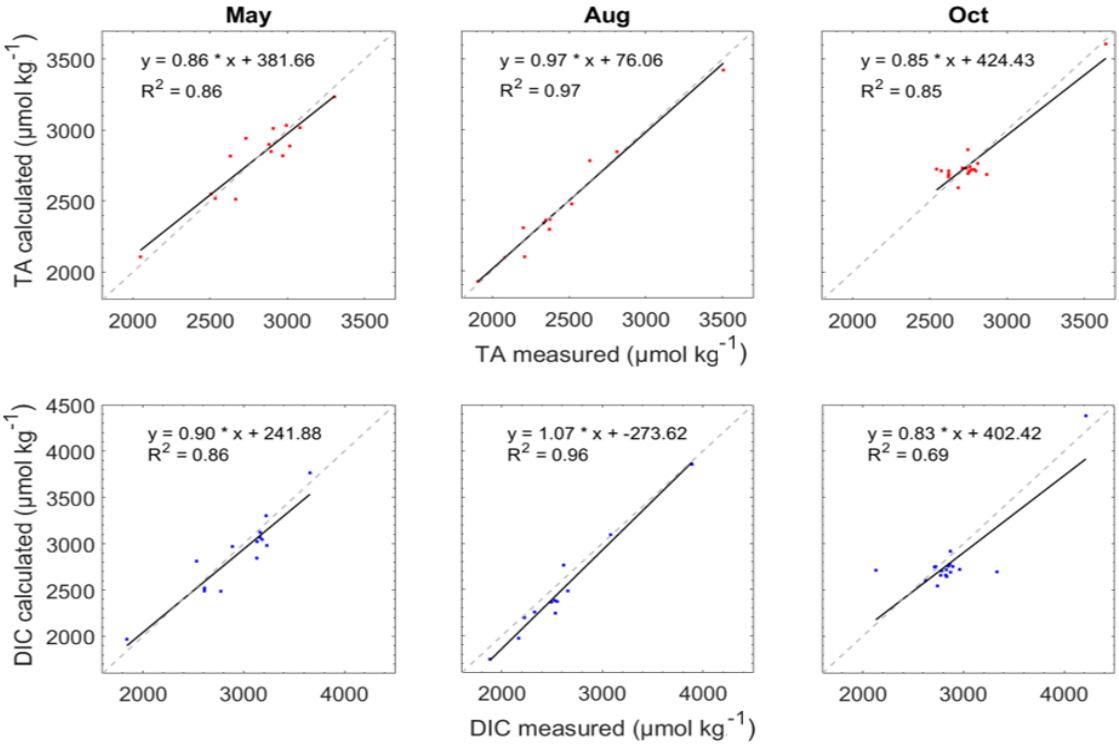

Figure 5.3: Both predicted and measured total alkalinity (TA, red top row) and dissolved inorganic carbon (DIC, blue bottom row) compared to the discrete samples with a linear regression fit (TA: R^2 between 0.85 – 0.97, DIC: R^2 between 0.69 – 0.96) across the three cruises: spring (May), summer (Aug) and autumn (Oct).

5.4.2 Seasonality and sectioning

Since the 1990s, the delta has been recovering from eutrophication (Enache et al., 2019), due to the nutrients stored within the sediments this process is slow (Geta et al., 2004). Within the delta, DIC is the dominant form of aquatic carbon (Tranvik et al., 2009), with seasonal discharge peaks in spring pushing the water into the delta, predominantly along the canals, while the autumn discharge minimum drains the water from the wetlands. The wetlands themselves and their influence on the surrounding regions change from season to season, which was observed with vast variability in pCO_2 and O_2 saturation, differing with season (Fig. 5.4, left) and water type (Fig. 5.4, right). Data are shown from just the daylight hours, excluding night cycles unless stated, given only few were conducted at night. For pCO_2, we found the entire delta as a whole to be supersaturated (73.9% of the delta over May, Aug and Oct) with respect to the atmospheric equilibrium (409.7, 405.1 and 403.6 μatm, at 25°C), with the largest median during May (1,212.8 $\pm$ 849.6 μatm ($\pm$SD)). Oct, although with the largest variability (from 177 to 22,984 μatm), had the smallest percentile range, with all 'extreme' values outside of the 75^{th} percentile (above 2,304 μatm); whereas in both May and Aug, the variability was distributed over a larger range, with the upper percentiles at 7,270 and 4,230 μatm respectively. With May and August being far more variable in both temperature and productivity, this would be expected to have more homogeneous concentrations over Oct, with only certain areas such as the 'hot spot' varying higher.

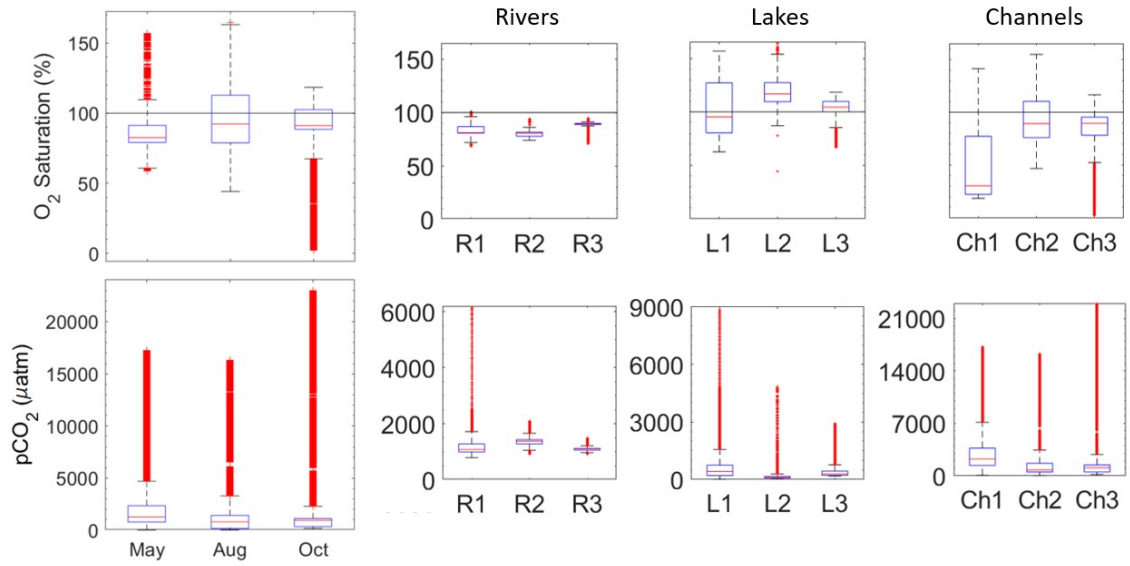

Figure 5.4: Left side: Overall variability during the cruises (excluding night data) for pCO_2 (μatm) (bottom) and O_2 saturation (%) (top, with 100% saturation indicated by horizontal line) throughout the entire Danube Delta for the three seasons covered in 2017: spring, May (1), summer, Aug (2) and autumn, Oct (3). Right side: Same data split into the three water types: lakes (L), rivers (R) and channels (Ch) for the respective season. The blue boxes represent the 25^{th} and 75^{th} percentiles, with the whiskers denoting 1.5 times that of the upper and lower box boundaries. Values outside the whiskers are shown as red symbols. Median values are shown as horizontal red lines.

pCO_2 varied from 14.1 – 17,264.8, 24.8 – 17,445.2 and 177.9 – 22,984.2 μatm for May, Aug and Oct, respectively, while T fluctuations during these months varied at 15.9 – 23.2, 25.4 – 33 and 14.4 – 17.3°C, with the largest range during Aug (table 5.2). However, pCO_2 showed a more skewed distribution mainly within channels (average difference median-mean = -985.9 μatm). In respect to DIC, May had the highest median (2,964.7 μmol L^{-1}), with Aug having the lowest (2,235.5 μmol L^{-1}), ruling out longer sunlight hours leading to enhanced photochemical oxidation, speeding up mineralisation of DOC to DIC as previously suggested (Brooks and Lemon, 2007; Song et al., 2013; Tobias and Böhlke, 2011).

O_2 was generally under saturated (medians: 87.2, 92.3, and 89.6 (%) for May, Aug and Oct respectively, and 71.4% of the delta over May, Aug and Oct, Fig. 5.4). the lakes during Aug and Oct exceeding 100% saturation (median 116.8 and 104.4%, table 2), suggesting the majority of the system (especially rivers, Figs. 5.5 + 5.6) are dominated by net heterotrophy and external processes. Throughout the entire delta, May O_2 ranged from 173.1 – 430.3 μmol L^{-1}, in Aug dropping slightly to 26.7 – 376.1 and then further in Oct to 6.9 – 376.4 μmol L^{-1}. When including the full diel cycles, O_2 showed little variation between the median and mean (ρ = -0.5, P = 0.667), with O_2 saturation staying around 80% (excluding the 'hot spot'). Excluding the night data, the overall O_2 saturation stays around the 100% (table 2, medians between 91.2 – 92.3% over 2 cruises, with May skewed by the 'anomaly' to 59.6%). During Oct, the river concentrations showed almost homogeneous behaviour, with relatively little variability for both pCO_2 and O_2 saturation compared to Ch and L (Fig. 5.5). Outliers seen for pCO_2 generally came from influence of the channels along the other regions (example, see Fig. 5.4: pCO_2 (μatm), R1).

pCO_2 (μatm) / O_2 (% Sat)	Rivers			Channels			Lakes		
	Min	Med	Max	Min	Med	Max	Min	Med	Max
May	**794.5**	**1,085.6**	**2,540.0**	**77**	**2,253.3**	**1,7264.8**	**41.1**	**425.5**	**8,868.9**
	68.5	81.9	101.1	18.6	30.5*	141	62.6	95.3	157
Aug	**927**	**1,381.8**	**2,118.4**	**32.9**	**796.3**	**1,7170.5**	**24.8**	**105.6**	**4,867**
	73.9	80.5	94	10.4	89.2	154.6	44.1	116.8	164.6
Oct	**926.5**	**1,113.9**	**1,500.2**	**205.8**	**1,092.3**	**22,984.2**	**177.9**	**292.3**	**2,959.8**
	71	89.4	95.1	2.2	89.5	116.4	66.5	104.4	118.5

* Potentially skewed distribution due to the largest proportion of data from the 'hot spot' (StCh) compared to that of the other months (Aug and Oct)

Table 5.2: The minimum, median, and maximum values for pCO_2 (μatm: bold) and O_2 saturation (%) for each season (May, Aug and Oct), further splitting into lakes, rivers and channels.Overall median for the entire Danube delta was 1,285.1, 792.3 and 947.8 for pCO_2 (μatm), and 59.6, 92.7 and 91.2 for O_2 saturation (%) for May, Aug and Oct respectively.

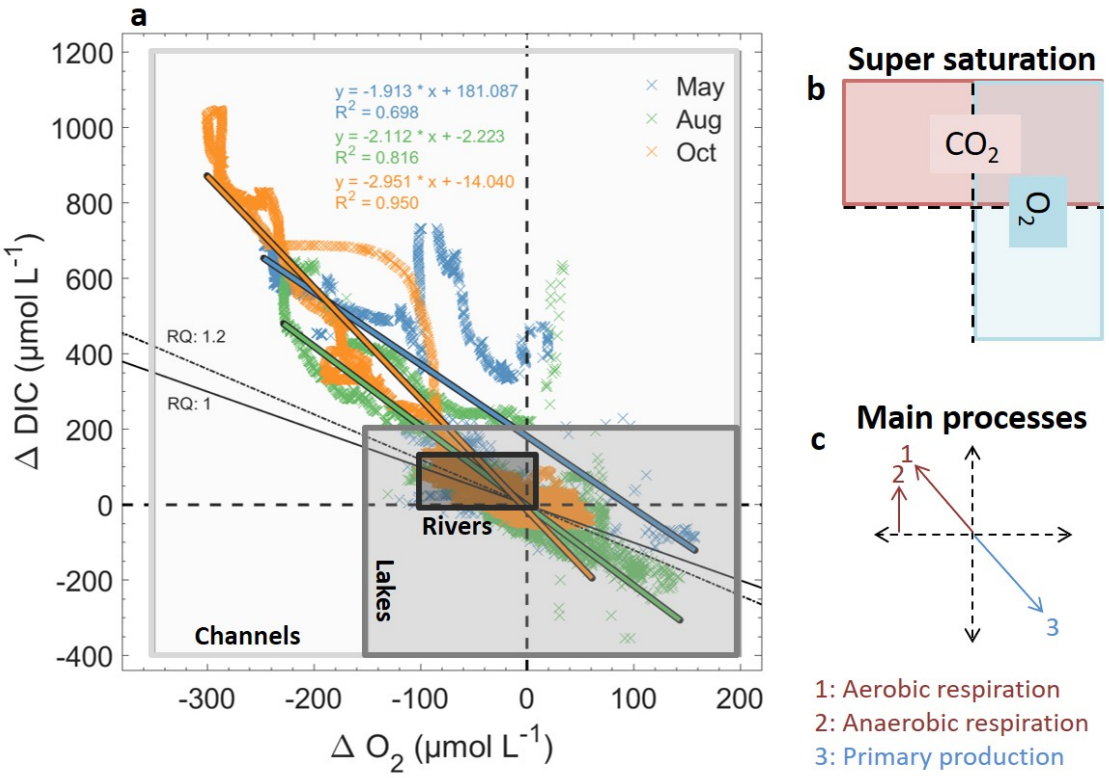

Figure 5.5: (a) Relationship between observed air-sea disequilibria for oxygen (ΔO_2) and dissolved inorganic carbon (ΔDIC) with symbols colour-coded for season: spring/May (blue), summer/Aug (green) and autumn/Oct (orange). Also shown are the equations and R^2 values of linear regressions fitted to the data for each season. The boxes indicate the parameter range into which the data from the three water types fall: R (rivers), L (lakes) and Ch (channels). (b) Explanatory graph to show the areas in which CO_2 and O_2 are supersaturated in respect to the atmosphere. As expected, most data fall into quadrants where one of the gases is in supersaturation while the other is in undersaturation. (c) Graph to represent the three main metabolic processes as vectors they would take on panel a, with RQ = 1 and 1.2 for standard RQ ratios in inland waters (Berggren et al., 2012).

ΔDIC and ΔO_2 were compared over the seasons (Fig. 5.5) to identify some of the

main processes and drivers (Figs. 5.5 c and b respectively). The $\Delta DIC/\Delta O_2$ ratio clearly shows a dependence on water type and location (Fig. 5.5 within the boxes: lakes, rivers and channels); Ch spanned by far the largest range reaching across both respiration- and production-dominated situations, R was primarily supersaturated in DIC and hence dominated by respiration while L was mainly supersaturated in O_2 as indicative of a net-productive environment.

The overall relationship between pCO_2, ΔDIC and ΔO_2 was as expected, with both carbonate system parameters correlating with O_2. This could be due to either production of respiration processes or outsources of abiotic processes and ground water intrusions (Crawford et al., 2014a; Kempe, 1979; Stets et al., 2017). Overall the results showed supersaturation in pCO_2, coinciding with the consensus that inland waters are typically supersaturated in relation to atmospheric pCO_2 (see Crawford et al., 2014; Raymond et al., 2013; Regnier et al., 2013; Torgersen and Branco, 2008) and therefore using this as quantitative evidence of net heterotrophy (Raymond et al., 2000). Aufdenkampe et al. (2011) found temperate regions to have median pCO_2 of 3,200, 3,500, 900 and 2,500 μatm for rivers, streams, lakes and wetlands respectively, all of which are higher than what we observed (table 5.2). Seasonally these changed throughout and within the delta, as flow changes can be seen with the use all parameters including temperature. During May, temperature distributions suggest colder river flood waters coming in through the fluvial delta, with only areas furthest away from the river inputs increasing in temperature (not shown here). During Aug, it appears within the core fluvial delta was where the warmest waters were, suggesting little movement of flowing waters allowing for heating. However, during Oct, the coldest waters appear to be within the core of the delta, with the warmest waters flowing in closer to the Black Sea.

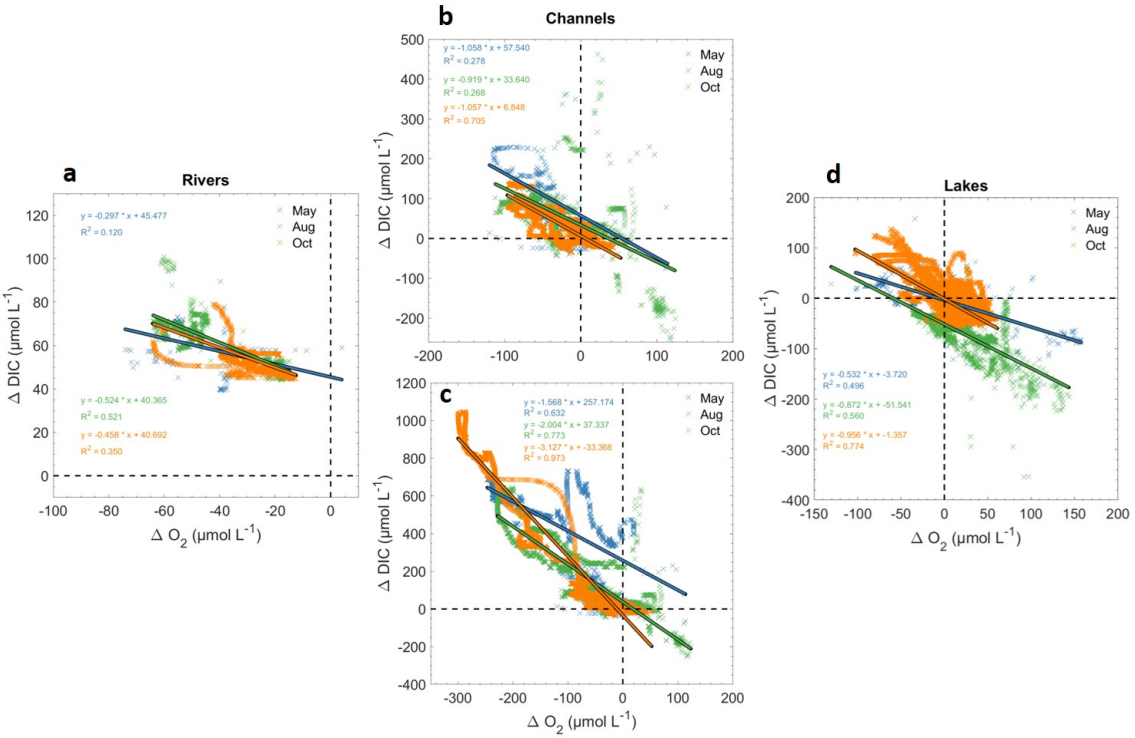

Figure 5.6: $\Delta DIC/\Delta O_2$ relationship for May (spring, blue), Aug (summer, green) and Oct (autumn, orange) for Rivers (a), Channels with (b), excluding and (c) including 'hot spot' StCh, and Lakes (d) with their fits in respective colours. Also shown are the equations and R^2 values of linear regressions fitted to the data for each season. Note that the scaling of x and y axes differs between panels.

Interestingly the pCO_2 and O_2 vary, sometimes not following the expected ratio,

potentially due to the different buffering capacity at high and low TA (< 1,000 and > 2,000 μmol L^{-1}, respectively) which was found and suggested by (Stets et al., 2017). Therefore, to be able to look closer into the interactions and potential drivers each season was then split by region (Fig. 5.6), where there is a clear boundary in the processes between each region, even when classification was done on a basic level. This will be further discussed in the following sections.

RQ, i.e. the amount of CO_2 released per O_2 consumed in a metabolic process, is atypically assumed to be 1 within inland waters, although multiple studies have since debated this, stating deviations in both directions, and can vary significantly (e.g. Allesson et al., 2016; Berggren et al., 2012; Cimbleris, 1998; Münzner and Berggren, 2019), with some more recent studies using 1.2, stemming from Berggren et al., (2012). Generally an RQ between 0.7-1 would be expected due to reaction stoichiometry for the algal material oxidation (Münzner and Berggren, 2019). In the marine realm, average O_2/C_{org} ratios of around 1.32 have been reported (Redfield et al., 1963; Körtzinger et al., 2001) corresponding to an RQ of about 0.75. However, an RQ systematically higher than 1 (Fig 5.6b and c), has been shown to occur when photoproducts (highly oxidized organic acids) are a large part of bacterial metabolism (Allesson et al., 2016). Given the span of all our RQs (figure 6), we must consider processes other than aerobic mineralisation of organic carbon, e.g. anaerobic methanogenesis (leading to high RQ) and subsequent methane oxidation (RQ = 0.5) (Bastviken et al., 2008). Nitrification may also lead to lower RQ (< 0.5, e.g. within the rivers) due to its potential to lower the RQ by accounting for $\sim$ 10% of the total O_2 consumption in water and soils (Hooijmans et al., 1990). (Bastviken et al., 2008).

Rivers

All of the rivers for each season were consistently supersaturated in pCO_2 with a maximum of 2,540 μatm to a minimum of 794.5 μatm both during May. In comparison, Raymond et al., (2013) who observed a median of 3,100 μatm following corrections of channels and rivers (variations depending on who investigated see Aufdenkampe et al., 2011; Cole et al., 2007; Lauerwald et al., 2015). We observed a lower overall median over the 3 seasons at 1,212.9 μatm, although consistently supersaturated in comparison with the atmosphere. The river concentrations split between the branches, with Sulina showing higher pCO_2 in two of the three months. The rivers had a constant DIC background level of around 40 μmol L^{-1} throughout the seasons. This background DIC supersaturation, unlike the observed slope, is probably not forced locally but rather suggests previous influence from within the waters and watersheds. The observed gentle slopes shown do not represent the clear respiration signal but are probably moderated by gas exchange with the atmosphere which is faster for O_2 than for DIC because of the buffering effect of the aquatic CO_2 system.

We found R to be less variable in terms of O_2 in respect to all other areas and consistently undersaturated, showing a maximum change of 182.7 μmol L^{-1} to 300 μmol L^{-1} (73.9% to 95% saturation: lowest in Aug, highest in Oct, appendix 5.3). May was the only month in which O_2 saturation went over 100% (table 5.2: 101.1%). Between the two branches O_2 shifted, with the median difference, St. George-Sulina; 65.9, -23.6 and -87.9 μmol L^{-1} for May, Aug and Oct respectively. During Aug, the ΔO_2 within rivers had the the steepest slope of -0.52 (intercept + 40.4 μmol L^{-1}, R^2 = 0.52: Fig. 5.6a), showing higher rate of O_2 uptake per DIC change.

Predicted DIC and TA showed similar variations with O_2 and CO_2 (appendix 5.3), with highest values and highest variability during May. Although each season showed some variability in the slope of the $\Delta DIC/\Delta O_2$ relationship, all had an intercept of about 40 μmol L^{-1}, showing the DIC input was from previous input given the RQ was not

expected of that for usual respiration (1.2: Berggren et al., 2012). Compared to other regions in the delta rivers are generally open systems with comparatively smaller biological activity, where mixing is prominent, enhanced by wind, waves and boat movement creating turbulence which results in outgassing (Borges and Abril, 2012). The change in the branches concentration levels, could be due to the proximity of the vast surrounding wetlands around the Sulina branch, along with the increase in water flow velocity within St George due to modifications to the river in recent years (Panin, 2003). This would allow for Sulina to retain and receive more pCO_2 and DIC over a longer period even though it is the shorter of the two.

When looking at the impact of the river on the delta system itself, it seemed it did not have as much impact overall throughout the seasons (see following sections) in which it seems in-delta processes may have a larger impact (appendix 5.13: DIC speciation). This is unlike what was suggested by Wang et al. (2013) for the Congo River where the river discharge had a large influence on the delta. An example of which is with the DIC speciation increasing in CO_3^{2-} concentration during Aug as soon as the transect entered the fluvial delta. If this was being formed you would expect changes in TA and DIC at a ratio of 1:2, however in areas where it increases in the fluvial delta, this is not the case. This suggests carbonate mineral precipitation with a drop in HCO_3^-potentially due to warming, given the lack of biogenic calcification and severe increase in temperature.

Channels

During the transect we experienced a 'hot spot' channel, StCh, which represents and extreme environmental setting that causes a distorted representation of channels observed throughout the delta. Final analyses are therefore split between channels excluding (Fig. 5.6b) and including StCh with its surrounding areas (Fig. 5.6c) during the three seasons.

The channels ranged in pCO_2 from 32.9 to 10,455 μatm for Aug and May respectively with an overall median of 968.1 μatm, showing an overall consistency with being supersaturated in respect to the atmosphere. Although the concentrations and DIC varied over the seasons, channels stayed almost homogenous over the three seasons, with little variability between them (Fig. 5.6b). DIC had the highest variability during Aug, such as with the other regions.

This variability was also experienced more net production of O_2 μmol L^{-1} during Aug (supersaturation of O_2, Fig. 5.6b) than the other two months. However, it was sparser and more scattered, potentially due to the extreme heat, the different transect track and resulting shallowness. Concentrations ranged from 113.4 to 396.1 μmol L^{-1} (saturations of 46.8% and 141.0% respectively), with May having the highest concentrations and Aug the lowest. The overall median of the channels for all seasons was 279.2 μmol L^{-1} (86.6% saturated), with overall being undersaturated in respect to O_2 which is also observed from ΔO_2 in figure 5.6b.

During Aug, an RQ of $\sim$ 0.9 is suggested to be a result of complete oxidation of terrestrial sourced bulk dissolved organic carbon (DOC) (Dilly, 2001). However, the other two months stayed almost exactly the same (- $\Delta DIC/\Delta O_2$ slope: 1.06, 0.92 and 1.06 for May, Aug and Oct respectively), in which net respiration was occurring throughout the seasons with little change. This steady ratio ($\Delta DIC/\Delta O_2$) was little seasonal variability, is consistent with the processes of aerobic respiration or production, with very few outliers from this 1:1 line.

Ch showed the largest variabilities of all parameters (table 5.2) within all the regions in the Danube Delta occurring during Aug (excluding StCh, appendix 5.4), excluding pCO_2 which was in May, potentially due to lower water levels leading to less homogeneous behaviour throughout with limited flowing waters in regions and extreme heat events.

One reason for this is they are the link between rivers and lakes and therefore can be the core of the nutrient and carbon transport.

One issue when analyzing parts of the Danube delta for all regions, especially the rivers, is due to the process of dredging throughout to allow access for larger vessels, in which this is normally unmonitored (Giosan et al., 2013). Within a 'natural' delta, channels tend to change and find the best way for the river (Overeem and Syvitski, 2009), however, due to the Danube being manually dredged this inevitably plays a role on the potential sedimentary release of CO_2 and CH_4. This will potentially release gases out of the sediments and create an 'unnatural' view of the system. On top of this, channels are surrounded by farmland, this too can also have a potential influence on the ratios and concentrations within the Ch. Yet assuming these impacts were not picked up on by our data, channels were constantly and consistently aerobically respiring throughout the seasons. This is consistent with previous work on streams and channels being a source of CO_2 (e.g. Abril and Borges, 2019; Raymond et al., 2013; Tranvik et al., 2018).

'Stinky' Channel

StCh had the highest pCO_2 and DIC dynamics out of all the regions, which is why it has been specifically separated. pCO_2 had a range from 491.1 to 22,984.2 μatm (Aug and Oct respectively), with the minimum peak for each month varying significantly (8,010.0, 491.1 and 2,967.2 μatm, May, Aug and Oct respectively). However, the upper range only vastly exceeded during Oct with both May and Aug staying roughly the same (17,263.8 and 17,170.5 μatm). DIC increased significantly within StCh with ΔDIC doubling to what is found in the channels (Fig 5.6c compared with Fig 5.6b). Both this specific channel, and connection channels, experienced some of the largest changes over the shortest distances ($\sim$ 13,000 pCO_2 μatm within 320 m of distance, Oct (appendix 5.12, autumn)).

O_2, unsurprisingly also showed greater extremes than any other region, such as with pCO_2. The concentrations ranged from 6.9 to 314.2 μmol L^{-1} (during Oct and Aug). Just with pCO_2, the same pattern was observed with May and Aug showing similar maximum values (312.0 and 314.2 μmol L^{-1}, 107.4% and 128.9% saturation), compared to Oct reaching just 237 μmol L^{-1} (78% saturation). If excluding the channel directly adjacent to StCh, which also shows high concentrations and is joint with the anomaly (appendix 5.12), only Aug O_2 reached above 100% saturation (108.2%) with May and Oct having a maximum of 68.6% and 25.3% respectively.

Using $\Delta DIC/\Delta O_2$, the change between Aug and Oct is visible, with the slope changing from 2.0 to 3.1 over the two seasons (R^2 = 0.77 to 0.97, Fig. 5.6c). Such positive slopes further indicate CO_2 input from anaerobic respiration, i.e. situations where respirative CO_2 release is not accompanied by matching oxygen consumption.

Reasons for this are more evidential for anaerobic respiration than ground waters, due to a limited passage through the reedbeds potentially create a 'microclimate' within the channel due to lack of flowing water. This in turn potentially leads to anaerobic metabolisation pathways leading to DIC release when there is little, or no oxygen left which is evident what we see in figure 5.6c. Given anaerobic respiration effects TA, this can signal anaerobic respiration from SO_4^{2-} reduction (Cai and Wang, 1998). This can further seen within appendix 5.13, with the highest CO_2 and lowest CO_3^{2-} during StCh, suggesting the DIC is made up of more CO_2 that has not had time to degas (Raymond et al., 2000). However, we also observe lower pH levels resulting in much higher CO_2 and decreased carbonate ion concentrations (CO_3^{2-}, appendix 5.13), causing DIC to increase higher than that of TA (i.e., $[CO_2] > [CO_3^{2-}]$); also suggesting potential ground water influxes. Although in general, small channels, such as StCh, potentially receive inputs of DIC and CO_2 from groundwater and reed runoff. This could suggest if the

receiving waters are low in TA then most of the DIC will be expressed as CO_2, therefore equilibrating faster than if the TA is higher, shown by Stets et al (2017). This could explain the continuously high pCO_2 following StCh and further into the surrounding channels, or during May (appendix 5.12) with DIC only gradually reducing while O_2 becomes almost saturated.

Using the CH_4 data measured, this theory can be tested. During Oct, the most extreme $pCH_4/\Delta O_2$ with the highest concentrations was observed during the day for all cruises (appendix 5.14). This extremity can be used to investigate processes going on within this anomaly. The extreme changes show a steep increase in pCH_4, with no more O_2 depletion, yet drop back within 1.2 km. pCO_2 (μatm) also shows an increase within this location, with O_2 correspondingly reaching the minimum of 6.9 μmol L^{-1}, yet these concentrations only slightly decreased/increased, respectively as abrupt as pCH_4. This would suggest at the end of the channel (for approx. 1 km) an anaerobic methanogenic environment, with any biomass fermented to methane via anaerobic bacteria (Thauer, 2010). With one channel entrance close to the end of StCh draining from a lake we did not measure; it could be suggested this plays a role. However, the advantages of having the continuous data, this can be disproved to a certain extent due to the concentrations being higher after the entrance, opposite to the direction of flow (appendix 5.12) and starting so abruptly after another drainage channel further up.

Lakes

In total, we mapped 5 lakes over the 3 seasons (appendix 5.15). Overall the pCO_2 within the lakes ranged significantly from 14.1 to 8,868.9 μatm both during May, with a median over all months of 217.5 μatm, showing an overall under saturation. The extreme pCO_2 concentrations usually coincided with channel of reed inflow and runoff given the proximity to the lake edges. Throughout two of the months each median showed undersaturation for Aug and Oct within the lakes: 425.5, 105.6 and 292.3 μatm for May, Aug and Oct respectively. In Fig.5.6d, the distribution of ΔDIC clearly changes over the months, with Aug being more productive and scattered compared to Oct in which it is more homogenous. DIC coincided with the highest pCO_2 median with May showing the highest concentrations (3,192.8 μmol L^{-1}).

O_2 μmol L^{-1} showed a range 104.3 to 430.3 (lowest in Aug, maximum in May) with an overall median of 328.7 μmol L^{-1} (104% saturation). Aug had the largest variability ranging from 104.3 to 376.1 μmol L^{-1} (44.1 to 164.6%). May was overall undersaturated at 95.3% (272.0 μmol L^{-1}), yet still had a high variability of 62.6 to 157.0% saturation (Table 5.2), coinciding with May having high rates of primary productivity, yet flood waters bringing in vast amounts of organic matter. This can also be observed from figure 5.6d, where there is a clear difference between the seasons with Aug showing high ranges within ΔO_2 μmol L^{-1}.

Looking at Oct is more consistently equal for both ΔDIC and ΔO_2 with a slope close to 1 (-0.96), which is within the typical oxidation of algal material reaction stoichiometry of 0.7-1 (Anderson, 1995; Körtzinger et al., 2001; Hedges et al., 2002; Münzner and Berggren, 2019; Takahashi et al., 1985). Lakes had the largest variability in $\Delta DIC/\Delta O_2$ ratio, excluding StCh, ranging from 0.53 to 0.96 (Fig. 5.6d). They tend to be the last regions to be influenced by the rivers, this variability could be due to lakes additionally affected by channels, reed beds and internal processes (Crawford et al., 2014a). We found very little direct influence from the rivers on the lakes, with them overall being undersaturated in pCO_2, which given the Danube delta is still slowly recovering from eutrophication follows Balmer and Downing, (2011), where the median of over 300 eutrophic lakes measured was also undersaturated. Only the lakes closest to the rivers appeared to have riverine influence with higher sediment transport, also observed by

Covaliov et al. (2003), especially seen in May, having just been flooded, more organic matter would have transported to the lakes.

A summary of the main, larger lakes will be discussed with further in-depth analyses on Lake Roșu, due to the largest and most well mapped of the lakes for seasonal comparability and shown to be within the most productive lake complexes in the Danube Delta (Enache et al., 2019).

Lake Uzlina and Lake Isac Lake Uzlina, the first of the lakes measured (Fig. 5.1), was the most impacted by the rivers, with higher pCO_2 concentrations compared to that of Lake Isac (adjacent to one another) also observed by Pavel et al, (2009). It had a range of 212.1 to 3,205.3 μatm (Oct and May respectively) with a varying median over the months however, consistently supersaturated: 1,102.7, 940.4 and 475.3 μatm (May, Aug and Oct) with an overall supersaturated median of 621.5 μatm. Lake Isac observed less variation, with only Oct reaching extremely high values (2,458.8 μatm) with the lowest values seen during Aug at 24.8 μatm. The over median for each month was undersaturated compared to Uzlina: 97.9, 96.9 and 249.9 μatm with an overall median of 197.9 μatm. Both May and Aug, had far higher pCO_2 average concentrations within the channel entering Lake Uzlina than within the lake itself (1,463.5 and 1,429.3. compared to 1,131 and 880.3 μatm respectively). This was further exaggerated when entering Lake Isac when it dropped to 192 and 115.8 μatm. However, during Oct the opposite occurred with both Lake Isac and Uzlina in terms of pCO_2 concentration, showing more homogenous pCO_2 behaviour (average pCO_2: 585.2 and 519 μatm respectively), with concentrations dropping from the river (mean: 1,048.5 μatm) to the channel (mean: 425.1 μatm), before rising in the lakes. DIC followed the same pattern, dropping from the Uzlina to lake Isac for May and Oct, yet staying similar to Oct, although still dropping (median DIC for lake Uzlina: 2,985.4, 2,179.4 and 2,714.1 μmol L^{-1} and Lake Isac: 2,095.3, 1,881.0 and 2,675.1 μmol L^{-1} for May, Aug and Oct).

O_2 varied between the two lakes. Lake Uzlina had more homogeneity across the seasons, varying between 232.0 (May) to 376.4 (Oct), with a median concentration of 327.6 μmol L^{-1} (103.3% saturation). Lake Isac showed higher concentrations and variability across all months ranging from 213.2 μmol L^{-1} in Oct to 430.3 μmol L^{-1} in May, with an overall median of 343.4 (107.7% saturation).

This variability between the two lakes is clear from the visual evidence of high macrophyte concentrations during both months especially in lake Isac, leading to high rates of primary productivity during the transects. From the dispersive spatial pattern (appendix 5.15), processes can be seen to influence these changes, from the proximity of the river inflowing via a channel, the surrounding reed beds and potential remineralization of organic matter transported in. Visible changes between the lakes showed Lake Uzlina experienced far higher organic matter transport compared to Lake Isac especially during May, further confirming the process of either remineralization before the use of CO_2 within primary production, or settlement of the matter. This could also explain the increase in macrophytes (and therefore net production) in Lake Isac due to greater visibility from the lack of organic matter. In comparison, during Aug, there was already some evidence of macrophytes beginning to break-down. Lake Uzlina was again greenish in colour, even with water levels lower from less river influence compared to May, combined with coverage in algae on the surface. This was also noted by Friedrich et al., (2003) within Lake Uzlina, where they suggested the C:N ratio in this environment were typical for plant detritus.

Although adjacent to one another, both lakes differ in depth and size but are still classed as shallow lakes, therefore, in theory, do not stratify (Friedrich et al., 2003) (depth: < 3 m and < 2 m for Lake Uzlina and Lake Isac respectively with Lake Isac

the bigger of the two). However, given the large amount of macrophytes during May and partially Aug, especially in Lake Isac where there was little fast flowing influence from the channels, stratification could have occurred due to light attenuation to the bottom waters and lack of mixing turbulence in the lower waters (Andersen et al., 2017). With DIC dropping throughout Lake Isac more dramatically compared to that of Lake Uzlina (steady drop), and would further suggest stratification throughout the day and nocturnal mixing. The stratified layers would mix during the night to replenish O_2 to the bottom layers and DIC to the surface, given in Lake Isac the DIC drops by half during the day, photosynthesis would be constrained by this (Andersen et al., 2017). With settlement of organic matter below the stratification line and within the sediments, would further fuel anaerobic respiration increases the depletion and release during the night from the bottom sediments. However, during Oct with the opposite occurring in terms of pCO_2 concentration, this implies respiration or remineralization of the degrading organic matter (the macrophytes) either from the lake itself or bought in via flooding which had occurred just previously creating a steady flow across both lakes with increased mixing.

Lake Puiu Lake Puiu varied significantly more than the previous two lakes, with pCO_2 concentrations ranging from 14.1 to 4,796.3 μatm (May), yet with an over median being undersaturated (302.2, 79.1 amd 376.9 μatm: May, Aug and Oct respectively, median overall of 252.1 μatm). The high concentrations were linked with an inflowing channel also showing levels of high DIC (3,066.1 μmol L^{-1}) during May, with a median of 2,698.7 μmol L^{-1}.

Aug was observed to have the highest variability for O_2 varying from 104.3 to 376.1 μmol L^{-1} (44 to 161.1% saturation). May and Oct stayed roughly the same spanning between 259.4 and 361.3 μmol L^{-1} (84.3 to 115.1% saturation), with Oct showing the least variability. Overall the median saturation was 97.0, 123.1 and 106.6 for May, Aug and Oct, with and over median of supersaturation (106.8%).

Influences into Lake Puiu came from Crisan channel during certain months (west channel entrance), with high CO_2-rich waters flowing in as also witnessed by Pavel et al., (2009). We found it to be originating from one fishing hut 'hotel', from potentially wastewater or farming pollution, yet adjacent to a small channel from a further lake within the wetlands. Streams that receive wastewater have been shown to more likely to become more anoxic, due to microbial consumption of O_2 within the sediment, especially during the night (Nimick et al., 2011). This could explain the steep increase in pCO_2 following this location, especially with higher concentrations in the morning along this transect during Oct, such as described before. However, like the lakes above, Puiu had large amounts of macrophytes and primary productivity within the waters which led to all saturation levels for pCO_2 are to be under atmospheric values, and supersaturated in O_2 (excluding May, which could also be due to lack of mapping (appendix 5.15)).

Lake Rosu Although higher than Lake Isac and similar to Puiu, pCO_2 (μatm) was generally supersaturated in respect to the atmosphere (medians of 347.4, 131.8 and 220.0 μatm for May, Aug and Oct). Concentrations ranged from 53.4 μatm (Aug) to 1,368.1 μatm in May, with the overall median of 194.0 μatm, showing an almost consistent undersaturated lake. Most of the high concentrations were linked to the lakes edge which is also observed in DIC (Fig. 5.7). Minimum CO_2 concentrations observed in Oct coincided when temperatures were at their lowest, also witnessed by Raymond et al., (2000). However, Lake Rosu is classed as a turbid lake (Coops et al., 1999) and therefore would explain the higher pCO_2 concentrations compared to Lake Isac.

O_2 varied between 186.6 μmol L^{-1} (62% saturation) in May to 353.2 μmol L^{-1}

(142.9%) in Aug, with medians of 233.4, 270.7 and 328.0 μmol L^{-1} for May, Aug and Oct. Generally Lake Rosu was over saturated (79.8, 109.3 and 104.8%) excluding May, which as stated with Lake Puiu, could be due to lack of efficient mapping. Just like with Lake Isac and Uzlina, the higher ranges for O_2 generally coincide with net primary production observed from the mass amounts of macrophytes, which play a role through growth and decay, giving way to both O_2 and DIC production and use over the seasons. Figure 5.6d shows both May and Aug appear to consist mainly within O_2 supersaturation.

Such as with DIC, TA shows the higher range during May and 588.8-3,386.3 μmol L^{-1} (appendix 5.6). Stronger inflow due to previous flooding appears to bring in higher lateral transport of DIC and TA during may, seen also with the other lakes. In regions of supersaturation, such as Oct and around the lake edges, calcification, by the shift in the speciation in aquatic CO_2 system leading to a release of CO_2, can explain the CO_2 supersaturation within the lakes (Brunskill 1969; Marce et al., 2015; Andersen et al., 2019) in addition to remineralization of organic matter to inorganic. This is also witnessed in TA, where the precipitation of 1 mole of $CaCO_3$ reduces TA by two molar equivalents and can be seen in certain regions around the lake edges (not shown here).

Transecting The extensive mapping of Lake Rosu (Fig. 5.7), with an initial transect conducted before/after mapping, shows patterns which represent both spatial and temporal variability. Temporal variability can be seen clearly with ΔO_2 during both Aug and Oct when comparing crossover locations which had been visited twice during transect and mapping. Both seasons were almost continuously supersaturated in O_2 (also visible in Fig. 8 box plots), with indications of spatial influences with inflow from the reeds surrounding the lake during Oct (supersaturation in ΔDIC, Fig. 5.7). Temperature change can account for $\sim$ 2% change in O_2 per T change of 1°C yet fails to explain the full variability. The distributions varied more during August, with a median of -80.6 μmol L^{-1} compared to that of Oct for DIC at -37.5 μmol L^{-1}, yet O_2 stayed comparatively the same (11.7 and 18.5 μmol L^{-1} for Aug and Oct respectively). Flow change over the seasons show the DIC influence reversing, originally from Lake Rosuelette in Aug, before changing direction to coming in from the west in Oct. Further seasonal variability could be linked with production, macrophyte degradation (as described previously) and varying flow regimes changing from reed bed influence to more in situ autotrophic processes during Aug.

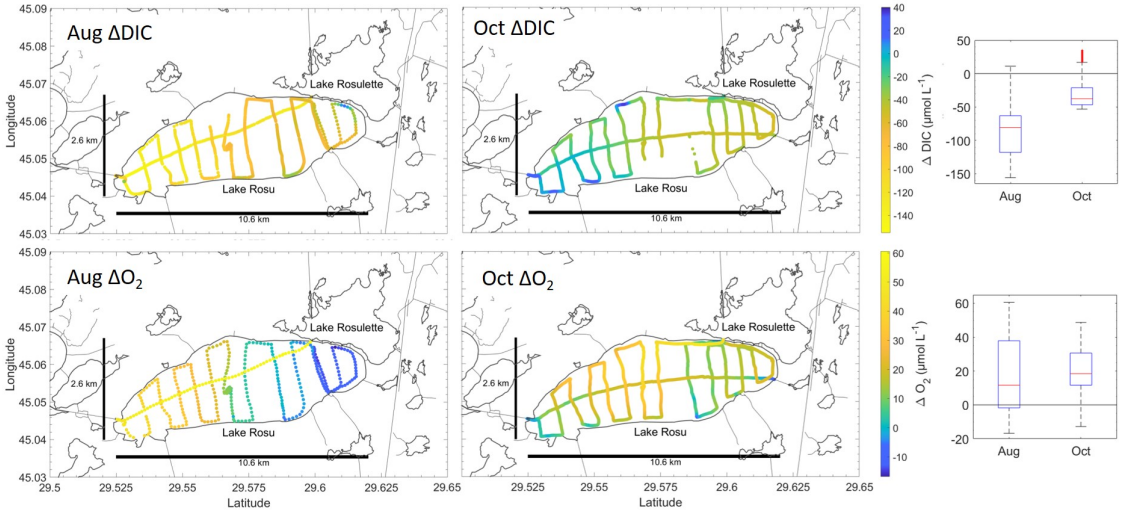

Figure 5.7: Lake Roşu mapping transect for ΔDIC (top) and ΔO_2 (bottom) from the Aug (left) and Oct (right) cruise. Note the inverse colour scale for DIC and O_2, with blue showing supersaturation for ΔDIC (top), and undersaturation for ΔO_2 (bottom). The entire transect took about 8 daylight hours, including the initial (Aug) or final (Oct) straight transect across the lake. Also shown are box plots (right) excluding night data for ΔDIC (μmol L^{-1}) and ΔO_2 (μmol L^{-1}) during Aug and Oct in Lake Roșu; with ΔDIC median at -80.6 μmol L^{-1} and -37.5 μmol L^{-1} and ΔO_2 with a supersaturated median of 18.5 μmol L^{-1} and 11.7 μmol L^{-1} for Aug and Oct, resp. The blue boxes represent the 25^{th} and 75^{th} percentiles, with the whiskers denoting 1.5 times the interquartile range away from the box top or bottom.

During Oct, the mapping measured over 2 consecutive days. During which, it was deemed to reliably use this with the same transect as it showed the same variability over a temporal scale from one day to another, with each day showing the same concentrations as the times of the previous day. DIC was slightly being replenished and O_2 reduced overnight to the values they were during the previous morning transect ($\sim$ -10 μmol L^{-1}). This was potentially due to nocturnal convection then mixing two water bodies described previously. This was also visible from the diel cycle (Fig. 5.8), during Aug where concentrations appear to reach the same level as the previous day at the same time. This can be seen in figure 5.8, except O_2 varying from 305 to 230 μmol L^{-1} compared to just 10 μmol L^{-1} during Oct.

O_2 Saturation over the course of the transect during day light hours, increases extremely linearly (Fig. 5.8), unlike pCO_2 (see below), from 94-124% over the course of an 8 hour transect. The mixing of the two water bodies from daily stratification, could be one explanation as to how this is such a strong diel relationship.

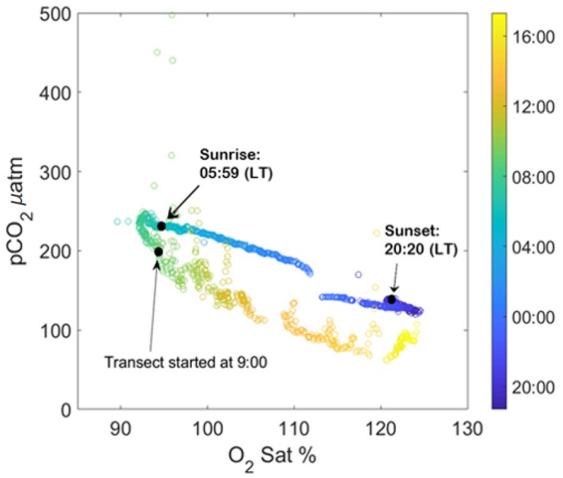

Figure 5.8: Stationary diel cycle of pCO_2 (μatm) over O_2 saturation (%) in the middle of lake Rosu during Aug with sunrise, sunset and when the transecting across the lake began. Colouration is of the time (hh:mm), with a clear hysteresis during the night as pCO_2 increases and O_2 saturation decreases, and a clear replenishment during the night (blue times) of pCO_2, while diminishing during the day with a clear increase in O_2 (green-yellow). In μmol L^{-1} of O_2 it accounts from 305 to 230 μmol L^{-1}.

Extracting anomalies Anomalies of pCO_2 ($pCO_{2,anom}$, ($R^2 = 0.97$, RMSE = 6.17)) were calculated as described in the methods section for Lake Roșu over the course of the transect ($\sim$ 8 h during daylight hours) and have signs of a clear diel cycle onto which small-scale spatial variability superimposed (Fig. 5.9a). A single sine function fitted to the temporal variation of $pCO_{2,anom}$ provides a quantitative representation of the average diel variability and point at a consistent diel cycle across Roșu. In figure 5.9b, the whole diel anomaly cycle from the lake is shown with figure 5.9c indicating the extraction for the sine-curve (Fig. 5.9a). As this was an experiment to ensure the feasibility of temporal extraction via daily data, this curve fits well, although potentially underestimating the entire diel cycle. Therefore, this function can be used to remove temporal variability on the diel time scale from the pCO_2 dataset which then should show only spatial plus short-term temporal variability. DIC was measured by the differences over the cross-over times throughout the transect (Figure 5.9d). Using this more linear fit, TA anomaly was then calculated from DIC and pCO_2 μatm (Fig. 5.10).

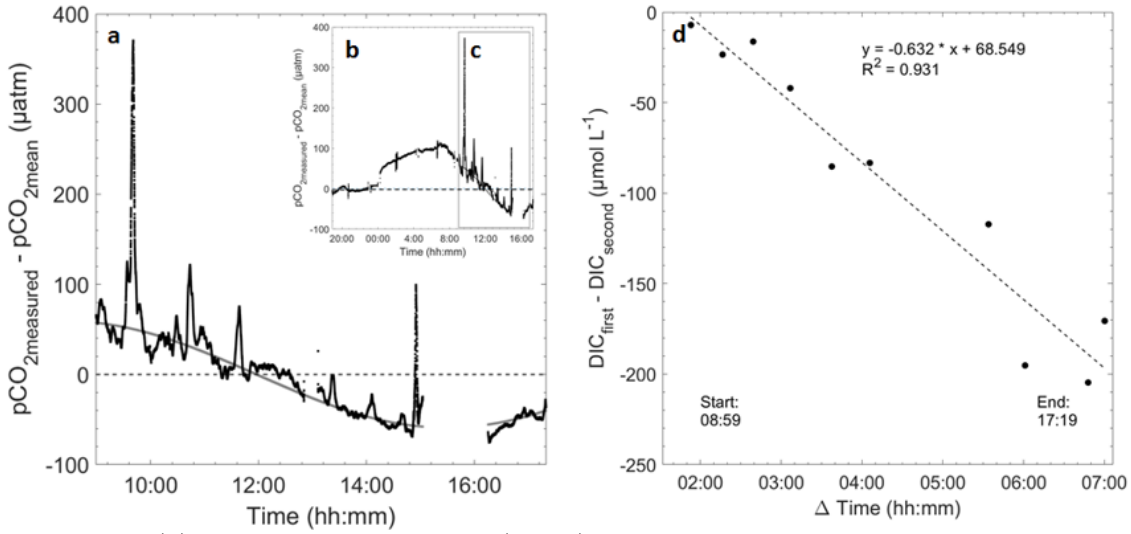

Figure 5.9: (a) A single Sine function (eq. 4) fitted to pCO_2,anom data from the 8 h mapping of Lake Roșu (see figure 1). The break between 15:00 and 16:00 was due to equipment not switched on. Data from 16:00 shows the return passing through the lake cutting across the previous mapping pattern (crossover locations). (b) The entire diel anomaly cycle from Lake Rosu over time showing the fit across the entire cycle, (c) box signalling the area in which figure a is taken from. (d) A linear fit for the temporal DIC change (DIC first transect – DIC second cross-over over difference in time (minutes)) observed through reoccupation of several locations in the lake during the detailed survey, where transects crossed over each other. The goal of this analysis is to exclude the diel variability across lake Roşu over the course of one day.

Removing the obsed/extracted diel cycle from pCO_2, DIC, pH, and TA (Fig. 5.10) reveals interesting differences in terms of spatial variability across the like. For all four parameters variability across the lake is reduced although small spatial scale (and possibly some unknown temporal) variability is still visible such as small peaks. For pCO_2 and pH, which in original data indicate a significant lateral gradient across the lake of about 140 μatm and 0.3, respectively, most of this variability is removed leaving pCO_2 of around 130 μatm and pH of 9.0. In contrast, both DIC and TA still retain a marked spatial gradient across the lake, with the DIC range reduced from originally 2,266-1,754 μmol L^{-1} to 2,355-1,908 μmol L^{-1} and the TA range from 2,262-1,953 μmol L^{-1} to 2,384-2,067 μmol L^{-1}, after removal of diel variability. This points at a large atmospheric control of pCO_2 (and hence pH) across the lake, whereas horizontal DIC and TA gradients appear to be driven by lateral hydrological input. This is further corroborated with the DIC (and TA) extrema being co-located with the channel entrances and the ends of the lake where water exchange could also be detected visibly.

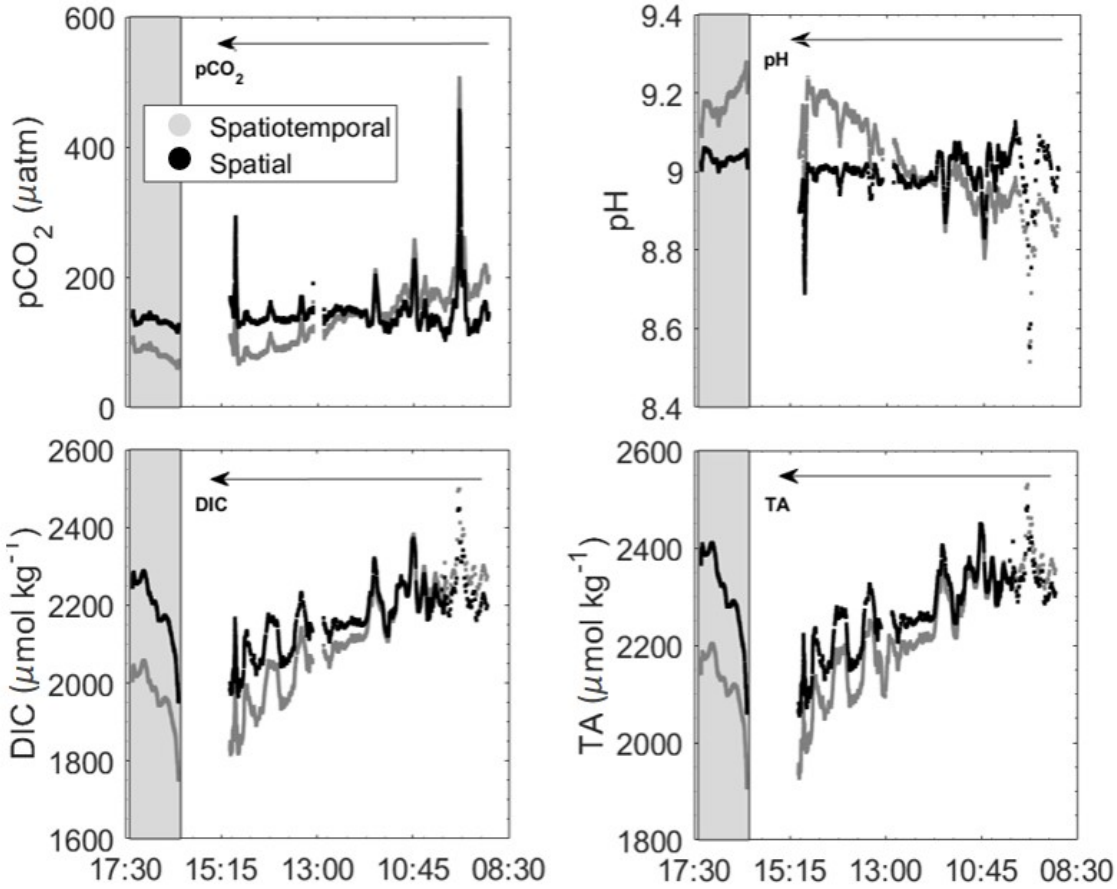

Figure 5.10: Both spatiotemporal and assumed spatial distributions (i.e. after removal of extracted diel cycle) of DIC, pCO_2, pH and total alkalinity (TA), across Lake Roșu over time (hh:mm) during Aug. Note the inverse time axis for better comparability to figure 5.7 where the zig-zag mapping pattern was carried out from east to west (see arrow in plots) while the straight return transect (grey box) went from west to east.

The gradient suggests hydrological inputs from one region of the lake, which can also be seen within appendix 5.13, with increased CO_3^{2-} (day: 06.08.2017). This provides further evidence in the applicability of doing such extractions (DIC speciation and temporal scale extraction). Within lakes, it has been previously found that in relatively high pH regions, under conditions of elevated CO_3^{2-} and reduced CO_2 concentrations, calcification is more pronounced (Andersen et al., 2019). Given the daily cycle of the DIC, if following a closed cycle this would suggest replenishment of DIC overnight, (Andersen et al., 2017). To fully assess this, stratification and its effects throughout the lake, vertical profiles would have been beneficial.

Using the extraction, the lake complex (Puiu, Roşu and Roşelette) has been shown to be influenced by Black Sea intrusions during the October months due to easterly winds (Durisch-Kaiser et al., 2008), however this is the opposite to what we found with input appearing to come in more from the West and the reed beds (Fig. 5.7). They also suggested, the lakes with the highest concentrations of CO_2 and CH_4 were closest to the Danube River, showing an influence from the inflow; this was only visible in our data from Lake Uzlina in May (appendix 5.15). Overall all lakes changed significantly both seasonally and spatially, further stressing the need for more characterised data due to vast seasonal and spatial variabilities.

Extraction of Diel Cycles

StCh show evidence of an extreme diel cycle (figure 5.11, $\sim$ 20.5 h) from the entrance of the StCh during Aug. There is an increase in ΔDIC after sunset, before dropping again with sunrise, in which the concentrations went from 17.7 to -228.3 μmol L^{-1} and 177.6 to 649.4 μmol L^{-1} for ΔO_2 and ΔDIC, respectively. An interesting feature of the observed diel cycle is the strong hysteresis in the data set, where during the net productive phase of the day (sunrise to sunset) DIC changes precede with oxygen changes lagging behind initially whereas during the net respirative phase (sunset to sunrise) oxygen changes precede with DIC lagging behind (Fig. 5.11). This may indicate that over the course of the entire cycle the contributions from aerobic (upper water column) and anaerobic (bottom waters or sediments) processes vary, either triggered by oxygen levels or by day-night changes in vertical mixing.

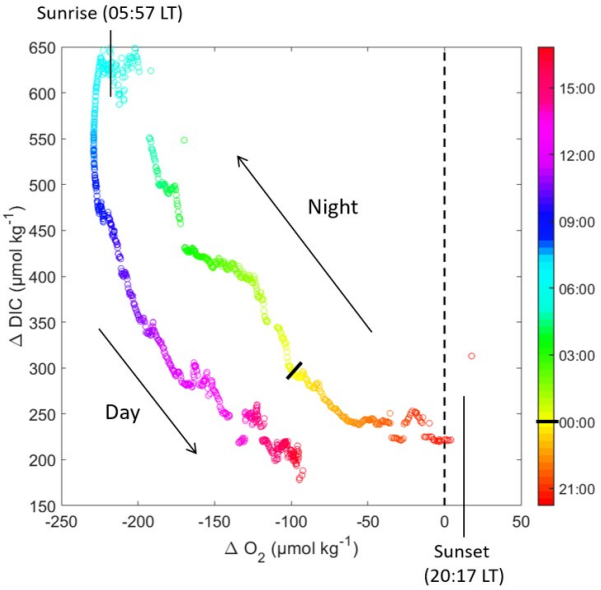

Figure 5.11: Diel cycle (20.5 h) of ΔDIC/ΔO_2 within the StCh during Aug (summer), with sunset (20:17 LT) and sunrise at 05:57 LT. Midnight (black thick line) is indicated as well as the time of day (colour bar, hh:mm). The fact that measurements do not cover a full 24 h cycle explains why the data do not perform a complete cycle.

Diel cycles within surface waters are regulated by multiple factors, however the consumption of O_2 overall was found to correlate to CO_2 (and therefore DIC) production, which is to be expected through respiration and also shown by others previously (Borges et al., 2004, 2015; Nimick et al., 2011; Stets et al., 2017). In general, if using the CO_2/O_2 stoichiometry of waters, you could expect predictable behavior. The results we show suggest external influences, given the slope varied from < 1 to > 1 depending on the time of the day, and CO_2 oversaturation exceeding that of O_2 consumption. When investigating StCh, combining the ratios with pCH_4 further enhances analysis justifications, with the potential influences suggesting anaerobic respiration, especially with the steep increase in pCH_4 (appendix 5.14). With wetlands being a known source for CH_4 due to anaerobic sediments (Bastviken et al., 2010), this can give further evidence for such water processes occurring within StCh both overnight (appendix 5.12, right) and during the transect along towards the end (appendix 5.12, left).

The StCh dynamics were found to be unique within our transects, however due to multiple other channels similar to this, it is highly unlikely it is the only 'hot spot' within the delta system. Especially given that the Danube has such vast reed beds coverage, these 'hot spots' could be scattered throughout yet are potentially highly influential on the carbon budget.

5.5 Conclusion

Overall, we observed that the Danube delta as a whole was supersaturated with respect to the atmospheric CO_2 concentration (722, 1,225 and 979 μatm, for May, Aug and Oct). Even though the full complexity of the system could not be fully captured, the spatial resolution of the data proved well enough to be able to successfully assess carbon and oxygen characteristics of main regions (lakes, rivers and channels). The delta showed strong spatial gradients throughout and within the region: both lakes and channels typically fluctuating between super- or undersaturated, yet the rivers staying consistently supersaturated with pCO_2. Lakes were only heavily influenced by channels in regions directly next to them, with the majority of lakes being undersaturated. However, with CO_2 and CH_4 emission from lakes projected to increase (Marotta et al., 2014), having the ability to consistently measure is of up-most importance to gather the biological dynamics within these diverse regions. On a seasonal scale, May had the largest variability for all regions (excluding the 'hot spot' that was observed), with Oct showing the most homogeneous patterns.

We were able to divulge further into this by extracting DIC from discrete samples and continuous data, showing the delta was almost completely net heterotrophic with net production only really occurring within the lakes during May and Aug. On top of processes such as aerobic remineralisation of organic matter transported into lakes, solely abiotic processes could be assessed. Including StCh ('hot spot') and diel cycles into the analyses enabled us to observe potential lateral (via reed beds and potential ground water intrusions, on top of that seen in lakes already) and vertical (within the lakes through day-time stratification and nocturnal mixing) inputs. Picking up on the 'hot spot' allowed for observations of potentially anaerobic methanogenesis towards the end of the StCh within a short distance during the day, where no more O_2 is used with a production of both pCO_2 and pCH_4, reaching extremely high values for both over all seasons. Seasonally the delta varied less than when split regionally, giving more of an importance to regional measuring comparison with influences on each system, rather than seasonal variability. When just focusing on one specific region within a vast delta system during day light hours, the diversity and variability across the delta is lost.

5.6 Appendices

Appendix 1

Rivers	**May**		**Aug**		**Oct**	
O_2 (μmol L^{-1})	207.4	289.9	182.7	227.5	233.7	300.0
pCO_2 (μatm)	794.5	2,540.0*	927.0	2,118.4	926.5	1,500.2
DIC (μmol L^{-1})	2,754.2	3,249.9	2,302.7	2,728.6	2,613.2	2,904.5
TA (μmol L^{-1})	2,742.4	3,244.1	2,271.9	2,674.5	2,572.5	2,853.8
Temperate (°C)	14.2	19.8	26.9	28.8	14.97	16.5

* Excluding 6 minutes of high concentrations dispersing and diluting in from the channels with a maximum value of 6149.4 μatm

Table 5.3: Maximum and minimum in rivers over each season (May, Aug and Oct) for O_2 (μmol L^{-1}), pCO_2 (μatm), DIC (μmol L^{-1}), TA (μmol L^{-1}) and Temperate (°C).

Appendix 2

Channels	May		Aug		Oct	
O_2 (μmol L^{-1})	173.1	396.1	113.4	355.4	220.7	359.9
pCO_2 (μatm)	77.0	10,455.1*	32.9	5,991.1	205.8	2,724.5
DIC (μmol L^{-1})	849.1	3,695.1	1,593.3	2,913.9	2,437.6	2,981.3
TA (μmol L^{-1})	864.6	3,599.4	1,826.9	2,723.8	2,472.7	2,899.3
Temperate (°C)	15.9	23.2	25.4	33	14.4	17.3

* Includes area where StCh influence continues for 5 minutes otherwise 8527.5 μatm.

Table 5.4: Max and min of each parameter over each season (May, Aug and Oct) found within channels (including channels around StCh).

Appendix 3

StCh	May		Aug		Oct	
O_2 (μmol L^{-1})	57.2	197.6	26.7	271.1	6.9	77.9
pCO_2 (μatm)	8,010.0	17,264.8	491.1	17,445.2	2,967.2	22,984.2
DIC (μmol L^{-1})	2,636.1	3,894.6	2,354.6	4,702.4	2,587.0	4,689.8
TA (μmol L^{-1})	2,323.9	3,267.7	2,380.6	4,324.2	2,466.8	3,803.3
Temperate (°C)	16.3	19.1	25.4	29.1	16.1	16.7

Table 5.5: Maximum and minimum of each parameters over each season (May, Aug and Oct) in StCh, excluding the channels surrounding it, for O_2 (μmol L^{-1}), pCO_2 (μatm), DIC (μmol L^{-1}), TA (μmol L^{-1}) and Temperate (°C). All parameters, excluding O_2, showing supersaturation.

Appendix 4

Lakes	May		Aug		Oct	
O_2 (μmol L^{-1})	186.6	430.3	104.3	376.1	213.2	376.4
pCO_2 (μatm)	14.1	8,868.9	24.8	4,867.0	177.9	2,959.8
DIC (μmol L^{-1})	765.4	3,192.8	1,552.9	2,640.3	2,303.2	2,918.2
TA (μmol L^{-1})	827.4	3,203.8	1,786.7	2,677.7	2,288.7	2,883.7
Temperate (°C)	15.1	22.9	25.6	33.4	14.2	17.8

Table 5.6: Min and max of each parameter (O_2 μmol L^{-1}, pCO_2 μatm, DIC μmol L^{-1}, TA μmol L^{-1} and Temperature °C) over the 3 seasons, spring (May), summer (Aug) and autumn (Oct) within lakes. pCO_2 μatm had the lowest values within lakes of all the regions for each season.

Appendix 5

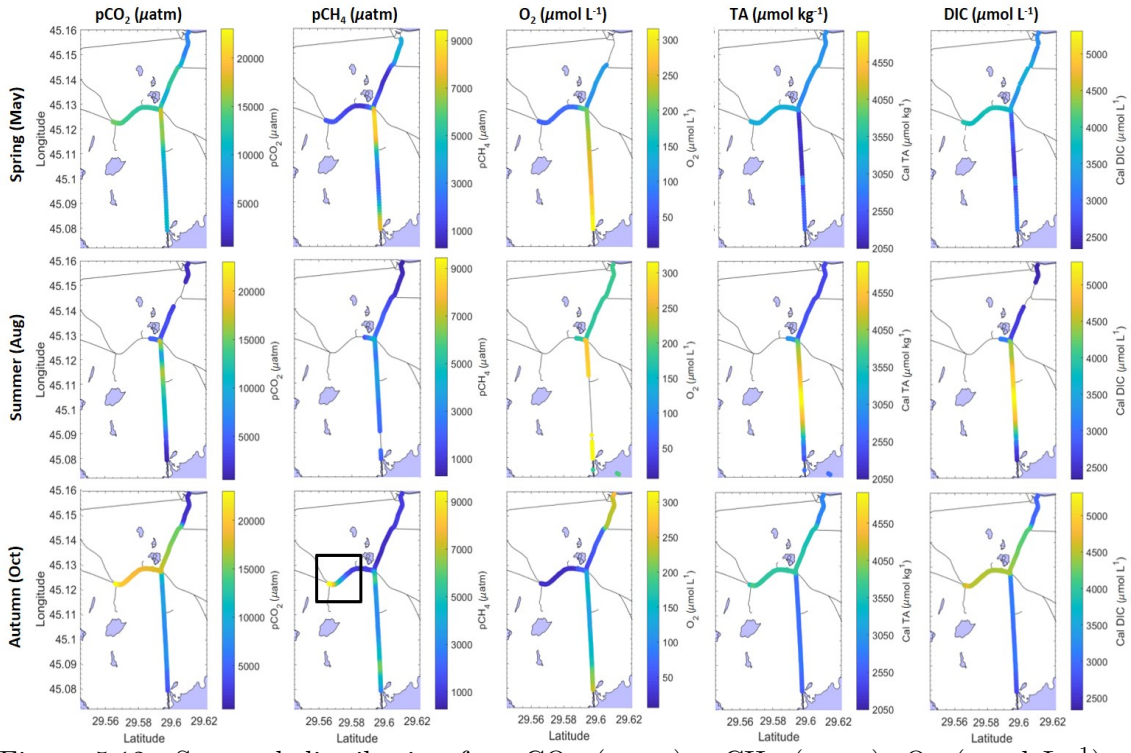

Figure 5.12: Seasonal distribution for pCO_2 (μatm), pCH_4 (μatm), O_2 (μmol L^{-1}), predicted total alkalinity (Cal TA) (μmol L^{-1}), and calculated dissolved inorganic carbon (Cal DIC) (μmol L^{-1}) during Spring (May), Summer (Aug) and Autumn (Oct). The black box in pCH_4 (μatm), Autumn, shows the extreme changes shown in appendix 5.15

Appendix 6

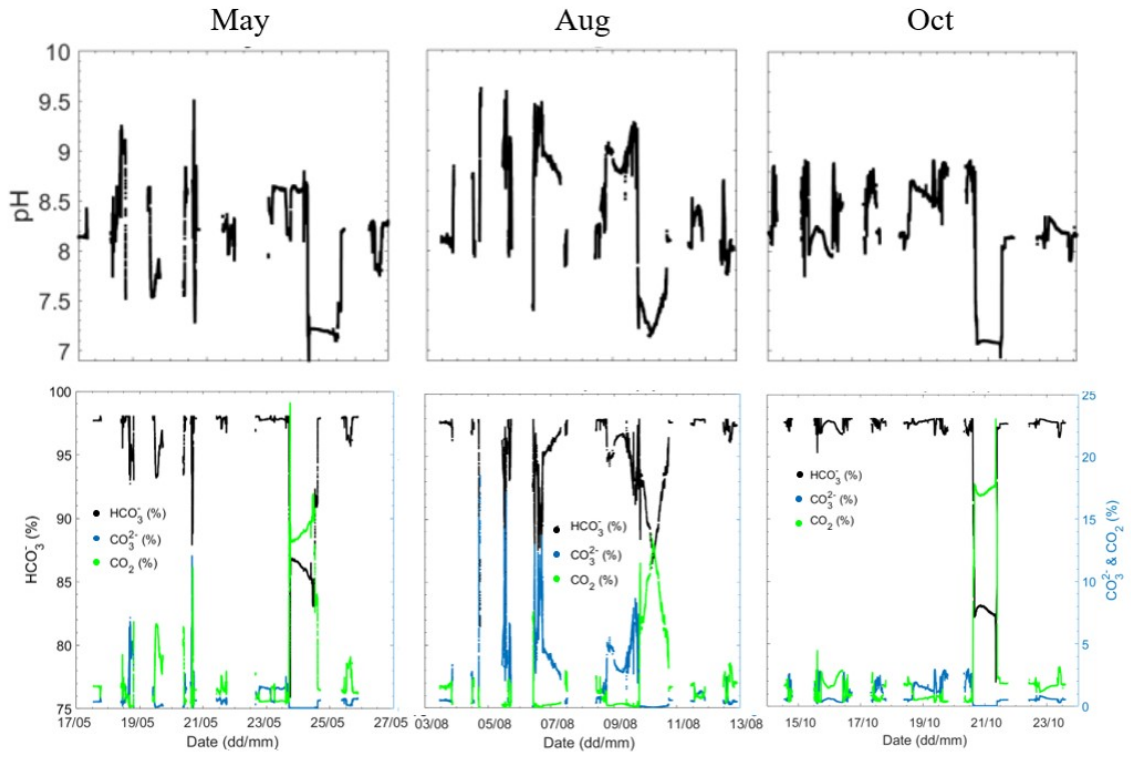

Figure 5.13: Speciation within the dissolved in organic carbon pool (DIC) and pH (top: black) as calculated using CO_2SYS (Lewis et al., 1998) for each season (May, Aug and Oct) along the entire cruise tracks.(Bottom) HCO_3^- on the left (black), CO_3^{2-} on the right (blue) and CO_2 (green).

Appendix 7

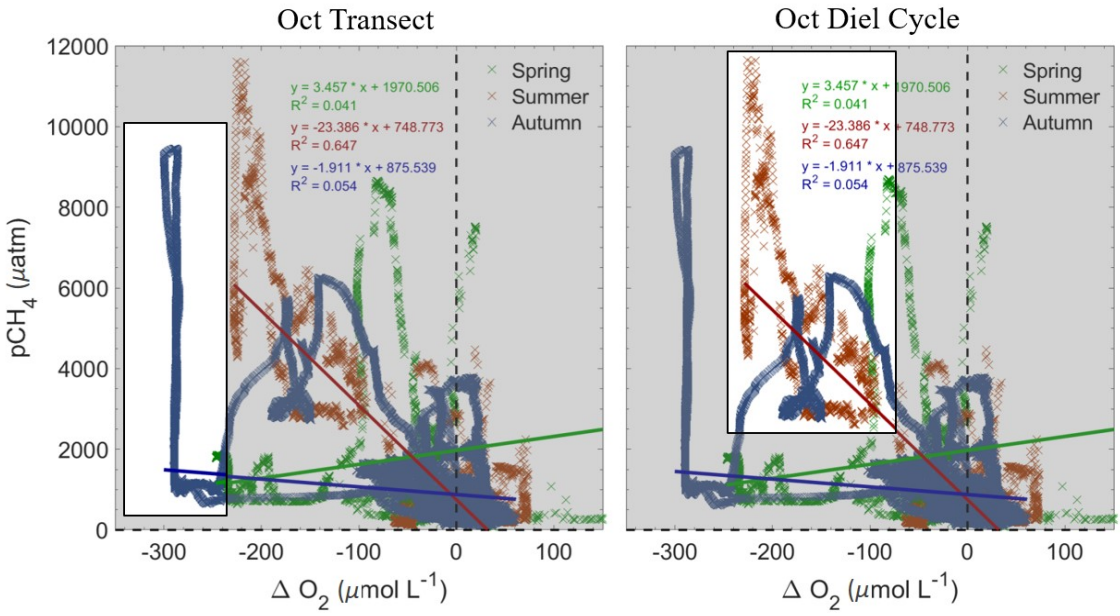

Figure 5.14: Correlation between pCH_4 and ΔO_2 including diel cycles. (left) Box indicates the location of the main part of 'stinky channel' spread over 1.2 km from half way along StCh in which O_2 stops being consumed. Over this period, pCO_2 increases just slightly as already supersaturated. (right) Box indicating day night cycle with pCH_4 dropping as the sun rose (same DN cycle as Fig. 5.11), giving a contrast as this effect as not occurring during Oct or May on quite this scale.

Appendix 8

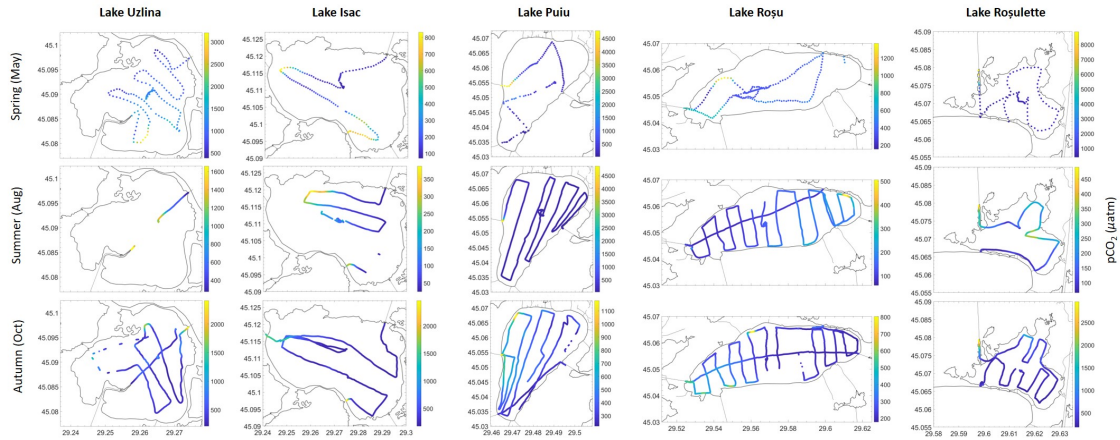

Figure 5.15: Mapping transects of all 5 lakes (Lake Uzlina, Isac, Puiu, Roșu and Roșulette) over the seasons (May, Aug and Oct) with pCO_2 excluding night cycles. Note the different pCO_2 scales, showing the full range of each lake. During May, only Lake Uzlina and Roșulette were oversaturated with pCO_2 μatm (median 1,102.7 $\pm$ 850.8 and 675.1 $\pm$ 408.8 ($\pm$SD) μatm), and in both Aug and Oct it was just Lake Uzlina (median of 940.4 $\pm$ 377.4 and 475.3 $\pm$ 249.6 ($\pm$ SD) μatm respectively); all other lakes were undersaturated. Influence of either channels or reed influence can be seen with increased concentration levels.

5.7 References

Abril, G. and Borges, A. V.: Carbon leaks from flooded land: do we need to re-plumb the inland water active pipe?, Biogeosciences, 769–784, doi:10.5194/bg-2018-239, 2019.

Allesson, L., Ström, L. and Berggren, M.: Impact of photo-chemical processing of dissolved organic carbon on the bacterial respiratory quotient in aquatic ecosystems, Geophys. Res. Lett., 43, 7538–7545, doi:10.1002/2016GL069621, 2016.

Andersen, M. R., Kragh, T. and Sand-Jensen, K.: Extreme diel dissolved oxygen and carbon cycles in shallow vegetated lakes, Proc. R. Soc. B Biol. Sci., 284(1862), doi:10.1098/rspb.2017.1427, 2017.

Anderson, L. A.: On the hydrogen and oxygen content of marine phytoplankton, Deep. Res. Part I, 42(9), 1675–1680, doi:10.1016/0967-0637(95)00072-E, 1995.

Antenucci, J. P., Tan, K. M., Eikaas, H. S. and Imberger, J.: The importance of transport processes and spatial gradients on in situ estimates of lake metabolism, Hydrobiologia, 700(1), 9–21, doi:10.1007/s10750-012-1212-z, 2013.

Aufdenkampe, A. K., Mayorga, E., Raymond, P. A., Melack, J. M., Doney, S. C., Alin, S. R., Aalto, R. E. and Yoo, K.: Riverine coupling of biogeochemical cycles between land, oceans, and atmosphere, Front. Ecol. Environ., 9(1), 53–60, doi:10.1890/100014, 2011.

Balmer, M. and Downing, J.: Carbon dioxide concentrations in eutrophic lakes: undersaturation implies atmospheric uptake, Inl. Waters, 1(2), 125–132, doi:10.5268/IW-1.2.366, 2011.

Bastviken, D., Cole, J. J., Pace, M. L. and Van de-Bogert, M. C.: Fates of methane from different lake habitats: Connecting whole-lake budgets and CH4H_4 emissions, J. Geophys. Res. Biogeosciences, 113(2), 1–13, doi:10.1029/2007JG000608, 2008.

Bastviken, D., Santoro, A. L., Marotta, H., Pinho, L. Q., Calheiros, D. F., Crill, P. and Enrich-Prast, A.: Methane emissions from pantanal, South America, during the low water season: Toward more comprehensive sampling, Environ. Sci. Technol., 44(14), 5450–5455, doi:10.1021/es1005048, 2010.

Berggren, M., Lapierre, J. F. and Del Giorgio, P. A.: Magnitude and regulation of bacterioplankton respiratory quotient across freshwater environmental gradients, ISME J., 6(5), 984–993, doi:10.1038/ismej.2011.157, 2012.

Bittig, H. C., Körtzinger, A., Neill, C., van Ooijen, E., Plant, J. N., Hahn, J., Johnson, K. S., Yang, B. and Emerson, S. R.: Oxygen Optode Sensors: Principle, Characterization, Calibration, and Application in the Ocean, Front. Mar. Sci., 4(January), 1–25, doi:10.3389/fmars.2017.00429, 2018.

Borges, A. V., Vanderborght, J.-P., Schiettecatte, L.-S., Gazeu, F., Ferrón-Smith, S., Delille, B. and Frankignoulle, M.: Variability of the Gas Transfer Velocity of Estuary (the Scheldt), Estuaries, 27(4), 593–603, doi:10.1007/BF02907647, 2004.

Borges, A. V., Darchambeau, F., Teodoru, C. R., Marwick, T. R., Tamooh, F., Geeraert, N., Omengo, F. O., Guérin, F., Lambert, T., Morana, C., Okuku, E. and Bouillon, S.: Globally significant greenhouse-gas emissions from African inland waters, Nat. Geosci., 8(8), 637–642, doi:10.1038/ngeo2$O_2$486, 2015.

Borges, A. V., Abril, G. and Bouillon, S.: Carbon dynamics and CO_2 and CH_4 outgassing in the Mekong delta, Biogeosciences, 15, 1093–1114, doi:10.5194/bg-15-1093-2018, 2018.

Borges, A. V and Abril, G.: Carbon Dioxide and Methane Dynamics in Estuaries, 2012.

Brennwald, M. S., Schmidt, M., Oser, J. and Kipfer, R.: A portable and autonomous mass spectrometric system for on-site environmental gas analysis, Environ. Sci. Technol., 50(24), 13455–13463, doi:10.1021/acs.est.6b03669, 2016.

Cai, W. J. and Wang, Y.: The chemistry, fluxes, and sources of carbon dioxide in the estuarine waters of the Satilla and Altamaha Rivers, Georgia, Limnol. Oceanogr., 43(4), 657–668, doi:10.4319/lo.1998.43.4.0657, 1998.

Cimbleris, A. C. P.: Planktonic bacterial respiration as a function of C:N:P ratios

across temperate lakes, Hydrobiologia, 384(1–3), 89–100, doi:10.1023/A:1003496815969, 1998.

Cole, J. J., Prairie, Y. T., Caraco, N. F., McDowell, W. H., Tranvik, L. J., Striegl, R. G., Duarte, C. M., Kortelainen, P., Downing, J. A., Middelburg, J. J. and Melack, J.: Plumbing the global carbon cycle: Integrating inland waters into the terrestrial carbon budget, Ecosystems, 10(1), 171–184, doi:10.1007/s10021-006-9013-8, 2007.

Coops, H., Hanganu, J., Tudor, M. and Oosterberg, W.: Classification of Danube Delta lakes based on aquatic vegetation and turbidity, Hydrobiologia, 415, 187–191, doi:10.1023/ A:1003856927865, 1999.

Couture, R. M., De Wit, H. A., Tominaga, K., Kiuru, P. and Markelov, I.: Oxygen dynamics in a boreal lake responds to long-term changes in climate, ice phenology, and DOC inputs, J. Geophys. Res. G Biogeosciences, 120(11), 2441–2456, doi:10.1002/2015 JG003065, 2015.

Covaliov, S., Van Geest, G., Hanganu, J., Hulea, O., Török, L. and Coops, H.: Seasonality of macrophyte dominance in flood-pulsed lakes of the Danube Delta, Hydrobiologia, 506–509(September), 651–656, 2003.

Crawford, J. T., Lottig, N. R., Stanley, E. H., Walker, J. F., Hanson, P. C., Finlay, J. C. and Striegl, R. G.: CO2O_2 and CH4H_4 emissionsfromstreams in a lake-rich landscape: Patterns, controls, and regional significance, Global Biogeochem. Cycles, (28), 197–210, doi:10.1002/2013GB004661.Received, 2014a.

Crawford, J. T., Loken, L. C., Casson, N. J., Smith, C., Stone, A. G. and Winslow, L. A.: High-Speed Limnology: Using Advanced Sensors to Investigate Spatial Variability in Biogeochemistry and Hydrology, Environ. Sci. Technol., 49(1), 442–450, doi:10.1021/es504773x, 2014b.

Cunada, C. L., Lesack, L. F. W. and Tank, S. E.: Seasonal Dynamics of Dissolved Methane in Lakes of the Mackenzie Delta and the Role of Carbon Substrate Quality, J. Geophys. Res. Biogeosciences, 123(2), 591–609, doi:10.1002/2017JG004047, 2018.

Deirmendjian, L. and Abril, G.: Carbon dioxide degassing at the groundwater-stream-atmosphere interface: isotopic equilibration and hydrological mass balance in a sandy watershed, J. Hydrol., 558, 129–143, doi:10.1016/j.jhydrol.2018.01.003, 2018.

Dickson, A. G., Sabine, C. L. and Christian, J. R.: Guide to Best Practices for Ocean CO_2 Measurements.North Pacific Marine Science Organization, 2007.

Dilly, O.: Microbial respiratory quotient during basal metabolism and after glucose amendment in soils and litter, Soil Biol. Biochem., 33(1), 117–127, doi:10.1016/S0038-0717(00)00123-1, 2001.

Drake, T. W., Raymond, P. A. and Spencer, R. G. M.: Terrestrial carbon inputs to inland waters: A current synthesis of estimates and uncertainty, Limnol. Oceanogr. Lett., 3(3), 132–142, doi:10.1002/lol2.10055, 2017.

Duarte, C. M. and Prairie, Y. T.: Prevalence of heterotrophy and atmospheric CO_2 emissions from aquatic ecosystems, Ecosystems, 8(7), 862–870, doi:10.1007/s10021-005-0177-4, 2005.

Durisch-Kaiser, E., Pavel, A., Doberer, A., Reutimann, J., Balan, S., Sobek, S., RĂDAN, S. and Wehrli, B.: Nutrient retention, total N and P export, and greenhouse gas emission from the Danube Delta lakes, Geo-Eco-Marina, (1), 81–90, doi:10.5281/zenodo.57332, 2008.

Duvert, C., Bossa, M., Tyler, K. J., Wynn, J. G., Munksgaard, N. C., Bird, M. I., Setterfield, S. A. and Hutley, L. B.: Groundwater-Derived DIC and Carbonate Buffering Enhance Fluvial CO 2 Evasion in Two Australian Tropical Rivers, J. Geophys. Res. Biogeosciences, 124(2), 312–327, doi:10.1029/2018JG004912, 2019.

Enache, I., Florescu, L. I., Moldoveanu, M., Moza, M. I., Parpală, L., Sandu, C., Turko, P., Rîșnoveanu, G. and Spaak, P.: Diversity and distribution of Daphnia across

space and time in Danube Delta lakes explained by food quality and abundance, Hydrobiologia, 842(1), 39–54, doi:10.1007/s10750-019-04025-y, 2019.

Friedrich, J., Dinkel, C., Grieder, E., Radan, S., Secrieru, D., Steingruber, S. and Wehrli, B.: Nutrient uptake and benthic regeneration in Danube Delta Lakes, Biogeochemistry, 64(3), 373–398, 2003.

Geta, R., Postolache, C. and Vădineanu, A.: Ecological significance of nitrogen cycling by tubificid communities in shallow eutrophic lakes of the Danube Delta, Hydrobiologia, 524(1), 193–202, doi:10.1023/B:HYDR.0000036133.92034.69, 2004.

Giosan, L., Constantinescu, S., Filip, F. and Deng, B.: Maintenance of large deltas through channelization: Nature vs. humans in the Danube delta, Anthropocene, 1, 35–45, doi:10.1016/j.ancene.2013.09.001, 2013.

Hanson, P. C., Bade, D. L., Carpenter, S. R., Kratz, T. K. and May, N.: Lake Metabolism: Relationships with Dissolved Organic Carbon and Phosphorus Lake metabolism: Relationships with dissolved organic carbon and phosphorus, Limnology, 48(3), 1112–1119, 2007.

Hanson, P. C., Carpenter, S. R., Kimura, N., Wu, C., Cornelius, S. P. and Kratz, T. K.: Evaluation of metabolism models for free-water dissolved oxygen methods in lakes, Limnol. Oceanogr. Methods, 6(9), 454–465, doi:10.4319/lom.2008.6.454, 2008.

Hedges, J. I., Baldock, J. A., Gélinas, Y., Lee, C., Peterson, M. L. and Wakeham, S. G.: The biochemical and elemental compositions of marine plankton: A NMR perspective, Mar. Chem., 78(1), 47–63, doi:10.1016/S0304-4203(02)00009-9, 2002.

Hooijmans, C. M., Geraats, S. G. M., van Neil, E. W. J., Robertson, L. A., Heijnen, J. J. and Luyben, K. C. A. M.: Determination of growth and coupled nitrification/denitrification by immobilized Thiosphaera pantotropha using measurement and modeling of oxygen profiles, Biotechnol. Bioeng., 36(9), 931–939, doi:10.1002/bit.260360908, 1990.

Hotchkiss, E. R., Sadro, S. and Hanson, P. C.: Toward a more integrative perspective on carbon metabolism across lentic and lotic inland waters, Limnol. Oceanogr. Lett., 3(3), 57–63, doi:10.1002/lol2.10081, 2018.

Istvánovics, V. and Honti, M.: Coupled simulation of high-frequency dynamics of dissolved oxygen and chlorophyll widens the scope of lake metabolism studies, Limnol. Oceanogr., 63(1), 72–90, doi:10.1002/lno.10615, 2018.

Kalcheva, H., Hristina, R., Beshkova, M., Berczik, Á., Kalchev, R., Tarjanyi, N. and Kiss, A.: Bacterioplankton of wetlands along the lower danube river (bulgaria) and its relation to environmental factors, Acta Zool. Bulg., 66(SUPPL. 7), 83–89, 2014.

Karim, A., Dubois, K. and Veizer, J.: Carbon and oxygen dynamics in the Laurentian Great Lakes: Implications for the CO_2 flux from terrestrial aquatic systems to the atmosphere, Chem. Geol., 281(1–2), 133–141, doi:10.1016/j.chemgeo.2010.12.006, 2011.

Kempe, S.: Carbon in the freshwater cycle., Glob. carbon cycle, (13), 317–342, 1979.

Koehler, B., Landelius, T. and Tranvik, L. J.: Photoproduction of dissolved inorganic carbon in Swedish lakes, , 14, 5119, 2012.

Kuhn, C., Bettigole, C., Glick, H. B., Seegmiller, L., Oliver, C. D. and Raymond, P.: Patterns in stream greenhouse gas dynamics from mountains to plains in northcentral Wyoming, J. Geophys. Res. Biogeosciences, 122(9), 2173–2190, doi:10.1002/2017JG003906, 2017.

Lauerwald, R., Laruelle, G. G., Hartmann, J., Ciais, P. and Regnier, P. A. G.: Global Biogeochemical Cycles, Global Biogeochem. Cycles, 29(5), 534–554, doi:10.1002/2014GB004941. 2015.

Lee, K., Tong, L.T., Millero, F.J., Sabine, C.L., Dickson, A.G., Goyet, C., Park, G.H., Wanninkhof, R., Feely, R.A. and Key, R.M., 2006. Global relationships of total alkalinity with salinity and temperature in surface waters of the world's oceans. Geophysical

research letters, 33(19).

Lewis, E., Wallace, D. and Allison, L. J.: Program developed for CO_2 system calculations, carbon dioxide information analysis center, Oak Ridge National Laboratory, Oak Ridge, Tenn., 1998.

Marotta, H., Pinho, L., Gudasz, C., Bastviken, D., Tranvik, L. J. and Enrich-Prast, A.: Greenhouse gas production in low-latitude lake sediments responds strongly to warming, Nat. Clim. Chang., 4(6), 467–470, doi:10.1038/nclimate2222, 2014.

Matache, M. L., Marin, C., Rozylowicz, L. and Tudorache, A.: Plants accumulating heavy metals in the Danube River wetlands, J. Environ. Heal. Sci. Eng., 11(1), 1–7, doi:10.1186/2052-336X-11-39, 2013.

Münzner, K. and Berggren, M.: In situ plankton community respiration measurements show low respiratory quotients in a eutrophic lake, Environ. Microbiol., 21(4), 1425–1435, doi:10.1111/1462-2920.14574, 2019.

Muraoka, K., Hanson, P., Frank, E., Jiang, M., Chiu, K. and Hamilton, D.: A data mining approach to evaluate suitability of dissolved oxygen sensor observations for lake metabolism analysis, , 16, 787–801, doi:10.1002/lom3.10283, 2018.

Nimick, D. A., Gammons, C. H. and Parker, S. R.: Diel biogeochemical processes and their effect on the aqueous chemistry of streams: A review, Chem. Geol., 283, 3–17, doi:10.1016/j.chemgeo.2010.08.017, 2011.

Obertegger, U., Obrador, B. and Flaim, G.: Dissolved oxygen dynamics under ice: Three winters of high-frequency data from Lake Tovel, Italy, Water Resour. Res., 53(8), 7234–7246, doi:10.1002/2017WR020599, 2017.

Oosterberg, W., Buijse, A. D., Coops, H., Ibelings, B. W., Menting, G. A. M. and Water, I. for I. W. M. and W.: Ecological gradients in the Danube Delta lakes: present state and man-induced changes, Lelystad Inst. Inl. Water Manag. Waste Water Treat. RIZA, doi:90.369.5309x, 2000.

Overeem, I. and Syvitski, J. P. M.: Dynamics and Vulnerability of Delta Systems, LOICZ Reports Stud. No. 35, GKSS Res. Center, (35), 54, 2009.

Palmer, S. C. J., Kutser, T. and Hunter, P. D.: Remote sensing of inland waters: Challenges, progress and future directions, Remote Sens. Environ., 157, 1–8, doi:10.1016/ j.rse.2014.09.021, 2015.

Panin, N. The Danube Delta. Geomorphology and Holocene Evolution: a Synthesis / Le delta du Danube. Géomorphologie et évolution holocène: une synthèse, Géomorphologie Reli. Process. Environ., 9(4), 247–262, doi:10.3406/morfo.2003.1188, 2003.

Pavel, A., Durisch-kaiser, E., Balan, S., Radan, S., Sobek, S. and Wehrli, B.: Sources and emission of greenhouse gases in Danube Delta lakes, Environ. Sci. Pollut. Res., 16, 86–91, doi:10.1007/s11356-009-0182-9, 2009.

Raymond, P. A., Bauer, J. E. and Cole, J. J.: Atmospheric CO_2 evasion, dissolved inorganic carbon production, and net heterotrophy in the York River estuary, Limnol. Oceanogr., 45(8), 1707–1717, doi:10.4319/lo.2000.45.8.1707, 2000.

Raymond, P. A., Zappa, C. J., Butman, D., Bott, T. L., Potter, J., Mulholland, P., Laursen, A. E., McDowell, W. H. and Newbold, D.: Scaling the gas transfer velocity and hydraulic geometry in streams and small rivers, Limnol. Oceanogr. Fluids Environ., 2(1), 41–53, doi:10.1215/21573689-1597669, 2012.

Raymond, P. A., Hartmann, J., Lauerwald, R., Sobek, S., McDonald, C., Hoover, M., Butman, D., Striegl, R., Mayorga, E., Humborg, C., Kortelainen, P., Dürr, H., Meybeck, M., Ciais, P. and Guth, P.: Global carbon dioxide emissions from inland waters, Nature, 503(7476), 355–359, doi:10.1038/nature12760, 2013.

Regnier, P., Friedlingstein, P., Ciais, P., Mackenzie, F. T., Gruber, N., Janssens, I. A., Laruelle, G. G., Lauerwald, R., Luyssaert, S., Andersson, A. J., Arndt, S., Arnosti, C., Borges, A. V., Dale, A. W., Gallego-Sala, A., Goddéris, Y., Goossens, N., Hartmann, J.,

Heinze, C., Ilyina, T., Joos, F., Larowe, D. E., Leifeld, J., Meysman, F. J. R., Munhoven, G., Raymond, P. A., Spahni, R., Suntharalingam, P. and Thullner, M.: Anthropogenic perturbation of the carbon fluxes from land to ocean, Nat. Geosci., 6(8), 597–607, doi:10.1038/ngeo1830, 2013.

Richey, J. E., Devol, A. H., Wofsy, S. C., Victoria, R. and Riberio, M. N. G.: Biogenic gases and the oxidation and reduction of carbon in Amazon River and floodplain waters, Limnol. Oceanogr., 33(4), 551–561, doi:10.4319/lo.1988.33.4.0551, 1988.

Rößger, N., Wille, C., Holl, D., Göckede, M. and Kutzbach, L.: Scaling and balancing carbon dioxide fluxes in a heterogeneous tundra ecosystem of the Lena River Delta, Biogeosciences Discuss., 1–40, doi:10.5194/bg-2019-10, 2019.

Song, K. S., Zang, S. Y., Zhao, Y., Li, L., Du, J., Zhang, N. N., Wang, X. D., Shao, T. T., Guan, Y. and Liu, L.: Spatiotemporal characterization of dissolved carbon for inland waters in semi-humid/semi-arid region, China, Hydrol. Earth Syst. Sci., 17(10), 4269–4281, doi:10.5194/hess-17-4269-2013, 2013.

Staehr, P. a, Bade, D., Koch, G. R., Williamson, C., Hanson, P., Cole, J. J. and Kratz, T.: Lake metabolism and the diel oxygen technique: State of the science, Limnol. Oceanogr. Methods, 8, 628–644, doi:10.4319/lom.2010.8.628, 2010.

Stets, E. G., Butman, D., McDonald, C. P., Stackpoole, S. M., DeGrandpre, M. D. and Striegl, R. G.: Carbonate buffering and metabolic controls on carbon dioxide in rivers, Global Biogeochem. Cycles, 31(4), 663–677, doi:10.1002/2016GB005578, 2017.

Takahashi, T., Broecker, W. S. and Langer, S.: Redfield ratio based on chemical data from isopycnal surfaces., J. Geophys. Res., 90(C4), 6907–6924, doi:10.1029/JC090iC04p06907, 1985.

Tamooh, F., Borges, A. V., Meysman, F. J. R., Van Den Meersche, K., Dehairs, F., Merckx, R. and Bouillon, S.: Dynamics of dissolved inorganic carbon and aquatic metabolism in the Tana River basin, Kenya, Biogeosciences, 10(11), 6911–6928, doi:10.5194/bg-10-6911-2013, 2013.

Thauer, R. K.: Functionalization of methane in anaerobic microorganisms, Angew. Chemie - Int. Ed., 49(38), 6712–6713, doi:10.1002/anie.201002967, 2010.

Torgersen, T. and Branco, B.: Carbon and oxygen fluxes from a small pond to the atmosphere: Temporal variability and the CO_2/O_2 imbalance, Water Resour. Res., 44(2), 1–14, doi:10.1029/2006WR005634, 2008.

Tranvik, L. J., Downing, J. A., Cotner, J. B., Loiselle, S. A., Striegl, R. G., Ballatore, T. J., Dillon, P. J., Finlay, K., Knoll, L. B., Kortelainen, P. L., Kutser, T., Larsen, S., Laurion, I., Leech, D. M., McCallister, S. L., McKnight, D. M., Melack, J. M., Overholt, E., Porter, J. A., Prairie, Y., Renwick, W. H., Roland, F., Sherman, B. S., Schindler, D. W., Sobek, S., Tremblay, A., Vanni, M. J., Verschoor, A. M., von Wachenfeldt, E. and Weyhenmeyer, G. A.: Lakes and impoundments as regulators of carbon cycling and climate, Limnol. Oceanogr., 54(6), 2298–2314, 2009.

Tranvik, L. J., Cole, J. J. and Prairie, Y. T.: The study of carbon in inland waters-from isolated ecosystems to players in the global carbon cycle, Limnol. Oceanogr. Lett., 3(3), 41–48, doi:10.1002/lol2.10068, 2018.

Tsutsui, H., Fujiwara, T., Inoue, D., Ito, R., Matsukawa, K. and Funamizu, N.: Relationship between respiratory quotient, nitrification, and nitrous oxide emissions in a forced aerated composting process, Waste Manag., 42, 10–16, doi:10.1016/j.wasman.2015.02.038, 2015.

Tweed, S., Leblanc, M., Bass, A., Harrington, G. A., Munksgaard, N. and Bird, M. I.: Leaky savannas: The significance of lateral carbon fluxes in the seasonal tropics, Hydrol. Process., 30(6), 873–887, doi:10.1002/hyp.10640, 2016.

Wang, Z. A., Bienvenu, D. J., Mann, P. J., Hoering, K. A., Poulsen, J. R., Spencer, R. G. M. and Holmes, R. M.: Inorganic carbon speciation and fluxes in the Congo River,

Geophys. Res. Lett., 40(3), 511–516, doi:10.1002/grl.50160, 2013.

Wilson, H. F. and Xenopoulos, M. A.: Effects of agricultural land use on the composition of fluvial dissolved organic matter, Nat. Geosci., 2(1), 37–41, doi:10.1038/ngeo391, 2009.

Woitke, P., Wellmitz, J., Helm, D., Kube, P., Lepom, P. and Litheraty, P.: Analysis and assessment of heavy metal pollution in suspended solids and sediments of the river Danube, Chemosphere, 51(8), 633–642, doi:10.1016/S0045-6535(03)00217-0, 2003.

Yiğiterhan, O. and Murray, J. W.: Trace metal composition of particulate matter of the Danube River and Turkish rivers draining into the Black Sea, Mar. Chem., 111(1–2), 63–76, doi:10.1016/j.marchem.2007.06.019, 2008.

Vannote, R. L., Minshall, G. W., Cummins, K. W., Sedell, J. R., and Cushing, C. E. (1980). The river continuum concept. Canadian journal of fisheries and aquatic sciences, 37(1), 130-137.

URL 1: https://www.icpdr.org/wq-db/wq

URL 2: http://www.ghiduldelteidunarii.ro/cotele-apelor-dunarii-la-tulcea/

Inland methane dynamics and diel cycles

In preparation as: Anna Canning, Arne Körtzinger, Bernhard Wehrli, 'Methane in the Danube Delta: the importance of spatial patterns and diel cycles for atmospheric emission estimates.' [In prep. for Biogeosciences]

6.1 Abstract

Methane (CH_4) is one of the substantial greenhouse gases in our atmosphere and over recent years has seen a significant increase from 1,775 ppb in 2006 to over 1,850 ppb in 2017. Although sources driving these increases are somewhat under debate, one potential contribution comes from wetlands. However, given the uncertainties around the fluxes, dynamics and concentrations within wetlands and other inland waters, there is considerable need to acquire higher resolution data to assist with explanations, monitoring and modelling of future predictions. Here we took a fully contained set-up measuring pCO_2, pCH_4, O_2 and auxiliary parameters and placed it on a houseboat for accessibility, to assess and analyse surface concentrations within the Danube Delta, Romania. Over 3 seasons we transected a $\sim$ 400 km route that consisted of extensive lake mapping and diel cycle stations. Overall the delta was a source for CH_4 throughout all seasons, with concentrations ranging between 0.113–15.6 μmol L^{-1}, and each system (lakes, rivers or channels) experiencing a variety of CH_4 ranges with channels having the highest variability. We found extreme diel cycles in both the lakes and channels, with concentrations varying by an order of magnitude between these two systems. The strong diel cycle within the lake suggested daily stratification due to macrophytes creating a temporal oxycline due to lack of light and movement between the stems as previously suggested. There was a clear linear trend with an O_2:CH_4 ratio of -50:1 due to nocturnal convection with the two water bodies mixing during the night. Throughout the day there was a consistent overall concentration of CH_4 at around 0.4 μmol L^{-1}. From our study we found, neglecting these diel cycles would reduce the average methane concentrations by 25% and increase by 3.3% for channels and lakes, respectively. Analyses also included a 'hot spot' in which a similar pattern was observed, with a far stronger methane cycle (from 4-15.6 μmol L^{-1}) overnight, with an almost immediate and extreme decrease in CH_4 following sunrise. Calculated diffusive CH_4 fluxes for the overall delta accounted for 49 $\pm$ 61 μmol m^{-2} h^{-1} corresponding to an annual flux of 0.43 $\pm$ 0.53 mol m^{-2} yr^{-1}. Our data illustrate the importance of collecting information on diel cycles to improve the emission estimates from wetland systems.

6.2 Introduction

Methane (CH_4) is one of the most relevant anthropogenic greenhouse gases following carbon dioxide (CO_2), has an estimated global emission of 572 Tg CH_4 yr^{-1} for the decade 2003-2012 (Saunois et al. 2019). More recently, we have seen an accelerated increase in atmospheric concentrations, rising from 1,775 ppb in 2006 to 1,850 ppb in

2017, with increased biogenic emissions from wetlands as a potential driver (Nisbet et al. 2019), contributing to the overall estimate of 159 (117-212) Tg CH_4 $yr^{-1}$from inland waters (Saunois et al. 2019). Although these emission numbers have high uncertainties, aquatic systems are known to act as sources (including sub-systems as sinks), with the majority of ocean and freshwaters to be substantial sources of CH_4 (Bastviken et al. 2011; Raymond et al. 2013). Inland waters only take up 3% of Earth's surface, yet combined with oceanic waters over recent years they account for 68% of all CH_4 emissions (Dean et al. 2018). In this however, the ocean only releases roughly 1-3% of the global CH_4 emissions (Saunois et al. 2016). Due to this difference in CH_4 source strength, inland waters have seen an increase in attention (see Abril and Borges 2005; Panneer Selvam et al. 2014; Richey et al. 2002; Wang et al. 2009; Zhang et al. 2018). Over a 100-year basis, CH_4 is 34 times more potent as a greenhouse gas than CO_2 when including climate carbon feedbacks (28 times without feedbacks: Myhre et al. 2013; Schubert and Wehrli 2019), and its continued increase has the potential to reverse any progress made for climate mitigation by reducing CO_2 emissions (Nisbet et al. 2019).

Wetlands are one of the single largest source within the inland waters with CH_4 emissions at 150–225 Tg CH_4 yr^{-1} accounting for roughly one third of total emissions (Dean et al. 2018). Rivers emit 1.5–26.8 Tg CH_4 yr^{-1}, and when combined with lakes contribute 73.1 Tg CH_4 yr^{-1} (Bastviken et al. 2011; Stanley et al. 2016), although these numbers have large uncertainties (Kirschke et al. 2013). However, given their potentially significant contribution to CH_4 in the atmosphere, they are still not included in some global greenhouse gas inventories and therefore further measurements are crucial for these systems (Bastviken et al. 2011).

Due to lakes being some of the easier systems to measure and compare, they are usually the most well measured systems components of inland waters and although only covering 0.9% of the Earth's surface give a range of around 8-73 Tg CH_4 yr^{-1} (Kirschke et al. 2013). They are known to generally be hot spots in terms of CH_4 emissions, even more so for shallow lakes (Cole et al. 2007; Davidson et al. 2018). Considering this, channels and rivers are more abundant than lakes and emit around 26.8 Tg CH_4 yr^{-1} excluding ebullition (Stanley et al. 2016). Yet there is a lot of contradicting work on river systems with uncertainties in values, processes and sources. Due to a lack of data coverage and consistency their role in the both carbon transport and storage is not well constrained (Tranvik et al. 2009). Rivers tend to be underrepresented within the world database (Crawford et al. 2014b; McGinnis et al. 2016; Stanley et al. 2016). Therefore, there is a need for more detailed assessment of the role of methane emissions from rivers and channels as they have been suggested to be more spatiotemporally variable for CH_4 than CO_2 (Stanley et al. 2016; Natchimuthu et al. 2017).

Surface inland waters, like ocean waters, are typically supersaturated with CH_4. However, given these surface waters also tend to be well-oxygenated and therefore should not host major methanogenic activity, this has led to the 'methane paradox' notion (Schmidt and Conrad 1993; Karl et al. 2008; Grossart et al. 2011; Tang et al. 2014; DelSontro et al. 2018). There is still a lot of debate on the ways CH_4 is being produced in oxic inland waters (Peeters et al. 2019). In the ocean, methanogenesis under oxic condition is thought to be largely driven by the process of bacterial degradation of dissolved organic matter in seawater (Repeta et al. 2016). When comparing these inland water systems to the ocean, oxic methane peaks are up to 1,000 times higher than those in marine waters and given the oxic methane layer depth is on a scale of roughly 1:10 (inland to ocean) this suggests that both marine and freshwaters have equal amounts of oxic methane (Tang et al. 2016).

Generally, CH_4 is biogenically produced within anaerobic environments (see Fig. 6.1 for details), where microbial fermentation of organic matter occurs and is controlled by

the interplay between input of organic matter and temperature (Stanley et al. 2016). This is generally the end of the line respiration process, through either hydrogenotrophic methanogenesis where oxidation of H_2 using CO_2 as a terminal electron acceptor produces CH_4 or by acetoclastic methanogenesis via the breakdown of simple substrates or acetate, which is a major pathway within the fresh water systems (Whiticar et al. 1986). Other processes also include ebullition, generally contributing far larger than that of diffusive fluxes with up to 50% of the total flux in certain systems (van Bergen et al. 2019), or more physical processes such as vertical mixing between surface and sub-surface layers, lateral transport and ground water inputs (Crawford et al. 2014a; Stanley et al. 2016).

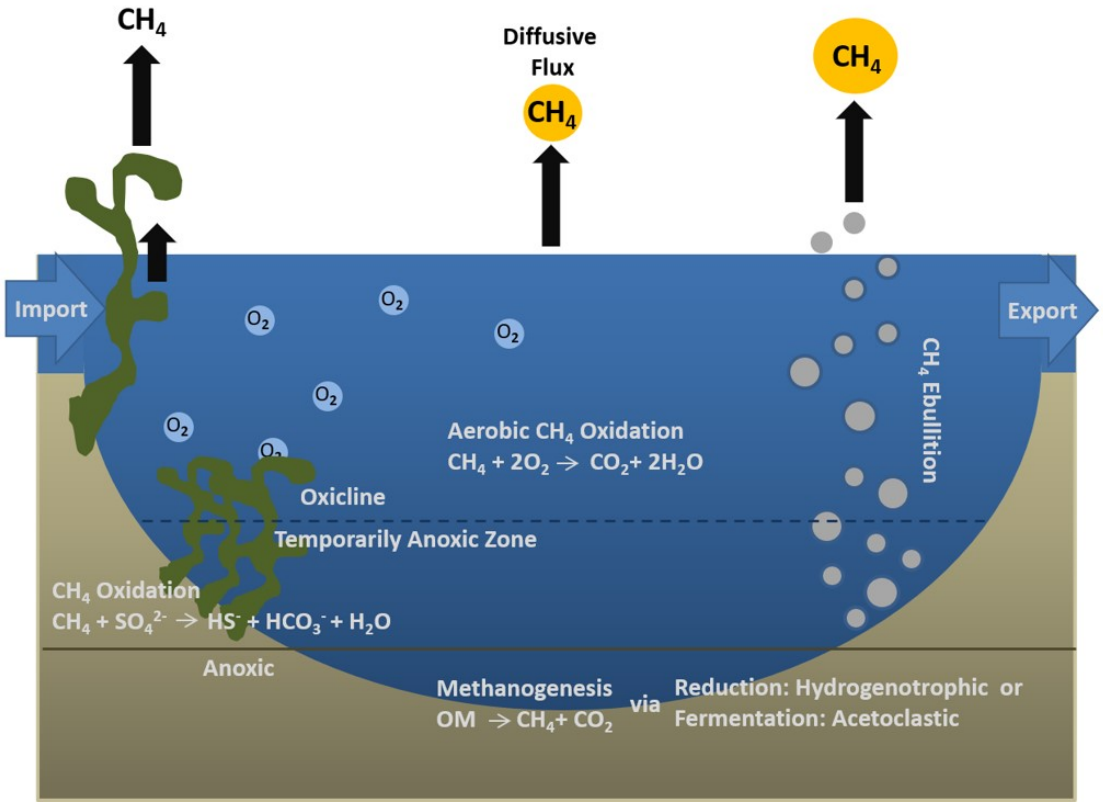

Figure 6.1: Some of the main processes within a lake. These are separated between the surface and sub-surface layers in a typical stratified situation. Well-oxygenated surface waters are places of CH_4 oxidation but also can host macrophytes which are known to produce methane some of which can be outgassed directly into the atmosphere. Sub-surface waters can host both methanogenic and methane oxidation pathways. Arrows pointing up symbolise the water-air fluxes resulting from typically observed supersaturation of methane in surface waters.

Most of these studies into the processes tend to ignore any potential diel cycle of CH_4. Diel cycles within inland waters have been observed, either due to the influence of biological processes such as photosynthesis and respiration or temperature dependent solubility (Nimick et al. 2011; Maher et al. 2015; Zhang et al. 2018). Although potentially substantial, these are rarely considered especially with fluxes due to general lack of data. Just as with overall data coverage of CH_4, both spatially and temporally, there is also need for refined and better understanding of the contributions and the controls of CH_4 production and sources (Bogard et al. 2014; Abril and Borges 2019).

The Danube River Delta, as most river deltas, is known to be an important natural source of CH_4 (Cuna et al. 2008; Durisch-Kaiser et al. 2008; Pavel et al. 2009). With climate warming, CH_4 production is set to increase from lakes as well as through

eutrophication (Marotta et al. 2014; Del Sontro et al. 2019, Sepulveda-Jauregui et al. 2018; Bartosiewicz et al. 2019). Bartosiewicz et al. (2019) suggest that increased warming and browning of the lakes will increase the warming of surface waters causing increasing stratification. This potentially will increase C storage below the pycnocline (between 0.22 – 4.5 Tg C yr^{-1}), which may lead to an increase the CH_4 production in bottom waters potentially leading to + 8% of the current global lake emissions from shallow (< 5 m) lakes. Therefore, having spatial and temporal (i.e. at least seasonal and diel) variability knowledge is important for future predictions through modelling efforts, analyses of processes and monitoring of CH_4 emissions. Given the complexity of inland water systems, especially wetlands, monitoring approaches tend to stay within one system. Here we use a set-up that can be deployed throughout the Danube delta, continuously measuring gas concentrations from a moving platform allowing for high resolution and high coverage data. Spatial variability of each individual systems (lakes, rivers and channels) have been recognized to have impacts on the subsequent systems, and therefore getting across-boundary data will get a better understanding of the linkage between the components of the delta. Our focus is more on the emission values from surface waters and how these change across the delta and during diel cycles.

6.3 Methods

6.3.1 Set up

A portable, versatile flow-through sensor set-up was placed on-board a small houseboat, continuously mapping throughout the Danube Delta. Campaigns took place over three seasons: May (17-26), Aug (3-12), and Oct (13-23) 2017. The set-up consisted of the HydroC® CO_2 FT (carbon dioxide partial pressure, pCO_2, Kongsberg Maritime Contros, Kiel, Germany: KMCON), HydroC® CH_4 FT (CH_4 partial pressure, pCH_4, KMCON), HydroFlash® O_2 (dissolved oxygen, O_2, KMCON) and a SBE 45 thermosalinograph (Sea-Bird Electronics, Bellevue, USA) to measure temperature and conductivity. All sensors ran simultaneously at a speed of up to 1 Hz on the same continuous water flow. The HydroC® CO_2 FT and the HydroC® CH_4 FT use NDIR and TDLAS technology respectively, while the HydroFlash® O_2 Optode sensor uses the principle of dynamic florescence quenching (Bittig et al. 2018). Further details on the setup, its calibration and validation can be found in Canning et al. (subm).

6.3.2 Study Site

The Danube River Delta is located on the Black Sea coast of Ukraine and Romania (44°25'-45°30'N and 28°45'-29°46'E). Originating in Germany, the Danube river travels across 2,857 km, with a drainage basin of 817,000 km2 (Panin 2003). The delta is a complex system made of wetlands, lakes, rivers and channels, both manmade and natural, with the largest compact reedbed zone in the world (Oosterberg et al. 2000; Panin 2003). The fluvio-marine delta system accounts for 51% (Pavel et al. 2009) in which it sees salt intrusions and through-flow from the Black Sea into the delta. Since the 1970s, the Danube Delta has been subject to eutrophication, with its peak during 1987-1988, largely due to the inflow of nutrients (Cristofor et al. 1993; Galatchi and Tudor 2006; Enache et al. 2019). After a decrease in 1990's, due to socioeconomic changes in Eastern Europe, a slow recovery of nutrient levels due to persistent loading was observed (Rîşnoveanu et al. 2004; Pavel et al. 2009), however more recent levels comparable to those in 1988 were reported (Tudor et al. 2016; Spiridon et al. 2018).

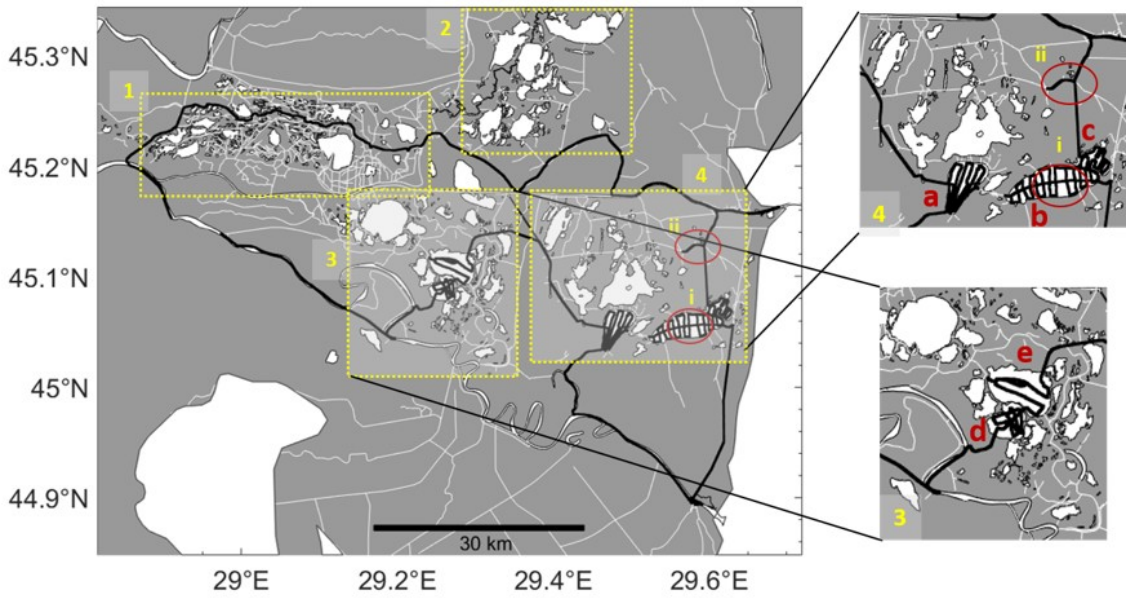

Figure 6.2: The Danube River Delta, Romania with the cruise tracks from the three seasonal campaigns in black, with only slight variations due to accessibility by boat. Systems of lake complexes: Contea-Furtuna (1), Matita-Merhei (2), Gorgova-Uzlina (3) and Roşu-Puiu (4), with only 3 (c) and 4 (b) extensively mapped and analysed here. Side figures show Lakes Puiu (a), Roşu (b), Roşulette (c), Uzlina (d) and Isac (e). Red circles indicate the two diel cycles at Lake Roşu (i) and the 'hot spot' channel (ii), both during the August campaign.

The delta is within the temperate system, however experiences extreme temperature ranges with air temperature from below freezing (< 0°C) to + 30°C (ICDP 2004). Deltas are continuously changing landscape, with moving lake systems and floating islands. The overall Danube delta is roughly 4423 km^2 with a 67-81% coverage in either aquatic ecosystems (rivers, lakes and channels) or wetlands (Cristofor et al. 1993). Using a small houseboat, the set-up was fixed, and a thorough transect throughout the delta was carried out with extensive lake transects completed in all three seasons for comparability (Fig 6.2). This study also features two stationary diel cycle measurements (Fig 6.2: red circles), one in lake Roşu and the other in the channel where we witnessed a major biogeochemical 'hot spot'.

6.3.3 Computations of Saturation and fluxes

The average global CH_4 concentration (ppb) was taken from NOAA/ESRL Global Monitoring Division program (Dlugokencky 2020) for May, Aug and Oct 2017 (1,847, 1,844.7 and 1,858.1 ppb respectively). As the delta is practically sea level, barometric pressure as well as wind speed measured at the Gorgova station were used. Schmidt numbers (Sc) were calculated for temperature dependence following (Wanninkhof 1992) for freshwater. The corrected Schmidt numbers varied between 296 and 824 in this study, consistent with temperature variance. Combined with CH_4 solubility, atmospheric equilibrium and saturation was calculated. Fluxes were calculated following the work from Peeters et al. (2019); supplementary material S3.2). Given slow stream velocities, we used the parameterisation from Cole and Caraco (1998) with constant gas-transfer velocity of ∼2 cm h^{-1} in the absence of wind

$$k_{600} = 2.07 + 0.215 \cdot U^{1.7}\,\mathrm{cm\,h^{-1}} \tag{6.1}$$

where U is wind speed at 10 m height in m s^{-1}, and $k600$ is the gas transfer velocity

normalised to a Schmidt number of 600, i.e. CO_2 in freshwater at 20°C (Jähne et al. 1987; Crusius and Wanninkhof (2003):

$$\mathrm{k}_{CH_4} = k_{600}\,(\frac{Sch\mathrm{CH_4}}{600})^n \tag{6.2}$$

$for\ U \leq 3.7\ ms^{-1}\ n = -\ \frac{2}{3},\ for\ U > 3.7\ ms^{-1}\ n = -\ \frac{1}{2}$

where k_{CH_4} is the transfer velocity at Sch_{CH_4} is the Schmidt number of CH_4 at a given temperature, and the exponential n reflects two wind speed regimes (Jähne et al. 1987). For rivers, due to differencing fetch and dynamics we used n = -0.5 throughout, consistent with multiple river studies (Borges et al. 2004; Guérin et al. 2007; Bange et al. 2019).

The flux was then calculated using the CH_4 concentration in the water and air:

$$Flux = k_{CH_4} \cdot (\mathrm{CH_{4,water}} - \mathrm{CH_{4,air}})\,\mathrm{mol\,m^{-2}\,s^{-1}} \tag{6.3}$$

Given that the effect of spatial variability of k_{CH_4} is relatively small in lakes with surface areas of 5x10^5 m^2 or larger, we disregarded size effects of lakes on emission fluxes (Schilder et al. 2013).

In the following analyses, both day and night data will be shown unless stated otherwise for CH_4, compared to the previous section (section 5) where it was excluded.

6.4 Results and discussion

6.4.1 Concentrations distribution and estimated fluxes

Overall CH_4 situation in Danube river delta

Our high spatiotemporal resolution CH_4 data showed constant supersaturation (113 to 15,600 nmol L^{-1}), throughout the delta. Significant variability both systemically and seasonally was observed, with channels having the highest concentrations of up to 15600 nmol L^{-1} (table 6.1) and showing a magnitude higher values compared to rivers. The concentrations are within the lower ranges previously observed (20 to 280,000 nmol L^{-1}) in methane in oxic freshwaters (Tang et al. 2016; Bižić-Ionescu et al. 2019).

High spatial variability was found across systems and water type boundaries (such as channels to lakes), which was also observed clearly by Crawford et al. (2017). More confined areas and in closer proximity to the wetlands, were found to have the highest concentrations. These boundary crossovers were due to seasonal changes in concentrations and change of flow direction varying throughout the delta. May and Aug show similar median CH_4 concentrations at 627 nmol L^{-1} and 951 nmol L^{-1}, respectively, however Oct CH_4 level had increased to 1440 nmol L^{-1} (Fig. 6.3). In each season, 3 specific locations stood out with extreme CH_4 concentrations: the two channels joining Lake Puiu (Crisan channel to the north and one from the south), and the 'hot spot' channel anomaly (red circle (i) on channel in Fig 6.2). Rivers and channels (including the anomaly) showed the highest variability during Aug and May, consistent with the directional flow regime bringing in the water from the surrounding wetlands after the flood waters. The highest median was during Oct for rivers, lakes and overall (median: 559, 693 and 1,500 nmol L^{-1} respectively), which coincides with the degradation of the macrophytes increasing the supply of biodegradable organic matter allowing for anoxic decomposition of organic carbon which releases CH_4 (Segers 1998).

Oxygen (O_2) was consistently undersaturated, however saturations were not distributed proportionally which potentially led to the lower median in May from the 'hot spot'. During all months, generally O_2 saturation (%) was above 60% with Aug showing the larges variability above 100% coinciding with both temperature and production. These values included the 'hot spot', given it is a natural feature and most likely not the only one within the Danube delta.

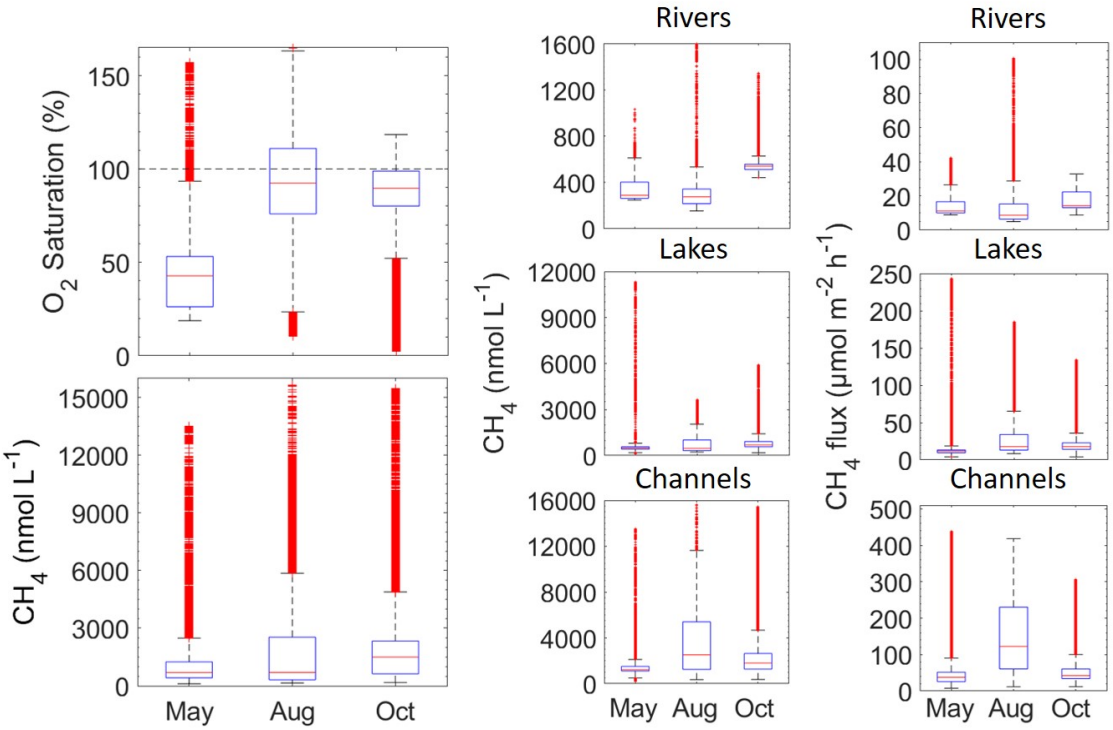

Figure 6.3: Left panel: oxygen saturation and methane concentration data from the three seasonal campaigns: May, August, and October. Central panel: CH_4 concentrations split by water type (rivers, channels and lakes). All data are included, including the hot spot and day/night cycle data. Right panels – CH_4 fluxes. The blue boxes represent the 25^{th} and 75^{th} percentiles, with the whiskers denoting 1.5 times that of the upper and lower box boundaries. Median values are shown as horizontal red lines.

Concentrations almost translate to the water-air fluxes (Fig. 6.3), with some variability ultimately due to temperature and wind. The diffusive fluxes have been suggested to underestimate total fluxes from lakes by 277% (Sanches et al. 2019) due to those and possibly other reasons such as micro-bubble flux enhancement, ebullition and direct plant emissions (Carmichael et al. 2014; McGinnis et al. 2015).

Taking the average across all 3 seasons we got an overall mean flux density of 49 $\pm$ 61 μmol m^{-2} h^{-1}. Using the area from Cristofor et al. (1993) according to which between 67-81% (2,963 to 3,582.6 km^2) of the delta consists of wetlands, rivers, lakes and stream, we estimated the delta's total emissions. We did this by using the above mean calculated flux for the area and applied this to the total area (2,963 - 3,582.6 km^2) over the entire year. This gave an emission range of 0.013- 0.042 Gg yr^{-1} CH_4 for the entire wetland, river, lake and stream covered region. The global overall average for wetlands, lakes, streams and rivers is 117-212 Tg CH_4 yr^{-1} (Saunois et al. 2019), from a total area of 596-894 million ha. The Danube delta therefore accounts for 0.0003 – 0.0006% of this total global area, and using the mean flux for the yearly calculation, scales up to between 0.00006 – 0.0004% of total emissions.

Table 6.1: Statistics (minimum (Min), median (Med), maximum (Max)) of CH_4 concentrations (nmol L^{-1}), CH_4 saturation (%) and CH_4 flux (μmol m^{-2} h^{-1}) of each system (rivers (R), channels (Ch) the hot spot channel (HS) and lakes (L)) over the 3 seasons: May, Aug and Oct 2017

System		CH_4 nmol L^{-1}			CH_4 Saturation %			CH_4 Flux μmol m^{-2} h^{-1}		
		May	**Aug**	**Oct**	**May**	**Aug**	**Oct**	**May**	**Aug**	**Oct**
R	**Min**	248	154	441	8564.0	6420.7	14232.1	8.9	4.9	8.8
	Med	302	290	541	10522.0	12235.3	17573.9	11.2	8.7	14.2
	Max	1040	1610	1350	35588.9	66618.4	44637.4	42.1	100.7	33.9
Ch	**Min**	221	355	369	7985.7	13960.9	11807.8	7.6	11.6	11.9
*	**Med**	1170	1300	2230	40858.3	55685.0	71423.5	39.1	63.4	49.4
	Max	6950	4270	6120	241534.6	179524.9	203121.8	225.4	219.9	165.5
HS	**Min**	1030	1830	994	33921.9	78643.9	32678.9	22.8	82.4	19.7
	Med	1210	5710	1730	40449.2	236897.6	56914.8	32.2	210.7	36.1
	Max	13500	15600	15500	468686.6	630620.8	507269.9	438.3	418.4	306.4
L	**Min**	113	224	177	4123.6	9449.6	5589.8	3.9	8.3	3.9
**	**Med**	465	466	693	16071.0	19291.3	22303.1	11.8	17.8	17.8
	Max	11300	3650	5930	394781.0	165378.2	187462.4	243.6	185.3	134.7

* Excluding Stinky channel ('hot spot') and channels connecting due to being an anomaly within our transect

** higher range in lakes due to influence of channels

We found very little evidence that intrusions from the Black Sea may have reached into the delta and have an impact such as suggested before (Durisch-Kaiser et al. 2008; Pavel et al. 2009). The highest conductivity observed was 0.08 S m^{-1} (overall mean ± SD of 0.038 ± 0.005 S m^{-1}), around the system of the 'hot spot', suggesting potential ground water influences, due to presence of more charged particles in the water. From our meteorological data, we found little correlation with external factors such as wind, however, given it was not measured in situ, this cannot be fully quantified. We therefore suggest the observed distribution patterns over the entire delta (as a whole) are mostly more driven by both biological and physical processes instead of external factors, as previously suggested (Bange et al. 2019; Sanches et al. 2019), further explored below.

Fluvial CH_4

The fluvial delta (rivers and channels) works as the supply of incoming water into the main part of the delta, accounting for the base level of CH_4 concentrations being laterally transported. Rivers had the lowest range of concentrations for CH_4 with the smallest variability out of all systems and the delta (Fig 6.3) ranging from 154 to 1,600 nmol L^{-1} (during Aug). Comparatively, channels experienced some of the highest concentrations due to the 'hot spot' within the Danube delta, ranging from 221 to 15,600 nmol L^{-1} for May and Aug respectively. When excluding the 'hot spot', medians were fairly consistent throughout May and Aug yet higher during Oct (1,170, 1,300 and 2,230 nmol L^{-1} respectively) within channels. When including this 'hot spot', the dynamics change with Aug observing the highest median of 5,710 nmol L^{-1}, showing the significant influence one hot spot can have on a system. This also provides evidence that most of the CH_4 production happens within the delta, not the rivers.

As stated before, CH_4 fluxes followed roughly the same trend as CH_4 concentration, only moderately modulated by variable wind speed. For rivers, such as with concentrations, Aug fluxes had the highest variability (table 6.1 and Fig. 6.3) spanning from 4.9 to 100.7 μmol m^{-2} h^{-1} CH_4, however had the lowest median of the seasons (8.7 μmol m^{-2}

h^{-1}). Comparing Oct to May and Aug for rivers, it had the largest percentile range and median (14.2 μmol m^{-2} h^{-1}). Channel fluxes from all months combined had a median of 47.9 ± 70.6 μmol m^{-2} h^{-1}, higher than both May and Aug alone (39.1 and 49.4 μmol m^{-2} d^{-1}: excluding the 'hot spot'). Potentially linked to the increased degradation of macrophytes and other organic matter during Oct compared to the previous months. Both rivers are channels varied, showing large dependence on both seasonal changes and sample location. Furthering evidence, just as with the 'hot spot', for significant influence from certain months for CH_4 fluxes. In Aug the 'hot spot' measured a median flux of 211 ± 86.3 μmol m^{-2} h^{-1}, however when compared al all months combined, the median from the 'hot sport' reduced to 54.9 ± 106 μmol m^{-2} h^{-1} and for all channels together showing 47.9 ± 70.6 μmol m^{-2} h^{-1}. Combining all months, overall our calculated flux from the fluvial delta was 594 ± 525 μmol m^{-2} h^{-1}, within the diffusive mean from the overall literature (342.5 ± 1,062.5 μmol m^{-2} h^{-1}). However, we found a far higher median of 473 μmol m^{-2} h^{-1} (compared to 33.3 μmol m^{-2} h^{-1}). The fluvial delta had a mean of 2,030 ± 2,110 nmol L^{-1}, with a median (1,520 nmol L^{-1}) comparable to that of Stanley et al. (2016) with a mean of 1,350 ± 5,160 nmol L^{-1}. When comparing within the fluvial system (rivers and channels separately), riverine CH_4 concentration during May and Aug had a median comparable to channels and therefore showed overall homogeneity, however channels appeared to have more extreme values and ranges than rivers. This difference would be due to less biological and physical processes occurring within the rivers due to depth, proximity to the wetlands and the flow generally being faster.

High concentrations and therefore fluxes during May, have previously been explained due to growth, temperature and biomass peak, linking plant biomass to CH_4 emissions during growing season (Milberg et al. 2017). This can be further linked to the previous flood waters just before the transect in May. The Danube delta is known to have high levels of nutrients (Panin 2003; Durisch-Kaiser et al. 2008; Spiridon et al. 2018) arriving from the Danube river. This could account for higher concentrations, and saturation due to plankton growth being a source of labile organic matter fuelling CH_4 productivity in the sediments, which then outfluxes (Mendonça et al. 2012; Ward et al. 2017). Aug showed the largest CH_4 range among the seasons, however with the lowest median coinciding with the theory that there is decreased CH_4 concentrations and emissions during lower water levels (Melack et al. 2004; Marín-Muñiz et al. 2015; McGinnis et al. 2016). Fluxes were greater than that found by Crawford et al. (2017) also within channels. In some systems of the delta the reduction in dissolved O_2 (Fig. 6.3) suggests more anoxic waters which would support the hypothesis of anoxic conditions close to the sediment and therefore methanogenesis (Crawford et al. 2014b; 2017). Although our methane peaks did sometimes inversely correlated with O_2 in the channels as Bižić-Ionescu et al. (2019) discussed, only the diel cycles or extreme did so. When changes were not extreme, there was little correlation. Channels are highly influenced by the surrounding reed beds, which are known to produce high levels of CH_4 (Bastviken et al. 2011), and have influence on the surrounding systems they flow into (e.g. lakes). This both explains the high variability (Fig. 6.3) and higher overall concentrations and fluxes (table 6.1). They are also influenced by the lakes, which are sources of labile organic carbon that fuels methanogenesis. However, given methanogenesis was not measured, we can only make assumptions for this. Channels are the links between the rivers and the lakes, surrounded by wetlands form which the collect water and therefore generally have the highest concentrations of CH_4 and lowest in O_2.

Situation of CH_4 in lakes

Lakes showed concentrations similar to those of Pavel et al. (2009) (see appendix table 6.3), although taken roughly 10 years later. The comparison to this earlier study indicates, that eutrophication and carbon turnover have not significantly changed during this period (Tudor et al. 2016; Spiridon et al. 2018). These concentrations ranged from the lowest 113 nmol L^{-1} to the highest 11,300 nmol L^{-1} both in May (largest concentration close to a channel). The median however, stayed roughly the same for both May and Aug (465 and 466 nmol L^{-1} respectively), with Oct reaching 630 nmol L^{-1}. We expect less productivity and more mineralization of macrophytes in Oct, leading to enhanced CH_4 production. Before entering each lake complex, the water had to travel through either the channels or the reed beds, increasing the concentrations coming into the lakes. The inflowing water however quickly dispersed, and was soon oxidized as seen before (Crawford et al. 2017). This was only visible on the edges of the lakes and although had influence on the overall concentration, were seen as outliers as the CH_4 due to being quickly oxidised (see Fig, 6.4). Morphology and seasonal changes were far clearer in the lakes than any of the other systems, due to noticeable influences from the channels are larger production and macrophyte distributions. This led to higher concentrations during Oct as the macrophytes broke down as mentioned before, but also potential stratification (Milberg et al. 2017).

Each lake system is assigned to a complex: Contea-Furtuna, Matita-Merhei, Gorgova-Uzlina and Rosu-Puiu (Fig. 6.2), of which the last two were measured during these campaigns. The total area of these complexes is 227.73 km^2, with Gorgova-Uzlina (Fig. 6.2c) being the largest of all at 68.48 km^2(Oosterberg et al. 2000; Panin 2003). By averaging over the lakes (appendix 1), we obtained the total lake area flux of 2.9, 6.5 and 4.8 mol CH_4 h^{-1} for May, Aug and Oct respectively. Sediment fluxes are one of the main sources of CH_4 diffusion fluxes Peeters et al. (2019), however, among other paths, ebullition can also be a significant source of CH_4 and its impact on the fluxes can vary from both system and location (see Bastviken et al. 2008, McGinnis et al. 2016, Schubert and Wehrli 2019 and van Bergen et al. 2019 for varying quantities). As it is not possible to capture ebullition through dissolved CH_4 surface measurements, such as in this study, this can potentially lead to mild-significant underestimations.

6.4.2 Diel CH_4 cycling

Extractions of temporal variability on the diel time scale (i.e. over nearly a full 24 h cycle) were successfully carried our while (partly) stationary in one location. For analyses and comparison below, two diel cycles were recorded: one in Lake Roşu (Fig. 6.2b(ii)), and the other within the so-called 'hot spot', a small channel system of extreme biogeochemical properties (Fig. 6.2b(i)), both locations < 3 m depth. Both covered just under a full 24 h but still documented a diel cycling (Fig. 6.4).

Lake Roşu's diel cycle (Fig. 6.4 left) shows clear indications of strong temporal variability on the diel time scale. The nocturnal buildup in CH_4 is linearly correlated with the loss of oxygen (molar CH_4:O_2 ratio 1:50). CH_4 concentrations started from 400 nmol L^{-1} at sunset and reached 1,400 nmol L^{-1} at sunrise. During the diurnal period, CH_4 concentrations quickly relaxed back to initial conditions. As the mapping transect in Lake Roşu started around 9:00, some spatial variability is superimposed from then on to the dominant diel cycle causing CH_4 concentrations to vary over the range 200-500 nmol L^{-1}. Overall, the CH_4 concentration shows a strong co-variation with oxygen. The diurnal relaxation of the CH_4 and O_2 concentrations to initial state has a more exponential shape. A possible explanation for this hysteresis is, that the water, which during the day becomes stratified, undergoes advective mixing as the water

is cooling during the night with the two formerly separate water bodies progressively mixing (hence the linear mixing line) as suggested by Milberg et al. (2017). Diurnal warming then quickly re-stratifies the water column so that the surface layer has no further entrainment from low-oxygen, high-methane waters below and undergoes rapid CH_4 loss due gas exchange (Fig. 6.4). In the case of CH_4, full equilibrium is not reached during the diurnal period. This could be due to background sources of CH_4 (e.g. from macrophytes, lateral transport, diffusive flux across the pycnocline or production via photoautotrophs (Bižić et al. 2020)). Given the rate and extent of the CH_4 increase, this shows potentially significantly CH_4 production during the day in the bottom waters (Grasset et al. 2019) which is more likely to lead to other effective transport of CH_4 such as ebullition. In turn potentially furthering the supply of CH_4 to the surface waters or the atmosphere. Oxygen, in contrast relaxes back to equilibrium during the day as both air-water fluxes and in-situ photosynthetic production of O_2 would drive the system towards equilibrium.

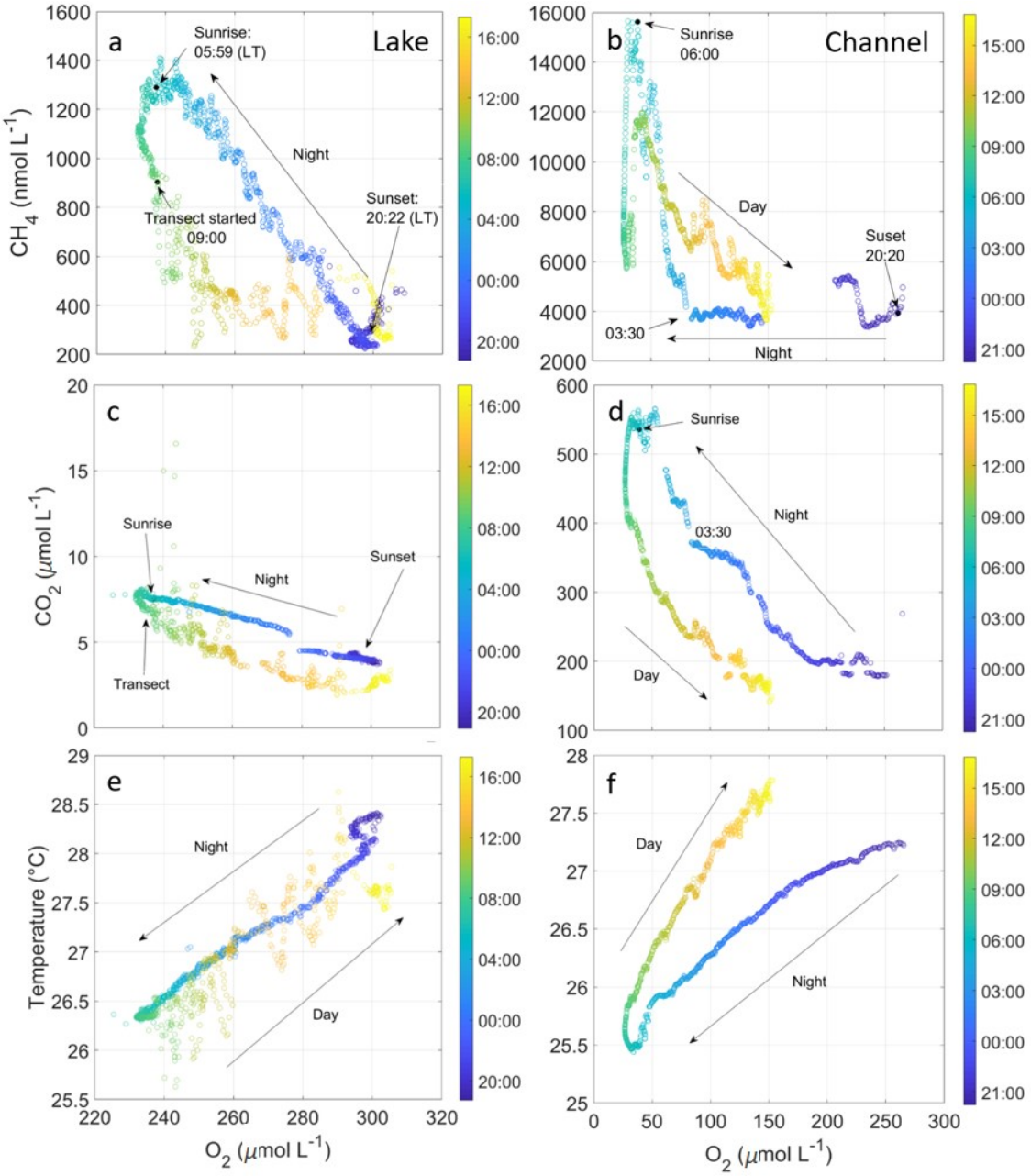

Figure 6.4: CH_4 (a + b), CO_2 (c + d) and temperature (e + f) against O_2 concentration as measured during diel cycle experiments in lake Roşu (left) the 'hot spot' (right). Colour bar denotes time of the day (hh:mm). Sunrise and sunset are also indicated. Both studies were carried out during the Aug (summer) campaign. During the night from just before 20:00 until 09:00, the boat was anchored and stationary. Transects through the following day continued to map the lake, whereas the channel was all in one anchored location.

The CO_2 peak of about 8 μmol L^{-1} (corresponding to a pCO_2 of about 100 μatm) just after sunrise is around 65% saturated, only during the transect do some values exceed 100%, reaching 130% (Fig. 6.4c few points over 15 μmol L^{-1}). The data show a slight decoupling from metabolism between CO_2 and O_2, such as CO_2 increasing significantly without the use of O_2, which has also been observed by Peeters et al. (2016). These concentrations, however, coincide with the mapping; higher CO_2 rates when closer to the lake edges (similar to the CH_4 pattern in Fig. 6.5), due to incoming waters form the wetlands. During the day, Lake Roşu is undersaturated for CO_2 in comparison with the atmosphere and supersaturated in O_2, showing high levels of productivity in

the surface waters. Overnight we observe respiration with the CO_2 increasing (and O_2 decreasing), however, never reaching above saturation for CO_2. This could be potentially due to the eutrophication and such high productivity during the day, and loss of organic matter to the bottom waters and sediment, therefore limiting CO_2 and staying well below saturation even during the night , also coinciding with other undersaturated eutrophic lakes (Balmer and Downing 2011). CO_2 was far lower than that found by Pavel et al. (2009), in which they found 26 ± 27 μmol L^{-1} during September, even when using the highest values measured.

The 'hot spot' (Fig. 6.4, right) also shows a clear co-variation with oxygen and strongly increases from roughly 4,000 to 16,000 nmol L^{-1} over the nocturnal period (sunset to sunrise), followed by a rapid return to values around 6,000 nmol L^{-1} during the diurnal period (sunrise to sunset). O_2 decreases while CH_4 stays roughly consistent until around 3:30 am when it appears to enter into hypoxic and even towards suboxic conditions as the ratio increases to about 1:3. This non-linearity maybe due to mixing with more than two endmembers, e.g., surface layer, sub-surface layer and bottom layer. The initial mixing encompasses only surface and sub-surface layer (similar to the lake situation) whereas later during the night near-bottom water are entrained that have extremely elevated CH_4 concentration (and no oxygen) as a consequence of anoxic methanogenesis in sediment pore waters.

CO_2 reaches saturation levels of close to 4,500% during the diel cycle in the 'hot spot', over the night with the lowest supersaturation of 1,175% at the end of the diel cycle ($\sim$ 150 to 550 μmol L^{-1}). It has almost mirrored relationship with temperature (Fig. 6.4f). The CO_2:O_2 relationship has a molar ratio 2:1 during the night and such as with CH_4, CO_2 show a steep decrease following sunrise, while little change in O_2. The diel hysteresis is far clearer with CO_2 than with CH_4, showing a steady increased and decrease. This is ultimately due to different processes, and potential methanogenesis occurring in the bottom waters before mixing, as stated above.

The changes in temperature are roughly the same for each system (± 2.5°C: Fig. 6.4), showing influence on all variables and induced strong density variations. The latter can be seen with the potential mixing of the bottom waters over the course of the night (Fig. 6.4), mixing the warmer top waters with the daily stratified bottom waters. Although it could be argued that temperature could have had an effect within the diel variability as previously suggested (Yvon-Durocher et al. 2014), temperature variability only causes a 3% change in methane solubility. Therefore, this observed temperature variation over the night (decrease of $\sim$ 2.5 °C) could not account for the full CH_4 increase in concentration (3% of ± 2.5°C causing a change of $\sim$ 0.0075 μmol L^{-1} from 0.3 μmol L^{-1}, Fig. 6.4a). Compared with the variability over the night, the transect during the day that covered the entire lake showed pCH_4 generally staying consistent once the sun rose ($\sim$ 200-400 nmol L^{-1} with peaks due to shorelines), roughly the same concentration as the previous day, such as with all other variables. Statistically we also found no correlation between temperature and CH_4 flux (van Bergen et al. 2019) over the entire lake ($P > 0.05$), therefore showing our diffusive fluxes are more reliant on the internal processes of the water.

Table 6.2: Mean distributions (± SD) and hourly and yearly fluxes within Lake Roşu and the 'hot spot' channel with the exclusion of the night data (day light only: DL, Fig. 6.5 map) and all data (full diel cycle: FD, Fig. 6.5 all black and red data) for CH_4 flux, CH_4, CO_2 and O_2 concentrations.

Mean ± SD			**Lake Roşu**		**'Hot Spot' Channel**	
DL CH_4 Flux density	μmol m^{-2} h^{-1}	mol m^{-2} yr^{-1}	18 ± 6.2	0.16 ± 0.05	263 ± 65.4	2.3 ± 0.6
FD CH_4 Flux density	μmol m^{-2} h^{-1}	mol m^{-2} yr^{-1}	19 ± 9.7	0.17 ± 0.08	224 ± 85	2 ± 0.7
DL CH_4 nmol L^{-1} Concentration			471 ± 148		7600 ± 2630	
FD CH_4 nmol L^{-1} Concentration			530 ± 300		6820 ± 2950	
DL CO_2 μmol L^{-1} Concentration			4.3 ± 1.8		307 ± 125	
FD CO_2 μmol L^{-1} Concentration			4.8 ± 1.8		315 ± 120	
DL O_2 μmol L^{-1} Concentration			271 ± 22.7		78 ± 47.1	
FD O_2 μmol L^{-1} Concentration			265 ± 23.5		105 ± 60.3	

To show the impact of these diel cycles, table 6.2 shows the mean CH_4 concentrations and calculated fluxes from the transect ($\sim$ 09:00 until 17:20, Fig. 6.5) and from the entire diel cycle (almost 24 hours: $\sim$ 18:55 8^{th} Aug 2017 until 17:20 9^{th} Aug 2017). The mapping is representative of a typical mapping routine performed during the day. The difference between the mapping (shown in Fig. 6.5), and when the full diel cycle is considered for concentrations and also fluxes and presented. As the mapping was part of the diel cycle (Fig. 6.4), we were able to extract this. These were then scaled up to year averages showing an underestimation by just day night data alone. For the 'hot spot', due to no mapping following the diel cycle, therefore we used the day night data (after sunrise) for this comparison.

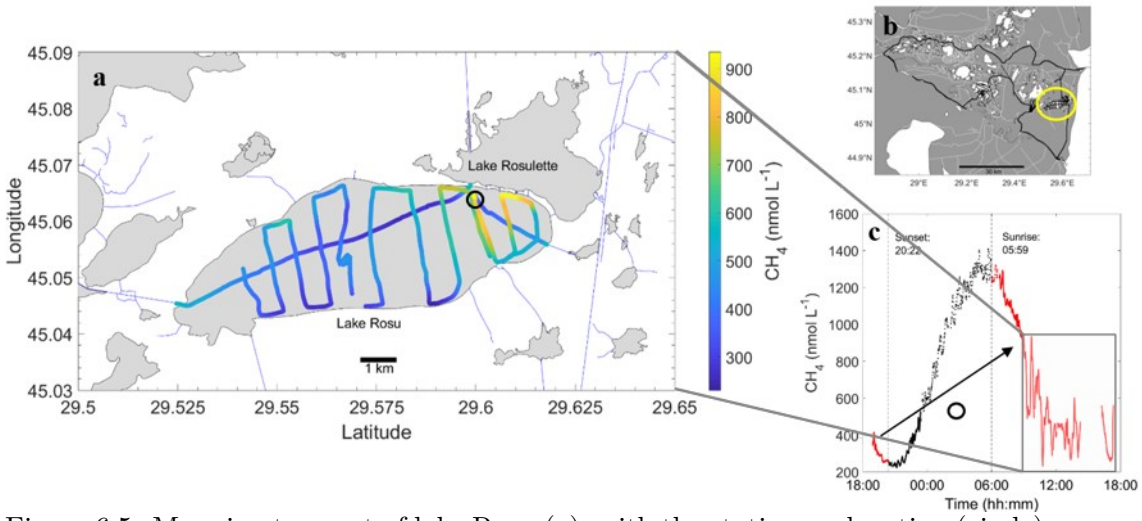

Figure 6.5: Mapping transect of lake Roşu (a), with the stationary location (circle), map the entire Danube delta with lake Roşu (b: yellow circle), and CH_4 concentration over time to show the distribution over the entire diel cycle (b: black showing between sunset and sunrise, red is day-time data, and box showing mapping transect). These were used to calculate the day light only data (b) and combined data (b: full data), with the diel cycle from lake Roşu (b: box) used for the day night data. Location of diel cycle during the night shown in a: black circle .

Overall, the values for day-light period and full day shows little change due to the

fact that the daily extremes are encountered around sunrise and sunset such that full coverage of the daylight hours captures the full dynamic range of the diel cycle. This has implications for on observational strategy. However, our extensive mapping throughout the day is not representative of typical sampling methods which are mostly based on discrete samples taken at some time during daylight hours. A comparison, for example for Lake Roşu, of the midday CH_4 concentration and flux (393 nmol L^{-1} and 13 μmol m^{-2} h^{-1}) to the full diel cycle values (530 nmol L^{-1} and 19 μmol m^{-2} h^{-1}) illustrates the magnitude of the potential bias (in this example about 30%) incurred by discrete sampling. For the 'hot spot', taking the concentration and flux at midday (6780 nmol L^{-1} and 230 μmol m^{-2} h^{-1}), this is roughly the same due to the peak throughout the mid-morning (Fig. 6.4c). This mid-morning peak potentially could have been a passing water body, or disruption to the bottom waters, as it does not follow the standard reduction in CH_4, that would be expected.

Combining the lakes (total area of 227.73 km^2, using Lake Roşu and this diel cycle, due to measuring roughly the middle of all lake values (appendix 1), the total lake fluxes would produce 36.4 $\pm$ 11.4 mol CH_4 yr^{-1} using day light data from sun rise to sunset (38.7 $\pm$ 18.2 mol CH_4 yr^{-1} for full diel cycle data), from the total lake area within the Danube.

Extracting all day night cycles and using just mapping data for every month, the mean CH_4 flux decreases from 49 $\pm$ 61 μmol m^{-2} h^{-1} to 34.9 $\pm$ 35.7 μmol m^{-2} h^{-1}. Scaling this by year it changes the fluxes for the Danube delta from 0.4 $\pm$ 0.5 mol m^{-2} h^{-1} to 0.3 $\pm$ 0.3 mol m^{-2} h^{-1}. Splitting between months, Aug showed the largest variability between extraction of night data (such as the diel examples above) from 84 $\pm$ 38 to 37 $\pm$ 33 μmol m^{-2} h^{-1}. This greater variability can be linked to higher temperatures, greater stratification and increased production and organic matter degradation, all leading to potential increases in CH_4 (Duc et al. 2010; Fuchs et al. 2016). To note, upscaling these numbers is to give more of an awareness of the difference between including and excluding diel cycle data. These values should not be taken at face value due to the major component of the Danube delta in terms of CH_4 influence (the wetland) was not measured.

Typically, delta systems tend to be either measured in specific regions (entrances or middle of lakes or channels), or with in situ measurements over time (e.g. Cuna et al. 2008; Wang et al. 2009; Olsson et al. 2015; Cunada et al. 2018). These measurements are then usually upscaled from a single location (e.g. Bouillon and Dehairs 2007; Borges et al. 2015; Joesoef et al. 2017), failing to include spatial variability, system specific impacts (such as the 'hot spot' we observed here), and monthly changes. Here we can see that all of these impacts can have significant effects on the observed measurements. In table 6.2 and Fig. 6.5, sampling time clearly has an impact, especially for upscaling.

There have been multiple studies looking into diel cycles (Nimick et al. 2011; Zhang et al. 2018; van Bergen et al. 2019), yet they are usually undetected or unresolved therefore are often ignored, particularly in studies with sampling during daylight hours. This can lead to substantial underestimation of emissions, as has also been noticed in systems with high CH_4 concentrations (Natchimuthu et al. 2017). From our evidence of lake diel cycles, we conclude, in terms of discrete sampling techniques to fully capture the full variable cycle, sampling should be conducted during 3 periods: before sunrise, just after sunset and during the early afternoon. This way there is potential to capture the peak amplitude, low and average concentrations, providing a better overall estimate of concentrations. Although, the best sampling techniques would be for complete mapping, however this is unfeasible in most cases.

In summary, when comparing overall concentration means with and then without diel cycles across all months, we found an underestimation of up to 25% for channels

whereas an overestimation in lakes by 3.3% CH_4 concentration if excluding the diel data (nmol L^{-1}) (as no diel cycles were conducted in rivers). In the lakes, this accounts for roughly an increase of 20.4% for channels yet a 4.2% decrease in fluxes when adding diel cycles. Although, in our study, diel cycles were vastly under represented compared to day data and therefore this could be even greater. From this one study, this shows compelling evidence diel cycles must be accounted for when measuring concentrations and calculating fluxes.

6.5 Summary and conclusion

Overall the Danube river delta surface waters were a source of CH_4, with the over mean of 1700 ± 1930 nmol L^{-1} (0.43 ± 0.53 mol m^{-2} yr^{-1}) over all months. This is comparable to other systems of this type and size (see Stanley et al. (2016) for literature comparison). However, given that wetland systems (and therefore the reed beds) are known to be the significant in CH_4 fluxes of high variability (Segers 1998; Nisbet et al. 2019), our data only cover that of the channels, rivers and lakes and therefore could potentially be greatly underestimating the overall fluxes. Being able to measure extensively within the lakes systems provided evidence that the reed bed concentrations were far higher than that of the lakes themselves. Our data has shown significant need for increased recordings of diel cycles in all systems, with channels and lakes show significantly lower concentrations and fluxes when excluding these. Of our three water types, rivers had the smallest fluxes, not only showing that most of the CH_4 production must come from further within the wetlands, but also signifying the important of the other systems. Most calculated CH_4 budgets, stem from extrapolations and data driven approaches due to lack of process-based models (Saunois et al. 2020), therefore knowledge the other systems are of potentially greater importance is vital for this.

With our analysis, diel cycles both in the channels and the lakes we were able to further confirm the importance of adequate data collection, through 24-h coverage or specific correction for sampling bias, and implementation into models. The diel cycle within the lake was consistent with stratification over the day, where vast amount of organic carbon from macrophytes creating anoxic subsurface waters, which slowly and steadily mix during the night. We showed this cycle could have major consequences on concentration measurements and fluxes. Far larger quantities of CH_4 are released during the night through this process and with most current sampling techniques, such variability would be lost. This diel cycle was also strong enough to be shown during the 'hot spot' where concentration changes varied between 4,000-16,000 nmol L^{-1}. Given this extreme variation, it appears other processes, not just stratification in the presence of macrophytes, but also thermal stratification, should also be considered in shallow systems.

Our data further proves, to improve our datasets of such areas, diel cycles must be included into the values and projections, especially with eutrophication predicted to increase in these vulnerable ecosystems. Given these cycles didn't just occur in lakes, a re-evaluation is needed on sampling techniques and data checks to include such cycles from all water systems.

6.6 Acknowledgements

The research leading to these results has received funding from the European Union's Horizon 2020 research and innovation program under the Marie Sklodowska-Curie grant agreement No 643052 (C-CASCADES project) and funding from Digital Earth which is coordinated by GEOMAR Helmholtz Centre for Ocean Research Kiel. We are grateful

to Dennis Booge for assistance with the flux calculation. All of the KMCON team with their support and help throughout my time with them and while on field work both day and night; all those who assisted on the cruises: our Romanian colleagues captain Nice, George, Marian, Christian Teodoru and Marie-Sophie Maier who drove the campaigns.

6.7 Appendices

Appendix 1

Table 6.3: Mean (±SD) for CH_4 concentration and flux (nmol L^{-1} and μmol m^{-2} h^{-1} respectively) and O_2 concentration (μmolL^{-1}) across all measured lakes during each expedition (May, Aug or Oct). Grey shows the comparison with Pavel et al. (2009) which was measured in 2006 as a comparison for CH_4 concentration and flux, in the same units for May and September.

	Lake Uzlina			**Lake Isac**			**Lake Puiu**			**Lake Roşu**			**Lake Roşulette**		
Month	May	Aug	Oct	May	Aug	Oct	May	Aug	Oct	May	Aug	Oct	May	Aug	Oct
2006	May	September		May	September		May	September		May	September		May	September	
Conc. CH_4 nmol L^{-1}	502 ± 81	2590 ± 391	722 ± 291	419 ± 62	1750 ± 827	539 ± 229	436 ± 301	n.d.	803 ± 635	468 ± 76	529 ± 297	756 ± 301	967 ± 1590	819 ± 426	1110 ± 515
Pavel et al. (2009) CH_4 nmol L^{-1}	714 ± 257	644 ± 224		569 ± 370	613 ± 161		891 ± 424	n.d.		534 ± 113	538 ± 119		738 ± 575	n.d.	
Flux $CH_4\mu$mol m^{-2} h^{-1}	13 ± 2.1	103.8 ± 15.4	17 ± 7.5	10.2 ± 1.7	82.6 ± 44.3	14.1 ± 6	11.9 ± 7.8	n.d.	17.8 ± 14.5	11.8 ± 2.5	19.3 ± 9.6	21.6 ± 11.2	21.7 ± 34.5	31.6 ± 18.1	29.3 ± 15.2
Pavel et al. (2009) CH_4 μmol m^{-2} h^{-1}	18 ± 7	26 ± 9		80 ± 51	62 ± 17		23 ± 11	n.d.		13 ± 3	7 ± 2		11 ± 9	n.d.	
Conc. O_2 μmol L^{-1}	267 ± 19	260 ± 8	324.5 ± 26.1	388 ± 39	294 ± 31.8	346 ± 16.3	280 ± 14.7	300 ± 39.1	75.3 ± 21.8	256 ± 13.5	255 ± 27.6	329 ± 11.4	218 ± 9.7	315 ± 3.6	311 ± 25

6.8 References

Abril, G., and A. V. Borges. 2005. Carbon Dioxide and Methane Emissions from Estuaries. 187–207. doi:10.1007/978-3-540-26643-38

Abril, G., and A. V. Borges. 2019. Carbon leaks from flooded land: do we need to re-plumb the inland water active pipe? Biogeosciences 769–784. doi:10.5194/bg-2018-239

Balmer, M., and J. Downing. 2011. Carbon dioxide concentrations in eutrophic lakes: undersaturation implies atmospheric uptake. Inl. Waters 1: 125–132. doi:10.5268/IW-1.2.366

Bange, H. W., C. H. Sim, D. Bastian, J. Kallert, A. Kock, A. Mujahid, and M. Müller. 2019. Nitrous oxide (N_2O) and methane (CH_4) in rivers and estuaries of northwestern Borneo. Biogeosciences Discuss. 1–25. doi:10.5194/bg-2019-222

Bastviken, D., J. J. Cole, M. L. Pace, and M. C. Van de-Bogert. 2008. Fates of methane from different lake habitats: Connecting whole-lake budgets and CH_4 emissions. J. Geophys. Res. Biogeosciences 113: 1–13. doi:10.1029/2007JG000608

Bastviken, D., L. J. Tranvik, J. A. Downing, P. M. Crill, and A. Enrich-Prast. 2011. Freshwater methane emissions offset the continental carbon sink. Science 331: 50. doi:10.1126/ science.1196808

van Bergen, T. J. H. M., N. Barros, R. Mendonça, and others. 2019. Seasonal and diel variation in greenhouse gas emissions from an urban pond and its major drivers. Limnol. Oceanogr. 64: 2129–2139. doi:10.1002/lno.11173

Bittig, H. C., A. Körtzinger, C. Neill, and others. 2018. Oxygen Optode Sensors: Principle, Characterization, Calibration, and Application in the Ocean. Front. Mar. Sci. 4. doi:10.3389/fmars.2017.00429

Bižić-Ionescu, M., D. Ionescu, M. Günthel, K. W. Tang, and H.-P. Grossart. 2019. Oxic Methane Cycling: New Evidence for Methane Formation in Oxic Lake Water. Biog. Hydrocarb. 379–400. doi:10.1007/978-3-319-78108-210

Bižić, M., T. Klintzsch, D. Ionescu, and others. 2020. Aquatic and terrestrial cyanobacteria produce methane. Sci. Adv. 6: 1–10. doi:10.1126/sciadv.aax5343

Bogard, M. J., P. A. Del Giorgio, L. Boutet, M. C. G. Chaves, Y. T. Prairie, A. Merante, and A. M. Derry. 2014. Oxic water column methanogenesis as a major component of aquatic CH_4 fluxes. Nat. Commun. 5: 1–9. doi:10.1038/ncomms6350

Borges, A. V., F. Darchambeau, C. R. Teodoru, and others. 2015. Globally significant greenhouse-gas emissions from African inland waters. Nat. Geosci. 8: 637–642. doi:10.1038/ngeO$_2$486

Borges, A. V., B. Delille, L. Schiettecatte, F. Gazeau, G. Abril, M. Frankignoulle, and F. Gazeau. 2004. Gas transfer velocities of CO_2 in three European estuaries. Limnol. Oceanogr. 49: 1630–1641.

Bouillon, S., and F. Dehairs. 2007. Biogeochemistry of the Tana estuary and delta (northern Kenya). Limnol. Oceanogr. 52: 46–59.

Carmichael, M. J., E. S. Bernhardt, S. L. Bräuer, and W. K. Smith. 2014. The role of vegetation in methane flux to the atmosphere: Should vegetation be included as a distinct category in the global methane budget? Biogeochemistry 119: 1–24. doi:10.1007/s10533-014-9974-1

Cole, J. J., and N. F. Caraco. 1998. Atmospheric exchange of carbon dioxide in a low-wind oligotrophic lake measured by the addition of SF6. Limnol. Oceanogr. 43: 647–656. doi:10.4319/lo.1998.43.4.0647

Cole, J. J., Y. T. Prairie, N. F. Caraco, and others. 2007. Plumbing the Global Carbon Cycle: Integrating Inland Waters into the Terrestrial Carbon Budget. Ecosystems 10: 172–185. doi:10.1007/s10021-006-9013-8

Crawford, J. T., L. C. Loken, W. E. West, and others. 2017. Spatial heterogeneity of within-stream methane concentrations. J. Geophys. Res. Biogeosciences 122: 1036–1048. doi:10.1002/2016JG003698

Crawford, J. T., N. R. Lottig, E. H. Stanley, J. F. Walker, P. C. Hanson, J. C. Finlay, and R. G. Striegl. 2014a. CO_2 and CH_4 emissions from streams in a lake-rich landscape: Patterns, controls, and regional significance. Global Biogeochem. Cycles 197–210. doi:10.1002/2013GB004661.Received

Crawford, J. T., E. H. Stanley, S. A. Spawn, J. C. Finlay, L. C. Loken, and R. G. Striegl. 2014b. Ebullitive methane emissions from oxygenated wetland streams. Glob. Chang. Biol. 20: 3408–3422. doi:10.1111/gcb.12614

Cristofor, S., A. Vadineanu, and G. Ignat. 1993. Importance of flood zones for nitrogen and phosphorus dynamics in the Danube Delta. Hydrobiologia 251: 143–148. doi:10.1007/BF00007174

Crusius, J., and R. Wanninkhof. 2003. Gas transfer velocities measured at low wind speed over a lake. Limnol. Oceanogr. 48: 1010–1017. doi:10.4319/lo.2003.48.3.1010

Cuna, S., E. Pendall, J. B. Miller, P. P. Tans, E. Dlugokencky, and J. W. C. White. 2008. Separating contributions from natural and anthropogenic sources in atmospheric methane from the Black Sea region, Romania. Appl. Geochemistry 23: 2871–2879. doi:10.1016/ j.apgeochem.2008.04.019

Cunada, C. L., L. F. W. Lesack, and S. E. Tank. 2018. Seasonal Dynamics of Dissolved Methane in Lakes of the Mackenzie Delta and the Role of Carbon Substrate Quality. J. Geophys. Res. Biogeosciences 123: 591–609. doi:10.1002/ 2017JG004047

Davidson, T. A., J. Audet, E. Jeppesen, F. Landkildehus, T. L. Lauridsen, M. Søndergaard, and J. Syväranta. 2018. Synergy between nutrients and warming enhances methane ebullition from experimental lakes. Nat. Clim. Chang. 8: 156–160. doi:10.1038/s41558-017-0063-z

Dean, J. F., J. J. Middelburg, T. Röckmann, and others. 2018. Methane Feedbacks to the Global Climate System in a Warmer World. Rev. Geophys. 56: 207–250. doi:10.1002/2017RG000559

DelSontro, T., P. A. del Giorgio, and Y. T. Prairie. 2018. No Longer a Paradox: The Interaction Between Physical Transport and Biological Processes Explains the Spatial Distribution of Surface Water Methane Within and Across Lakes. Ecosystems 21: 1073–1087. doi:10.1007/s10021-017-0205-1

Dlugokencky, E, NOAA/ESRL: www.esrl.noaa.gov/gmd/ccgg/trendscH_4/, last access: 12 December 2019

Duc, N. T., P. Crill, and D. Bastviken. 2010. Implications of temperature and sediment characteristics on methane formation and oxidation in lake sediments. Biogeochemistry 100: 185–196. doi:10.1007/s10533-010-9415-8

Durisch-Kaiser, E., A. Pavel, A. Doberer, J. Reutimann, S. Balan, S. Sobek, S. Rădan, and B. Wehrli. 2008. Nutrient retention, total N and P export, and greenhouse gas emission from the Danube Delta lakes. Geo-Eco-Marina 81–90. doi:10.5281/zenodo.57332

Enache, I., L. I. Florescu, M. Moldoveanu, and others. 2019. Diversity and distribution of Daphnia across space and time in Danube Delta lakes explained by food quality and abundance. Hydrobiologia 842: 39–54. doi:10.1007/s10750-019-04025-y

Fuchs, A., E. Lyautey, B. Montuelle, and P. Casper. 2016. Effects of increasing temperatures on methane concentrations and methanogenesis during experimental incubation of sediments from oligotrophic and mesotrophic lakes. J. Geophys. Res. Biogeosciences 121: 1394–1406. doi:10.1002/2016JG003328

Galatchi, L., and M. Tudor. 2006. Europe as a source of pollution – the main factor for the eutrophication of the Danube delta and black sea, Chemicals. L. Simeonov and E. Chirila [eds.]. Springer.

Grasset, C., G. Abril, R. Mendonça, F. Roland, and S. Sobek. 2019. The transformation of macrophyte-derived organic matter to methane relates to plant water and nutrient contents. Limnol. Oceanogr. 64: 1737–1749. doi:10.1002/lno.11148

Grossart, H. P., K. Frindte, C. Dziallas, W. Eckert, and K. W. Tang. 2011. Microbial methane production in oxygenated water column of an oligotrophic lake. Proc. Natl. Acad. Sci. U. S. A. 108: 19657–19661. doi:10.1073/pnas.1110716108

Guérin, F., G. Abril, D. Serça, C. Delon, S. Richard, R. Delmas, A. Tremblay, and L. Varfalvy. 2007. Gas transfer velocities of CO_2 and CH_4 in a tropical reservoir and its river downstream. J. Mar. Syst. 66: 161–172. doi:10.1016/j.jmarsys.2006.03.019

ICPDR international commission for the protection of the Danube river, 2004. The Danube River Basin District, Part A - Basin-wide over- view. WFD Roof Report

Jähne, B. J., K. O. M. Münnich, R. Bösinger, A. Dutzi, W. Huber, and P. Libner. 1987. On the Parameters Influencing Air-Water Gas Exchange of magnitude lower in the water than in the air, information, which in turn has also hindered transfer in the water k +. J. Geophys. Res. 92: 1937–1949. doi:10.1029/JC092iC02p01937

Joesoef, A., D. L. Kirchman, C. K. Sommerfield, and W. C. Cai. 2017. Seasonal variability of the inorganic carbon system in a large coastal plain estuary. Biogeosciences 14: 4949–4963. doi:10.5194/bg-14-4949-2017

Karl, D. M., L. Beversdorf, K. M. Björkman, M. J. Church, A. Martinez, and E. F. Delong. 2008. Aerobic production of methane in the sea. Nat. Geosci. 1: 473–478. doi:10.1038/ngeO$_2$34

Kirschke, S., P. Bousquet, P. Ciais, and others. 2013. Three decades of global methane sources and sinks. Nat. Geosci. 6: 813–823. doi:10.1038/ngeo1955

Maher, D. T., K. Cowley, I. R. Santos, P. Macklin, and B. D. Eyre. 2015. Methane and carbon dioxide dynamics in a subtropical estuary over a diel cycle: Insights from automated in situ radioactive and stable isotope measurements. Mar. Chem. 168: 69–79. doi:10.1016/j.marchem.2014.10.017

Marín-Muñiz, J. L., M. E. Hernández, and P. Moreno-Casasola. 2015. Greenhouse gas emissions from coastal freshwater wetlands in Veracruz Mexico: Effect of plant community and seasonal dynamics. Atmos. Environ. 107: 107–117. doi:10.1016/j.atmosenv.2015.02.036

McGinnis, D. F., N. Bilsley, M. Schmidt, P. Fietzek, P. Bodmer, K. Premke, A. Lorke, and S. Flury. 2016. Deconstructing Methane Emissions from a Small Northern European River: Hydrodynamics and Temperature as Key Drivers. Environ. Sci. Technol. 50: 11680–11687. doi:10.1021/acs.est.6b03268

McGinnis, D. F., G. Kirillin, K. W. Tang, S. Flury, P. Bodmer, C. Engelhardt, P. Casper, and H. P. Grossart. 2015. Enhancing surface methane fluxes from an oligotrophic lake: Exploring the microbubble hypothesis. Environ. Sci. Technol. 49: 873–880. doi:10.1021/es503385d

Melack, J. M., L. L. Hess, M. Gastil, B. R. Forsberg, S. K. Hamilton, I. B. Lima, and E. M. Novo. 2004. Regionalization of methane emissions in the Amazon Basin with microwave remote sensing. Glob. Chang. Biol. 530–544. doi:10.1111/j.1529-8817.2003.00763.x

Mendonça, R., S. Kosten, S. Sobek, N. Barros, and J. Cole. 2012. Hydroelectric carbon sequestration. Nat. Geosci. 5: 838–840. doi:10.1038/ngeo1653

Milberg, P., L. Törnqvist, L. M. Westerberg, and D. Bastviken. 2017. Temporal variations in methane emissions from emergent aquatic macrophytes in two boreonemoral lakes. AoB Plants 9. doi:10.1093/aobpla/plx029

Myhre, G., D. Shindell, F.-M. Bréon, and others. 2013. Anthropogenic and Natural Radiative Forcing. In: Climate Change 2013: The Physical Science Basis. Contribution of Working Group I to the Fifth Assessment Report of the Intergovernmental

Panel on Climate Change [Stocker, T.F., D. Qin, G.-K. Plattner, M. Ti. Cambridge Univ. Press. Cambridge, United Kingdom New York, NY, USA, Chapter 8: 659–740. doi:10.1017/CBO9781107415324.018

Natchimuthu, S., M. B. Wallin, L. Klemedtsson, and D. Bastviken. 2017. Spatio-temporal patterns of stream methane and carbon dioxide emissions in a hemiboreal catchment in Southwest Sweden. Sci. Rep. 7: 1–12. doi:10.1038/srep39729

Nimick, D. A., C. H. Gammons, and S. R. Parker. 2011. Diel biogeochemical processes and their effect on the aqueous chemistry of streams: A review. Chem. Geol. 283: 3–17. doi:10.1016/j.chemgeo.2010.08.017

Nisbet, E. G., M. R. Manning, E. J. Dlugokencky, and others. 2019. Very Strong Atmospheric Methane Growth in the 4 Years 2014–2017: Implications for the Paris Agreement. Global Biogeochem. Cycles 33: 318–342. doi:10.1029/2018GB006009

Olsson, L., S. Ye, X. Yu, M. Wei, K. W. Krauss, and H. Brix. 2015. Factors influencing CO_2 and CH_4 emissions from coastal wetlands in the Liaohe Delta, Northeast China. Biogeosciences 12: 4965–4977. doi:10.5194/bg-12-4965-2015

Oosterberg, W., A. D. Buijse, H. Coops, B. W. Ibelings, G. A. M. Menting, and I. for I. W. M. and W. Water. 2000. Ecological gradients in the Danube Delta lakes: present state and man-induced changes. Lelystad Inst. Inl. Water Manag. Waste Water Treat. RIZA. doi:90.369.5309x

Panin, N. 2003. The Danube Delta. Geomorphology and Holocene Evolution: a Synthesis / Le delta du Danube. Géomorphologie et évolution holocène: une synthèse. Géomorphologie Reli. Process. Environ. 9: 247–262. doi:10.3406/morfo.2003.1188

Panneer Selvam, B., S. Natchimuthu, L. Arunachalam, and D. Bastviken. 2014. Methane and carbon dioxide emissions from inland waters in India - implications for large scale greenhouse gas balances. Glob. Chang. Biol. 20: 3397–3407. doi:10.1111/gcb.12575

Pavel, A., E. Durisch-kaiser, S. Balan, S. Radan, S. Sobek, and B. Wehrli. 2009. Sources and emission of greenhouse gases in Danube Delta lakes. Environ. Sci. Pollut. Res. 16: 86–91. doi:10.1007/s11356-009-0182-9

Peeters, F., D. Atamanchuk, A. Tengberg, J. Encinas-Fernández, and H. Hofmann. 2016. Lake Metabolism: Comparison of lake metabolic rates estimated from a diel CO_2- and the common diel O_2- Technique. PLoS One 11: 1–24. doi:10.1371/journal.pone.0168393

Peeters, F., J. Encinas Fernandez, and H. Hofmann. 2019. Sediment fluxes rather than oxic methanogenesis explain diffusive CH_4 emissions from lakes and reservoirs. Sci. Rep. 9: 1–10. doi:10.1038/s41598-018-36530-w

Raymond, P. A., J. Hartmann, R. Lauerwald, and others. 2013. Global carbon dioxide emissions from inland waters. Nature 503: 355–359. doi:10.1038/nature12760

Richey, J. E., J. M. Melack, A. K. Aufdenkampe, V. M. Ballester, and L. L. Hess. 2002. Outgassing from Amazonian rivers and wetlands as a large tropical source of atmospheric CO_2. Nature 416: 617–620. doi:10.1038/416617a

Rîşnoveanu, G., C. Postolache, and A. Vădineanu. 2004. Ecological significance of nitrogen cycling by tubificid communities in shallow eutrophic lakes of the Danube Delta. Hydrobiologia 524: 193–202. doi:10.1023/B:HYDR.0000036133.92034.69

Sanches, L. F., B. Guenet, C. C. Marinho, N. Barros, and F. de Assis Esteves. 2019. Global regulation of methane emission from natural lakes. Sci. Rep. 9. doi:10.1038/s41598-018-36519-5

Saunois, M., P. Bousquet, B. Poulter, and others. 2016. The global methane budget 2000-2012. Earth Syst. Sci. Data 8: 697–751. doi:10.5194/essd-8-697-2016

Saunois, M., A. R. Stavert, B. Poulter, and others. 2019. The Global Methane Budget 2000-2017. Earth Syst. Sci. Data. doi:10.1017/CBO9781107415324.004

Schilder, J., D. Bastviken, M. Van Hardenbroek, P. Kankaala, P. Rinta, T. Stötter, and O. Heiri. 2013. Spatial heterogeneity and lake morphology affect diffusive

greenhouse gas emission estimates of lakes. Geophys. Res. Lett. 40: 5752–5756. doi:10.1002/2013GL057669

Schmidt, U., and R. Conrad. 1993. Hydrogen, carbon monoxide, and methane dynamics in Lake Constance. Limnol. Oceanogr. 38: 1214–1226. doi:10.4319/lo.1993.38.6.1214

Schubert, C. J., and B. Wehrli. 2019. Contribution of Methane Formation and Methane Oxidation to Methane Emission from Freshwater Systems. A.J.M. Stams and D.Z. Sousa [eds.]. Springer.

Segers, R. 1998. Methane production and methane consumption: A review of processes underlying wetland methane fluxes. Biogeochemistry 41: 23–51. doi:10.1023/A:1005929032764

Spiridon, C., L. Teodorof, A. Burada, and others. 2018. Seasonal variations of nutrients concentration in aquatic ecosystems from Danube delta biosphere reserve. AACL Bioflux 11: 1882–1891.

Stanley, E. H., N. J. Casson, S. T. Christel, J. T. Crawford, L. C. Loken, and S. K. Oliver. 2016. The ecology of methane in streams and rivers: Patterns, controls, and global significance. Ecol. Monogr. 86: 146–171. doi:10.1890/15-1027

Tang, K. W., D. F. McGinnis, K. Frindte, V. Brüchert, and H. P. Grossart. 2014. Paradox reconsidered: Methane oversaturation in well-oxygenated lake waters. Limnol. Oceanogr. 59: 275–284. doi:10.4319/lo.2014.59.1.0275

Tang, K. W., D. F. McGinnis, D. Ionescu, and H. P. Grossart. 2016. Methane production in oxic lake waters potentially increases aquatic methane flux to air. Environ. Sci. Technol. Lett. 3: 227–233. doi:10.1021/acs.estlett.6b00150

Tranvik, L. J., J. A. Downing, J. B. Cotner, and others. 2009. Lakes and impoundments as regulators of carbon cycling and climate. Limnol. Oceanogr. 54: 2298–2314.

Tudor, I., L. Teodorof, A. Burada, M. Tudor, and O. Ibram. 2016. Long-term nutrients and heavy metals concentration dynamics in aquatic ecosystems of the Danube Delta. Sci. Ann. Danube Delta Inst. 22: 149–156.

Wang, D., Z. Chen, W. Sun, B. Hu, and S. Xu. 2009. Methane and nitrous oxide concentration and emission flux of Yangtze Delta plain river net. Sci. China, Ser. B Chem. 52: 652–661. doi:10.1007/s11426-009-0024-0

Wanninkhof, R. H. 1992. Relationship between wind speed and gas exchange. J. Geophys. Res. 97: 7373–7382.

Ward, N. D., T. S. Bianchi, P. M. Medeiros, M. Seidel, J. E. Richey, R. G. Keil, and H. O. Sawakuchi. 2017. Where Carbon Goes When Water Flows: Carbon Cycling across the Aquatic Continuum. Front. Mar. Sci. 4: 1–27. doi:10.3389/fmars.2017.00007

Whiticar, M. J., E. Faber, and M. Schoell. 1986. Biogenic methane formation in marine and freshwater environments: CO_2 reduction vs. acetate fermentation-Isotope evidence. Geochim. Cosmochim. Acta 50: 693–709. doi:10.1016/0016-7037(86)90346-7

Yvon-Durocher, G., A. P. Allen, D. Bastviken, R. Conrad, C. Gudasz, A. St-Pierre, N. Thanh-Duc, and P. A. Del Giorgio. 2014. Methane fluxes show consistent temperature dependence across microbial to ecosystem scales. Nature 507: 488–491. doi:10.1038/nature13164

Zhang, C., S. Cheng, L. Long, H. Xie, X. Mu, and W. Zhang. 2018. Diel and seasonal methane flux across water–air interface of a subtropic eutrophic pond. Toxicol. Environ. Chem. 100: 413–424. doi:10.1080/02772248.2018.1499231

Conclusions and outlook

The main goal of this work was to evaluate and assess oceanographic sensors for their suitability of high-resolution data acquisition across the land ocean aquatic continuum (LOAC). The LOAC is generally split between oceanographers and limnologists, each focusing on their specific regions. This split has led to lack of unification with quality standards, lack of data in areas where these regions mix, and differences between measuring techniques and therefore unknown additional uncertainties. With the high accuracy of oceanographic sensors tested in inland waters, this is another step forward to unifying these two regions. These sensors measure carbon dioxide (CO_2), methane (CH_4), oxygen (O_2) as well as temperature and salinity (conductivity) to primarily gather information about the carbon cycle budgets and dynamics. These parameters are known to be highly variably between different regions within the LOAC, with little to no data coverage from the majority of inland waters. Due to atmospheric CO_2 and CH_4 ever increasing, knowing correct quantities, budgets and potential inland dynamics is of upmost importance. This can assist with modelling efforts and monitoring, while furthering our scientific knowledge of these highly complex systems.

To attempt to close this boundary, evaluate if the sensors have to potential to do this and assess what advances high-resolution data can acquire for the scientific community, this thesis has been split into three chapters. 1) Set-up, deployment and evaluation of the oceanic-sensor flow through package across three sections of the LOAC (oceanic, brackish and limnic waters), which led on to look at the 2) dynamics of carbonate species throughout the inland water campaign. Using the mapping technique, diel extractions were performed to see the overall impact on the system over a full diel cycle. This was then taken a step further where 3) CH_4 diel cycles were specifically assessed. Focusing on whether measuring at only one time (i.e. when taking a discrete sample), only during the day or over a full 24-hour cycle would have significant implications on the overall methane budget estimates. Each of theses sections addresses the research questions that were presented in sections 4-6 and provides the following answers:

1. **Can a set of oceanographic sensors provide high-quality data across the entire Land-Ocean Aquatic Continuum and under a wide range of operation conditions?**

   To assess the oceanic sensors, three regional campaigns took place: across the Atlantic Ocean (oceanic), the Baltic Sea (brackish) and the Danube River Delta (limnic). Each campaign also took place in different seasons (spring, summer and autumn) and over different durations (10 days to 1 month) to ensure the capabilities of the sensors to handle extreme environmental conditions, varying waters types while consistently stable over this period of time. The sensors were exposed to concentrations ranging from 14.1 - 6,000 μatm (pCO_2), 1.5 - 11,633 μatm (pCH_4), 6.9 - 431 μmol kg^{-1} (O_2) and ranging across a temperature and salinity range of 8.5 - 34.6 °C and 0 - 36.25, respectively.

   Extensive corrections were evaluated for ensuring the best quality of data for every

region. Along with the basic corrections (e.g. drift correction and temperature correction), a response time correction proved to be one of the most vital corrections for the CH_4 sensor (HydroC CH_4 FT). The ocean tends to have small spatial variabilities in comparison to limnic waters, due to biological activities and multiple other processes occurring when multiple factors are closely linked (e.g. wetland run off, anthropogenic influences, system run over such as channels to lakes and close sediment fluxes).

The limnic campaign was the largest test for this response time correction and ability to pick-up large-scale variabilities with some regions for CO_2 changing from >14,000 μatm to $\sim$ 1,600 μatm in less than 400 meters of distance. The advantage of measuring simultaneously with the O_2 data, allowed for CH_4 data corrections to be assessed due, although not always, inverse relationship between CH_4 and O_2. As both sensors were in no way linked through this correction it proved that the sensor was providing correct variabilities following the correction.

In summary, the sensors were able to perform to a high standard across all water bodies. They were tested in extreme conditions (< 10 to + 30 °C), extreme environments, from platforms of drastically different sophistication and across large and sometimes extremely steep concentration gradients. Although improvements could be made on the set-up, such as size, it proved to be versatile enough to measure on multiple vessels, including a house boat running on a generator. Even with this, I was able to show stability within variable waters to across longer transect, and even able to pick up the smallest of variabilities from all parameters. This enabled further in-depth analyses into the data and showing options for combining both the oceanic and limnological worlds. Furthering this, it allowed the following questions to be answered.

2. Can high-resolution mapping data be applied to a simple model to predict TA and further carbonate species measurements, while enabling diel extractions?

To answer this question and to calculate the carbonate species, discrete samples for TA were used, along with the continuous data for temperature and specific conductivity. From this, applied to a simple multilinear regression model, a continuous dataset for TA was generated. Quadratic terms for specific conductivity and temperature were introduced to consider the slightly non-linear relationship and improved the average error by 1.19% and R^2 by -0.12. Combined with the continuous pCO_2 data, the full carbonate species (including DIC) was then calculated using CO_2SYS (Lewis et al., 1998). This model output was verified against the measured TA and DIC samples which were collected simultaneously to the sensor measurements. Overall the model was able to calculate across the full range for TA (< 2,000 to > 3,500 μmol kg^{-1}) with R^2 ranging from 0.85 to 0.97. DIC calculated from measured pCO_2 and the estimated TA, showed roughly the same comparison to TA for both concentration and R^2 (< 2,000 to > 4,000 μmol kg^{-1} and R^2 = 0.69, to 0.96).

The outcomes from the model were then used to look further into the carbon dynamics within the delta. From the measured pCO_2 it was observed that 73.9% of the entire delta over three seasons were supersaturated in respect to atmospheric (during day hours). The delta was split between seasons (May, Aug or Oct) as well as systems (rivers, channels and lakes). Each of these systems showed large variety between concentrations, with rivers having a maximum of just over 6,000 μatm, to channels reaching over 21,000 μatm. Using the O_2 data collected, ΔDIC and ΔO_2 were compared over the seasons identifying the main processes and drivers.

The ratio between $\Delta DIC/\Delta O_2$ had a strong dependence on both water system and season. Between systems, rivers were consistently oversaturated with DIC for all months, identifying that the incoming DIC was potentially from further upstream. Although lakes were the most productive (supersaturated in ΔO_2, undersaturated in ΔDIC), both lakes and channels showed roughly similar values and there was a clear inter-linking between these two systems. We therefore focused on these two regions, as there was comparatively little variability within rivers implying most of the variability came from the processes within the delta.

From mapping experiments across Lake Roşu featuring an extensive mapping transect with cross overs, a diel cycle was extracted. This was completed by fitting a simple harmonic function for the pCO_2 data, and a linear fir from DIC extraction cross over values over the difference in time. These corrected values were then used to calculate TA and pH anomalies across the lake. Removing this revealed further spatial variability between the parameters than just a daily cycle. While pCO_2 and pH stayed roughly consistent throughout the entire lake after the diel cycle anomaly extraction (excluding some spatial variability coming form proximity to the reed beds), DIC and TA still showed a gradient from the incoming channel. This allowed us to observe a lateral hydrological input coinciding with the DIC and TA extreme co-locating with channel input and exits. The diel cycle was then compared to that of the full diel cycle for pCO_2, showing a consistent hysteresis, with nocturnal replenishment of pCO_2 from the diurnal depletion, to the same levels as the previous day.

In comparisons, the diel cycle was also extracted from a channel, showing the comparison between the two. The channel, such as with the concentrations, was far greater in variability than in the lake, however showed a similar (just elongated) hysteresis, yet different processes due to consistent supersaturation in DIC (unlike the lake which was undersaturated).

In summary, extracting carbonate species with the use of continuous temperature and specific conductivity data (and furthering pCO_2) is possible and shows good correlation with discrete samples taken for TA and DIC. This is one way to gather more in-depth data on a continuous scale within individual systems. This can then help assess and understand variations within systems, such as lakes, with transport either via lateral transport or more biological processes. Extracting the anomalies via mapping cross-over data also enhances this and provides further evidence for reasons behind concentration gradients. Overall, the delta varied less by season than between systems. Each system showed large spatial variability, due to multiple processes. Therefore, high-resolution mapping is one way of fully understanding such a system and can assist with daily cycling variability explanations. It can successfully be used to provide insights into diel cycles while enabling further extractions of various species and modelling of parameters.

3. Can high-spatio-temporal methane data and diel-cycle extraction advance the improvement of methane budget estimates?

From the results of the previous study, focus was turned more to the CH_4 data due to high uncertainties within the global methane budget (Saunois et al., 2019). From the extraction of the diel cycles proving potentially significant and having a major influence within the delta, this was further explored to answer this question. First, concentrations and overall fluxes were calculated using the entire dataset collected, including the diel cycles. Two strong diel cycles were the extracted as examples from Lake Roşu and the hot spot channel to get comparisons (such as the section above).

From the lake we observed a nocturnal build-up of CH_4 with a molar CH_4:O_2 ratio of 1:50, going from 400 nmol L^{-1} to 1,400 nmol L^{-1}. With the slow gradient over the night, decreasing in O_2, it is suggested to be due to stratification during the day within the lake (Milberg et al., 2017). Over the night, as the water cools, it undergoes advective mixing joining the two water bodies: deeper more anoxic waters with high CH_4 build-up and surface waters high in O_2 and low in CH_4. During the day, this re-stratifies, increasing in O_2 and decreasing in CH_4, which is lost as diffusive flux across the water-air interface. This process was vastly amplified within the channel, showing a potential bottom layer having been further stratified and therefore experiencing a sudden increase in CH_4 later during the night. It was linked with a decrease in O_2 as a CH_4:O_2 molar ratio of 1:3, going from roughly 4,000 nmol L^{-1} to 16,000 nmol L^{-1}.

Using this knowledge and data, CH_4 concentrations and fluxes were calculated with using the diel cycles, compared with excluding them. This showed a significant decrease in the over concentrations for channel concentrations and fluxes, however a slight unexpected increase in lakes. Given our mapping data in the lakes was such resolution, this biased our results, therefore showing if taking the average from the early afternoon only, it would have decreased the overall mean in CH_4. From this, the suggestion that to include the same benefit of high-resolution data, sampling should be completed during the low and high peak to gather the amplitude: before sunrise and after sunset.

In summary, the high-resolution data provided evidence that within channels, CH_4 concentrations were reduced by up to 25% when the full diel-cycle (and therefore night data) was not included. For lakes, values were increased with the extraction of the diel-cycle by 3.3% showing the potential of overestimation. These account for roughly an increase of 20.4% and decrease of 4.2% from fluxes for channels and lakes respectively when adding the full diel-cycle. Scaling this up to the entire delta, extraction of all diel-cycles, and using just the daily mapped data decreases the mean CH_4 flux from 49 $\pm$ 61 μmol m^{-2} h^{-1} to 34.9 $\pm$ 35.7 μmol m^{-2} h^{-1}. Although our day cycle values were far more extensive than most discrete collection techniques and therefore could be underestimating the influence, out data strongly suggests that high-spatial and diel-cycle inclusions have the potential to completely change regional CH_4 budget estimates.

The results of this thesis show the feasibility of combining the two disciplines together across the entire LOAC. It showed that with little to no modifications, the oceanic sensors were capable of measuring with high precision across all water bodies. This included highly diverse inland waters varying over concentration and temperature. Specific corrections were shown to be extremely important within these specific regions, specifically response time corrections for the CH_4 data. The success of this correction allowed for the deployment across extremely diverse regions, accessing even the little spatial variabilities. It has been acknowledged multiple times about the lack of data, especially spatiotemporally data within inland waters (e.g. Abril and Borges, 2019; Crawford et al., 2017; Saunois et al., 2016). Working with the knowledge of these gaps in data, we deployed our instruments across the entire spectrum (oceanic, brackish and limnic). Given these sensors are already used within ocean and brackish waters, the main focus for the success was on the limnic system. Using the high-resolution data we collected from intensive mapping, we were able to show the possibilities of data extraction.

In section two, we provided a means to calculate continuous TA data. Currently there is no limnic, and only one (to our knowledge, see Seelmann et al., (2019))

proven working TA instrument to continuously measure TA within water. Therefore, we enabled a way to extract TA from temperature and specific conductivity. Alongside continuous pCO_2 data, allowed for the carbonate species to be extracted. Having a complete dataset for all these parameters also in such high resolution allows for multiple processes to investigated which can provide further data into the processes within inland waters. It was observed that boundary crossing between the regions had an effect on overall concentrations, and that most of the CO_2 and CH_4 concentrations were produced within the delta and not in the rivers. In sections two and three, extraction of the daily cycles provided a way for the daily cycle to be extracted to further look at the processes within the waters.

CH_4 has large uncertainties in terms of carbon fluxes, storage and overall budgets (Saunois et al., 2019). Therefore, focusing on the extraction of CH_4 concentrations and fluxes both on a daily scale over complete diel variations, enabled an insight into potential missing fluxes. This is due to currently most datasets consisting mainly of discrete or daily data, with few studies focusing on diel variation. Although, these studies are growing in numbers, this is one that assists and shows strong evidence of the impacts this could have on overall global CH_4 budgets.

The thesis overall has shown that the advances in technology over the years, in terms of efficiency and precision, have leaped forward significantly. The combination of both the ocean and limnological realms should not be considered as two separate systems but start combining and learning from each other. It showed such high-resolution data is needed both on a regional but also global scale. With diel cycles and hot spots occurring in most limnic systems, focus should start be turning from selective discrete sampling, to forms of mapping with the use of continuous data. Although, as this is not always feasible, even continuous collection of daily cycles through day light hours is far more accurate than discrete sampling. We suggest if this is still not possible, collecting data at the peak and trough of the diel cycle may give a better average than midday sampling. Although, given every region will differ in terms of amplitude and processes therefore we suggest better classification of the diel cycles, with multiple examples is needed. However, this data gives further evidence that diel cycles should be accounted for in regional models and that the potential CH_4 and CO_2 budgets could be grossly underestimating fluxes in these regions, especially from channels.

Therefore, in all, understanding the limnic system is greatly improved by combining the work of oceanographers and limnologists. Thus, helping stretch the understanding of the biogeochemical processes of these highly diverse regions and getting a better overall estimate for the carbon budget.

7.1 References

Abril, G. and Borges, A. V.: Carbon leaks from flooded land: do we need to re-plumb the inland water active pipe?, Biogeosciences, 769–784, doi:10.5194/bg-2018-239, 2019.

Crawford, J. T., Loken, L. C., West, W. E., Crary, B., Spawn, S. A., Gubbins, N., Jones, S. E., Striegl, R. G. and Stanley, E. H.: Spatial heterogeneity of within-stream methane concentrations, J. Geophys. Res. Biogeosciences, 122(5), 1036–1048, doi:10.1002/2016JG003698, 2017.

Lewis, E., Wallace, D. and Allison, L. J.: Program developed for CO_2 system calculations, carbon dioxide information analysis center, Oak Ridge National Laboratory, Oak Ridge, Tenn., 1998. Milberg, P., Törnqvist, L., Westerberg, L. M. and Bastviken, D.: Temporal variations in methane emissions from emergent aquatic macrophytes in

two boreonemoral lakes, AoB Plants, 9(4), doi:10.1093/aobpla/plx029, 2017.

Saunois, M., Bousquet, P., Poulter, B., Peregon, A., Ciais, P., Canadell, J. G., Dlugokencky, E. J., Etiope, G., Bastviken, D., Houweling, S., Janssens-Maenhout, G., Tubiello, F. N., Castaldi, S., Jackson, R. B., Alexe, M., Arora, V. K., Beerling, D. J., Bergamaschi, P., Blake, D. R., Brailsford, G., Brovkin, V., Bruhwiler, L., Crevoisier, C., Crill, P., Covey, K., Curry, C., Frankenberg, C., Gedney, N., Höglund-Isaksson, L., Ishizawa, M., Ito, A., Joos, F., Kim, H. S., Kleinen, T., Krummel, P., Lamarque, J. F., Langenfelds, R., Locatelli, R., Machida, T., Maksyutov, S., McDonald, K. C., Marshall, J., Melton, J. R., Morino, I., Naik, V., O'Doherty, S., Parmentier, F. J. W., Patra, P. K., Peng, C., Peng, S., Peters, G. P., Pison, I., Prigent, C., Prinn, R., Ramonet, M., Riley, W. J., Saito, M., Santini, M., Schroeder, R., Simpson, I. J., Spahni, R., Steele, P., Takizawa, A., Thornton, B. F., Tian, H., Tohjima, Y., Viovy, N., Voulgarakis, A., Van Weele, M., Van Der Werf, G. R., Weiss, R., Wiedinmyer, C., Wilton, D. J., Wiltshire, A., Worthy, D., Wunch, D., Xu, X., Yoshida, Y., Zhang, B., Zhang, Z. and Zhu, Q.: The global methane budget 2000-2012, Earth Syst. Sci. Data, 8(2), 697–751, doi:10.5194/essd-8-697-2016, 2016.

Saunois, M., Stavert, A. R., Poulter, B., Bousquet, P., Canadell, J. G., Jackson, R. B., Raymond, P. A., Dlugokencky, E. J., Houweling, S., Patra, P. K., Ciais, P., Arora, V. K., Bastviken, D., Bergamaschi, P., Blake, D. R., Brailsford, G., Bruhwiler, L., Carlson, K. M., Carrol, M., Castaldi, S., Chandra, N., Crevoisier, C., Crill, P. M., Covey, K., Curry, C. L., Etiope, G., Frankenberg, C., Gedney, N., Hegglin, M. I., Höglund-Isaksson, L., Hugelius, G., Ishizawa, M., Ito, A., Maenhout, J. G., Jensen, K. M., Joos, F., Kleinen, T., Krummel, P. B., Langenfelds, R. L., Laruelle, G. G., Liu, L., Machida, T., Maksyutov, S., McDonald, K. C., McNorton, J., Miller, P. A., Melton, J. R., Morino, I., Müller, J., Murguia-Flores, F., Naik, V., Niwa, Y., Noce, S., O'Doherty, S., Parker, R. J., Peng, C., Peng, S., Peters, G. P., Prigent, C., Prinn, R., Ramonet, M., Regnier, P., Riley, W. J., Rosentreter, J. A., Segers, A., Simpson, I. J., Shi, H., Smith, S. J., Steele, L. P., Thornton, B. F., Tian, H., Tohjima, Y., Tubiello, F. N., Tsuruta, A., Viovy, N., Voulgarakis, A., Weber, T. S., Weele, M. van, Werf, G. R. van der, Weiss, R. F., Worthy, D., Wunch, D., Yin, Y., Yoshida, Y., Zhang, W., Zhang, Z., Zhao, Y., Zheng, B., Zhu, Q., Zhu, Q. and Zhuang, Q.: The Global Methane Budget 2000-2017, Earth Syst. Sci. Data, doi:10.1017/CBO9781107415324.004, 2019.

Seelmann, K., Aßmann, S. and Körtzinger, A.: Characterization of a novel autonomous analyzer for seawater total alkalinity: Results from laboratory and field tests, Limnol. Oceanogr. Methods, 17(10), 515–532, doi:10.1002/lom3.10329, 2019.

Acknowledgements

I'd first like to thank my main supervisors, Arne Kortzinger and Peer Fietzek who helped, supported and had faith in me for this thesis. For their ideas, input and general enthusiasm for the project. I would also like to thank my second supervisor Bernhard Werhli for his input, especially for the third manuscript and the combined work in Romania. I would also like to thank the funding bodies which led to this thesis; funding from the European Union's Horizon 2020 research and innovation program under the Marie Sklodowska-Curie grant agreement No 643052 (C-CASCADES project) and funding from Digital Earth which is coordinated by GEOMAR Helmholtz Centre for Ocean Research Kiel.

I'd also like to thank all the people that helped along the way, from my friends and family in the UK to those in Germany, including those who helped with programming: Chris and Sergei. To my family who were always there for support and encouragement whenever it was needed. This also includes the Oval Office family, Dennis and Alex and more recently, Lili, who not only kept up the energy throughout the 4 years, but assisted with with snack provisions, laughter and continuous help with the actual thesis work.

I would like to acknowledge and send a massive thanks to those who helped with both laboratory work, teamwork and enjoyment on the cruises on top of my personal learning and growth: Mario and all the guys from the East Shore in Kiel, Insa, Roberto, Damian, Annette, Katharina, Tobi Hahn (also with optode processing), Melf, Max and especially Patricia, Dagmara and Jen Clarke. Without the final 3, this work would have been much more of a struggle in different ways.

I am grateful for all those who also helped along the process; Björn Fiedler and Tobias Steinhoff who gave me the first lot of scripts when first starting out and any help needed along the way. All of the KMCON team, especially Nadja, with their support and help throughout my time with them and while on field work both day and night.

Many thanks goes to those who helped and worked on the many campaigns: the teams and crew on RV EMB, RV Meteor and RV Littorina; my Romanian colleagues captain Nice, George, Marian and especially Teo who helped, and drove the campaigns. Especially to those in Romania who took us into their home, including Teo, and showed us life in the Danube Delta.

I'd also like to thank Thomas Braun who kept me well-supplied with chocolate care packages from Switzerland towards the end. To my main climbing and coffee break buddies including Thomas, Ole, Chris, Phillipp and Anna.

I would also like to send a massive thank-you the C-CASCADES group, without whom, none of this would have been possible due to their support and continued drive. For all those weeks together through our training activities and our summer school, we bonded well and kept up the enthusiasm for our projects.

And finally, the warmest thank-you goes to Marie-Sophie Maier who maintained my sanity during the Romanian campaigns, discussed and devised ideas with enthusiasm and whose input was invaluable. Her patience and attention to detail is unbelievable. I think we made quite a team and it was an absolute pleasure!